UNIVERSIDADE DE BRASÍLIA – UnB
INSTITUTO DE GEOCIÊNCIAS
PROGRAMA DE PÓS-GRADUAÇÃO EM GEOLOGIA

GEOLOGIA, GEOQUÍMICA, Sm-Nd E GEOCRONOLOGIA U-Pb E Lu-Hf EM ZIRCÃO DO EMBASAMENTO DO ORIENTE BOLIVIANO: IMPLICAÇÕES PARA A EVOLUÇÃO GEODINÂMICA DO SW/S DO CRÁTON AMAZÔNICO

TESE DE DOUTORADO
Nº 172

Letícia Alexandre Redes

Brasília, DF, março de 2021.

UNIVERSIDADE DE BRASÍLIA – UnB
INSTITUTO DE GEOCIÊNCIAS
PROGRAMA DE PÓS-GRADUAÇÃO EM GEOLOGIA

ÁREA DE CONCENTRAÇÃO: Geologia Regional

TESE DE DOUTORADO
Nº 172

GEOLOGIA, GEOQUÍMICA, Sm-Nd E GEOCRONOLOGIA U-Pb E Lu-Hf EM ZIRCÃO DO EMBASAMENTO DO ORIENTE BOLIVIANO: IMPLICAÇÕES PARA A EVOLUÇÃO GEODINÂMICA DO SW/S DO CRÁTON AMAZÔNICO

Letícia Alexandre Redes

Banca Examinadora:
Natalia Hauser (UnB - Orientadora)
Amarildo Salina Ruiz (UFMT – Coorientador)
Valmir da Silva Souza (UnB, Brasil)
Umberto Giuseppe Cordani (USP, Brasil)
Víctor Alberto Ramos (UBA, Argentina)
Catarina L. B. Toledo (Suplente interno)

Brasília, DF, março de 2021.

Alexandre Redes, Letícia
A757g GEOLOGIA, GEOQUÍMICA, Sm-Nd E GEOCRONOLOGIA U-Pb E Lu-Hf EM ZIRCÃO DO EMBASAMENTO DO ORIENTE BOLIVIANO: IMPLICAÇÕES PARA A EVOLUÇÃO GEODINÂMICA DO SW/S DO CRÁTON AMAZÔNICO / Letícia Alexandre Redes; orientador Natalia Hauser; co orientador Amarildo Salina Ruiz. -- Brasília, 2021.
220 p.

Tese (Doutorado - Doutorado em Geologia) -- Universidade de Brasília, 2021.

1. Geologia. 2. Pré-cambriano do Leste da Bolívia. 3. Bloco Rio Apa. 4. Bloco Paraguá. 5. Sm-Nd, U-Pb e Lu-Hf. I. Hauser, Natalia, orient. II. Salina Ruiz, Amarildo, co orient. III. Título.

Dedicado à Sylvana Redes e Edvaldo Redes

AGRADECIMENTOS

O presente trabalho foi realizado com apoio da Coordenação de Aperfeiçoamento de Pessoal de Nível Superior - Brasil (CAPES) - Código de Financiamento 001. Sou grata ao suporte financeiro que me foi oferecido.

Agradeço imensamente a todos que me deram apoio na realização do doutorado. Aos que me motivaram, quando eu já não tinha forças, aos que me inspiraram, e que mesmo sem saber, foram exemplos para eu continuar.

Agradeço aos meus pais, minha irmã, alguns membros da minha família e amigos da vida, que foram essenciais nessa jornada, pois foram como uma fortaleza, que me apararam nos meus momentos de fragilidade. Me ofertando amor, carinho e cuidado em livre demanda. Obrigada Joniel, pelos momentos essenciais de companheirismo, compreensão e apoio durante a caminhada que me trouxe aqui.

Sou muito grata aos amigos e colegas do Programa de Pós-graduação em Geologia, por todas as trocas de conhecimento e todo tipo de ajuda.

De maneira especial gostaria de agradecer a minha querida orientadora, professora Natalia Hauser, que veio preencher de forma brilhante e acalentadora, o papel anteriormente atribuído ao saudoso professor Márcio Martins Pimentel (*in memoriam*), que antes de partir deixou um legado de conhecimento incrível e contribuiu muito na realização do meu doutorado.

Obrigada, Natalia! Eu sou extremamente grata por toda a sua contribuição intelectual e dedicação, prestadas nas diversas e inúmeras correções, necessárias para a produção e finalização dos artigos científicos e desta Tese. Agradeço por me fornecer afeto e muito carinho, como reflexo de um dos seres humanos mais incríveis que já conheci.

Agradeço ao professor Uwe, por todas as revisões e correções pertinentes. Obrigada por todo tempo dedicado.

Obrigada professores Amarildo Ruiz e Ramiro Matos, por me acompanharem em campo e terem sido muito importantes nessa trajetória.

De modo geral, agradeço a todos os professores pelo conhecimento destinado a mim. E aos técnicos dos laboratórios pelo suporte fornecido.

E obrigada Deus, por não soltar da minha mão!

SUMÁRIO

ÍNDICE DE FIGURAS

ÍNDICE DE TABELAS

RESUMO

Geoquímica e isótopos de Sm-Nd e U-Pb/Hf zircão foram obtidos em granitoides e gnaisses do embasamento paleoproterozoico do Leste da Bolívia (EBB). Foram estudados os granitoides Santo Corazón, Correreca e Santa Terezita (Bolívia) e o Gnaisse Santana da região de Corumbá (Brasil) do Bloco Rio Apa e vários gnaisses do Complexo Chiquitania do vizinho Bloco Paraguá. O objetivo era melhorar a compreensão da evolução desses terrenos e das relações entre eles e o Cráton Amazônico. Os dados obtidos durante esta pesquisa foram apresentados na forma de dois artigos: (1) *"U–Pb and Hf isotopes in granitoids from the Eastern Bolivian basement: Insights into the Paleoproterozoic evolution of the western part of South America"*, e (2) "*The polycyclic evolution of the Paraguá Block, Bolivia-SW Brazil: a Sm-Nd and U-Pb/Hf isotope study of the Paleo- to Mesoprotrozoic Chiquitania Complex*". O primeiro artigo foi publicado em 2020 no *Journal of South American Earth Sciences*, edição especial dedicada a Márcio Pimentel, e o segundo foi submetido ao *Precambrian Research* e encontrasse em processo de avaliação. Os granitos Santo Corazón, Correreca e Santa Terezita têm um caráter cálcio-alcalino de médio a alto potássio, são peraluminosos do tipo S. Foram obtidas idades U-Pb de intercepto superior em zircão de 1874±15 Ma e 1862±7 Ma para o quartzo-monzonito Santo Corazón e granito Correreca, e de 1849±11 e 1852±6 Ma para o granito Santa Terezita. Os dados geoquímicos e de isótopos Sm-Nd e U-Pb sugerem que esses granitoides representam o retrabalho durante a tempo Orosiriano de uma crosta criada entre 2,23 e 1,96 Ga. O retrabalho ocorreu em uma configuração de arco magmático. Isto é ainda suportado por dados de isótopos Hf para zircão do granito Correreca. O Gnaisse Santana trata-se de um granada-hornblenda-biotita gnaisse com uma idade U-Pb de intercepto superior em zircão de 1764±23 Ma, que é interpretada como a idade de cristalização do protólito ígneo, um quartzo-monzonito ou granodiorito. Os dados petrológicos, geoquímicos e de isótopos de Nd e U-Pb mostram semelhança entre os granitos do embasamento oriental da Bolívia (EBB) e o Gnaisse Santana com a Suíte Intrusiva Alumiador e o Gnaisse Caracol, respectivamente. Isso sugere que este fragmento crustal poderia ter sido uma extensão em direção ao oeste do Bloco Rio Apa, que hoje se estende por 300 km do sudoeste de Mato Grosso do Sul e do nordeste do Paraguai ao leste da Bolívia. A presença de crosta continental que remonta a 1,7-1,8 Ga é inferida a partir de dados de isótopos para os núcleos de zircão do Gnaisse de Santana e os granitos da Bolívia Oriental. Os protólitos dos gnaisses do Complexo Chiquitania eram de composição granítica a tonalítica e metaluminosa a peraluminosa. Eles também tinham caráter cálcio-alcalino e foram relacionados a uma configuração de arco magmático. Com base nas idades de cristalização U-Pb interpretadas para seus protólitos, os gnaisses estudados foram divididos em duas unidades: a unidade mais antiga do Complexo Chiquitania, o gnaisse Miraflores com idades de intercepto superior de 1747±11 Ma, e a unidade mais jovem conformada pelos gnaisses Rio Fortuna, San Miguel e Rosário com idades de intercepto superior de 1699±9

Ma, 1681±13 Ma e 1678±21 Ma, respectivamente. Valores negativos de $\varepsilon_{Nd(t)}$ para o gnaisse Miraflores indicam principalmente crosta retrabalhada, enquanto os gnaisses Rio Fortuna, San Miguel e Rosário renderam valores positivos de $\varepsilon_{Nd(t)}$ e $\varepsilon_{Hf(t)}$ em zircão, o que indica que os magmas parentais representavam a mistura entre material derivado do manto e crosta retrabalhada. As idades modelos Nd e Hf paleoproterozoicas indicam que a crosta mais velha de 2,64-1,97 Ga foi retrabalhada em um arco magmático entre ~ 1,75 e ~ 1,69 Ga. Com base nos dados de idade U-Pb atualmente disponíveis, o embasamento oriental a Bolívia teve uma evolução policíclica. Assim, três eventos magmáticos / metamórficos principais foram reconhecidos: *Evento 1* foi relacionado com a colocação de granitos Orosirianos do Bloco Rio Apa em ~ 1,84 Ga; O *Evento 2* foi relacionado com o desenvolvimento de arcos magmáticos acrecionários no Bloco Paraguá entre ca. 1,75 e 1,65 Ga, e o *Evento 3* foi relacionado com a Orogenia San Ignacio em ~ 1,3 Ga. O Evento 2 pode estar relacionado com a construção do Bloco Paraguá em três ciclos: Ciclo 1 relacionado ao Arco granodiorítico Miraflores em ~ 1,75 Ga, Ciclo 2 relacionado com os arcos mais juvenis circundantes, o arco tonalítico do Rio Fortuna e o arco monzogranitico de San Miguel/Rosário de ~ 1,69 Ga, e o Ciclo 3 relacionado com o arco Triunfo/Matão/Turvo e pelo arco Refúgio, mais juvenil de ~ 1,65 Ga. Neste trabalho, o Bloco Paraguá foi interpretado como um bloco composto pela acreção sucessiva de arcos, com uma parte central mais antiga (Arco granodiorítico Miraflores), circundado por arcos magmáticos progressivamente mais jovens, aqueles representados pelos ciclos 2 e 3. A colisão entre o Bloco Paraguá e o Cráton Amazônico provavelmente ocorreu a 1,5 Ga; mas esses blocos continentais foram posteriormente destacados em ~ 1,4 Ga. A colisão final dos blocos Paraguá e Rio Apa com o Cráton Amazônico ocorreu em ~ 1,3 Ga durante a Orogenia San Ignácio. Esta assembleia permaneceu estável durante a estruturação do Supercontinente Rodínia.

Palavras-chave: Pré-cambriano do Leste da Bolívia; Bloco Paraguá; Bloco Rio Apa; Sm-Nd; Geocronologia U-Pb e Lu-Hf

ABSTRACT

Geochemical, Sm-Nd and U-Pb/Hf on zircon isotope analysis was conducted on granitoids and gneisses from the Paleoproterozoic basement of Eastern Bolivia (EBB). The Santo Corazón, Correreca, and Santa Terezita granitoids (Bolivia) and the Santana Gneiss from the Corumbá region (Brazil) from the Rio Apa Block and several Chiquitania Complex gneisses from the neighboring Paraguá Block were studied. The aim was to improve understanding of the evolution of these terranes and the relationships between these blocks and the Amazonian Craton. The data obtained during this research were presented as two manuscripts: 1) "U–Pb and Hf isotopes in granitoids from the Eastern Bolivian basement: Insights into the Paleoproterozoic evolution of the western part of South America", and 2) "The polycyclic evolution of the Paraguá Block, Bolivia-SW Brazil: a Sm-Nd and U-Pb/Hf isotope study of the Paleo- to Mesoprotrozoic Chiquitania Complex". The former was published in 2020 in the Journal of South American Earth Sciences, Special Issue dedicated to Marcio Pimentel, and the latter has just been submitted to Precambrian Research, that at the moment is under review. The Santo Corazón, Correreca, and Santa Terezita granites have a medium to high calc-alkaline potassium character and are typically peraluminous S-type granites. Upper intercept U-Pb zircon ages of 1874±15 Ma and1862±7 Ma were obtained for the Santo Corazón quartz monzonite and Correreca granite, whereas two U-Pb upper intercept zircon ages of 1849±11 and 1852±6 Ma were obtained for the Santa Terezita granite. The geochemical, Sm-Nd and U-Pb isotope data suggest that these granitoids represent reworking during Orosirian times of a crust created between 2.23 and 1.96 Ga. The reworking occurred in a magmatic arc setting. This is further supported by Hf isotope data for zircon from the Correreca granite. The garnet-hornblende-biotite Santana Gneiss gave an upper intercept U-Pb zircon age of 1764±23 Ma, which is interpreted as the crystallization age of the igneous protolith, a quartz-monzonite or granodiorite. The petrological, geochemical and Nd as well as U-Pb isotope data show similarity between the Eastern Bolivian Basement granites (EBB) and the Santana Gneiss with the Alumiador Intrusive Suite and the Caracol Gneiss, respectively. This suggests that this crustal fragment could have been an extension towards the west of the Rio Apa Block, which today extends for 300 km from the southwest of Mato Grosso do Sul and northeast Paraguay to Eastern Bolivia. The presence of continental crust that dates back to 1.7-1.8 Ga is inferred from isotope data for the cores of zircon from the Santana Gneiss and the Eastern Bolivian granites. The protoliths of the Chiquitania Complex gneisses were granitic to tonalitic, and metaluminous to peraluminous in composition. They also had calc-alkaline character and can be related to a magmatic arc setting. On the basis of the interpreted U-Pb crystallization ages for their protoliths, the studied gneisses were divided into two units: the older unit of the Chiquitania Complex, the Miraflores gneiss with an upper intercept ages of 1747±11 Ma, and the younger Rio Fortuna, San Miguel and Santo Rosario gneisses with upper intercept ages of 1699±9 Ma,

1681±13 Ma, and 1678±21 Ma, respectively. Negative $\varepsilon_{Nd(t)}$ values for the Miraflores Gneiss indicate mainly reworked crust, whereas the younger Rio Fortuna, San Miguel and Santo Rosario gneisses yielded positive values and positive $\varepsilon_{Hf(t)}$ on zircon values, which indicates that parental magmas represent mixing between mantle-derived material and reworked crust. Paleoproterozoic Nd and Hf T_{DM} indicate older 2.64-1.97 Ga crust was reworked in a volcanic arc setting at ~1.75 and ~1.69 Ga. Based on currently available U-Pb age data, the Eastern Bolivian Basement had a polycyclic evolution. In this waythree major magmatic/metamorphic events were recognized: *Event 1* was related with the emplacement of Orosirian granites of the Rio Apa Block at ~1.84 Ga; *Event 2* was related with the development of accretionary magmatic arcs on the Paraguá Block between ca. 1.75 and 1.65 Ga, and *Event 3* was related with the San Ignacio Orogeny at ~1.3 Ga. Event 2 can be related with the assembly of the Paraguá Block that probably involved three cycles: Cycle 1 related to the Miraflores Tonalite Arc at ~1.75 Ga, Cycle 2 related with the surrounding more juvenile arcs involving the Rio Fortuna Tonalite and San Miguel/Santo Rosario monzogranite arcs of ~1.69 Ga age, and Cycle 3 is indicated by the Triunfo/Matão/Turvo Granitoid Arc and the more juvenile Refugio Granite Arc of ~1.65 Ga age. In this work is interpreted that the Paraguá Block is a composite block formed by the successive accretion of arcs, with an older central part (the Miraflores Granodiorite Arc), intruding the Lomas Maneches terrane, surrounded by progressively younger magmatic arcs, those represented by Cycles 2 and 3. Collision between Paraguá Block and Amazonian Craton probably occurred at 1.5 Ga; these continental blocks were later detached at ~1.4 Ga. Final amalgamation of the Paraguá and Rio Apa blocks with the Amazonian Craton occurred at ~1.3 Ga during the San Ignacio Orogeny. This assemblage remained stable during the amalgamation into the Rodinia supercontinent.

Keywords: Precambrian of Eastern Bolivia; Paraguá Block; Rio Apa Block; Sm-Nd; Geochronology U-Pb e Lu-Hf

CAPÍTULO 1 – INTRODUÇÃO

1.1. Introdução

O conhecimento atual da geologia pré-cambriana do oriente da Bolívia é em grande parte uma consequência do mapeamento sistemático chamado de Proyecto Precambrico (Litherland e Bloomfield, 1981; Berrangé, 1982; Litherland *et al*., 1986, 1989). O projeto era parte de um programa cooperativo britânico-boliviano na década de 1980. Poucas pesquisas integram os estudos geológicos entre o Brasil e a Bolívia, e as existentes buscaram correlacionar a história geológica e tectônica da Bolívia com o SW do Cráton Amazônico no Brasil (por exemplo, Boger *et al*., 2005; Vargas-Mattos, 2006; Cordani e Teixeira, 2007; Santos *et al*., 2002, 2008; Cordani *et al*., 2009; Matos *et al*., 2009; Bettencourt *et al*., 2010; Teixeira *et al*., 2010; Faleiros *et al*. 2015).

O embasamento boliviano em sua totalidade sempre foi descrito como integrante do Bloco Paraguá (Litherland *et al*., 1986, Boger *et al*., 2005, Bettencourt *et al*., 2010). O Bloco Paraguá está inserido no contexto da Província Rondoniana-San Ignácio (1.5 – 1.3 Ga; Bettencourt *et al*., 2010) e faz parte da evolução do supercontinente paleoproterozoico Columbia (Zhao *et al*., 2004). A posição e o papel que ele teria tido ainda não é claro, porque nos últimos anos poucas unidades paleoproterozoicas foram identificadas na Bolívia. O embasamento desse bloco compreende principalmente granulitos, paragnaisses e ortognaisses, migmatitos e xistos, com idades entre 1900 e 1600 Ma.

A sequência estratigráfica proposta por Litherland *et al.* (1986) consiste no Complexo Lomas Maneches (cerca de 1900 Ma) composto por granulitos, seguido por uma associação de ortognaisses e paragnaisses do Complexo Gnáissico Chiquitania, e por uma unidade mais jovem, constituída por xistos do Grupo San Ignácio (~1650 Ma) (Boger *et al.*, 2005; Litherland *et al.*, 1986; Santos *et al.*, 2008; Faria *et al.*, 2014; Figueiredo *et al.*, 2013; Matos *et al*., 2013; Nedel *et al.*, 2017). Além dessas unidades, anteriormente Mitchell (1979) tinha descrito os granitos paleoproterozoicos Correreca e Santo Corazón no leste da Bolívia. Posteriormente Vargas-Mattos *et al*. (2010) descreveram um magmatismo paleoproterozoico no território boliviano relacionado à colocação de granitos de médio potássio, cálcio-alcalinos, peraluminosos, compatíveis com

ambiente de arco e com idades entre 1925±32 e 1894±13 Ma. Com base nesses dados, Vargas-Mattos *et al*. (2010) e Faleiros *et al*. (2016) sugeriram que o Granito Correreca poderia ser uma peça do Bloco Rio Apa que se estendia ao território boliviano. A Orogenia San Ignácio (~1300 Ma), responsável pela colisão do Bloco Paraguá com o Cráton Amazônico (Ruiz 2005, 2009), causou deformação, metamorfismo de alto grau e fusão parcial durante o pico metamórfico, que afetou principalmente o embasamento do Bloco Paraguá (Bettencourt *et al*., 2010). Essa colisão gerou um arco magmático representado por vários granitoides com idades em torno de 1300 Ma (Matos *et al.*, 2009, Jesus *et al.*, 2010, Nalon *et al.*, 2013, França *et al.*, 2014). Essa suíte foi chamada de Complexo Granitoide Pensamiento (1,3 Ga; Litherland *et al*., 1986; Boger *et al*., 2005; Matos, 2010). Posteriormente a Orogenia Sunsas (1,0 Ga) afetou parcialmente as unidades do embasamento, gerando deformação e metamorfismo de baixo grau (Teixeira *et al*., 2010).

1.2. Objetivos da Tese

O presente trabalho tem como objetivo aprofundar no conhecimento sobre o embasamento boliviano, especificamente na porção leste da Bolívia. Antes deste estudo o embasamento da área era conhecido pela ocorrência do Granito Santo Corazón de dimensões batolíticas, pelo Granito Correreca de idade orosiriana (Vargas-Matos, 2010) e pelas unidades denominadas de pré-San Ignácio: Complexo Lomas Maneches (granulitos), Complexo Chiquitania (orto e paragnaisses) e Grupo San Ignácio (xistos) (Bettencourt *et al*., 2010).

A proposta central desta tese consiste em descrever a ocorrência e a evolução dos blocos Rio Apa e Paraguá, com enfoque nas unidades paleoproterozoicas: Complexo Chiquitania (Bloco Paraguá), Suíte Intrusiva Alumiador (Bloco Rio Apa) no oriente boliviano e da Suíte Caracol (Bloco Rio Apa) em Corumbá-MS.

Assim os dados obtidos através da caracterização petrográfica, mineralógica, litogeoquímica, geocronológica (U-Pb em zircão) e isotópica (Sm-Nd e Lu-Hf), ajudaram a compreender a evolução pré-cambriana deste embasamento. Os processos envolvidos nesta evolução irão contribuir para o conhecimento geológico regional, através de:

a) Individualização dos períodos de geração de crosta continental e retrabalhamento crustal durante o Proterozoico, ligado ou não a períodos de acreção, bem como a distinção de eventos e ciclos magmáticos;

b) Caracterização dos eventos (ciclos) magmáticos-deformacionais;

c) Caracterização das fontes magmáticas e idades dos protólitos envolvidos;

d) Investigação das possíveis correlações entre os eventos magmatismo e metamórficos dos blocos Rio Apa e Paraguá com as orogenias comumente registradas no Crato Amazônico.

e) Proposição de um modelo evolutivo para o embasamento boliviano.

1.3. Localização e Vias de acesso

A área de estudo está situada entre as cidades de Corumbá (MS – Brasil) e San Ignácio de Velasco (Departamento de Santa Cruz – Bolívia), compreende a parte leste do departamento de Santa Cruz, abrangendo as folhas 1: 250.000 de San Ignácio de Velasco, Las Petas e San José de Chiquitos.

Como a área de estudo localiza-se na divisa entre o Brasil e a Bolívia, durante as etapas de campo o acesso foi feito pelos estados de Mato Grosso e Mato Grosso do Sul (Fig.1.1).

Partindo de Cuiabá, capital do Estado de Mato Grosso (MT), pela rodovia BR-070 até a cidade de Cáceres – MT, chega-se à divisa entre os países. A partir da divisa essa rodovia passa a se chamar *Ruta* 10. Tem-se acesso então ao primeiro município em território boliviano, San Matías, que dista aproximadamente 100 Km de Cáceres-MT. Segue-se pela *Ruta* 10 até San Ignácio de Velasco, onde é necessário seguir por aproximadamente 70 km pela *Ruta* 17, para chegar em San Rafael (675 km de Cuiabá-MT), pela mesma rota chega-se a San José de Chiquitos. Outras cidades em torno de San Rafael foram acessadas pelas *Rutas* 9, 10, 39 e Carretera Hardeman, e ainda por estradas vicinais, que ligam zonas rurais a rota principal.

Como uma segunda opção de acesso e também para estudar os Gnaisse Santana, segue-se por Campo Grande capital do Estado de Mato Grosso do Sul (MS), onde percorreu-se 430 km até Corumbá-MS, município localizado na porção noroeste do Mato Grosso do Sul, que abrange

parte da Folha Corumbá (SE. 21-Y-D). Nesta região fica localizado parte da área de estudo, na qual o acesso é feito pela rodovia BR-262 e MS-228 e pelas estradas secundárias que interligam assentamentos, sedes e retiros dentro de fazendas.

Partindo de Corumbá-MS, para acessar a área de estudo na Bolívia, passa-se pela cidade de Porto Suaréz, cidade que faz divisa com Corumbá-MS. Em território boliviano se percorre cerca de 240 Km pela RN-4 de Porto Suaréz até Roboré, cidade principal que forneceu acesso por vias secundárias até a região de Santo Corazón.

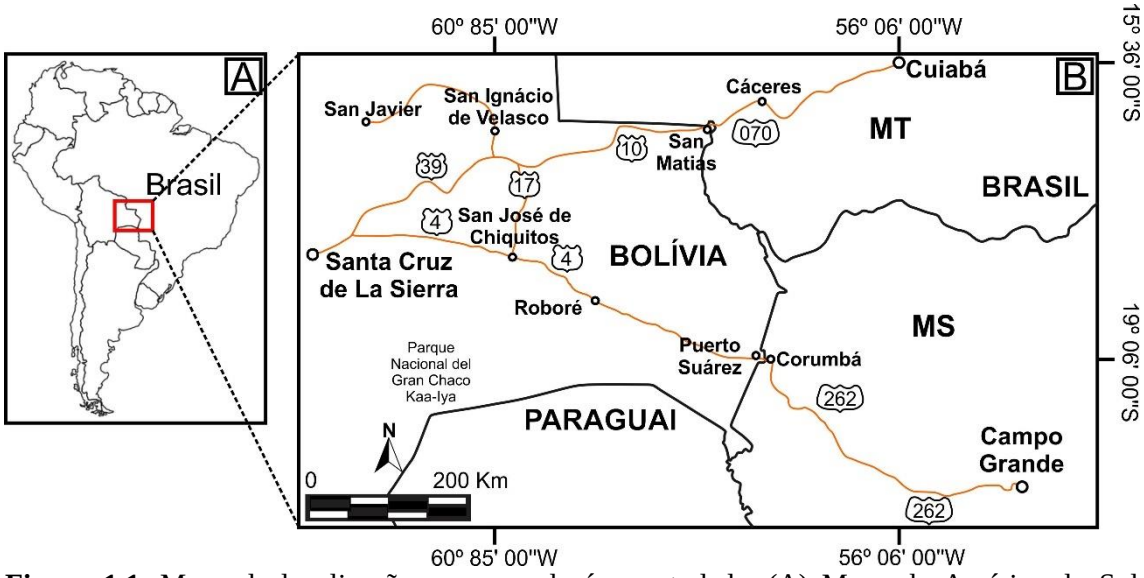

Figura 1.1. Mapa de localização e acesso da área estudada. (A) Mapa da América do Sul mostrando a localização da área de estudo. (B) Destaque da área de estudo na região oriental da Bolívia.

1.4. Estrutura da Tese

A presente Tese de Doutorado encontra-se dividida em sete (7) capítulos. O Capítulo 1 da pesquisa é composto pelos tópicos de introdução, que contempla o motivo da seleção do tema e histórico da área e sua relevância, seguido dos objetivos da Tese, onde é elucidado brevemente os alvos desta pesquisa, logo após é explicado a localização e vias de acesso da área pesquisada, e subsequente este subtópico, “Estrutura da tese”.

O Capítulo 2 aborda a contextualização geológica da área de estudo, onde é apresentada uma síntese a respeito do embasamento do leste boliviano e dos blocos Rio Apa e Paraguá.

O Capítulo 3 apresenta aspectos sobre a preparações pré-campo, seguida por aspectos sobre as etapas de campo e de laboratório, e posteriormente é revelado os métodos analíticos empregados nesta pesquisa.

Os capítulos 4 e 5 apresentam os resultados obtidos durante o desenvolvimento da pesquisa, na forma de dois artigos científicos:

1) O Capítulo 4 contém o artigo intitulado: "*U–Pb and Hf isotopes in granitoids from the Eastern Bolivian basement: Insights into the Paleoproterozoic evolution of the western part of South America*", publicado em Agosto de 2020 no no *Journal of South American Earth Sciences*. Neste artigo são abordadas a caracterização petrografica e isotópica dos granitos orosirianos do leste da Bolívia, e dos gnaisses estaterianos de Corumbá-MS, bem como a importância deste estudo no contexto da América do Sul;

2) O Capítulo 5 compreende o artigo "*The polycyclic evolution of the Paraguá Block, Bolivia-SW Brazil: A Sm-Nd and U-Pb/Hf isotope study of the Paleo- to Mesoproterozoic Chiquitania Complex*". Neste artigo são abordados os múltiplos eventos de atividades magmáticas e metamórficas, registrados nos gnaisses de idade estateriana do Complexo Chiquitania do Bloco Paraguá. Este manuscrito foi submetido recentemente ao *Precambrian Research* e encontrasse na etapa de revisão.

O Capítulo 6 inclui uma síntese conclusiva da Tese, destacando a história evolutiva integrada, a partir dos diversos registros preservados nas rochas que compõem o Bloco Rio Apa e Paraguá, mediante os dados que foram apresentados nos artigos científicos dos capítulos 4 e 5.

Finalmente o capítulo 7 contém referências bibliográficas utilizadas do capítulo 1 a 3 do trabalho.

CAPÍTULO 2 – CONTEXTO GEOLÓGICO REGIONAL

2.1. Embasamento do oriente boliviano

O embasamento pré-cambriano do oriente da Bolívia (Fig. 2.1) pertence a Província Rondoniana- San Ignácio (1.5 – 1.3 Ga; Tassinari *et al*., 1996; Bettencourt *et al*., 2010) e é composto, principalmente, pelos gnaisses do Complexo Chiquitania, gnaisses e granulitos do

Complexo Lomas Maneches e xistos do Grupo San Ignacio (Litherland *et al*., 1986; Boger *et al*., 2005), inseridos no Bloco Paraguá (1,74-1,32 Ga; Bettencourt *et al*., 2010). Além dessas unidades, rochas graníticas paleoproterozoicas foram reconhecidas no extremo leste boliviano, na região de Santo Corazón. Vargas-Mattos *et al*. (2010) e Faleiros *et al*. (2016) sugeriram que o granito Correreca, parte destas rochas graníticas, poderia ser uma peça do Bloco Rio Apa que se estendia ao território boliviano.

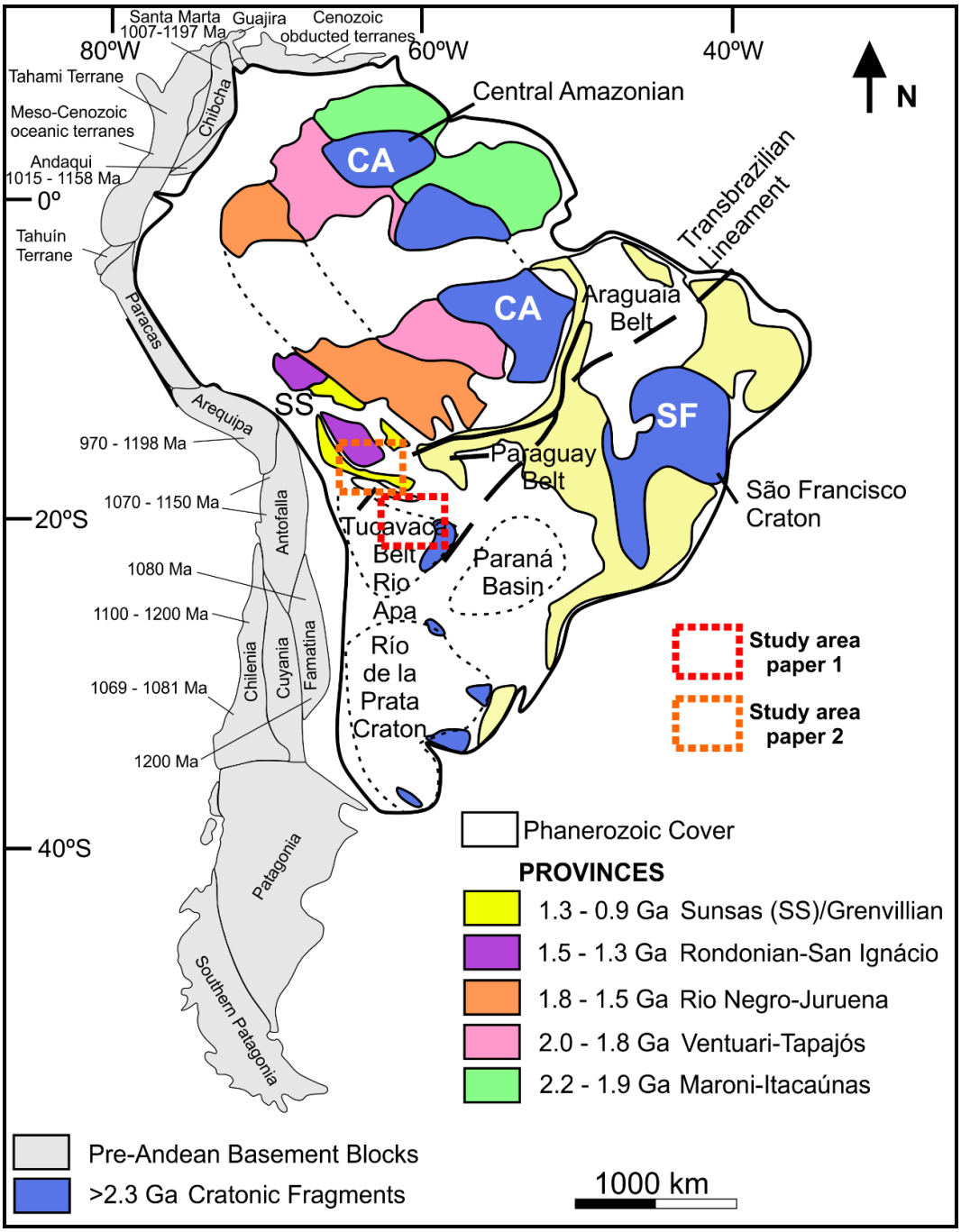

Figura 2.1. Províncias geológicas do continente sul-americano. Adaptado de Cordani *et al*. (2000), Tassinari *et al*. (2000), Loewy *et al*. (2004) e Ramos (2010).

2.2. Bloco Rio Apa

O Bloco Rio Apa está localizado na parte central da América do Sul (Fig. 2.2 A), as rochas do mesmo afloram no Brasil, na fronteira com a Bolívia e com o Paraguai, e se estende a sul em território paraguaio, e na região sudoeste do estado de Mato Grosso do Sul (Teixeira *et al*., 2020; Fig. 2.3 B). Este bloco foi divido em dois terrenos tectônicos principais: o ocidental e o oriental (Cordani *et al*., 2010; Teixeira *et al*., 2020). O conjunto de unidades litoestratigráficas que fazem parte deste bloco, estão formadas por segmentos infra e supracrustais, cuja evolução tectônica dá-se, em grande parte, nos períodos Orosiriano e Estateriano, representando, assim um importante papel na consolidação do Supercontinente Rodínia. Este fragmento é parte de um domínio cratônico da Faixa Paraguai composto por rochas do Paleo-Mesoproterozoico de médio grau metamórfico, intrudido por rochas graníticas. As mesmas são cobertas pelos depósitos carbonáticos neoproterozoicos dos Grupos Corumbá e Itapocumi (Almeida, 1965 e 1967; Alvarenga *et al*., 2000; Boggiani e Alvarenga 2004).

O bloco é marcado por setores com características tectono-estruturais e geocronológicas distintas, que levaram Lacerda Filho *et al*., (2006) a sugerir a presença de quatro compartimentos geotectônicos: (i) Remanescente de Crosta Oceânica (2,20-1,95 Ga), representado pelo Grupo Alto Tererê; (ii) Arco magmático Rio Apa (1,95-1,97 Ga), formado pelo Complexo Rio Apa; (iii) Arco Magmático Amonguijá (1,87-1,75 Ga), compreendendo as rochas da Suíte Amonguijá (Granito Alumiador e rochas vulcânicas Serra da Bocaina) e (iv) Domínio Amolar (1,2-0,9 Ga).

O Bloco Rio Apa foi definido como um terreno formado pela colagem de uma série de arcos magmáticos diacrónicos fragmentados e outros segmentos tectônicos em uma margem acrescionária de longa duração (Faleiros *et al*., 2016). E as relações espaciais dos três mais jovens eventos magmáticos presentes nos terrenos ocidentais e orientais exibem um zoneamento geocronológico claro, o que poderia refletir numa paleogeografia parcialmente preservada (Faleiros *et al*., 2016).

De acordo com Faleiros *et al*. (2016) este zoneamento geocronológico é refletido nos arcos magmáticos; (i) 1,90-1,88 Ga, localizado na parte mais ocidental do Bloco Rio Apa; (ii) 1,84-1,81 Ga, situado na parte central e (iii) 1,78- 1,72 Ga localizado na parte oriental do Bloco

Rio Apa. Este zoneamento geocronológico sugere a migração do orógeno devido à subducção progressiva de leste a oeste, com subducção da placa do leste sob a placa a oeste (Faleiros *et al*., 2016).

Diferentemente do que foi proposto anteriormente, Lacerda Filho *et al*., (2016) sugere que o Arco Magmático Amonguijá do Bloco Rio Apa é formado pelo Complexo Porto Murtinho (1,98-1,94 Ga) Suíte Amonguijá (Formação Serra Bocaina-1,87 Ga; Suíte Alumiador-1,84), Complexo Paso Bravo (1,84 Ga), Intrusões Morro do Triunfo e Serra da Alegria (1,79 Ga), Grupo Alto Tererê (1,70 Ga), Complexo Rio Apa (1,79-1,72 Ga), Grupo Amolar e Suíte Rio Perdido (1,58 Ga).

Recentemente foi proposto que o Bloco Rio Apa é composto por três arcos magmáticos (Teixeira *et al*., 2020, Ribeiro *et al*., 2020?), sendo eles: os (i) arcos magmáticos Porto Murtinho (2,07–1,94 Ga) e (ii) Amonguijá (1,87–1,82 Ga), que geraram o Terreno Ocidental, e é representado por componentes crustais, enquanto o (iii) Arco Caracol (1,80-1,74 Ga), juntamente com o Grupo Alto Tererê, Suíte Baía das Garças (1,77 Ga) e unidade Paso Bravo (1,77-1,75 Ga) constituem o Terreno Oriental com características isotópicas que indicam derivação de uma fonte magmática predominantemente juvenil com contaminação crustal (Teixeira *et al*., 2020). Eles são descritos em continuação.

(i) Arco Porto Murtinho (2,07 a 1,94 Ga)

O Arco magmático Porto Murtinho é composto pelo Complexo Porto Murtinho, que por sua vez representa o embasamento Riaciano/Orosiriano do Terreno Ocidental do Bloco Rio Apa. Tambem é composto por um conjunto granito-gnáissico, constituídos por ortognaisses bandados com enclaves de anfibolitos e migmatitos (Cordani *et al*., 2010), paragnaisses (Pavan *et al*., 2014), e de granitos e gabros. Os complexos o Gnaisse Morraria (Cordani *et al*., 2010), Gnaisse Córrego Jiboia (Faleiros *et al*., 2014), Granito Morro da Lenha (Faleiros *et al*., 2014), granitos Piatã e Chatelodo (1902±11 Ma; Faleiros *et al*., 2016) e Gabro Matão (1969±5 Ma; Faleiros *et al*., 2016) também fazem parte do mesmo. Um estudo de proveniência realizado por Faleiros *et al*. (2016) no Complexo Porto Murtinho revelou duas populações de zircão detríticos (2220-1960 e 2980-2520 Ma), além de alguns grãos de zircão retrabalhados de crosta Paleoarqueana. Esses dados

associados com a idade encontrada U-Pb (SHRIMP) de 2069±4 Ma (Teixeira *et al*., 2020) em um zircão de um migmatito do Complexo Porto Murtinho, sugerem que a formação do Complexo de Porto Murtinho pode ter envolvido protólitos sedimentares distintos e que o primeiro evento magmático no Bloco Rio Apa durou cerca de 100 Ma (Teixeira *et al*., 2020).

As assinaturas negativas ε_{Nd} e afinidade cálcio-alcalina das rochas do Terreno Ocidental possibilitaram Teixeira *et al*. (2020) a sugerirem uma dinâmica colisional semelhante a configuração de um arco. O conjunto dos dados isotópicos disponíveis, permitiram também a Teixeira *et al*. (2020), interpretar que grande parte do Terreno Ocidental foi construído sobre (ou foi adjacente a uma crosta continental antiga de entre 2.07 e 1,95 Ga, gerado a partir de um magmatismo juvenil, e por eventos magmáticos tardios com contribuição de material crustal reciclado.

(ii) Arco Amonguijá (1,87-1,82 Ga): Suíte Intrusiva Alumiador

O arco magmático Amonguijá compreende o segundo evento magmático granítico (1880-1830 Ma) que afetou a área do Bloco Rio Apa. É caracterizado por um magmatismo cálcio-alcalino de médio a alto K, peraluminoso, e reúne os granitos cálcio-alcalinos intrusivos da Suíte Alumiador e as rochas vulcânicas e piroclásticas félsicas da Formação Serra da Bocaina (Lacerda Filho *et al*., 2006; Godoy *et al*., 2010; Brittes *et al*., 2013; Faleiros *et al*., 2016). Além da afinidade geoquímica, as relações entre riolitos e andesitos sugerem magmatismo de arco relacionado à zona de subducção (Faleiros *et al*., 2016). Diques básicos, como por exemplo, aquele encontrado no Córrego Cabrito (1,82 Ga), que intrude rochas gnáissicas do embasamento, parecem pertencer ao mesmo evento (Lacerda Filho, 2015).

As rochas plutônicas da Suíte Intrusiva Alumiador, assim como as rochas pertencentes à Suíte Vulcânica Serra da Bocaina, encontram-se agrupadas na Supersuíte Amonguijá, baseado na cogeneticidade das rochas vulcânicas com as plutônicas (Godoi e Martins, 1999; Lacerda Filho *et al*., 2006). A Suíte Intrusiva Alumiador abrange biotita granitos, de composição entre granodiorito a sienogranito, cálcio-alcalinas, da série de alto potássio a shoshonítica, de caráter metaluminoso a peraluminoso, originadas em ambiente sin-colisional a pós-colisional. (Correia Filho *et al*., 1981, Godoy *et al*., 2007, Manzano *et al*., 2012). No entanto, alguns dos tipos de

rochas graníticas da Suíte Intrusiva Alumiador possuem assinaturas alcalinas típico de configurações pós-orogênicas ou anorogênicas (Manzano *et al*., 2012).

A Suíte Intrusiva Alumiador (Fig. 2.2 B) aflora nas serras do Alumiador, São Miguel, São Paulo (Mato Grosso do Sul, Brasil) e Paraguai, e em alguns locais isolados da borda ocidental da serra da Bodoquena e na região de Corumbá.

O Batólito Alumiador, é o principal integrante da Suíte Intrusiva Alumiador. Tem composição sieno a monzogranítica, ocorre como uma grande intrusão alongada com lineamentos NNE observados ao longo da Serra do Alumiador que desviam para NW ao longo da Serra da Alegria (Lacerda Filho *et al*., 2006, Cordani *et al*., 2010). Outros corpos menores também fazem parte desta suíte; como os granitos São Francisco (1874±5 Ma; Souza *et al*., 2016), Taquaral (1861±5 Ma; Redes *et al*., 2015), Coimbra (1859±4 Ma; Santos *et al*., 2019), Aquidabã (1811±7; Nogueira, 2015), Piatã (1892±31 Ma; Lacerda Filho, 2015) e Córrego Cervo (1841±7 Ma; Pavan *et al*., 2014). De acordo com Faleiros *et al*., (2015), a Suíte Intrusiva Alumiador situa-se no Terreno Ocidental, que é composto tanto pelas rochas gnáissicas e graníticas do Complexo Porto Murtinho, como pelas intrusões graníticas do Granito Chatelodo e da Suíte Intrusiva Alumiador, que são recobertos por rochas vulcânicas e piroclásticas da Formação Serra da Bocaina.

(iii) Arco Caracol (1800-1740 Ma): Suíte Caracol

A Suíte Caracol, abrange rochas granito-gnáissicas de composição cálcio-alcalina e de alto-K (1776±13 – 1748±19 Ma; Plens, 2018), localiza-se no Terreno Oriental do Bloco Rio Apa (Plens, 2018). Lacerda Filho *et al*. (2006) trata os gnaisses da Suíte Caracol como integrante do Complexo Rio Apa, e o relaciona com a evolução do Arco Magmático Rio Apa, que se desenvolveu durante o Orosiriano. No entanto, Teixeira *et al*. (2020) incluem além da Suíte Caracol, a Suíte Baía das Garças e as rochas granitoides da Província Paso Bravo na evolução do Arco Caracol, pois mostram idades U-Pb em zircão, semelhantes com aquelas do Gnaisse Caracol. Novos dados isotópicos sugerem que o Arco Caracol esteve ativo entre 1780 e 1740 Ma, período que foi formado o Terreno Oriental (Cordani *et al*., 2010). Neste contexto, Teixeira *et al*. (2020) consideram que a sequência vulcâno-sedimentar do Grupo Alto Tererê, foi formada em uma configuração de back-arc, como parte da evolução do Arco Caracol.

Compartimentalização geotectônica o Bloco Rio Apa

Os autores Lacerda Filho *et al*. (2006), Cordani *et al*. (2010), Faleiros *et al*. (2016) e Lacerda Filho (2015) propuseram alguns modelos, que serão explicados a seguir.

O Bloco Rio Apa foi dividido por Cordani *et al*. (2010) em dois diferentes terrenos tectônicos, denominados de ocidental e oriental, baseados em idades modelo Sm-Nd, idades de cristalização e de metamorfismo. De acordo com Cordani *et al*. (2010), esses terrenos possuem histórias evolutivas distintas, limitados por zonas de sutura aproximadamente N-S. Estes autores também sugeriram que estes terrenos foram justapostos em ~1690 Ma, e posteriormente foram afetados por um evento metamórfico de baixo grau (300º-400º C) em 1300 Ma.

Além dos terrenos ocidental e oriental, Faleiros *et al*. (2016) individualizaram o terreno sudeste (Fig.2.2). Os terrenos são limitados por zonas de cisalhamento e sua evolução magmática se deu por meio de eventos acrescionários distintos, refletindo regime tectônico extremamente móvel (Faleiros *et al*., 2016).

O Terreno Ocidental (Cordani *et al.,* 2010) é formado por rochas do Complexo Porto Murtinho (constituído pelo Gnaisse Córrego Jiboia e Granito Morro da Lenha; Faleiros *et al*., 2016), Granito Chatelodo (1902±12; Faleiros *et al*., 2016), Supersuíte Amoguijá e Formação Naitaca (Faleiros *et al*., 2013). O terreno oriental é constituído pelos gnaisses Morraria e Caracol e pela Suíte Baia das Garças, formada pelo Granito Sanga Bonita (1721±25 Ma; Remédio *et al*., 2013) e ortognaisses Santa Clarinha e Espinilho (Remédio *et al*., 2013; 1716±11Ma e 1735±12 Ma, respectivamente), além do Granito Cerro Porã (1749±45 Ma; Plens *et al*., 2013), até então descrito como pertencente ao terreno ocidental. No terreno sudeste são descritos os gnaisses João Candido e Rio Areia (1820±18 Ma; Faleiros *et al*., 2016) e o Granito Scardine (1791±19 Ma; Faleiros *et al*., 2016).

Lacerda Filho (2015), posteriormente modifica sua proposta inicial e compartimenta o Bloco Rio Apa em três segmentos (ocidental, central e oriental). Os autores sugerem cinco principais eventos magmáticos graníticos (2.07-1.71 Ga) que constituem uma evolução progressiva e representam vários estágios de acresção do Arco Magmático de Amoguijá.

O Terreno Oriental (Cordani *et al.*, 2010) é constituído pela associação de rochas já citada nas duas compartimentações acima, com algumas modificações: ao Complexo Porto Murtinho são adicionadas as unidades Gnaisse Piatã, Paragnaisse Tonalítico, Granito Chateolo (1902±11 Ma; Faleiros *et al*., 2016) e Gabro Matão (1969±5 Ma; Faleiros *et al*., 2016). Os granitos Córrego Servo e Aquidabã também são acrescentados.

Para o Terreno Central (Lacerda Filho, 2015) é mantida a denominação de Complexo Rio Apa, caracterizado como uma associação de granitos e gnaisses representados pelas unidades recentemente propostas por Cordani *et al*. (2010), Remédio *et al.* (2013), e Faleiros *et al*. (2016), além de terminologias inéditas como Granito Tamanduá (1736±19 Ma; Lacerda Filho *et al*., 2016) e Granito Santo Antônio (1794±14 Ma; Lacerda Filho, 2015), e incluem também a Província Passo Bravo (Wiens, 1986; 1559±55 Ma; Cordani *et al*., 2010) em território paraguaio. O Complexo Paraíso é constituído pelos gnaisses e granitos descritos no terreno sudeste de Faleiros *et al*. (2016).

Recentemente, Teixeira *et al*. (2020) elaboraram um trabalho de revisão sobre o Bloco Rio Apa, no qual foi renomeado de Terreno Rio Apa (Fig. 2.2), e foi subdividido em Terreno Ocidental, Terreno Oriental e Terreno Sudeste. Conforme proposto por Teixeira *et al*. (2020), o Terreno Ocidental (Teixeira *et al*., 2020) é constituído pelo Complexo Porto Murtinho (2074 – 1941 Ma; Lacerda Filho, 2015; Cordani *et al*., 2010; Faleiros *et al*., 2016), Cinturão Continental Amonguijá (1841 – 1839 Ma) e Sequências Supracrustais (1710 – 1800 Ma; Cabrera, 2015; Lacerda Filho, 2015). O Terreno Oriental (Teixeira *et al*., 2020) compreende distintas rochas gnáissicas, migmatíticas e granitoides, que compõem o Gnaisse Morraria e Suíte Caracol (1783 – 1721 Ma; Cordani *et al*., 2010; Plens, 2018), bem como a Suíte granítica Baía das Garças (1719 – 1754 Ma; Cordani *et al*., 2010), que intrudem no Gnaisse Morraria e na Província de Paso Bravo (1935±15 Ma; Cordani *et al*., 2010) no Paraguai (Wiens, 1986). Todo o terreno é parcialmente coberto pelas rochas metavulcâno-sedimentares altamente deformadas e metamorfizadas do Grupo Alto Tererê (Teixeira *et al*., 2020). O Terreno Sudeste (Teixeira *et al*., 2020) foi sugerido como um terceiro compartimento tectônico do Bloco Rio Apa (Faleiros *et al*. 2016), limitado pela

zona de cisalhamento dextral da Serra do Perdido, sendo composto por gnaisses de 1791 a 1820 Ma (Faleiros *et al*., 2016), que se assemelham aos gnaisses do Terreno Oriental.

Na região de Corumbá-MS (Fig. 2.3) o cenário geológico é representado pelo o Granito Taquaral, Granito Coimbra e Gnaisse Santana, essas unidades compõem o embasamento granítico-gnáissico das coberturas neoproterozoicas dessa região (Araújo *et al*., 1982, Godoi *et al*., 2001 e Redes *et al*., 2013). Esse embasamento granítico-gnáissico faz contato de natureza tectônica, e em parte por discordância, com as formações Tamengo e Bocaina (Grupo Corumbá) e com as formações Urucum e Santa Cruz (Grupo Jacadigo), encontrando-se parcialmente recoberto pela Formação Pantanal do Quaternário (Redes *et al*., 2015). Baseados em dados geocronológicos, isotópicos, petrológicos e estruturais, o embasamento granítico da região de Corumbá foi considerado como um prolongamento do Bloco Rio Apa, sendo integrante da Suíte Intrusiva Alumiador (Redes *et al*., 2015 e Santos *et al*., 2019, Teixeira *et al*., 2020).

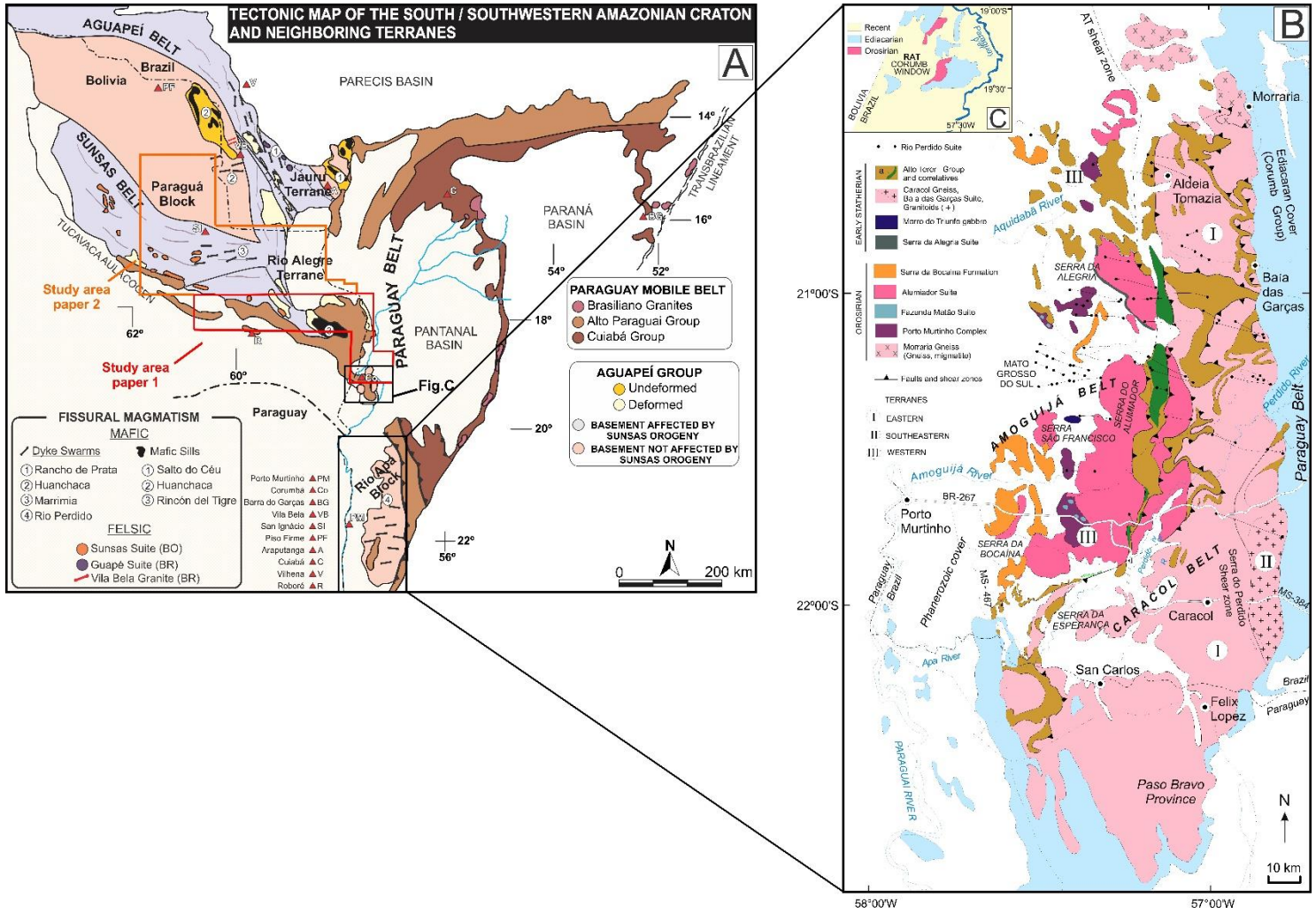

Figura 2.2. (A) Mapa tectônico do Sudoeste/sul do Cráton Amazônico e áreas vizinhas, principalmente, Bloco Rio Apa e Bloco Paraguá (modificado de Ruiz *et al*., 2010). No mesmo são destacadas as áreas de estudo. (B) Mapa geológico do Bloco Rio Apa (extraído de Teixeira *et al*., 2020).

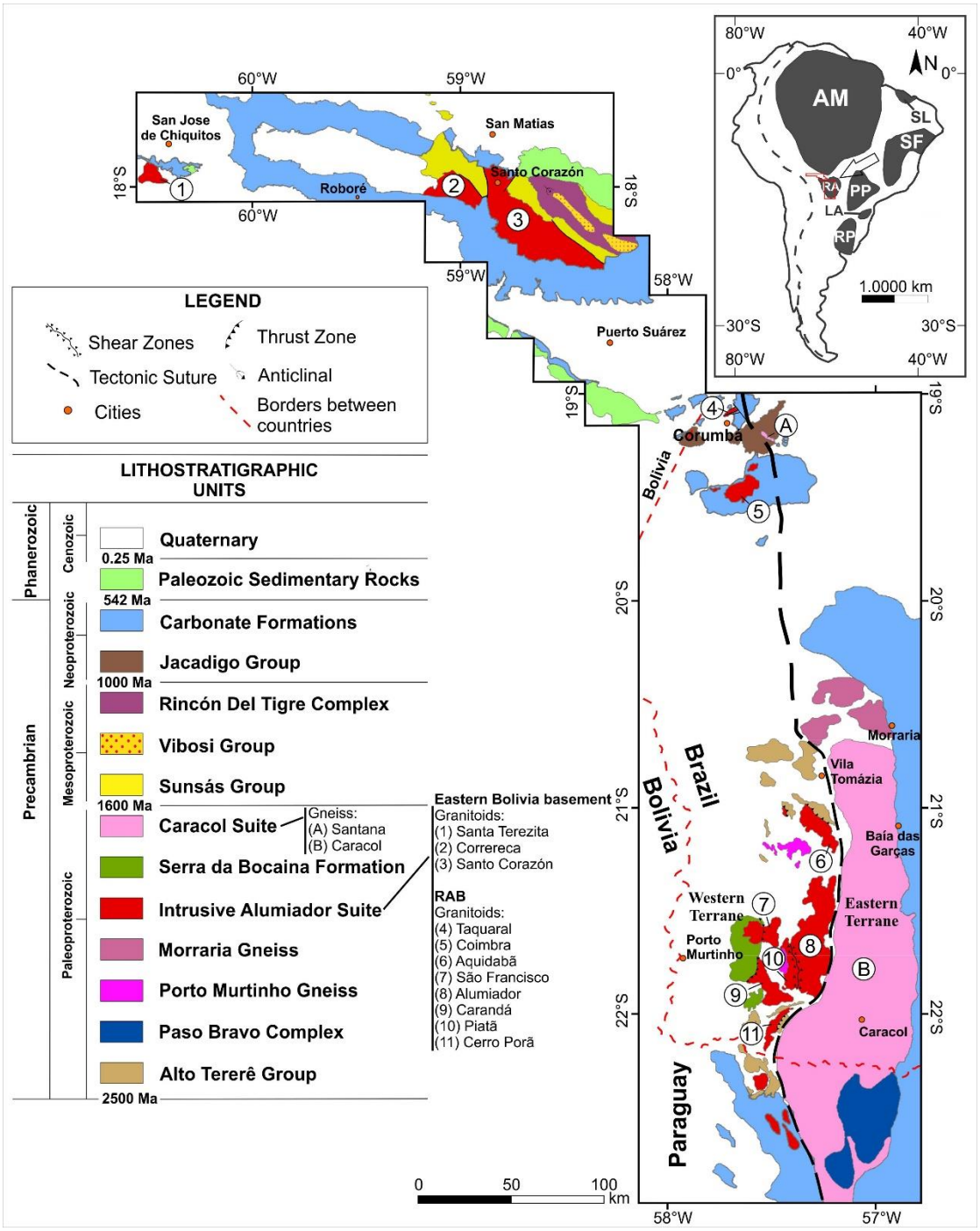

Figura 2.3. Mapa geológico simplificado do Bloco Rio Apa (modificado após Matos, 2010; Cordani *et al*., 2010; Redes *et al*., 2015; Santos *et al*., 2019) e a relação com os granitos do embasamento do oriente boliviano e o Gnaisse Santana, todos investigados neste trabalho. AM: Cráton Amazônico, SL: Cráton São Luiz, SF: Cráton São Francisco, PP: Cráton Paranapanema, RA: Bloco Rio Apa, LA: Cráton Luís Alves, RP: Cráton Rio de La Plata.

2.3. Bloco Paraguá

O Bloco Paraguá (1,74-1,32 Ga) faz parte da Província Rondoniana-San Ignácio (Fig. 2.4), se estende por grande parte do território boliviano e abrange o SW do estado do Mato Grosso no Brasil. O mesmo hospeda as unidades pré-San Ignácio (>1640 Ma): Complexo Lomas Maneches, Complexo Chiquitania e Grupo San Ignácio, que são intrudidas pelo Complexo Granitoide Pensamiento (1,37-1,34 Ga), que foi desenvolvido em um arco magmático tipo andino (Bettencourt *et al*. 2010). O Grupo Sunsas recobre por inconformidade os complexos Lomas Maneches e Chiquitania e o Grupo San Ignácio e foi deformado junto com o embasamento durante a Orogenia Sunsas (~1000 Ma). O Grupo Tucavaca foi depositado após a orogenia Sunsas, e corresponde a uma cobertura não-deformada do Neoproterozoico (Boger *et al*., 2005). Berrangué e Litherland (1982), já indicavam que o Paleoproterozoico em território boliviano foi afetado por eventos que resultaram na cratonização da área, enquanto o Neoproterozoico é composto pelos depósitos de transgressão do ciclo Orogênico Brasiliano do Cinturão Tucavaca.

Originalmente a região a sul da Zona de Cisalhamento San Diablo foi denominada de Bloco Cristal por Klinck e Litherland (1982), e posteriormente foi denominada por Saes *et al*. (1992) de Terreno San Pablo e descrita como um terreno alóctone de história geologicamente distinta. O termo Cráton Paraguá foi introduzido por Litherland *et al*. (1986) no escudo pré-cambriano da Bolívia oriental para denotar uma região tectonicamente estável durante a deformação Meso-Neoproterozoica relacionadas com as Faixas Sunsas e Aguapeí.

Com base em idades Rb-Sr, a crosta pré-San Ignácio (Complexo Chiquitania e Complexo Lomas Maneches) foi considerada com mais de 1961 Ma por Litherland *et al*. (1986). Existe até hoje um forte impasse sobre a posição estratigráfica entre essas unidades. U-Pb (via SHRIMP) em zircão nos granitos com e sem ortopiroxênio do Complexo Lomas Maneches e de um biotita-gnaisse do Complexo Chiquitania, permitiram Boger *et al*. (2005) obter idades U-Pb em zircão de 1689±5, 1663±4 Ma e 1765±12 Ma. As bordas de zircão magmático e metamórfico teriam registrado a orogenia San Ignácio no período 1340 – 1320 Ma. Desta forma, Boger *et al*. (2005) estabelecem que o Complexo Chiquitania e o Grupo San Ignácio são derivados de fontes de 1765 Ma e que não foram depositados antes de 1690 Ma. Boger *et al*. (2005) consideram a colocação

da Suíte Lomas Maneches entre 1690 – 1660 Ma, e que esta unidade juntamente com o Complexo Chiquitania é sincrônica, e mais velhas que o Grupo San Ignácio.

Santos *et al*. (2008) identificaram idade $^{207}Pb/^{206}Pb$ de 1818±13 Ma para zircão magmático do Complexo Lomas Maneches. Santos *et al*. (2008), também encontraram zircão herdados formados entre 1772 e 1729 Ma nos ortognaisses Rio Fortuna e Santa Rita do Complexo Chiquitania.

Matos (2010) somente reforça que o Complexo Lomas Maneches, Complexo Gnáissico Chiquitania e o Grupo de Xisto San Ignácio constituem o embasamento polimetamórfico paleoproterozoico formado durante o intervalo de tempo de 1,82-1,69 Ga.

Entretanto estudos recentes, como o de Nedel *et al*. (2017) sugerem que a Zona de Cisalhamento San Diablo (Fig. 2.4) não representa uma zona de sutura entre o Bloco Paraguá e o Terreno San Pablo, e que o Bloco Paraguá se prolonga para o sul dessa zona de cisalhamento. O Bloco Paraguá tem sido descrito como um fragmento crustal alóctone, acrescido à margem do proto-Cráton Amazônico durante o Mesoproterozoico ou Neoproterozoico (Berrangué e Litherland 1982, Boger *et al*. 2005, Ruiz, 2009, Bettencourt *et al*. 2010). Segundo Boger *et al*. (2005) sua aglutinação teria ocorrido durante a Orogenia Sunsas (1,0 a 0,9 Ga), enquanto Ruiz (2005, 2009) sugeriu que a Orogenia San Ignácio (1,37 a 1,3 Ga) seria a responsável pela colisão do Bloco Paraguá (BP) ao Cráton Amazônico (CA).

Bettencourt *et al*. (2010) com base nos processos de deformação, metamorfismo de alto grau e fusão parcial, que afetaram principalmente o Complexo Chiquitania e o Complexo Lomas Maneches, também postula que a colisão entre o Bloco Paraguá e o Cráton Amazónico teria ocorrido durante a orogenia San Ignácio (1,34-1,32 Ga).

Boger *et al*. (2005) defende que Orogenia Sunsas resultou no crescimento do Cráton Amazônico pelo acréscimo de dois blocos litosféricos alóctones – o Cráton Paragua e o embasamento dos blocos Arequipa-Antofalla (Litherland *et al*., 1989; Loewy *et al*., 2004; Tohver *et al*., 2004), e que ambas as regiões preservam uma história geológica alternativa, e uma margem onde se acumulam, com *trends* estruturais com ângulos para NW, que se alinham a margem paleocontinental do Cráton Amazônico.

Ruiz (2005, 2009), baseado na ausência de registros deformacionais e metamórficos relacionados ao Evento Sunsas no embasamento pré-cambriano do oriente boliviano, sugere que a aglutinação BP+CA ocorreu durante a Orogenia San Ignácio. Pelo contrário este mesmo embasamento registra os efeitos da Orogenia San Ignácio, assim como as unidades localizadas na margem do SW do Cráton Amazônico.

Para o Bloco Paraguá no Brasil, Faria (2015) opta pelo termo Complexo Serra do Baú para denominar os ortognaisses correlatos ao Complexo Chiquitania, e Complexo Metamórfico Ricardo Franco para os granulitos de origem paraderivada, correspondentes ao Complexo Lomas Maneches. Dessa forma, o ortognaisse Rio Fortuna estudado neste trabalho, estaria inserido no Complexo Serra do Baú, uma vez que este gnaisse aflora também em território brasileiro e o Complexo Serra do Baú corresponde ao Complexo Chiquitania.

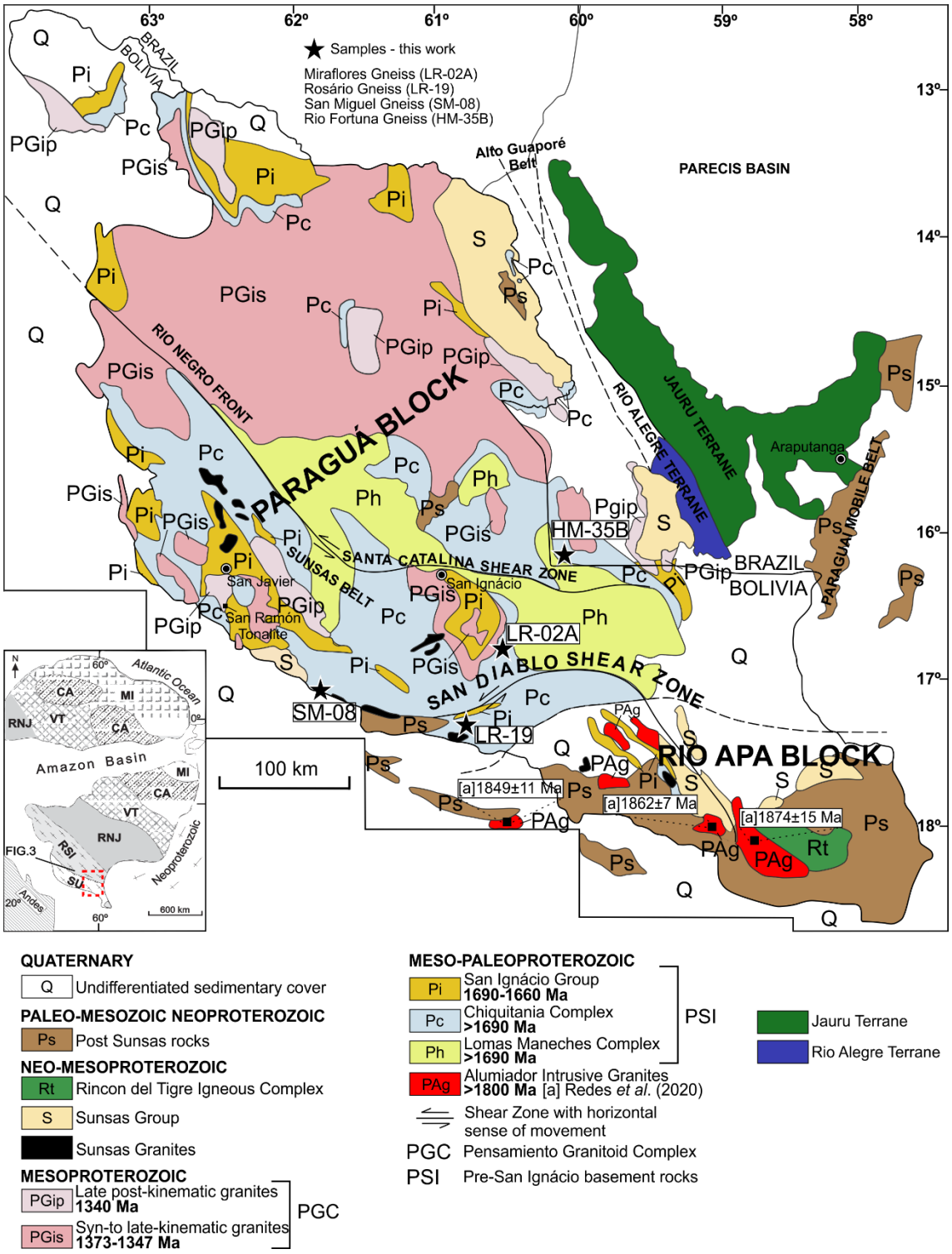

Figura 2.4. (A) Principais unidades geológicas e elementos tectônicos do Bloco Paraguá. Parte noroeste do Bloco Rio Apa no leste da Bolívia (modificado de Litherland *et al*., 1986, Ruiz, 2005, Matos *et al.*, 2009). Figura inserida: Cráton amazônico com os limites inferidos entre as províncias proterozoicas de Cordani e Teixeira (2007). Siglas: Amazônia Central – CA (> 2,6 Ga); Maroni-Itacaiúnas – MI (2,25 – 2,05 Ga); Ventuari-Tapajós – VT (1,98 – 1,81 Ga); Rio Negro-Juruena – RNJ (1,78 – 1,55 Ga); Rondoniana-San Ignácio – RSI (1,55 – 1,30 Ga) e Sunsas – SU (1,25 – 0,97 Ga).

Complexo Lomas Maneches

Das unidades que compreendem o Bloco Paraguá, o Complexo Lomas Maneches é considerado por Berrangué e Litherland (1982), como mais antigo e estruturalmente mais profundo, composto por granulitos. No entanto, Boger *et al*. (2005) interpretam que esse complexo foi formado sincronicamente com o Complexo Chiquitania. A unidade Lomas Maneches apresenta enderbitos, charnoquitos com predominância de feldspato potássico, granulitos com hyperstênio, granulitos calcissilicáticos com cordierita e gnaisses quartzo-feldspáticos, com bandas concordantes de até 1 m de espessura de granulitos e rochas graníticas metaluminosas a peraluminosas (Berrangué e Litherland 1982; Litherland *et al*., 1986; Vargas-Matos, 2006). Elas estão expostas nos núcleos de dobras antiformais regionais (Berrangué e Litherland, 1982; Litherland e Bloomfield, 1981); (Fig. 2.4).

Os protólitos do Complexo Lomas Maneches foram gerados em ambiente pré-colisional a tardi-orogênico, representado preferencialmente por rochas graníticas. Eles ocorrem intercaladas com rochas metassedimentares calcissilicáticas ou psamíticas (Berrrangé e Litherland, 1982).

Complexo Chiquitania

Litherland *et al*. (1986) dividiram os gnaisses do Complexo Chiquitania em dois tipos, A e B. Os gnaisses tipo A são compostos por biotita paragnaisses a gnaisses graníticos, que possuem maior grau metamórfico, com estruturas migmatíticas desenvolvidas, e nas zonas de contato com o Complexo Lomas Maneches apresenta bandas transicionais que contém hyperstênio e cordierita metamórfica. Os gnaisses tipo B são principalmente paragnaisses derivados do Grupo San Ignácio (<1690 Ma). A distinção entre os dois tipos também foi feita com base nas diferentes proporções de bandas de quartzitos, rochas calcissilicáticas e anfibolitos.

Litherland *et al*. (1986) descreveu os gnaisses Las Madres, La Bella, San Juan, Ascensión, Paquiosal, San Diabo, Pataju, Rio Blanco e Santa Rita, que afloram em território boliviano, como pertencentes ao Complexo Chiquitania (Fig. 2.5). Posteriormente Santos *et al*. (2008), verificou que o Gnaisse Santa Rita era um ortognaisse de 1319±6 Ma com zircão herdado de 1746 Ma, indicando que o Gnaisse de Santa Rita é mais jovem que o Complexo Chiquitania.

Em território boliviano também foram identificados o Gnaisse Refúgio e o Gnaisse Rio Fortuna por Santos *et al*. (2008). O Gnaisse Refúgio, que ocorre cerca de 100 km a norte do afloramento o Gnaisse San Miguel, estudado aqui, é descrito como ortognaisse leucocrático de composição sieno a monzogranítica, com idade de cristalização de 1641±4 Ma, ε_{Nd} positivo de +4,06 e T_{DM} Nd de 1, 66 Ga (Santos *et al*., 2008). Enquanto o Gnaisse Rio Fortuna, que faz parte deste trabalho, é um ortognaisse cinza escuro, de composição granodiorítica a tonalítica, com duas idades principais: 1336±3 Ma que corresponde a zircão magmático e bordas metamórficas, e o intervalo 1772-1734 Ma, que representa núcleos de zircão herdados (Santos *et al*., 2008).

Nedel *et al.* (2017) caracterizou os ortognaisses Miraflores e Rosário do Complexo Chiquitania, localizados no oriente Boliviano. Para o Gnaisse Rosário obteve uma idade de cristalização em 1685±5 Ma (Fig. 2.5) e provável idade de metamorfismo em 1111±10 Ma. Ambos estudados neste trabalho.

No Brasil, mais precisamente no Mato Grosso, na região da Serra de Santa Bárbara, na fronteira Brasil-Bolívia, os gnaisses correlatos ao Complexo Chiquitania, correspondem ao Complexo Metamórfico Serra do Baú (Ruiz, 2005). Este complexo é composto pelos gnaisses ortoderivados (Fig.1.6): Rio Fortuna, Shangri-lá, Matão, Triunfo, Turvo e Retiro (Faria, 2015, Nascimento, 2015). Para o Gnaisse Turvo foi encontrada a idade de 1651±4 Ma, sendo interpretada como idade de colocação do protólito ígneo (Figueiredo *et al*., 2013). Para o Gnaisse Rio Fortuna a idade de 1711±13 Ma, foi descrita como idade de cristalização do protólito ígneo de composição tonalítica (Faria *et al*., 2014). O Gnaisse Triunfo foi descrito como ortognaisses de composição monzo a granodiorítica, e a idade U-Pb em zircão de 1722±68 Ma, foi interpretada como correspondente à idade de cristalização do protólito ígneo (Faria, 2015).

Relação estratigráfica entre o Complexo Lomas Manchis e o Complexo Chiquitania

Boger *et al*. (2005), sugerem que os protólitos graníticos do Complexo Lomas Maneches, intrudem no Complexo Chiquitania, e que invariavelmente contém todas as estruturas preservadas em suas rochas hospedeiras e comumente mostram evidências de fusão parcial subsequente à sua intrusão.

No extremo norte do Bloco Paraguá o Complexo Lomas Maneches ocorre como megaxenólitos dentro do Complexo Granitoide Pensamiento. Na região de San Ignácio na Bolívia, os granulitos deste complexo encontram-se tectonicamente sobrepostos por xistos do Grupo San Ignácio (Berrangué e Litherland, 1982). Os granulitos ocorrem de maneira transicional com o Complexo Gnáissico Chiquitania, principalmente entre a região de San Ignácio e a Zona de Cisalhamento San Diablo (Berrangué e Litherland 1982; Litherland *et al*., 1986).

Grupo San Ignácio

O Grupo San Ignácio encontra-se afetado por um metamorfismo de menor grau. Caracteriza-se por apresentar um grau metamórfico médio à baixo, compreendendo quartzitos, metapsamitos feldspáticos, xistos de duas micas e filitos de origem vulcânica (Litherland *et al*., 1986; Fig. 2.5)

A complexidade desta faixa deve-se a superimposição das estruturas do evento orogênico Sunsas sobre as do evento San Ignácio, fator que localmente favoreceu a formação de corpos mineralizados com ouro, como no caso da mina de Puquio Norte (Adamek *et al*.,1996).

No sul do Bloco Paraguá este cinturão de xistos mostra um contato transicional com o Complexo de gnaisses do Complexo Chiquitania e no extremo norte este cinturão se apresenta como megaxenolitos no Complexo Granitoide Pensamiento (Berrangé e Litherland 1982).

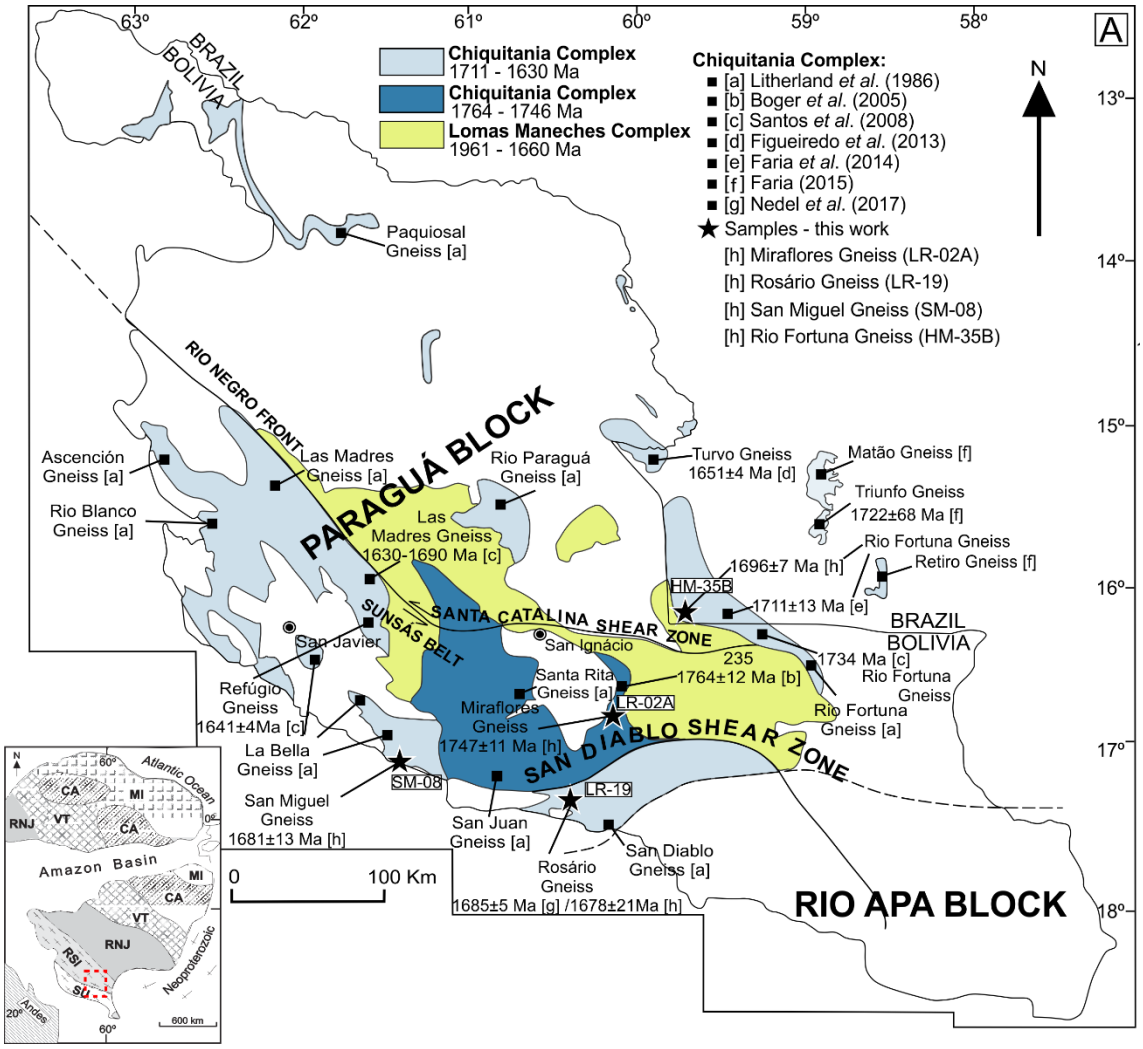

Figura 2.5. Principais divisões e nomes dos gnaisses do Complexo Chiquitania (Bloco Paraguá). Modificado de Litherland *et al*. (1986) e Faria (2015).

CAPÍTULO 3 – MÉTODOS ANALÍTICOS

Para a elaboração desse trabalho, foram realizadas idas a campo para a coleta de dados e amostras para análises laboratoriais, em que foi adotado um cronograma de quatro etapas principais: etapa preliminar, etapa de aquisição de dados (em campo e em laboratório), etapa de tratamento e sistematização de dados e etapa de conclusão e divulgação dos resultados.

3.1. Etapa Preliminar

Nesta etapa exerceu-se o levantamento bibliográfico disponível referente a geologia do embasamento boliviano, e suas relações com os terrenos e blocos vizinhos, também foi realizada a fotointerpretação de imagens Geocover e satélite da parte sudoeste da América do Sul.

3.2. Etapa de Aquisição de Dados

Esta etapa corresponde às atividades desenvolvidas para a obtenção de dados em campo através do mapeamento geológico, e em laboratório por meio de análises petrográficas, geoquímicas, geocronológicas e isotópicas

3.2.1. Trabalhos de Campo

Os trabalhos de campo foram realizados em três fases. A primeira se deu durante os dias 22 e 30 de julho de 2015, a segunda entre os dias 18 e 29 de junho de 2016 e a terceira do dia 11 a 22 de maio de 2018. Em campo foi realizada a descrição afloramentos, o reconhecimento das unidades geológicas, a coleta de dados estruturais e de amostras para os estudos geoquímicos, petrológicos, geocronológicos e isotópicos. Foram coletadas quarenta amostras no total, das quais sete correspondem aos granitos da Suíte Intrusiva Alumiador, doze ao Gnaisse Santana, e vinte e uma pertencem aos gnaisses do Complexo Chiquitania. Todas foram identificadas e orientadas para estudos laboratoriais (macroscópicos e microscópicos).

3.2.2. Trabalhos de Laboratório e Análises Petrográficas

As amostras coletadas nas etapas de campo foram descritas macroscopicamente considerando os aspectos texturais, estruturais, deformacionais e composicionais. Seguidamente foram confeccionadas cerca de 60 seções delgadas no Laboratório de Laminação do Instituto de Geociências da UnB (IG-UnB). A atividade de descrição das lâminas foi desenvolvida em microscópio óptico binocular da marca Olympus, modelo BX50, no Laboratório de Microscopia, no IG-UnB, tendo como objetivos a caracterização petrográfica dos gnaisses e granitos (composição mineralógica e feições texturais e aspectos deformacionais). A contagem modal em escala microscópica foi realizada em todas as seções delgadas com auxílio de um *charriot*. Os

critérios adotados quanto à granulação (em mm) foram os sugeridos pela IUGS: muito fina (Ø≤0,1); fina (0,1<Ø≤1,0); média (1,0<Ø≤5,0) e grossa (5,0<Ø≤20,0).

Análises Litogeoquímicas

Para as análises geoquímicas foram estudados os resultados um total de 25 amostras mais representativas dos granitos da Suíte Intrusiva Alumiador, do Gnaisse Santana e dos gnaisses do Complexo Chiquitania, considerando sua distribuição na área, diversidade mineralógica e granulação. Para tanto, foram analisadas sete amostras da Suíte Intrusiva Alumiador, onze amostras do Gnaisse Santana e sete amostras do Complexo Chiquitania.

Essas amostras foram lavadas para a remoção de impurezas e cortadas com serra diamantada para a retirada das camadas alteradas a fim de evitar a contaminação química. Posteriormente, elas foram britadas e pulverizadas em moinho de mandíbulas do Laboratório de preparação de amostras do IG-UnB. Após quarteamento, separou-se cerca de 100 gramas de cada amostra para serem enviadas ao Museum für Naturkunde, localizado em Berlim (Alemanha), onde foram analisados os elementos maiores (SiO_2, TiO_2, $Al2O_3$, FeOt, MnO, MgO, CaO, Na_2O, K_2O e P_2O5) por espectroscopia de fluorescência de raios-X (XRF) em um espectrômetro Bruker ASX S8 TIGER, no qual os métodos adotados e a quantificação dos resultados foram descritos em detalhes por Schmitt *et al*. (2004). A amostra de pó para análise de elementos menores, incluindo elementos de terras raras, foram enviados para ALS Brasil Ltda para análise na ALS em Lima, Peru. Cerca de 0,1 g das amostras foram diluídas em um fluxo de metaborato/tetraborato de lítio. O pó depois foi dissolvido em 100 mL de ácido nítrico a 4% / ácido clorídrico a 2%. As análises dos elementos menores e traços, foram realizadas por Espectrometria de Massa de Plasma (ICP-MS). A descrição completa dos métodos analíticos está disponível na página da ALS Chemex: (www.alsglobal.com).

O tratamento dos dados de litogeoquímica foram realizados com o auxílio dos softwares GCDkit 3.0., IGPet e Excel. A interpretação dos resultados das análises buscou a caracterização geoquímica, a natureza do magmatismo e sua ambiência tectônica.

Análises Isótopicas – U-Pb e Lu-Hf

As análises isotópicas U-Pb e Lu-Hf em zircão foram realizadas por LA-ICP-MS no Laboratório de Geocronologia e Geoquímica Isotópica da Universidade de Brasília (UnB). Foi analisado para isótopos de U-Pb o zircão das amostras graníticas: ST-02, ST-03, CO-820, SC-824, e das amostras gnáissicas: CLR-04, LR-2ª, HM-35B, SM-08 e LR-19. As amostras CO-820 e CLR-04, assim como as amostras HM-35B, SM-08 e LR-19 também foram analisadas pelo método Lu-Hf, após serem analisadas pelo método U-Pb.

Inicialmente, cerca de 10 kg de cada amostra de rocha bruta foi triturada em britador de mandíbula, moída em moinho de discos no Laboratório de Geocronologia e Geoquímica Isotópica da UnB, em seguida foi peneirada em tamanhos diversos (100-400 μm). Após ser peneirada, a amostra foi submetida a um processo de separação dos minerais leves e pesados, por densidade em água, com o auxílio da bateia. Posteriormente foi utilizado também um imã para que os minerais magnéticos fossem removidos. O concentrado de minerais pesados foi depositado no separador magnético Frantz, onde acontece a dissociação da fração menos magnética. Do material resultante, foi separado manualmente, com o auxílio de lupa óptica binocular, 50 cristais de zircão, que foram colocados em um suporte de resina *epoxy (mount)*, que foi polido até aproximadamente metade da espessura. O *mount* foi conduzido ao Microscópio Eletrônico de Varredura (MEV) FEI QUANTA 450 (SEM), no Laboratório de Geocronologia e Geoquímica Isotópica da (UnB), para a geração de imagens de BSE e CL, a fim de caracterizar os cristais de zircão.

Finalmente os cristais de zircão foram analisados pelos métodos U-Pb e Lu-Hf, usando um espectrômetro de massa de plasma acoplado indutivamente multicoletor de alta resolução Thermo-Fisher Neptune (HR-MC-ICP-MS) acoplado a um sistema de ablação a laser Nd: YAG UP213 *New Wave* no Laboratório de Geocronologia da UnB. As análises de U-Pb nos cristais de zircão foram realizadas pelo método de agrupamento de amostra padrão (Albarède *et al*., 2004), usando o zircão padrão GJ-1 (Jackson *et al*., 2004), para quantificar o fracionamento de ICP-MS. As massas sintonizadas foram 238, 207, 206, 204 e 202. O tempo de integração foi de 1 segundo e o tempo de ablação foi de 40 segundos. O tamanho do *spot* realizado foi de 30 μm, e o laser foi

ajustado para operar em 10 Hz e 2-3 J/cm^2. O zircão 91500 (Wiedenbeck *et al*., 1995, 2004) também foi analisado como um padrão externo durante as sessões analíticas. Para as análises dos granitos, o zircão 91500 (Tabela 3.1) apresentou as idades de intercepto superior de 1064±13 Ma e 1070±67 Ma, durante as análises das amostras ST-03 e CO-820, respectivamente. Enquanto para as análises dos gnaisses, se obteve as seguintes idades de intercepto superior do zircão 91500; LR-2ª: 1024±230 Ma; HM-35B: 1055±54 Ma; SM-08: 1052±25 Ma; LR-19: 1066±53 Ma; CLR-04: 1056±57 Ma (Tabela 3.1).

As relações $^{206}Pb/^{207}Pb$ e $^{206}Pb/^{238}U$ foram corrigidas com o tempo. Os dados brutos foram processados off-line e reduzidos com o software interno Chronus do Laboratório de Geocronologia da UnB (ver Oliveira, 2015).

O ^{204}Pb comum foi monitorado usando as massas ^{202}Hg e (^{204}Hg + ^{204}Pb). As correções de Pb comum não foram feitas devido a sinais muito baixos de ^{204}Pb (<30cps) e altas taxas de ^{206}Pb / ^{204}Pb. Os erros relatados são propagados por adição quadrática [(2SD2 + 2SE2) ½] (SD = desvio padrão; SE = erro padrão) de reprodutibilidade externa e precisão dentro da execução. A reprodutibilidade externa é representada pelo desvio padrão obtido a partir de análises repetidas (~ 1,1% para $^{207}Pb/^{206}Pb$ e até ~ 2% para $^{206}Pb/^{238}U$) do padrão de zircão GJ-1 durante as sessões analíticas, e a precisão dentro da execução é o erro padrão calculado para cada análise. Diagramas Concordia (elipses de erro 2σ), gráficos de densidade de probabilidade e idades médias ponderadas foram calculados usando o software Isoplot-3/Ex (Ludwig, 2012).

Cristais de zircão previamente analisados para isótopos de U-Pb e com dados concordantes a ligeiramente discordantes (<10%) foram selecionados para análises de Lu-Hf. Os dados isotópicos de Lu-Hf foram coletados ao longo de 50 s de tempo de ablação e usando um *spot* de 50 μm. Durante as sessões analíticas, várias análises do zircão padrão GJ-1 foram realizadas, obtendo-se uma relação $^{176}Hf/^{177}Hf$ média de 0,282006±16 (2σ), em boa concordância com o valor de referência para o zircão padrão GJ (Morel *et al*., 2008). Os pontos de medição foram diligentemente posicionados na mesma área de crescimento, mas não no mesmo local analisado para dados de U-Pb. Os sinais dos isótopos livres de interferência ^{171}Yb, ^{173}Yb e ^{175}Lu foram monitorados durante a análise para corrigir as interferências isobáricas de ^{176}Yb e ^{176}Lu no

sinal ^{176}Hf. As contribuições de ^{176}Yb e ^{176}Lu foram calculadas usando a abundância isotópica de Lu e Hf (Chu *et al*., 2002). Medições contemporâneas de ^{171}Yb e ^{173}Yb fornecem um método para corrigir o enviesamento de massa de Yb usando um fator de normalização $^{173}Yb/^{171}Yb$ de 1,132685 (Chu *et al*., 2002). As razões de isótopos Hf foram normalizadas para ^{179}Hf /^{177}Hf de 0,7325 (Patchett, 1983). A descrição detalhada dos procedimentos e métodos foi fornecida por Matteini *et al*. (2010). O valor de $\varepsilon_{Hf(t)}$ foi calculado usando a constante de decaimento $\lambda = 1,86 *$ 10-11 (Scherer *et al*., 2006) e os valores CHUR $^{176}Lu/^{177}Hf$ e $^{176}Hf/^{177}Hf$ de 0,0336 e 0,282786 (Bouvier *et al*., 2008), respectivamente. As idades T_{DM} foram calculadas a partir da composição isotópica Hf inicial do zircão, usando uma razão média de Lu/Hf crustal (Gerdes e Zeh, 2009; Nebel *et al*., 2007). Os valores de $^{176}Lu/^{177}Hf = 0,0384$ e $^{176}Hf/^{177}Hf = 0,28325$ foram usados para o manto depletado (Chauvel e Blichert-Toft, 2001) e $^{176}Lu/^{177}Hf = 0,0113$ para a crosta média (Taylor e McLennan, 1985; Wedepohl, 1995). A composição inicial de Hf do zircão é representada pelo valor $^{176}Hf/^{177}Hf$, que foi calculado para a idade de cristalização do zircão U – Pb registrada anteriormente para o mesmo cristal.

Análises Isotópicas – Sm-Nd

Análises isotópicas Sm-Nd em amostras de rocha total foi realizada nas seguintes amostras graníticas: ST-02, ST-03, SC-824, SC-1328, CO-1329, CO-822, CO-820. E nas amostras gnáissicas: LR-2ª, HM-35B, SM-08, LR-19, CLR-04 e RM-33.

As amostras graníticas (ST-02, ST-03, SC-824, SC-1328, CO-1329, CO-822 e CO-820) e os gnaisses (LR-2ª, HM-35B, SM-08 e LR-19) foram analisados no Laboratório de Geocronologia e Geoquímica Isotópica da UnB, enquanto as amostras CLR-04 e RM-33 foram analisadas no Isótopo Laboratório de Geologia da Universidade Federal do Pará (Para-Isso).

As análises isotópicas de Sm-Nd realizadas no Laboratório de Geocronologia e Geoquímica Isotópica da UnB, seguiram o método descrito por Gioia e Pimentel (2000). As rochas foram pulverizadas (~ 50 mg) e misturadas com solução de pico ^{149}Sm -^{150}Nd e dissolvidos em béqueres Savillex. A extração de Sm e Nd de amostras de rocha total seguiu técnicas convencionais de cromatografia de troca catiônica, com colunas de Teflon contendo resina LN-

Spec (HDEHP – ácido dietilhexil fosfórico suportado em pó de PTFE). As frações Sm e Nd foram carregadas em filamentos de evaporação de reevaporação de conjuntos de filamento duplo, e as medidas isotópicas foram realizadas em um espectrômetro de massa de ionização térmica multicoletor TRITON em modo estático. As incertezas das relações ^{147}Sm / ^{144}Nd e $^{143}Nd/^{144}Nd$ foram melhores do que ±0,1% (erro padrão 2 σ) e ±0,0015% (1σ), respectivamente, de acordo com análises repetidas do padrão internacional de rocha BHVO-2. As razões $^{143}Nd/^{144}Nd$ foram normalizadas para $^{146}Nd/^{144}Nd = 0,7219$, e a constante de decaimento usada foi (σ) $6,54 \times 10^{-12}$ (Lugmair e Marti, 1978). Os valores de T_{DM} foram calculados usando o modelo DePaolo (1981).

As amostras CLR-04 e RM-33, foram analisadas no laboratório de Geologia Isotópica (Pará-Isso) da Universidade Federal do Pará, no qual o método Sm-Nd aplicado em rocha total, seguiu o procedimento analítico descrito por Oliveira *et al*. (2008). Primeiramente, em cerca de 100 mg de amostra pulverizada, foram adicionadas um traçador misto $^{149}Sm/^{150}Nd$ para a determinação dos teores de Sm e Nd por diluição isotópica. Em seguida, foram dissolvidas com HNO3, HCl e HF em forno de micro-ondas, logo foi realizada a separação química por cromatografia em resinas de troca iônica (Biorad DOWEX AG50x8 e Ln Eichrom®) em duas etapas, a primeira, para separação do grupo dos ETRs dos elementos maiores, utilizando uma coluna de teflon e na segunda coluna, foi feita a separação de Sm e Nd dos ETRs. Após a coleta e secagem, as frações concentradas de Sm e de Nd foram solubilizadas com HNO_3. A análise é realizada em um espectrômetro de massa com fonte de plasma (ICP-MS) modelo Thermo-Finnigan – Neptune. As razões isotópicas medidas do Nd são corrigidas para o fracionamento de massa utilizando, como parâmetro de normalização, a razão $^{146}Nd/^{144}Nd=0,7219$. A constante de decaimento usada foi o valor de $6,54 \times 10^{-12}$/ano-1 (Lugmair e Marti, 1978). Os cálculos das idades-modelo foram feitos com base na curva de evolução do manto empobrecido de DePaolo (1981).

Tabela 3.1. Dados da análise de U-Pb realizada por meio de LA-ICP-MS em zircão do padrão 91500.

PADRÃO	91500											Idades aparentes						
GRÃO	*f* 206 (%)	Th/U	$^{206}Pb/^{204}Pb$	$^{207}Pb/^{206}Pb$	err (%) 1 σ	$^{207}Pb/^{235}U$	err (%) 1 σ	$^{206}Pb/^{238}U$	err (%) 1 σ	Rho	$^{207}Pb/^{206}Pb$	2 σ abs	$^{207}Pb/^{235}U$	2 σ abs	$^{206}Pb/^{238}U$	2 σ abs	conc. (%)
Amostra ST-03 – 91500																		
025-91500	0.22	0.257	71323	0.07427	0.51	1.809	0.88	0.1766	0.62	0.70	1049	20	1049	11	1048	12	100
023-91500	0.29	0.261	52858	0.07429	0.47	1.804	0.82	0.1761	0.56	0.68	1049	19	1047	11	1045	11	100
008-91500	0.96	0.277	161717	0.07443	0.40	1.782	0.87	0.1736	0.68	0.78	1053	16	1039	11	1032	13	98
007-91500	0.12	0.279	123804	0.07445	0.45	1.774	0.83	0.1728	0.59	0.71	1054	18	1036	11	1027	11	97
006-91500	0.12	0.288	130400	0.07451	0.41	1.769	0.80	0.1722	0.58	0.73	1055	16	1034	10	1024	11	97
005-91500	0.12	0.286	133183	0.07456	0.42	1.784	0.81	0.1735	0.59	0.73	1057	17	1040	11	1032	11	98
017-91500	0.14	0.262	106630	0.07460	0.43	1.840	0.82	0.1789	0.60	0.73	1058	17	1060	11	1061	12	100
004-91500	0.22	0.283	69006	0.07466	0.56	1.811	0.99	0.1759	0.72	0.73	1059	23	1050	13	1045	14	99
024-91500	0.17	0.259	89831	0.07471	0.62	1.816	0.96	0.1762	0.63	0.65	1061	25	1051	13	1046	12	99
021-91500	0.12	0.272	128528	0.07476	0.42	1.814	0.78	0.1760	0.55	0.70	1062	17	1051	10	1045	11	98
011-91500	0.12	0.288	130791	0.07477	0.48	1.804	0.96	0.1749	0.74	0.77	1062	19	1047	12	1039	14	98
009-91500	0.14	0.290	114315	0.07480	0.36	1.788	0.78	0.1733	0.58	0.75	1063	15	1041	10	1030	11	97
026-91500	0.18	0.258	87309	0.07482	0.49	1.813	0.89	0.1757	0.65	0.73	1064	19	1050	12	1044	12	98
019-91500	0.12	0.268	131072	0.07497	0.51	1.835	0.88	0.1775	0.62	0.70	1068	20	1058	12	1053	12	99
010-91500	0.14	0.290	107651	0.07497	0.42	1.784	0.82	0.1726	0.60	0.73	1068	17	1040	11	1026	11	96
020-91500	0.20	0.271	77824	0.07498	0.48	1.837	0.85	0.1777	0.59	0.70	1068	19	1059	11	1054	11	99
018-91500	0.18	0.265	88106	0.07500	0.47	1.860	1.01	0.1798	0.81	0.80	1068	19	1067	13	1066	16	100
022-91500	0.19	0.272	80879	0.07518	0.52	1.811	0.85	0.1747	0.57	0.66	1073	21	1049	11	1038	11	97
Amostra CO-820 – 91500																		
050-91500	0.10	0.23	36308	0.07486	0.36	1.869	2.09	0.1810	1.50	0.72	1065	56	1070	28	1073	30	101

003-91500	0.13	0.23	72639	0.07517	0.52	1.960	1.88	0.1891	1.52	0.81	1073	42	1102	25	1117	31	104
020-91500	0.11	0.23	44036	0.07558	0.41	1.929	1.94	0.1851	1.26	0.65	1084	57	1091	26	1095	25	101
Amostra LR-02[a] – 91500																	
003-91500	0.15	0.26	69364	0.07456	1.0	1.81181	2.1	0.17562	1.8	0.87	1064	38	1050	27	1043	35	98
035-91500	0.11	0.26	41523	0.07482	0.7	1.84299	2.0	0.17925	1.5	0.71	1057	56	1061	27	1063	28	101
056-91500	0.11	0.27	36317	0.07647	0.9	1.92677	1.9	0.18272	1.4	0.73	1107	48	1090	25	1082	27	98
Amostra HM-35B – 91500																	
003-91500	0.10	0.20	43652	0.07531	1.6	1.84405	2.3	0.17759	1.6	0.70	1077	65	1061	31	1054	32	98
023-91500	0.06	0.19	20891	0.07683	2.9	1.87662	4.2	0.17713	3.1	0.73	1117	112	1073	55	1051	59	94
Amostra SM-08 – 91500																	
003-91500	0.12	0.21	40539	0.07555	1.3	1.79416	1.9	0.17222	1.4	0.71	1083	52	1043	25	1024	26	95
022-91500	0.09	0.22	42013	0.07392	1.7	1.82874	2.7	0.17942	2.1	0.76	1039	69	1056	35	1064	40	102
044-91500	0.08	0.21	25585	0.07466	2.0	1.80620	2.8	0.17545	2.0	0.70	1059	79	1048	37	1042	38	98
Amostra LR-19 – 91500																	
003-91500	0.11	0.22	31972	0.07511	1.1	1.80424	2.3	0.17421	1.7	0.77	1071	56	1047	29	1035	33	97
023-91500	0.09	0.22	56501	0.07495	1.3	1.79187	2.4	0.17449	1.7	0.72	1054	64	1043	31	1037	33	98
050-91500	0.08	0.22	37499	0.07447	1.2	1.88839	2.5	0.18272	1.8	0.69	1067	71	1077	33	1082	35	101
Amostra CLR-04 – 91500																	
038-91500	0.10	0.25	58086	0.07533	1.39	1.799	1.97	0.1732	1.34	0.68	1077	55	1045	26	1030	25	96
003-91500	0.12	0.25	52532	0.07554	1.53	1.810	2.52	0.1738	1.97	0.78	1083	61	1049	33	1033	38	95
017-91500	0.15	0.25	81059	0.07632	1.14	1.781	1.84	0.1693	1.40	0.76	1103	45	1039	24	1008	26	91

CAPÍTULO 4 – ARTIGO 1

"U–Pb AND Hf ISOTOPES IN GRANITOIDS FROM THE EASTERN BOLIVIAN BASEMENT: INSIGHTS INTO THE PALEOPROTEROZOIC EVOLUTION OF THE WESTERN PART OF SOUTH AMERICA"

Letícia A. Redes[1], Natalia Hauser[1], Amarildo S. Ruiz[2], Ramiro S. Matos[3], Wolf Uwe Reimold[1], Elton L. Dantas[1], Ralf-Thomas Schmitt[4], Barbara Alcântra Ferreria Lima[1], Erico Natal Pedro Zacchi[1], Jeane Grasyelle Silva Chaves[1], Luis Felipe Baumotte Osorio[1], Márcio Martins Pimentel[1] (*in memoriam*)

[1]Laboratorio de Geocronologia e Geoquimica Isotópica, Instituto de Geociências, Universidade de Brasília, Asa Norte, Brasília, DF, Brasil, 70910-900. E-mail: leticiaredes@hotmail.com

[2]Faculdade de Geociências, Universidade de Mato Grosso, Avenida Fernando Corrêa da Costa, 2367, Boa Esperança, Cuiabá, MT, Brasil, 78060-900.

[3]Instituto de Geologia Economica e Medio Ambiente, Universidad Mayor de San Andrés, Calle 27, Geologia Pabellón, La Paz, Bolivia.

[4]Museum für Naturkunde, Leibniz-Institute for Evolution and Biodiversity Science, Invalidenstrasse 43, 10115, Berlin, Germany.

ABSTRACT

Granitoids from Eastern Bolivian basement at Santo Corazón, Correreca, and Santa Terezita, and the Santana Gneiss from the Corumbá region (Mato Grosso de Sul state, Brazil) were studied by geochemistry and Sm-Nd and U-Pb isotope analysis. The granites have a medium to high calcium-alkaline potassium character and are typically peraluminous S-type granites. For The Santo Corazón quartz monzonite and Correreca granite we obtained Orosirian upper intercept U-Pb zircon ages of 1874±15 Ma and1862±7 Ma. For Santa Terezita granite two upper intercept U-Pb zircon ages of1849±11 and 1852±6 Ma were obtained. The geochemical and Nd and U-Pb isotope data suggest that these complexes were part of a crust created between 2.23 and 1.96 Ga, which was reworked mainly in Orosirian times in a magmatic arc setting. This is further supported by

Hf isotope data for zircon from the Correreca granite. The garnet-hornblende-biotite Santana Gneiss gave an upper intercept zircon U-Pb age of 1764±23 Ma, which is interpreted as the crystallization age of the igneous protolith, a quartz-monzonite to granodiorite. The petrological, geochemical and Nd as well as U-Pb isotope data show similarity between the Eastern Bolivian basement granites (EBB) and the Santana Gneiss with the Alumiador Intrusive Suite and the Caracol Gneiss, respectively. This suggests that this crustal fragment could have been an extension to the west of the Rio Apa Block, which today extends for 300 km from the southwest of Mato Grosso do Sul and northeast of Paraguay to Eastern Bolivia. The presence of continental crust that dates back to 1.7-1.8 Ga is inferred from isotope data for the cores of zircon from the Santana Gneiss and the Eastern Bolivian granites (EBB). In contrast, U-Pb ages obtained in rims of zircon crystals may indicate that two collisional events took place: a first one at 1.7 Ga, which we can relate to the collision of the Eastern and Western terranes of the Rio Apa Block with the Paraguá Block located to the west; and a second one at 1.3 Ga, related to the collision between the Paraguá Block, Eastern Bolivian basement granite terrane and the Rio Apa Block (EBB+RAB) with the Amazonian Craton during the San Ignacio Orogeny. This assemblage remained stable during the amalgamation into the Rodinia supercontinent.

Keywords: Basement, Eastern Bolivia, Paleoproterozoic granites, U-Pb/Lu-Hf geochronology, Sm-Nd isotopes, Rio Apa Block.

4.1. INTRODUCTION

The Precambrian basement in Eastern Bolivia (Fig. 4.1 A) comprises gneiss of the Chiquitania Complex, gneiss and granites of the Lomas Maneches Complex, and schist of the San Ignacio Group. These units have provided U-Pb ages in zircon between 1660 and 1700 Ma, but also a zircon U-Pb age of 1820 Ma (Litherland *et al.*, 1986; Boger *et al.*, 2005; Santos *et al.*, 2008). This basement was first assessed by the "*Proyecto Precámbrico*", a cooperation program between England and Bolivia (Litherland and Bloomfield, 1981; Berrangé, 1982; Litherland *et al.*, 1986, 1989). The terrane was initially considered the basement of the Paraguá Block,

interpreted as an extension of the SW Amazonian Craton (Boger *et al.*, 2005; Vargas-Mattos, 2006; Cordani and Teixeira, 2007; Santos *et al.*, 2002, 2008; Cordani *et al.*, 2009; Matos *et al.*, 2009; Teixeira *et al.*, 2010; Faleiros *et al.*, 2016).

The only geochronological study carried out until now on the basement of Bolivia was done by Vargas-Mattos *et al.* (2010), who studied the Correreca Granite and obtained $^{207}Pb/^{206}Pb$ ages on zircon. Later, Faleiros *et al.* (2016) interpreted this body as a northerly extension of the Rio Apa Block, exposed in Brazil at the border with Bolivia and Paraguay and extending into Bolivian territory.

The present study involves geochemical and Sm-Nd (ID-TIMS) analyses, as well as U-Pb and Lu-Hf isotope analyses on zircon (LA-ICP-MS) for three granites from the basement of Eastern Bolivia, the Santa Terezita, Correreca, and Santo Corazón granites (from west to east) the Santana Gneiss that crops out in the Corumbá region along the Brazil/Bolivia border. The results data allow us to infer the nature and evolution of the Bolivian basement. One important objective for this work has been to search for evidence of a possible geological correlation of the Eastern Bolivian basement with neighboring units, such as the Rio Apa Block, and the relationship of this basement with the southern part of the Amazonian Craton (Fig 4.1 B). Eventually, this work may help to understand the evolution of the western sector of South America between ~1900 and 1300 Ma, also in the overall context of amalgamation of the Columbia supercontinent during that time (Zhao *et al.* 2004; Fig. 4.1 C).

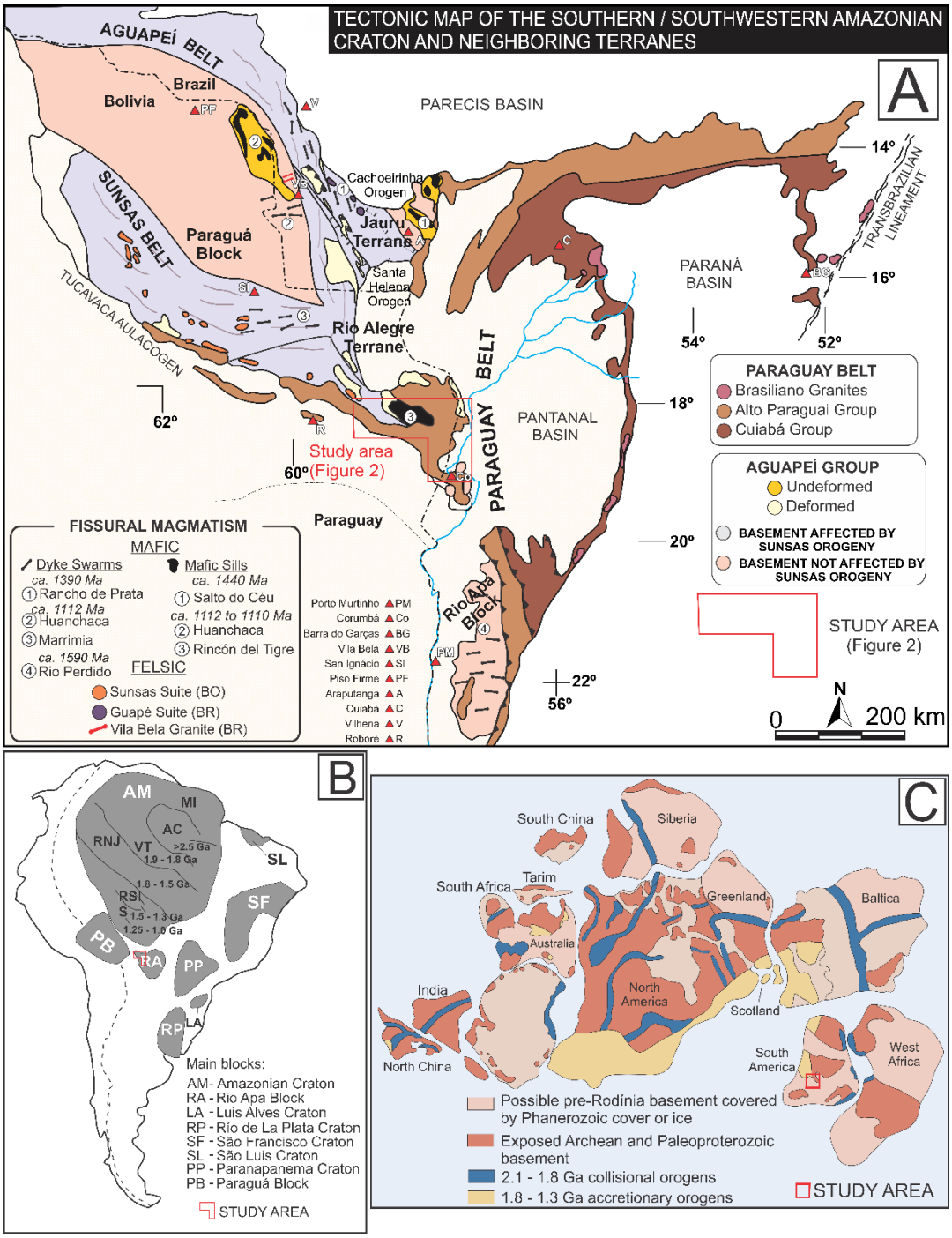

Figure 4.1. (A) Tectonic map of the South/Southwest of South America. Modified after Ruiz *et al.* (2010). (B) Distribution of the main cratonic blocks in South America with emphasis on the provinces of the Amazonian Craton: Amazônia Central – (CA, > 2.6 Ga); Maroni-Itacaiúnas (MI, 2.25 – 2.05 Ga); Ventuari-Tapajós (VT, 1.98 – 1.81 Ga); Rio Negro-Juruena (RNJ,1.78 – 1.55 Ga); Rondoniana-San Ignácio (RSI, 1.55 – 1.30 Ga) e Sunsas – (SU,1.25 – 0.97 Ga) (Tassinari and Macambira, 2004). (C) Columbia Supercontinent configuration after Zhao *et al.* (2004). The framed area in A corresponds to Figure 4.2, and the framed areas in B and C indicate the study area for this work.

4.2. GEOLOGICAL SETTING

As only a few geological studies have been published about the basement of Bolivia, the geology of this country is still poorly known. The Precambrian rocks in Bolivia, mainly exposed in the eastern part of this country, are only represented by gneiss from the Chiquitania Complex, gneiss and granulites from the Lomas Maneches Complex, and schist from the San Ignacio Group (Litherland *et al*., 1986; Boger *et al*., 2005). All of these occur in the area previously called the Crystal Block (Litherland and Klinck, 1982) or the San Pablo Block (Saes *et al*., 1992).

Litherland *et al*. (1986) introduced the name Paraguá Craton for the Precambrian shield of Eastern Bolivia (Fig. 4.1). Boger *et al*. (2005) established that the Chiquitania Gneiss Complex and the San Ignacio Group were derived from sedimentary rocks from 1765 Ma old sources and that these gneisses had not been deposited prior to 1690 Ma. These authors considered the emplacement of the Lomas Maneches Complex between 1690 and 1660 Ma; according to them, this unit is younger than the Chiquitania Gneiss Complex and the San Ignacio Group. U-Pb data from magmatic and metamorphic zircon delimited the age of the San Ignacio Group to 1340-1320 Ma. In contrast, Matos (2010) indicated that the Lomas Maneches Complex, the Chiquitania Complex, and the San Ignacio Group were Paleoproterozoic polymetamorphic basement formed between 1.82 and 1.69 Ga ago.

Sm-Nd whole rock isotopic data suggested three main granitic magmatic periods for the Bolivian Precambrian basement: the Yarituses Suite (1.63 to 1.62 Ga), the San Ramón Granite (1.42 Ga), and the San Ignacio Granite (1.33 to 1.27 Ga), with the Yarituses Suite representing a juvenile amalgamation event between 1.67 and 1.62 Ga (Matos, 2010).

The Paraguá Block (Fig. 4.1A and B) was described as an allochthonous crustal fragment attached to the margin of the Amazonian Proto-Craton during the Mesoproterozoic or Neoproterozoic (Boger *et al*., 2005; Ruiz, 2009; Bettencourt *et al*., 2010). According to Boger *et al.* (2005), the agglutination of this fragment may have occurred during the Sunsas Orogeny (1.0 to 0.9 Ga), whereas Ruiz (2005, 2009) suggested that the collision of the Paraguá Block with the Amazonian Craton took place during the San Ignácio Orogeny (1.37 to 1.34 Ga). Bettencourt *et al.* (2010) advocated that most of the Paraguá Block was formed during the San Ignácio Orogeny,

and that this process had affected basement rocks older than 1.64 Ga (Litherland *et al*., 1986; Darbyshire, 2000; Santos *et al*., 2008; Matos *et al*., 2009). In addition, during this orogeny, several granitic plutons were emplaced. This assemblage was collectively called the Pensamiento Granitoid Complex (1.3 Ga; Litherland *et al.*, 1986; Boger *et al.*, 2005; Matos, 2010).

Mitchell (1979) pioneered studies of Eastern Bolivian Paleoproterozoic granites, which indicated that the Correreca Granite (Fig. 4.2) was covered to the north by Sunsas Group sedimentary rocks, to the west by the Boquí Group, to the south by the Murciélago Group, and had a fault contact with the Santo Corazón Granite to the east.

Vargas-Mattos *et al*. (2010) described a Paleoproterozoic magmatism in the Bolivian territory related to emplacement of calc-alkaline, medium potassium granites of peraluminous affinity, compatible with a tectonic arc environment of 1925±32 Ma to 1894±13 Ma age. On the basis of these data, Vargas-Mattos *et al*. (2010) and Faleiros *et al*. (2016) suggested that the Correreca Granite could actually be a portionof the Rio Apa Block (Alumiador Intrusive Suite) that extended into Bolivian territory.

In the Corumbá region in the extreme western part of the state of Mato Grosso do Sul (MS) near the Brazil-Bolivia border occur the Taquaral and Coimbra granites, and the Santana Gneiss (Redes *et al*., 2015; Santos *et al*., 2019). The basement there is in tectonic contact with the Tamengo and Bocaina formations (Corumbá Group) and the Urucum and Santa Cruz formations (Jacadigo Group). The basement is partially covered by the Pantanal Formation (Redes *et al*., 2015). Based on geochronological, isotopic, petrological and structural data, the granitic basement of the Corumbá region has been considered an extension of the Alumiador Intrusive Suite of the Rio Apa Block (Redes *et al*., 2015; Santos *et al*., 2019, Teixeira *et al*., 2020).

The gneisses outcropping along the Brazil-Paraguay border in southwestern Mato Grosso do Sul and in far western Paraguay have been grouped together into the Caracol Suite (Fig. 4.2; Faleiros *et al*., 2016; Plens, 2018). They are classified as granite-gneiss of high-K calc-alkaline composition of 1776±13 to 1748±19 Ma age (Plens, 2018). The Caracol Suite constitutes the Eastern Terrane of the Rio Apa Block (Plens, 2018, Teixeira *et al*., 2020).

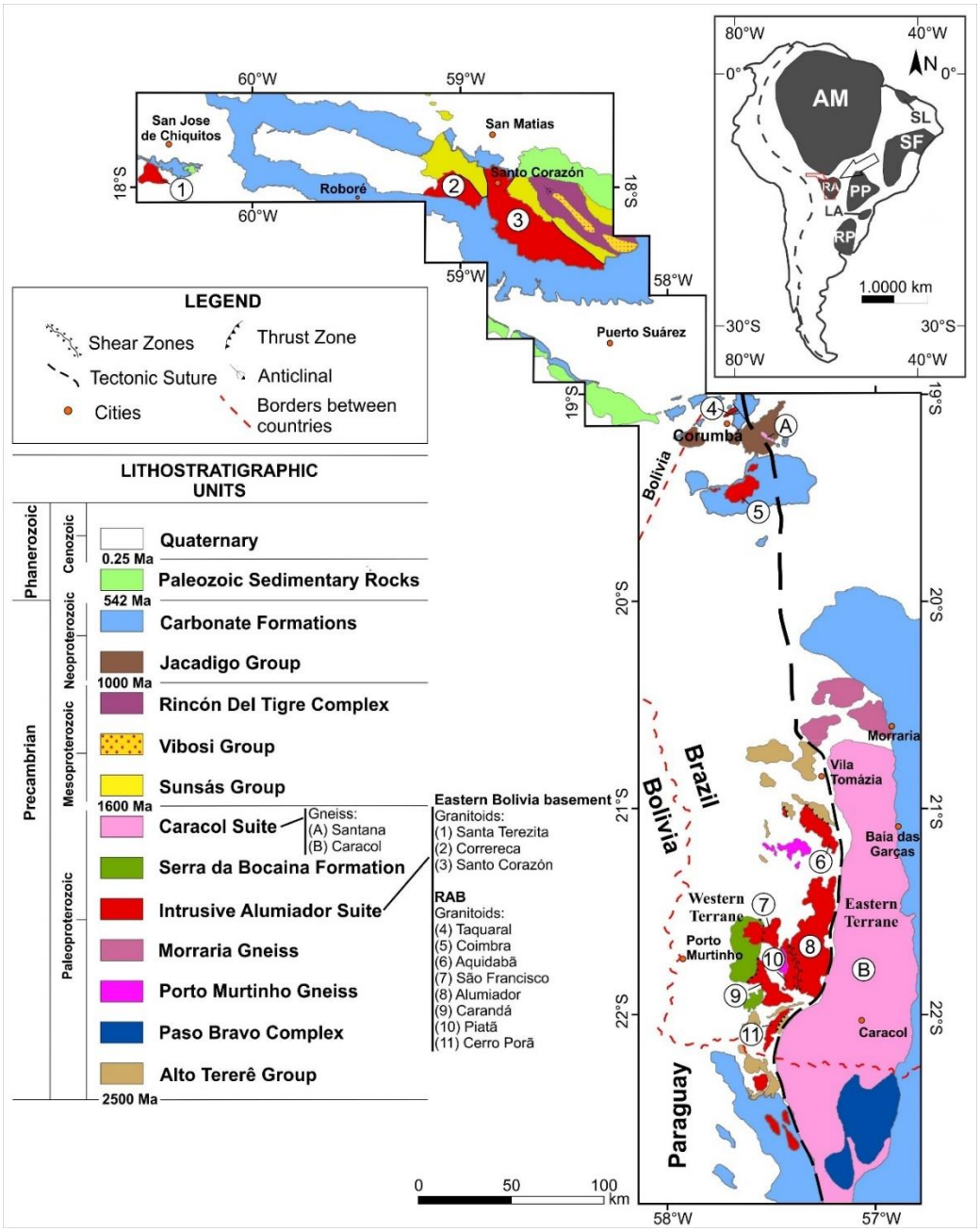

Figure 4.2. Simplified geological map of the Rio Apa Block (modified after Matos 2010; Cordani *et al*., 2010; Redes *et al*., 2015; Santos *et al*., 2019) and the relationship with the Eastern Bolivian basement granites and the Santana Gneiss investigated in this work.

4.3. MATERIALS AND ANALYTICAL METHODS

Several granite samples from the Eastern Bolivian basement were collected for petrographic analysis, geochemistry, U-Pb and Lu-Hf isotope analysis of zircon, and Sm-Nd isotope geochemistry on whole rock samples. Twenty thin sections were prepared in the Lamination Laboratory of the Instituto de Geociências of the Universidade de Brasília (IG-UnB)

for determination of mineral compositions, textural features, metamorphic grade, and deformation features.

4.3.1. Geochemistry

Samples were crushed and powdered in the IG-UnB sample preparation laboratory. Chemical analyses for major and trace elements were carried out on eighteen samples from the Correreca, Santo Corazón, and Santa Terezita granites (data in Table 4.1) and Santana Gneiss (Table 4.2). Major elements were analyzed by X-ray fluorescence spectroscopy (XRF) on a Bruker ASX S8 TIGER spectrometer at the Museum für Naturkunde Berlin (Germany), on powder (major elements) and fused glass discs (trace elements); the adopted methods and the quantification of results were described in detail by Schmitt *et al*. (2004). Powder aliquot for analysis of trace elements, including rare earth elements, were sent to ALS Brasil Ltda for analysis at ALS in Lima, Perú. The samples (0.1 g) were digested in a lithium metaborate/tetraborate flux. The powder was then dissolved in 100 mL of 4% nitric acid / 2% hydrochloric acid. The analyses were performed with Inductively Coupled Plasma (ICP) spectrometry to analyze the major elements and Inductively Coupled Plasma-Mass Spectrometry (ICP-MS) to analyze the trace elements. A full description of the analytical methods and quality parameters isavailable on the ALS Chemex webpage: (www.alsglobal.com).

4.3.2. U-Pb and Lu-Hf isotope analysis on zircon

U-Pb and Lu-Hf dating of zircon was performed by LA-ICP-MS at the Geochronology and Isotope Geochemistry Laboratory of the Universidade de Brasília. Zircon from samples ST-02, ST-03, CO-820, SC-824 and CLR-04 was analyzed for U-Pb isotopes. Only samples CO-820 from the Correreca granite and CLR-04 from the Santana gneiss were also analyzed by the Lu-Hf isotope method. Results for U-Pb and Lu-Hf analyses in zircon are given in Supplementary Tables 4.II.1 to 4.II.5, and Table 4.3, respectively.

Approximately 10 kg of each sample were crushed, followed by grinding in a vibratory cup mill, and sieving to different grain sizes (100 to 400 μm). Then, lighter and heavier minerals

were separated by their densities with water. The concentrate of heavy minerals was subjected to magnetic separation with a Frantz isodynamic separator; no chemical treatment was applied. Over 50 zircon grains were separated from samples ST-03, ST-02, CO-820, SC-824 and CLR-04 each. After separation, the grains were cast into an epoxy mount, polished to approximately half thickness, and the polished surfaces were characterized by back-scattered electron (BSE) and cathodoluminescence (CL) imaging using a FEI QUANTA 450 scanning electron microscope (SEM) at the Laboratory of Geochronology of the Universidade de Brasília.

Isotopic analysis of zircon was performed with a Thermo-Fisher Neptune HR-MC-ICP-MS instrument, coupled to a Nd:YAG UP213 New Wave laser ablation system – also at the Geochronology and Isotope Geochemistry Laboratory of the University of Brasilia. U-Pb analyses (Tables 4.II.1 to 4.II.5, Figures 4.10 to 4.12) were performed based on the standard-sample bracketing method (Albarède *et al*., 2004) using the GJ-1 standard (Jackson *et al*., 2004) in order to measure ICP-MS fractionation. The 91500 zircon (Wiedenbeck *et al.*, 1995, 2004) was also analyzed as an unknown during analytical sessions. Tuned masses were 238, 207, 206, 204 and 202. Integration time was 1 second, and ablation time was 40 seconds. Spot size was 30 μm, and laser adjustment was 10 Hz and 2-3 J / cm^2. In addition, the $^{206}Pb/^{207}Pb$ and $^{206}Pb/^{238}U$ ratios were time corrected. Data reduction was carried out with the in-house Chronus software at the UnB Geochronology Laboratory (see Oliveira, 2015).

Common ^{204}Pb was monitored based on ^{202}Hg and (^{204}Hg + ^{204}Pb) masses. Common Pb corrections were not carried out due to very low signals for ^{204}Pb (< 30 cps) and high signals for ^{206}Pb / ^{204}Pb ratios. Reported errors were propagated by the quadratic addition [(2SD ^ 2 + 2SE ^ 2) ½] (SD = standard deviation; SD = standard error) of external reproducibility and performance accuracy. External reproducibility was represented by the standard deviation based on repeated analyses (n = 20, ~ 1.1% for $^{207}Pb/^{206}Pb$ and up to ~ 2% for $^{206}Pb/^{238}U$) of the GJ-1 zircon standard during the analytical sessions, whereas performance accuracy is the standard error calculated for each analysis. Concordia diagrams (2σ error ellipses) and weighted mean ages were calculated with the Isoplot-3 / Ex software (Ludwig, 2012). The adopted geological time scale is in compliance with the one by Cohen *et al*., (2013, updated).

Lu-Hf isotopes (Table 4.3) were analyzed on zircon grains that had been previously analyzed for U-Pb isotopes (Supplementary Table 4.II.1 to 4.II.5) and that had given concordant data (concordance of 6/8 and 7/6 ages). Whenever possible, both the U-Pb and Lu-Hf analysis points were set as close as possible to enable analysis of zircon grain portions with the same isotopic features. Before the Hf isotope measurements, replicate analyses of a 200 ppb Hf JMC 475 standard solution doped with Yb (Yb/Hf=0.02) were carried out ($^{176}Hf/^{177}Hf$=0.282162±13 2s, n=4). The analysis of the GJ-1 standard was replicated during the analytical session and recorded $^{176}Hf/^{177}Hf$ ratios averaged to 0.282006±16 (2σ, n = 25), as compared to the reference value of 0.282000±0.000005 recorded by Morel *et al.* (2008) for this standard. The value recorded for GJ-1 was 0.282015±0.000009 (n = 5.2 SD) at an intensity of 2.03±0.08 V for ^{178}Hf. Lu-Hf isotope data were collected for 40-50 seconds of ablation, yielding 40 μm spot diameters, for 85% energy. The signals of the interference-free isotopes ^{171}Yb, ^{173}Yb and ^{175}Lu were monitored during analysis in order to correct for isobaric interferences of ^{176}Yb and ^{176}Lu on the ^{176}Hf signal. The ^{176}Yb and ^{176}Lu contributions were calculated using the isotopic abundance of Lu and Hf, as proposed by Chu *et al*. (2002). Contemporaneous measurement of ^{171}Yb and ^{173}Yb provides a means to correct for mass-bias of Yb using a $^{173}Yb/^{171}Yb$ normalization factor of 1.132685 (ibid). Hf isotope ratios were normalized to the $^{179}Hf/^{177}Hf$ value of 0.7325 (Patchett, 1983). Detailed description of procedures and methods was provided by Matteini *et al.* (2010).

The ε_{Hf} value of each grain was recalculated for the U-Pb age that had been previously recorded for the same zircon grain. The $\varepsilon_{Hf(t)}$ values were calculated based on the decay constant $\lambda = 1.86 * 10\text{-}11$ suggested by Scherer *et al.* (2006), as well as on the $^{176}Hf/^{177}Hf$ and $^{176}Lu/^{177}Hf$ CHUR values (0.282786 and 0.0336, respectively) suggested by Bouvier *et al.* (2008). *Depleted mantle Hf* model ages (T_{DM} Hf) were calculated based on the $^{176}Hf/^{177}Hf$ and $^{176}Lu/^{177}Hf$ DM values (0.28325 and 0.0384, respectively) suggested by Chauvel and Blichert-Toft (2001). The value of $^{176}Lu/^{177}Hf$ ratio (0.0113) was used as a mean crust reference (Taylor and McLennan, 1985; Wedepohl, 1995). Thus, T_{DM} ages were calculated based on the initial Hf isotopic composition of zircon by using mean Lu/Hf crustal values (Gerdes and Zeh, 2009; Nebel *et al.*, 2007). The initial Hf composition of zircon is represented by the ^{176}Hf / ^{177}Hf value, which was

calculated for the zircon crystallization time–the U-Pb age previously recorded for the same crystal.

4.3.3. Zircon characteristics

Santa Terezita Granite: Two samples were analysed from this granite. Zircon crystals from sample ST-02 are colorless, pinkish or brown, with prismatic to roundish habits, euhedral or subhedral, with length/width ratios ranging from 1/1 to 3/1, and sizes ranging from 50 to 130 µm. The grains are mostly regular and sometimes irregular with chaotic oscillatory zonation (Supplementary Figure I.1). Sample ST-03 yielded mostly colorless to pinkish zircon crystals, with roundish to prismatic habits, and subhedral crystals with a length/width ratio of 2/1. Grains are often fractured, contain some inclusions, and grain size ranges from 100 to 140 µm. Backscattered electron (BSE) imaging showed well-defined oscillatory zonation, and in some instances prominent metamorphic overgrowths (bright rims) (Supplementary Figure 4.I.2).

Santo Corazón Granite: The zircon crystals from sample SC-824 are prismatic, bipyramidal, and colorless to pinkish, with variably long or short habits. Most crystals are fractured or broken, ranged in length from 80 to 235 µm, and the average length/width ratio is 3/1. In cathodoluminescence imaging, the oscillatory zonation of well-defined dark and light bands is striking. These bands are interpreted as the result of variable U contents (Sato *et al*., 2008) and linked to igneous growth. Some crystals provide evidence for late growth phases, with prominent overgrowths along the margins of crystals (Supplementary Figure I.3).

Correreca Granite: The CO-820 sample yielded mostly colorless to pinkish crystals that are elongated and have bipyramidal prismatic habit; the length/width ratio is 3/1. Grains are often fractured; they range in size from 110 to 330 µm. Backscattered electron (BSE) images showed relatively regular, dark and light zonation, typical for igneous growth (Supplementary Figure I.4). *Santana Gneiss*: Zircon crystals from the CLR-04 sample are roundish to prismatic, colorless, and have short habit. They are often fractured and have some inclusions; sizes range from 70 to 200 µm; the length/width ratio was 2/1. Based on cathodoluminescence imaging, zonation is

prominent but not well defined. There are distinct metamorphic overgrowths on some crystals, in the form of transparent rims (Supplementary Figure I.5).

4.3.4. Sm-Nd isotopic analysis of whole rock samples

Sm-Nd isotope analysis of-whole rock samples was carried out for selected samples from the Santa Terezita (ST-02 and ST-03 samples), Santo Corazón (samples SC-824 and SC-1328), and Correreca granites (samples CO-1329, CO-822 and CO820), as well as the Santana gneiss (samples CLR-04 and RM-33), also at the Geochronology and Isotope Geochemistry Laboratory of the University of Brasilia, whereas the gneiss samples were analyzed at the Isotope Geology Laboratory of the Federal University of Pará (Para-Iso).

Isotope Geochemistry and Geochronology Laboratory – UnB (Universidade de Brasília)

The separation procedures and analytical method applied at UnB were reported by Gioia and Pimentel (2000). Approximately 50 mg of rock powder were mixed with $^{149}Sm/^{150}Nd$ rapid solution and dissolved in Savillex capsules. All whole rock samples used for Sm-Nd extraction were subjected to conventional cation exchange techniques based on Teflon® columns containing LN-Spec resin (HDEHP – Di-(2-ethylhexyl) phosphoric acid supported by polytetrafluoroethylene powder). Isotopic measurements were recorded with a Finnigan Triton multi-collector mass spectrometer in static mode. The uncertainties in $^{147}Sm/^{144}Nd$ and $^{143}Nd/^{144}Nd$ ratios were better than ±0.5% (2 σ) and ±0.005% (2 σ), respectively, based on repeated analysis of the international BHVO-2 and BCR-1 rock standards. The $^{143}Nd/^{144}Nd$ proportions were normalized to $^{146}Nd/^{144}Nd = 0.7219$; the decomposition constant was 6.54×10^{-12} (Lugmair and Marti, 1978). T_{DM} values were calculated based on the model by DePaolo (1981). Neodynium blanks were < 100 pg.

Isotope Geology Laboratory at Universidade Federal do Pará (Para-Iso)

The Isotope Geology Laboratory at Universidade Federal do Pará (Para-Iso) adopted the analytical procedure described by Oliveira *et al.* (2008). Approximately 100 mg of powdered

sample were dissolved in Teflon® pumps, based on the addition of HNO_3, HCl and HF, and placed into a microwave oven. A $^{149}Sm/^{150}Nd$ tracer was introduced to enable determining Sm and Nd concentrations through isotope dilution. Chemical separation was carried out by two-stage ion exchange chromatography with the use of Biorad DOWEX™ AG50x8 and Ln Eichrom® resins. Isotopic analyses were carried out with a Thermo Finnigan Neptune ICP-MS. The Nd isotope ratios were corrected for mass fractionation and normalized to $^{146}Nd/^{144}Nd = 0.7219$; the decay constant applied was 6.54×10^{-12} $year^{-1}$ (Lugmair and Marti, 1978). Model ages were calculated based on the depleted mantle curve over time (DePaolo, 1981). Sm-Nd isotope results for the analyzed samples are given in Table 4.4.

4.4. RESULTS

4.4.1. LITHOLOGY

Granites

Santa Terezita Granite: The rocks of the Santa Terezita Granite are light gray, generally leucocratic, equigranular to granular, and medium- to fine-grained, and they variably show incipient foliation to marked schistosity, with local evidence of strong deformation. Alkali feldspar (40-33 vol%), quartz (38-35 vol%), plagioclase (24-20 vol%) ranging from albite to oligoclase (An_{10-25}), and biotite (≤5 vol%) are the main minerals. These rocks are classified as monzogranitic to syenogranitic. Apatite, zircon, opaque minerals are the main accessory minerals sericite, phyllosilicate minerals, epidote, clinozoisite, zoisite, calcite, muscovite and chlorite are alteration products (Fig. 4.3 A and B).

Santo Corazón Granite: The granite of the Santo Corazón batholith is grey to pink in color, leucocratic, medium- to coarse-grained, and has a strong foliation. The granite is composed of plagioclase (40-29 vol%), quartz (40-29 vol%), alkali feldspar (30-25 vol%), and biotite (2-4 vol%). The plagioclase has albite ($An_{1.4}$) composition, and the samples are classified as monzogranite. Apatite, zircon and opaques are accessory minerals; sericite, phyllosilicate minerals, epidote, clinozoisite, zoisite, calcite, muscovite, and chlorite are alteration products **(**Fig. 4.3 C and D).

Correreca Granite: The Correreca Granite forms bodies of red to pink, leucocratic rocks with medium grain size and slight foliation. The granite is composed of plagioclase (40-32 vol%), quartz (36-32 vol%), alkali feldspar (29-19 vol%), and biotite (3-6 vol%). The composition of the plagioclase is albite ($An_{0.4–3}$). Quartz with undulatory extinction and recrystallization . The rocks are classified as granodiorite to monzogranite. Apatite, zircon and opaques are accessory minerals (≤1 vol%). There is evidence for some hydrothermal alteration that caused sericitization, argillitization, and saussuritization of feldspar, and chloritization of biotite (Fig. 4.3 E and F).

Santana Gneiss

This gneiss presents continuous and discontinuous banding is observed. In some places, mylonitic deformation zones can be found. It consists of light to dark gray bands of fine to medium grain size. Composed mainly of plagioclase, quartz, K-feldspar, amphibole, and biotite. The porphyroblast of K-feldspar, surrounded by quartz and plagioclase, which generated the augen texture. Titanite, garnet, apatite, zircon and opaque minerals are accessory phases. The rock is classified as a garnet-hornblende-biotite gneiss, of quartz-dioritic to syenogranitic composition. The Santana Gneiss varies in metamorphic grade from greenschist to amphibolite facies. Petrographic impressions are shown in Fig. 4.3 G and H.

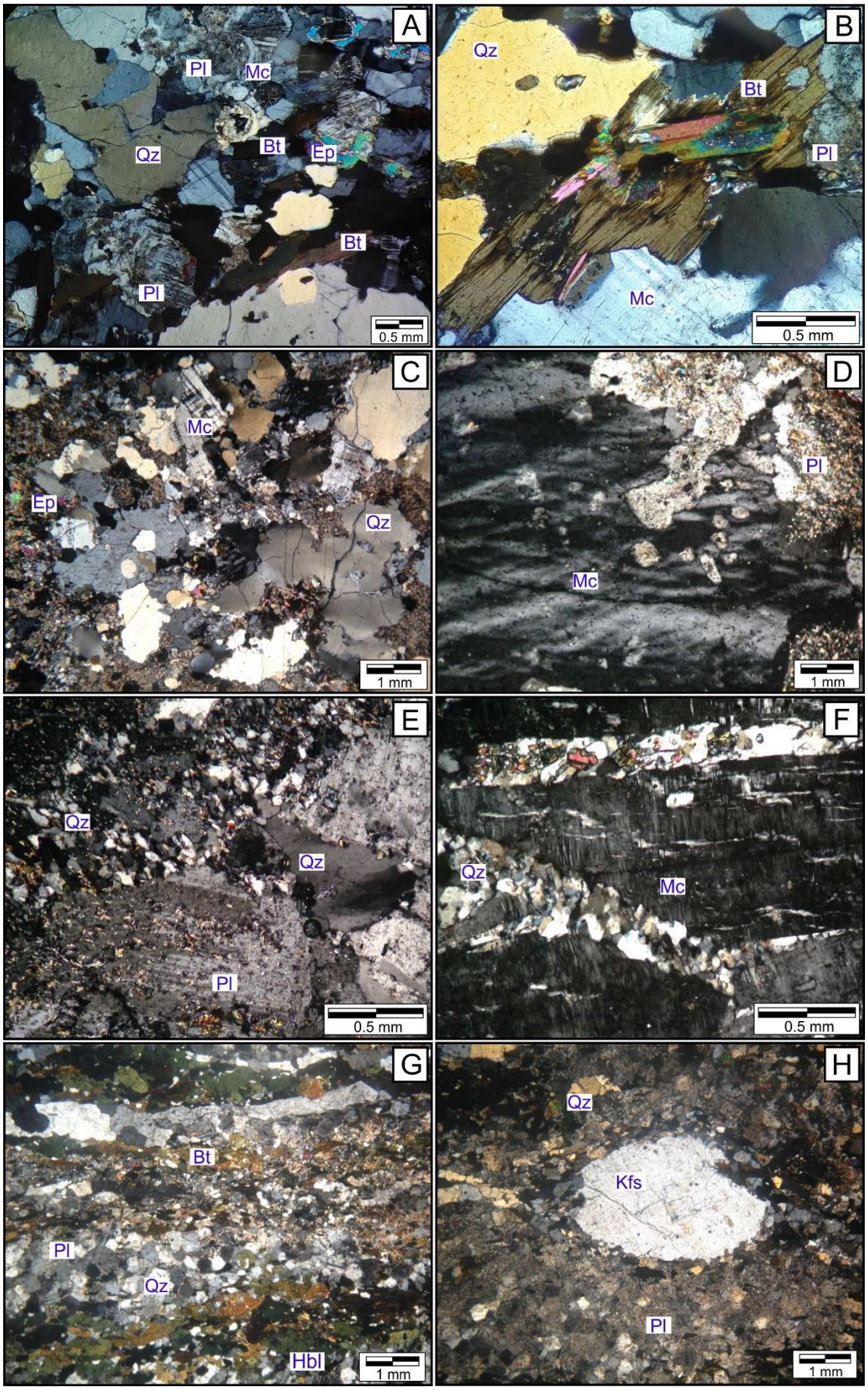
A
Pl
Mc
Qz
Bt
Ep
Bt
Pl
0.5 mm
B
Qz
Bt
Pl
Mc
0.5 mm
C
Mc
Ep
Qz
1 mm
D
Pl
Mc
1 mm
E
Qz
Qz
Pl
0.5 mm
F
Qz
Mc
0.5 mm
G
Bt
Pl
Qz
Hbl
1 mm
H
Qz
Kfs
Pl
1 mm

Figure 4.3. Microscopic aspects granites and the Santana Gneiss: (A) Syenogranite, medium-grained, inequigranular, Santa Terezita Granite. (B) Syenogranite: partially chloritized biotite aggregate, Santa Terezita Granite. (C) Monzogranite, medium to coarse grain size, Santo Corazón Granite. (D) Monzogranite with perthitic alkali feldspar and intensely altered plagioclase, Santo Corazón Granite. € Granodiorite, Correreca Granite. (F) Monzogranite with perthitic alkali feldspar surrounded by recrystallized quartz, Correreca Granite. (G) Quartz-dioritic with granoblastic texture to lepidonematoblastic texture, Santana Gneiss. (H) Syenogranitic, augen texture, Santana Gneiss. Pl = plagioclase; Qz = quartz; Kfs = K-feldspar feldspar; Mc = microcline, Bt = biotite; Hbl = hornblende; Ep = epidote. Abbreviations based on Siivola and Schmid (2007).

4.4.2. GEOCHEMISTRY

Granites

The Santo Corazón, Santa Terezita and Correreca granite samples mostly fall into the granite domain, in the Na_2O+K_2O-CaO versus SiO_2 diagram after Middlemost (1985; Fig. 4.4 A), except for sample ST-02 that falls into the alkali-granite field,. The samples plot into the quartz-monzonite and granite fields in the Ab-An-Or diagram of O'Connor (1965, modified by Barker, 1979; Fig. 4.4 B). The Na_2O+K_2O-CaO versus SiO_2 diagram by Frost *et al*. (2001; Fig. 4.5 A) indicates that the Paleoproterozoic granitic rocks from Bolivia have a calc-alkaline character that corresponds to subduction-related environments, except for sample ST-02 that plots into the alkaline field. A magnesian signature is indicated in the FeO_t/(FeOt+MgO) versus SiO_2 diagram of Frost *et al*. (2001; Fig. 4.5 B). Based on the index by Shand (1943), according to the A/CNK versus A/NK diagram by Maniar and Piccoli (1989; Fig. 4.5 C), the samples are peraluminous. The granites plot into the S-type field of the modified ACF diagram (Fig. 4.6 A) after White and Chappell (1977) and in the Fe_2O_3+FeO versus A/CNK diagram (Fig. 4.6 B) after Pearce *et al*. (1984).

Table 4.1. Chemical data of the Correreca (triangle), Santo Corazón (square) and Santa Terezita (start) granites (major element data in wt % and trace elements in ppm).

Samples	**CO-820** ▲	**CO-822** ▲	**CO-1329** ▲	**SC-824** ■	**SC-1328** ■	**ST-03** ✱	**ST-02** ✱
Major elements (wt %)							
SiO_2	70.00	73.10	73.40	70.30	72.00	71.50	71.8
TiO_2	0.44	0.36	0.40	0.44	0.30	0.38	0.34
Al_2O_3	14.40	13.90	13.90	14.20	13.20	14.50	12.5
Fe_2O_3	2.62	1.99	1.90	2.96	1.97	2.09	2.44
MnO	0.07	0.12	0.11	0.08	0.04	0.04	0.1
MgO	0.82	0.55	0.56	1.09	0.57	0.94	0.75
CaO	1.82	1.38	1.11	2.37	1.47	1.77	0.24
Na_2O	4.61	4.45	4.35	2.87	2.95	3.41	1.48
K_2O	3.71	3.02	3.32	4.22	4.50	4.43	8.79
P_2O_5	0.09	0.07	0.07	0.12	0.08	0.08	0.05
LOI	0.70	0.70	0.60	1.10	2.30	0.50	0.60
Total	99.28	99.64	99.72	99.75	99.38	99.64	99.09
Trace elements (ppm)							
Sc	7.00	8.00	8.00	9.00	5.00	7.00	5.00
Ni	7.00	7.00	6.00	16.00	9.00	10.00	11.00
Cu	15.00	15.00	15.00	25.00	15.00	15.00	15.00
Zn	41.00	52.00	68.00	65.00	27.00	28.00	74.00
Ga	18.10	19.00	18.90	15.90	14.70	16.40	14.50
Rb	108.00	93.90	101.50	149.00	165.00	189.50	250.00
Sr	334.00	346.00	189.00	375.00	160.50	115.00	99.30
Y	23.00	32.50	29.50	20.60	14.00	37.80	35.30
Zr	271.00	281.00	272.00	160.00	122.00	227.00	224.00
Nb	10.30	12.30	11.80	9.60	9.80	15.50	30.90
Cs	1.42	0.62	0.71	2.64	0.83	2.63	1.75
Ba	1150.00	1010.00	1085.00	796.00	564.00	823.00	1710.00
Hf	6.30	6.50	6.70	4.40	3.80	6.20	6.20
Ta	1.30	1.40	1.50	1.20	1.80	2.20	2.60
Pb	15.00	15.00	15.00	15.00	15.00	15.00	41.00
Th	11.75	10.75	11.10	15.05	17.10	19.75	23.40
U	1.05	1.64	1.38	2.28	2.37	4.04	4.97
La	51.80	61.10	53.40	44.50	32.40	46.40	58.00
Ce	94.10	108.50	103.00	79.50	56.80	88.10	119.00
Pr	11.00	14.30	12.70	8.99	6.37	10.60	13.10
Nd	40.80	54.70	48.70	32.30	22.40	38.40	52.30
Sm	6.59	9.29	8.58	5.75	3.90	7.25	9.77
Eu	1.67	2.32	2.14	1.14	0.75	1.32	1.66
Gd	5.50	7.98	7.80	4.40	3.33	7.86	8.31
Tb	0.79	1.13	1.07	0.74	0.48	1.26	1.18
Dy	4.41	6.25	5.92	4.05	2.59	6.59	6.99
Ho	0.81	1.20	1.03	0.77	0.45	1.44	1.26
Er	2.39	3.28	3.44	2.30	1.43	4.02	3.90

Tm	0.35	0.47	0.47	0.32	0.21	0.57	0.60
Yb	2.49	3.11	2.90	2.29	1.57	3.80	35.30
Lu	0.37	0.47	0.46	0.32	0.23	0.53	0.56
(La/Yb)N	14.92	14.09	13.21	13.94	14.80	8.76	10.30
(La/Sm)N	5.07	4.25	4.02	5.00	5.36	4.13	3.83
(Gd/Yb)N	1.83	2.12	2.23	1.59	1.75	1.71	1.70
Ba/La	22.20	16.53	20.32	17.89	17.41	17.74	29.48
Sr/Y	14.52	10.65	6.41	18.20	11.46	3.04	2.81
Eu/Eu*	0.06	0.06	0.06	0.06	0.06	0.06	0.06

Table 4.2. Chemical data for samples from the Santana Gneiss (major element data in wt % and trace elements in ppm).

Samples	**CLR-01**	**CLR-02A**	**CLR-03**	**CLR-04**	**CLR-04A**	**CLR-44**	**CLR-44A**	**CLR-46**	**RM-30**	**RM-33**	**RM-44B**
Major elements (wt %)											
SiO_2	61.80	63.70	55.40	58.40	55.80	54.80	62.50	59.40	59.30	57.70	58.70
TiO_2	0.71	0.59	0.89	0.77	0.63	1.04	0.69	0.86	0.79	0.66	0.83
Al_2O_3	17.00	16.50	17.00	15.70	15.60	17.30	17.30	16.80	17.60	16.30	16.30
Fe_2O_3	5.13	4.95	8.06	7.10	7.94	8.91	5.02	6.84	6.61	7.19	6.87
MnO	0.08	0.09	0.14	0.10	0.12	0.17	0.10	0.13	0.13	0.13	0.10
MgO	1.93	1.62	4.41	3.56	4.78	4.36	1.93	2.99	2.49	4.54	2.35
CaO	4.20	4.22	7.06	5.86	6.42	6.79	4.45	5.08	5.14	5.94	5.35
Na_2O	3.98	3.62	3.33	3.81	3.64	3.63	4.07	3.74	4.13	3.32	4.59
K_2O	3.19	3.52	1.82	2.25	2.46	1.44	2.44	1.67	1.97	2.16	2.27
P_2O_5	0.15	0.15	0.27	0.14	0.09	0.29	0.17	0.22	0.20	0.11	0.17
LOI	1.40	0.80	1.30	1.50	1.80	1.00	1.70	1.90	1.30	1.80	1.50
Total	99.57	99.76	99.68	99.19	99.28	99.73	100.37	99.63	99.66	99.85	99.03
Trace elements (ppm)											
Sc	11.00	12.00	25.00	22.00	23.00	25.00	15.00	16.00	20.00	24.00	14.00
Ni	17.00	14.00	42.00	33.00	67.00	51.00	15.00	35.00	22.00	61.00	23.00
Cu	22.00	30.00	30.00	70.00	33.00	153.00	22.00	19.00	25.00	333.00	34.00
Zn	55.00	49.00	70.00	57.00	60.00	85.00	59.00	79.00	77.00	65.00	66.00
Ga	18.00	18.00	18.00	16.00	16.00	20.00	19.00	19.00	19.00	16.00	19.00
Rb	99.00	86.00	54.00	58.00	79.00	42.00	82.00	59.00	62.00	72.00	55.00
Sr	428.00	398.00	465.00	336.00	314.00	447.00	402.00	363.00	443.00	278.00	491.00
Y	26.00	26.00	28.00	23.00	18.00	36.00	29.00	30.00	29.00	20.00	27.00
Zr	201.00	252.00	181.00	161.00	99.00	222.00	213.00	165.00	222.00	133.00	224.00
Nb	10.00	10.00	10.00	10.00	10.00	10.00	10.00	10.00	10.00	10.00	10.00
Cs	1.12	1.02	1.04	0.54	0.97	1.05	2.14	1.02	1.06	0.77	0.99
Ba	1350.00	1350.00	519.00	668.00	662.00	489.00	880.00	626.00	510.00	852.00	795.00

Hf	7.50	7.90	5.30	3.10	3.20	7.50	7.90	5.00	7.50	4.30	7.90
Ta	0.80	1.30	0.70	0.40	0.70	0.80	1.20	0.90	0.80	0.50	1.00
Pb	15.00	15.00	15.00	15.00	15.00	15.00	15.00	15.00	15.00	15.00	15.00
Th	15.00	15.00	15.00	15.00	15.00	15.00	15.00	15.00	15.00	15.00	15.00
U	10.00	10.00	10.00	10.00	10.00	10.00	10.00	10.00	10.00	10.00	10.00
La	27.00	30.00	25.00	29.00	16.00	36.00	30.00	30.00	34.00	19.00	31.00
Ce	65.80	61.80	74.80	45.20	44.10	68.30	81.90	50.70	64.80	44.70	80.80
Pr	8.15	7.76	9.84	5.16	4.96	8.97	9.43	6.99	8.10	5.27	10.30
Nd	32.60	31.40	40.60	19.10	19.80	37.30	37.30	29.20	33.30	20.60	41.80
Sm	5.81	5.65	7.54	3.41	3.57	7.75	6.46	5.29	6.13	3.61	7.76
Eu	1.84	1.35	2.07	1.07	1.04	1.95	1.76	1.51	1.88	1.19	2.00
Gd	4.70	5.07	6.56	2.83	3.41	7.45	5.74	5.57	5.90	3.85	6.86
Tb	0.79	0.79	1.07	0.45	0.50	1.08	0.94	0.84	0.91	0.57	1.07
Dy	4.81	5.06	6.19	2.91	3.35	7.09	6.23	5.05	6.06	3.73	6.27
Ho	0.97	0.91	1.20	0.59	0.71	1.41	1.14	1.05	1.15	0.74	1.17
Er	2.62	2.74	3.52	1.46	2.05	4.08	3.37	2.98	3.33	2.13	3.23
Tm	0.43	0.40	0.46	0.21	0.27	0.58	0.52	0.39	0.46	0.32	0.49
Yb	2.69	2.98	3.04	1.66	1.99	4.01	3.96	2.88	2.92	1.94	3.13
Lu	0.37	0.39	0.42	0.23	0.33	0.62	0.58	0.39	0.49	0.33	0.49
(La/Yb)n	8.43	7.00	8.45	10.24	8.25	5.38	6.48	6.85	7.71	8.17	8.53
(La/Sm)n	3.51	3.32	3.07	4.49	4.14	2.51	3.58	3.36	3.31	3.95	3.09
(Gd/Yb)n	1.45	1.41	1.79	1.41	1.42	1.54	1.20	1.60	1.67	1.64	1.81
Ba/La	49.84	51.20	15.92	21.01	33.23	16.64	26.87	23.09	18.15	42.26	23.60
Sr/Y	17.96	15.35	15.24	15.67	16.40	12.05	13.53	13.18	15.95	15.80	17.13
Eu/Eu*	0.06	0.06	0.06	0.06	0.06	0.06	0.06	0.06	0.06	0.06	0.06

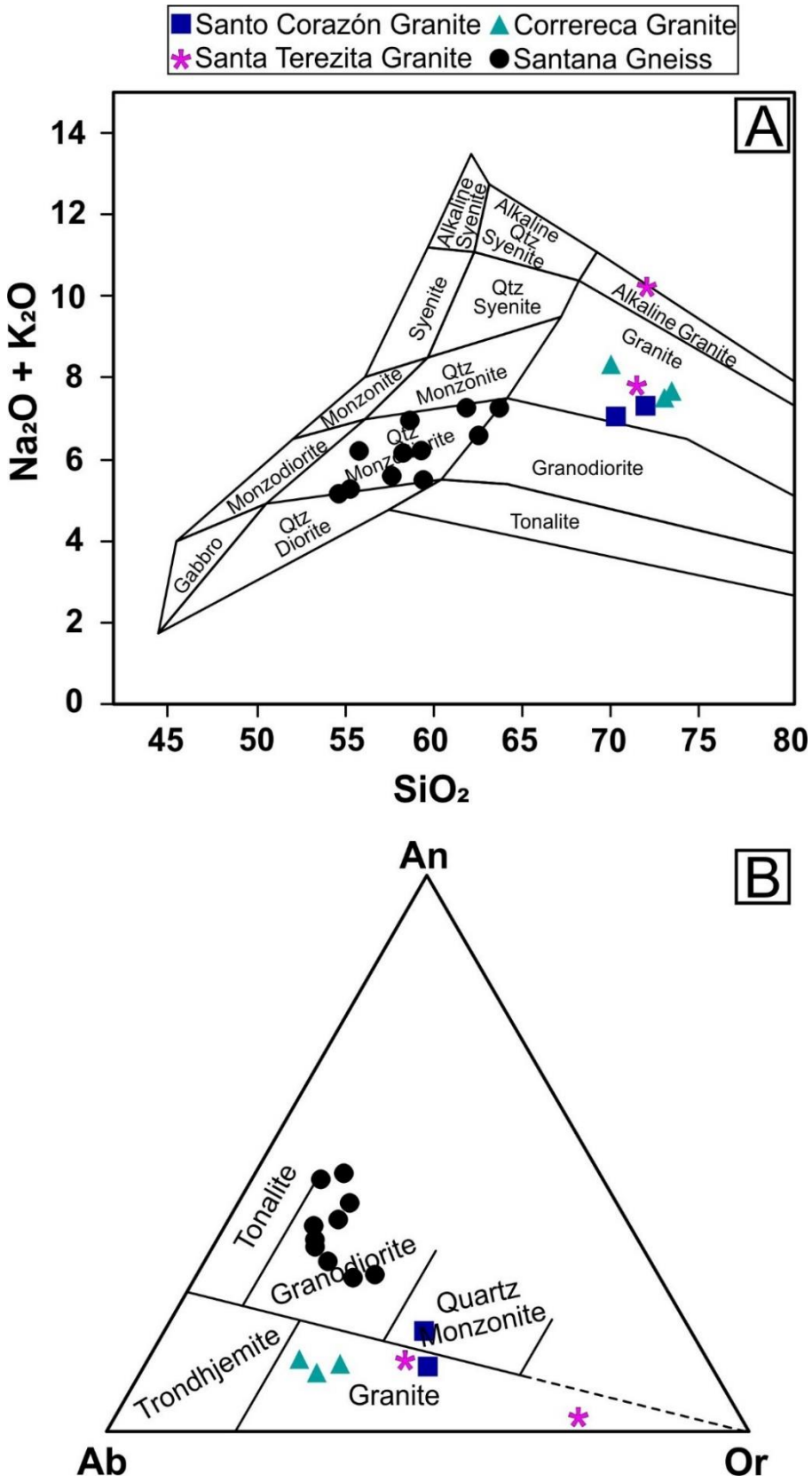

Figure 4.4. Classification of the studied rocks using the (A) Na_2O+K_2O *versus* SiO_2 plot after Middlemost (1985) and (B) An-Ab-Or normative plot (O'Connor, 1965, modified by Barker, 1979).

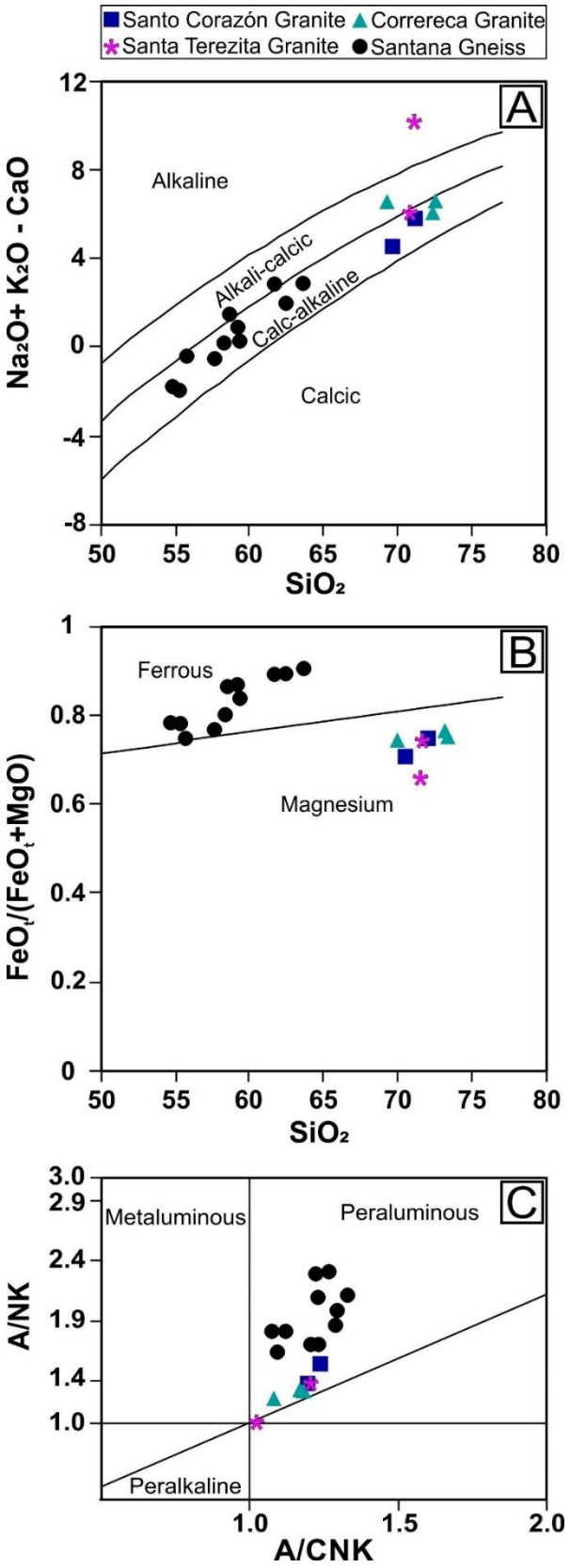

Figure 4.5. Classification of the studied rocks using (A) Na_2O+K_2O-CaO *versus* SiO_2 (Frost *et al.*, 2001); (B) $FeO_t/(FeO_t+MgO)$ *versus* SiO_2 (Frost *et al.*, 2001*);* (C) A/NK *versus* A/CNK (Maniar and Piccoli, 1989).

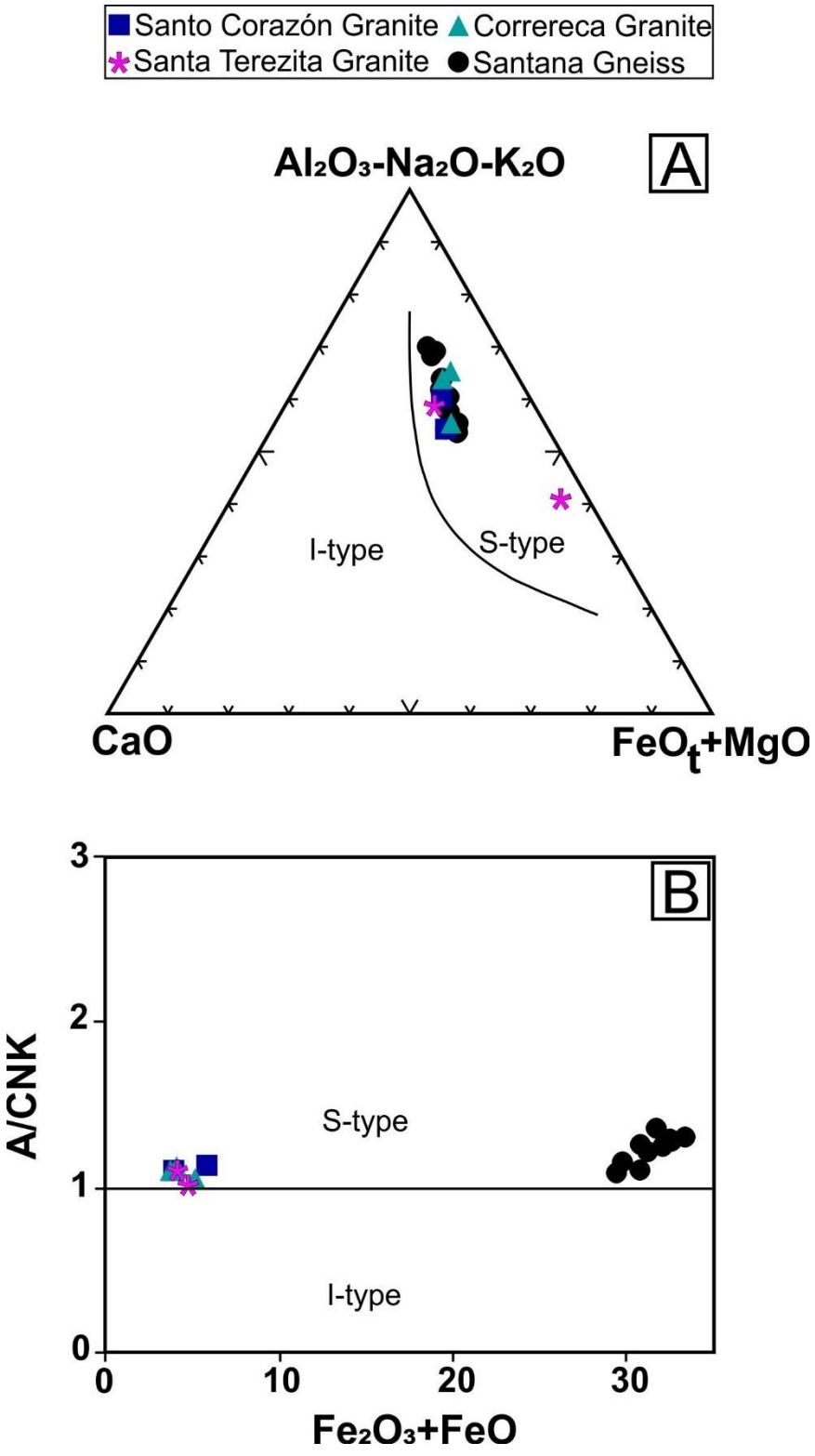

Figure 4.6. Classification of granites using (A) Al_2O_3-Na_2O-K_2O – CaO – FeO_t+MgO plot (White and Chappell, 1977) and (B) Fe_2O_3+FeO *versus* A/CNK plot (Pearce *et al*., 1984).

These granites have little variation in silica content, which is between 70 and 73.4 wt% (Table 4.1). The patterns for trace element and K_2O data, normalized against granite from Mid-Ocean Ridges, after Pearce *et al.* (1984; Fig. 4.7 A), show enrichment of large ion lithophile elements (LILE) in comparison to the elements with high ionic potential (HFSE) (negative Nb and Ta typical for crustal contribution) (Rollinson, 1993) or subduction-zone settings (Kelemen *et al.*, 1993). The multi-element diagram by Sun and McDonough (1989; Fig. 4.7 B) shows that the granites are at least 100 times enriched in large lithophile elements in comparison to primitive mantle. This is particularly evident in the Ba/La ratio, which ranges from 16.5 to 22.2, and by the Sr/Y ratio, which varies between 3 and 18.2 (Table 4.1).

Rare Earth Element (REE) patterns for the Santo Corazón, Santa Terezita and Correreca granite samples (data normalized to the CI chondrite data after Sun and McDonough, 1989; Fig. 4.7 C) are similar to patterns for calc-alkaline granitoids, with Heavy REE depletion in comparison to the Light REE. The Heavy REE have a sub-horizontal pattern with $(Gd/Yb)_N$ ratios between 1.5 and 2.2, whereas the Light REE show stronger fractionation expressed by $(La/Sm)_N$ ratios between 4 and 5.3. The Santo Corazón rocks have comparatively more homogeneous patterns with La/Yb ratios of 19.4 to 20.6. The La/Yb ratio for samples from the Santa Terezita Granite is 12.2, and for the Correreca Granite between 18.4 and 20.8. The Eu/Eu* ratios for these granites are homogeneous around 0.58 for all samples (Table 4.1).

In tectonic environment diagrams, these granites plot into the Arc field (Fig. 4.8 A) after Pearce *et al*. (1984), and into the Subduction and Collision domains in the $(Nb/Zr)_N$ versus Zr diagram after Thiéblemont and Tegyey (1994), where the Nb/Zr ratios are normalized by [Zr = 9.714 and Nb = 0.6175] after Hoffman (1988; Fig. 4.8 B).

Santana Gneiss

The protoliths for the Santana Gneiss samples are classified as quartz-monzonite based on the Na_2O+K_2O-CaO *versus* SiO_2 diagram by Middlemost (1985; Fig. 4.4 A). The Santana Gneiss falls into the granodiorite field in the Ab-An-Or diagram by O'Connor (1965, modified by Barker 1979; Fig. 4.4 B), but it has a significant similarity to granodiorite composition, because

the silica content of Santana Gneiss samples varies widely – from intermediate, with values between 54.8 and 63.7 wt% (Table 4.2).

The Santana Gneiss samples plot in the Na_2O+K_2O-CaO *versus* SiO_2 diagram by Frost *et al.* (2001; Fig. 4.5 A) into the cal-alkaline to alkaline fields, with a general calc-alkaline tendency. Most of these rocks have a ferrous signature in the $FeO_t/(FeO_t+MgO)$ *versus* SiO_2 (Fig. 4.5 B) diagram of Frost *et al.* (2001) and are classified as peraluminous in the A/CNK *versus* A/NK diagram (Maniar and Piccoli, 1989; Fig. 4.5 C).

The protoliths of the Santana Gneiss plot into the S-type field of the modified ACF diagram (Fig. 4.6 A) after White and Chappell (1977) and in the Fe_2O_3+FeO versus A/CNK diagram (Fig. 4.6 B) after Pearce *et al*. (1984).

The multi-element distribution patterns of samples from the Caracol Intrusive Suite - normalized to values for granite from Mid-Ocean Ridges (Pearce *et al.*, 1984; Fig. 4.7 A) - show enrichment of large ion lithophile elements (LILE) in comparison to the high field-strength elements (HFSE). The LILE have positive potassium, Rb and Th anomalies; according to Rollinson (1993) this suggests crustal contamination. On the other hand, the HFSE display positive Ce and Sm anomalies. The diagram by Pearce *et al.* (1984) (Fig. 4.7 A) also shows a negative Ta and Nd trend typical for granites from volcanic arcs, as well as positive Ce and Sm anomalies, in comparison to the other HFSE.

The multi-element diagram by Sun and McDonough (1989; Fig. 4.7 B) indicates enrichment of the large ion lithophilic elements (LILE) by at least 100 times, in comparison to primitive mantle, for the protoliths for the Santana Gneiss. This is supported by the Ba/La ratios, which vary from 15.9 to 51.2, and by the Sr/Y ratios, which vary between 12.1 and 18.0 (Table 4.2). The protoliths of the Santana Gneiss plot into the Volcanic Arc Granite (VAG) field (Fig. 4.8 A and B), after Pearce *et al*. (1984) and Thiéblemont and Tegyey (1994).

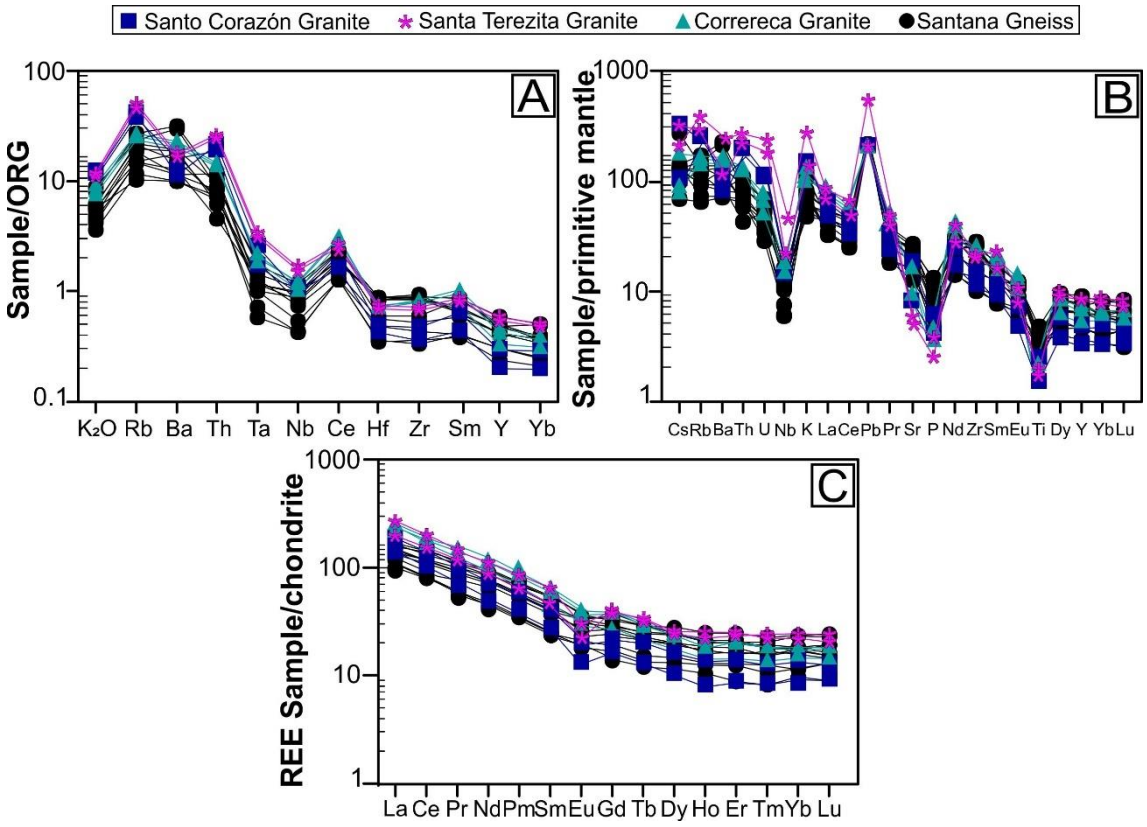

Figure 4.7. Element distribution patterns for the samples from the Santana Gneiss and from the Corazón, Santa Terezita and Correreca granites. (A) Trace elements and K_2O normalized to granites from Mid-Ocean Ridges (ORG – Ocean Ridge Granites; Pearce *et al.*, 1984). (B) Multi-element diagram (Sun and McDonough, 1989). (C) REE diagram normalized to C1 chondrite (Sun and McDonough, 1989).

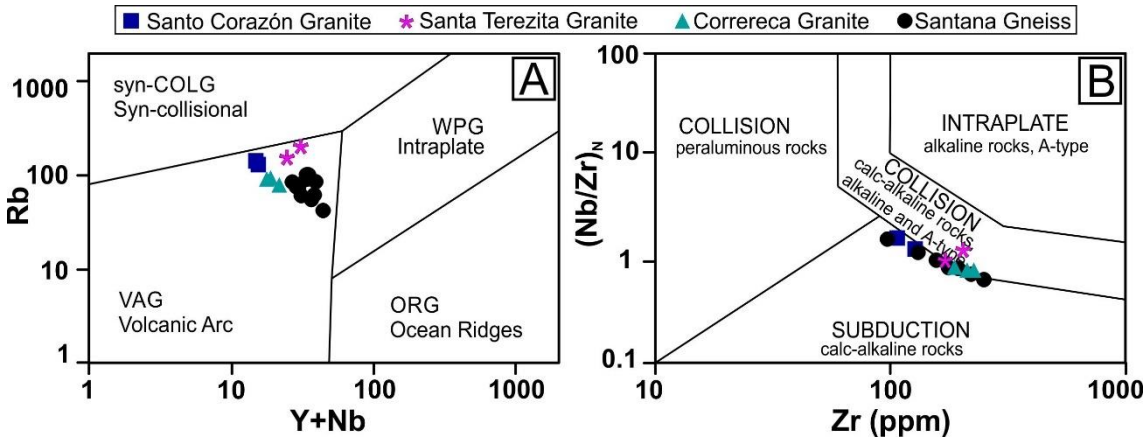

Figure 4.8. Geochemical plots for the Santana Gneiss and the Eastern Bolivian basement granites, the Santo Corazón, Santa Terezita, and Correreca granites: (A) Rb *versus* Y+Nb (Pearce *et al.*, 1984); (B) $(Nb/Zr)_N$ *versus* Zr (Thiéblemont and Tegyey, 1994). The Nb/Zr ratio was normalized by values (Zr = 9.714 and Nb = 0.6175) suggested by Hofmann (1988).

4.4.3. U-Pb and Lu-Hf GEOCHRONOLOGY ON ZIRCON

Santa Terezita Granite

Sample ST-02:

In total, 44 U-Pb isotope analyses were performed on 39 zircon crystals (Supplementary Table 4.II.1). The data with ages between 1873 and 1810 Ma, comprises 11 data with concordance between 94 and 104 % (Fig. 4.9 A). These data were obtained on cores and rims of crystals characterized by regular zonation, typical for magmatic origen, and sometimes irregular, chaotic oscillatory zonation (CL image in Fig. 4.9). The upper intercept age of 1849±11 Ma (MSWD=1.4; Fig. 4.9 B) is interpreted as the crystalization age of this granite. These zircon crystals display Th/U ratios between 0.06 and 0.77.

Taking into account that there is a continuos range in ages between 1873 and 1810 Ma, with concordance of 94 to 104 %, the slightly older population of ~1870 Ma could correspond to antecrysts, i.e., zircon crystals that crystallized from an earlier pulse of magma and were incorporated into later pulse(s) (Miller *et al*., 2007); the crystals ranging in age between 1861 and 1838 Ma could represent a second pulse, during which the major population of crystals was generated; the crystals with ages between 1833 and 1810 Ma could correspond to crystals generated during the last pulse and would be classified as autocrysts (Miller *et al*., 2007), namely crystals that grow only within the youngest intrusive pulse.

On the basis of $^{207}Pb/^{206}Pb$ apparent ages, the data allowed us to indentifie two olders groups, with upper intercept ages of 2212±77 Ma, 2104±220 Ma (Fig. 4.9 A), respectively. These upper intercept ages were obtained in cores of zircon crystals with typical magmatic characteristics, such as regular concentric zonation. Their Th/U ratios range from 0.04 to 0.84.

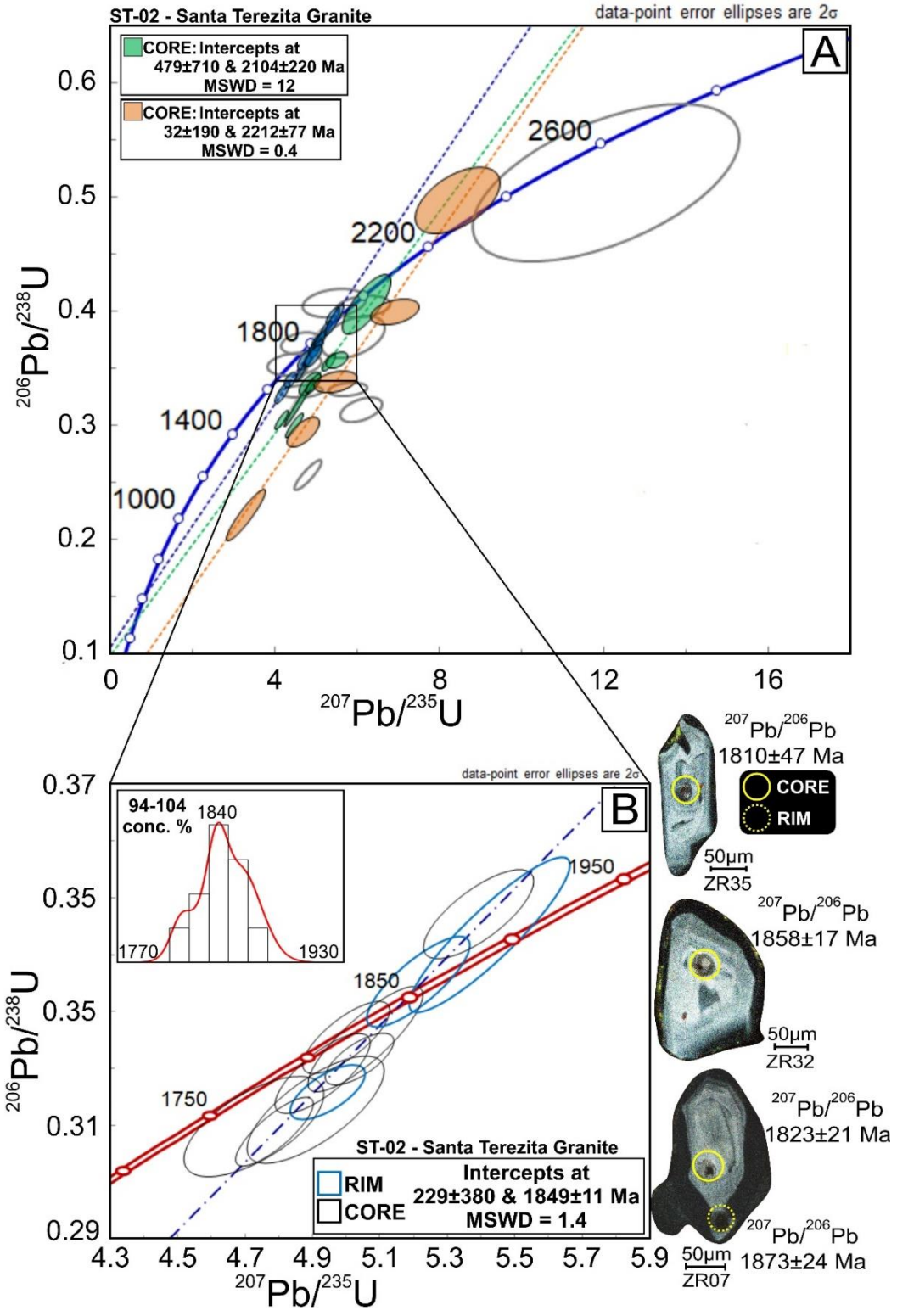

Figure 4.9. U-Pb isotope analysis for the Santa Terezita granite, sample ST-02. (A) Distribution of U-Pb data in the Wetherill Concordia Diagram. Several populations with different upper intercept ages of 1849±11 Ma and 2104±11 Ma, 2212±77 Ma, can be distinguished. (B) The youngest upper intercept age of 1849±11 Ma is proposed as the crystallization age of this body. To the right, cathodoluminescence images of zircon crystals and positions of the U-Pb analyses (30 µm spots) in the yellow circles.

Sample ST-03:

From this sample, 58 zircon crystals were analyzed (Supplementary Table 4.II.2, Fig. 4.10 A). On the basis of $^{207}Pb/^{206}Pb$ apparent ages, the obtained data were organized into two groups, a group with an older upper intercept age of 1853±5 Ma (Fig. 4.10 B) and a younger group with a concordia age of 1722±7 Ma (Fig. 4.10 C).

For the group with age range between 1916 Ma and 1844 Ma (concordance between 97% and 104%), the two ages of 1916 and 1903 Ma could correspond to xenocrystic zircons; the slightly older population with ages between 1892-1875 Ma could correspond to zircon antecrysts gnerated during an older magmatic pulse; and the youngest interval of ages between 1864 and 1844 Ma could represent the last magmatic pulse, and, thus, the corresponding crystals could represent autocrysts. This last group (with concordance between 97-104%, and Th/U ratios from 0.21 to 0.80) allowed to obtain an upper intercept age of 1853±5 Ma (MSWD = 0.2; Fig. 4.10 B) for zircon cores. This age is interpreted as the crystallization age for this granite.

Some zircon crystals exhibit light rims around darker areas (e.g., the BSE image in Fig. 4.10). These relatively light rims are interpreted as metamorphic overgrowths. These areas are related with five concordant ages of 1738, 1716, 1611,1346 and 1275 Ma. The data between 1638 and 1738 Ma define a Concordia age of 1722±7 Ma (MSWD = 4.4; Fig. 4.10 C), and the corresponding grains have Th/U ratios from 0.02 to 0.10.

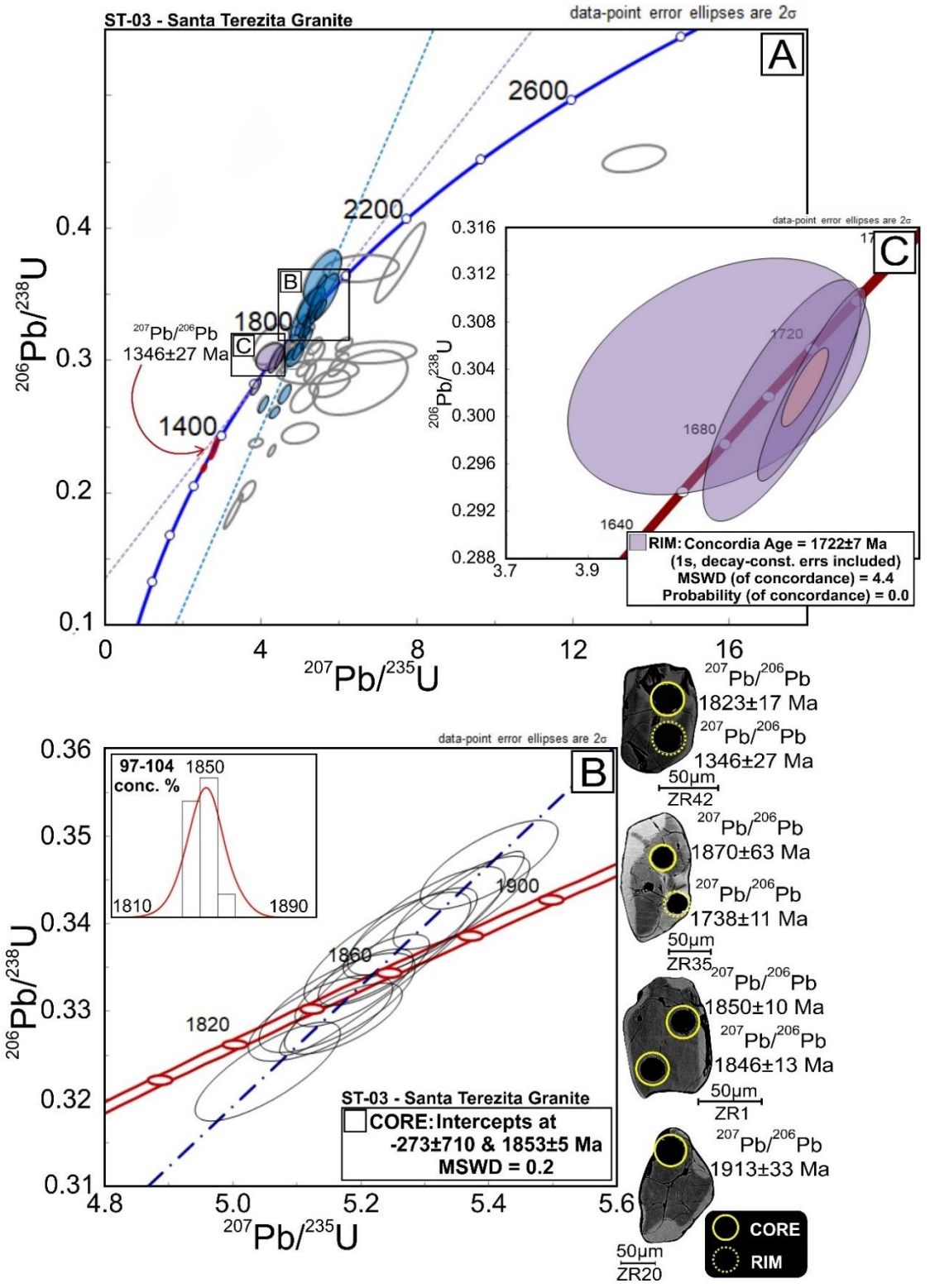

Figure 4.10. U-Pb isotope analysis for the Santa Terezita granite, sample ST-03. (A) Distribution of U-Pb data in the Wetherill Concordia Diagram. (B) The youngest upper intercept age of 1853±5 Ma is interpreted as the crystallization age of this granite. Note that the two ages obtained for ST-02 and ST-03 overlap within error limits. To the right, Backscattered electron images of zircon crystals and positions of the U-Pb analyses (30 µm spots) in the yellow circles are shown. (C) The youngest Concordia age of 1722±7 Ma is based on three analyses of zircon rims.

Santo Corazón Granite

Sample SC-824:

The results for 44 concordant to discordant analyses on 34 zircon crystals are presented in Figure 11 (Supplementary Table 4.II.3).

The data with concordance between 92 and 102% yielded an upper intercept age of 1874±15 Ma (MSWD = 1.3, Fig. 4.11 B). The data were obtained in cores with magmatic zonation and high Th/U ratios from 0.64 to 1.09 This age is interpreted as the crystalization age of this granite.

According to the continuous range of ages between 1889 and 1846 Ma, with concordance between 92 and 102 %, the slightly older population of grains with ages between 1889 and 1871 Ma could represent antecrysts generated in older pulses, whereas the crystals with ages between 1857 and 1846 Ma could be considered autocrysts.

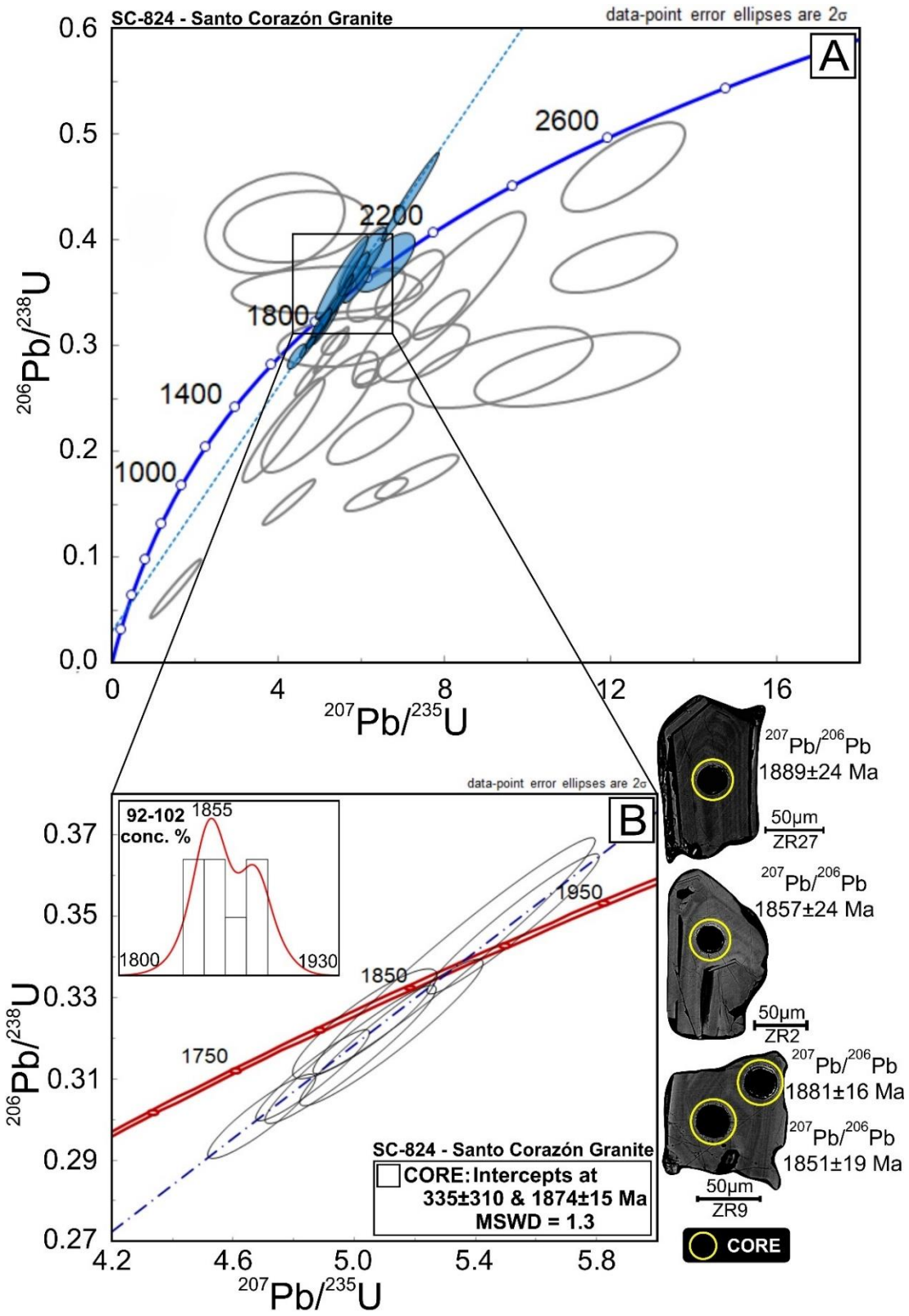

Figure 4.11. (A) U-Pb isotope analysis for the Santo Corazón Granite, sample SC-824. (A) The distribution of U-Pb data in the Wetherill Concordia Diagram. (B) The upper intercept age at 1874±15 Ma is interpreted as the crystallization age of this granite. To the right, BSE images of zircon crystals with typical magmatic zonation are shown. The position of the U-Pb analyses (30 µm spots) are indicated in the yellow circles.

Correreca Granite

Sample CO-820:

The 44 U-Pb isotope analyses were performed in 34 zircon crystals from this sample (Supplementary Table 4.II.4). Of these, 42 data, yielded an upper intercept age of 1861±7 Ma (MSWD = 2.1; Fig. 4.12) from magmatic domains in cores with high Th/U ratios from 0.42 to 1.56. For this reason, this upper intercept age is interpreted as the crystalization age of the Correreca Granite. Twelve concordant data (98 to 102 % concordance) with ages between 1874 and 1809 Ma represent the magmatic event responsible for the generation of the Correreca Granite. These data allow to postulate that the zircon crystals with ages between 1874 and 1868 Ma could represent antecrysts related to an older magmatic pulse. The population of zircon crystals with ages between 1858 and 1835 Ma could also indicate the presence of zircon antecrysts generated in a second magmatic pulse, and the youngest population of crystals with ages between 1821 and 1809 Ma could be considered as autocrysts related to the last magmatic pulse. Analyses on 13 rims demonstrated that there is no difference in terms of age between the cores and rims (BSE image in Fig. 4.12) of these grains, and no metamorphic event is registered by these crystals.

Lu-Hf isotope analysis was done on 12 zircon crystals with U-Pb ages beetween 1809 and 1891 Ma (correspondig to the magmatic event). These grains gave variably negative to positive $\varepsilon_{Hf(t)}$ values between -4.63 and +2.76, and Hf model ages between 2.68 and 2.29 Ga (Table 4.3; Fig.4.14).

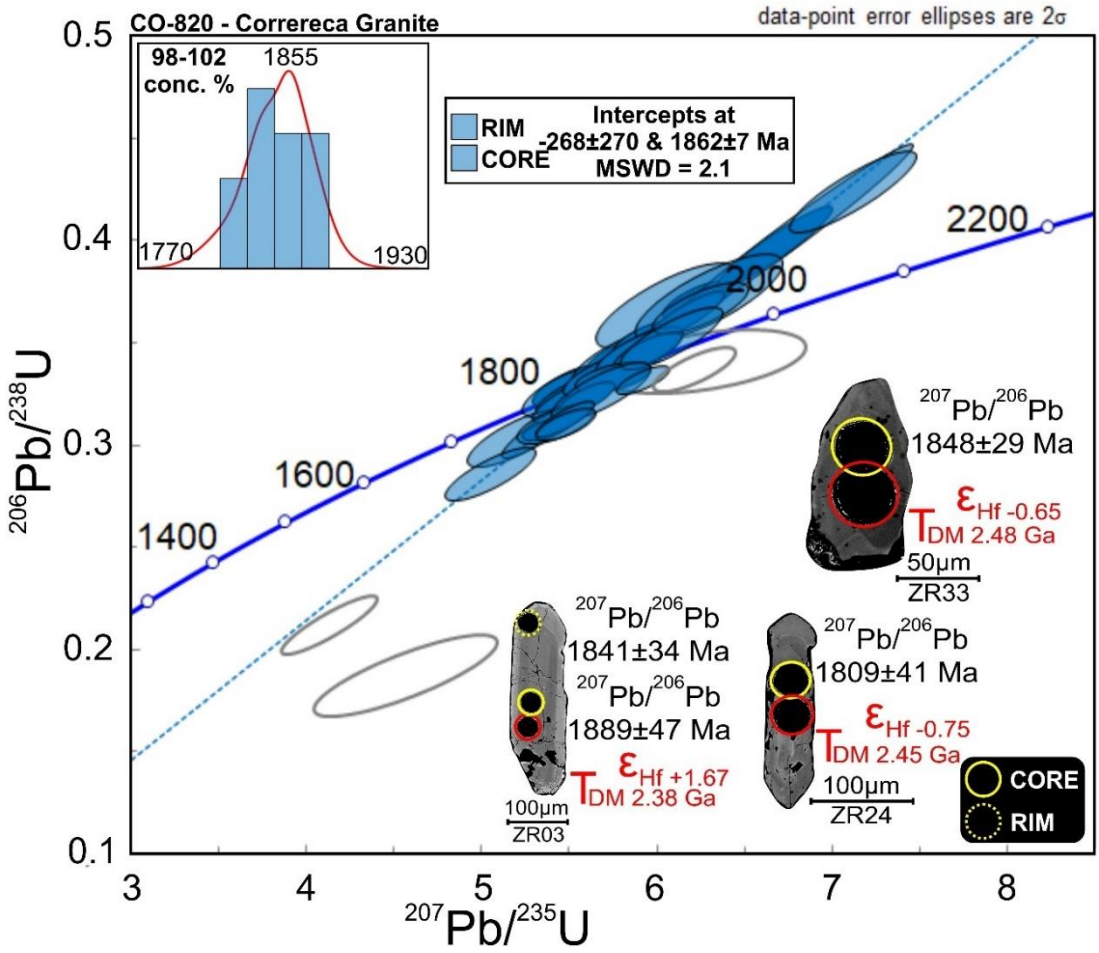

Figure 4.12. U-Pb isotope analysis for the Correreca Granite, sample CO-820. The distribution of U-Pb data in the Wetherill Concordia Diagram indicates an upper intercept age at 1861±7 Ma, which is interpreted as the crystallization age of this granite. BSE images of zircon with 30 µm spots (yellow circles) for U-Pb isotope analysis of zircon, and 40 µm spots (red circles) for Lu-Hf isotope analysis are shown as well.

Santana Gneiss

Sample CLR-04:

From this sample 21 zircon grains were analyzed (Supplementary Table 4.II.5). On the basis of apparent $^{207}Pb/^{206}Pb$ ages, two groups of zircon with upper intercept ages of 1764±23 Ma and 1475±45 Ma are defined. The upper intercept age of 1764±23 Ma (MSWD = 6.2; Fig. 4.13), obtained on cores of crystals that show irregular and chaotic zonation and have Th/U ratios of 0.35 to 0.95, is considered the crystalization age of the protolith of this gneiss. These cores show metamorphic overgrowths with ages averaged to 1693±21 Ma (BSE image in Fig. 4.13).

Two data with ages of 1458 and 1521 Ma define an upper intercept age of 1475±45 Ma (MSWD = 0.0; Fig. 4.13). These data correspond to zircon rims of high Th/U ratios of 0.35 and 0.54. The two oldest ages of 1803 and 1790 Ma from cores correspond to xenocrysts, and the youngest ages between 1768 and 1755 Ma could represent antecrysts/autocrysts. The two youngest ages of 1726 and 1693 Ma could be interpreted as metamorphic ages.

The Lu-Hf isotope analysis was carried out in four zircon crystals. Two crystals with ages of 1766 and 1768 Ma (Table 4.3; Fig.4.14) that are related to the magmatic event that generated the protolith of Santana Gneiss gave slightly negative ε_{Hf} values of -2.07 and -2.55 and Hf model ages of 2.49 and 2.51 Ga. Two grains with U-Pb ages of 1722 and 1755 Ma yielded two slightly positive ε_{Hf} values of +0.22 and +1.53, and Hf model ages of 2.32 and 2.22 Ga.

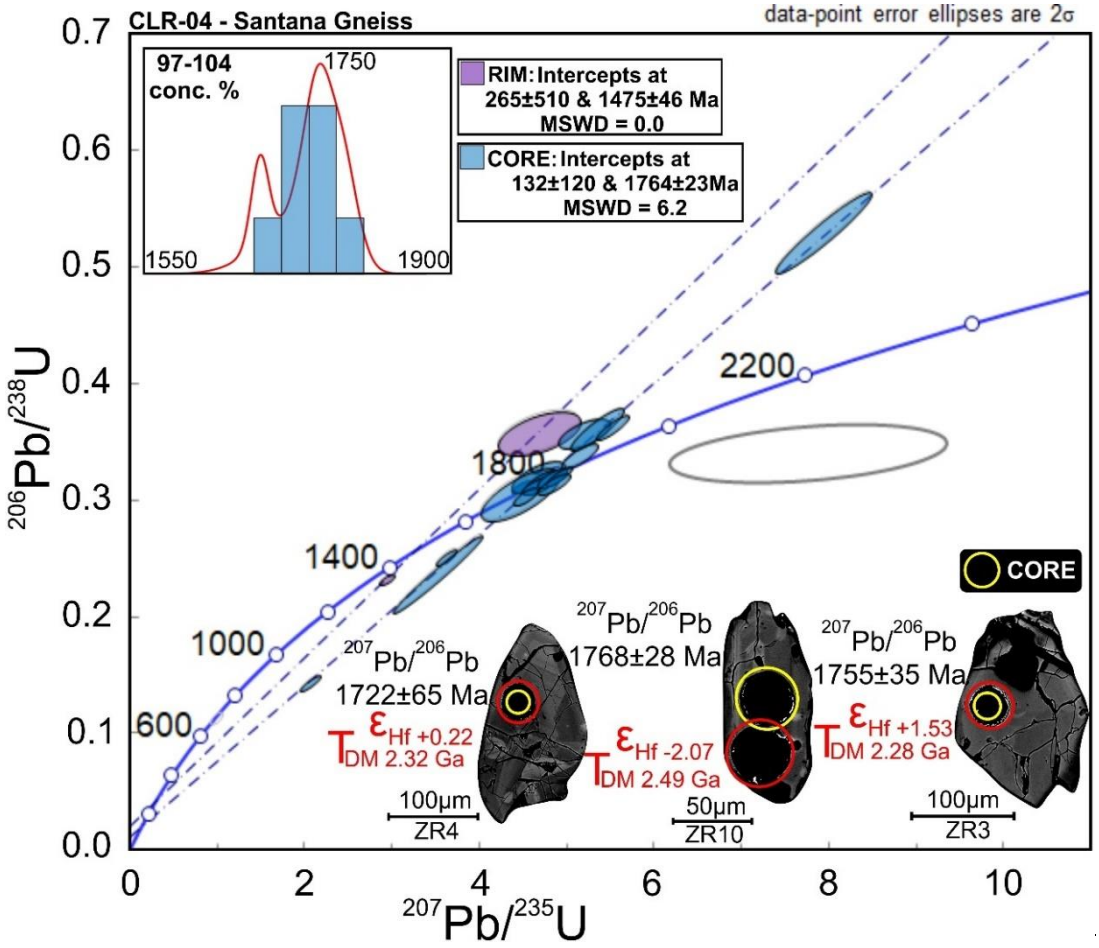

Figure 4.13. U-Pb isotope analysis for the Santana Gneiss, sample CLR-04. The distribution of U-Pb data in the Wetherill Concordia Diagram indicates two upper intercept ages of 1764±23 Ma and 1475±46 Ma. The older upper intercept age of 1764±23 Ma is interpreted as the crystallization

age of the granodioritic protolith. BSE images of representative zircon, with yellow circles representing spots of 30 µm diameter for U-Pb analyses, and red circles representing spots of 40 µm diameter for Lu-Hf analyses, are shown as well.

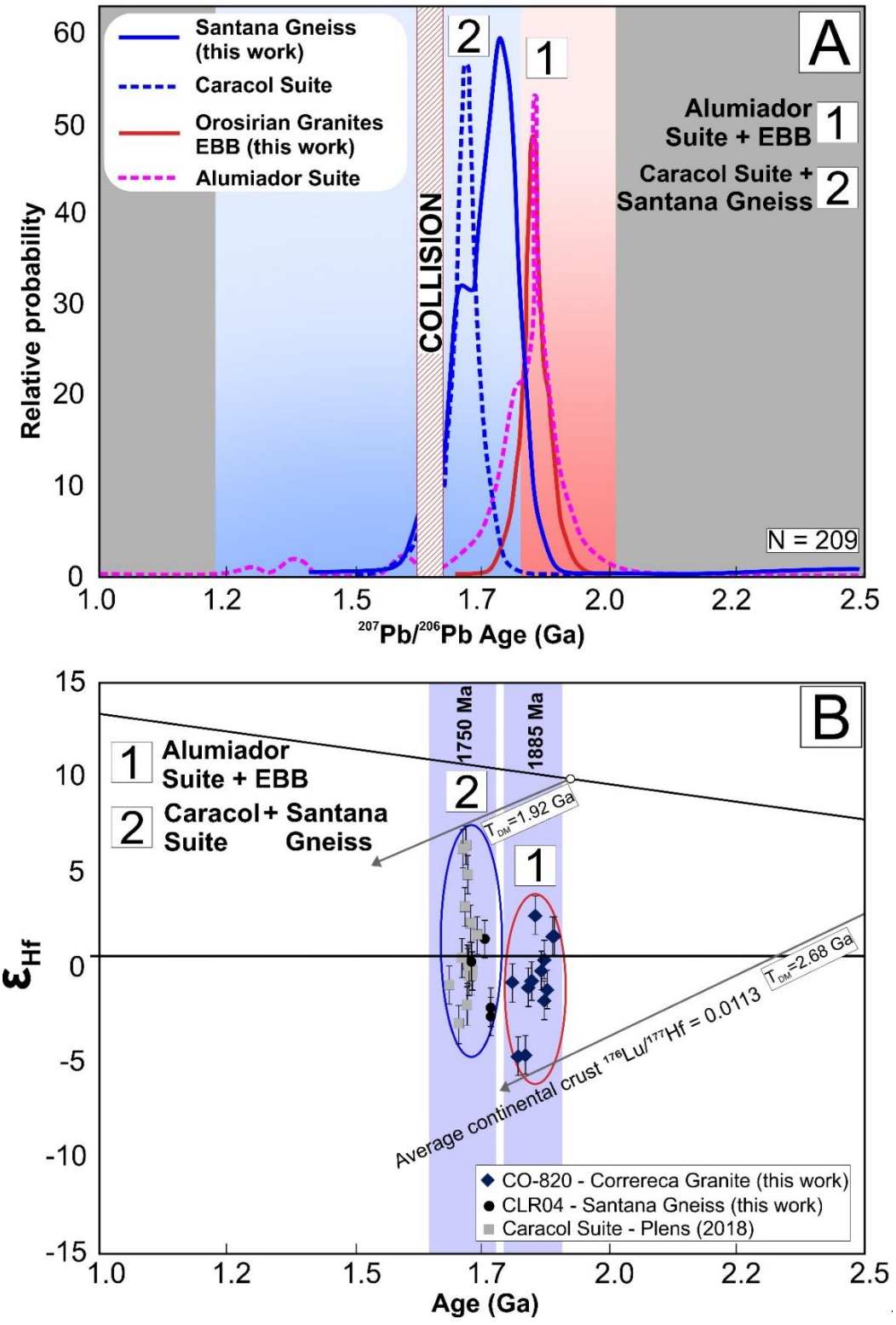

Figure 4.14. (A) Integrated $^{207}Pb/^{206}Pb$ age (with concordance between 95 % and 105%) histogram for samples of this study and data from several authors. Two main magmatic cycles C1 and C2 are observed. (B) Age (Ga) versus ε_{Hf} evolution diagram for zircon crystals from the Santana Gneiss (CLR-04; the present study), Correreca Granite (CO-820; the present study), and Caracol Gneiss (Plens, 2018). The C1 cycle is related to the crustal evolution of the Eastern Bolivian basement granites and the Alumiador Intrusive Suite, part of the Eastern Terrane of the Rio Apa Block , and the much younger cycle C2, is related with the evolution of the Western Terrane of the Rio Apa Block, represented by the Santana and Caracol gneisses. The two arrows indicate the $\varepsilon_{Hf(t)}$ bulk-rock evolution trend for these two terranes. The vertical gray areas indicate the position of these two main cycles. Note that C2 is much younger and more juvenile than C1. The U-Pb data are from: (a) Lacerda Filho *et al.* (2006); (b) Cordani *et al.* (2010); (c) Redes *et al.* (2015); (d) Nogueira (2015); (e) Souza *et al.* (2016); (f) Plens (2018); (g) Santos *et al.* (2019); and (h) the present study.

Table 4.3. Representative results of in situ Lu–Hf LA–ICP-MS–MC zircons analyses for the Correreca Granite and Santana Gneiss.

SAMPLE		CO-820 (Correreca Granite)								
GRAIN	**T (Ma)**	$\frac{^{176}Lu}{^{177}Hf}$	**± 2 б**	$\left(\frac{^{176}Hf}{^{177}Hf}\right)$	**± 2 б**	$\left(\frac{^{176}Hf}{^{177}Hf}\right)$	**± 2 б**	$\varepsilon_{Hf(t)}$	**±1 б**	T_{DM} **(Ga)**
ZR24	1809	0.106741	0.0005419	0.28171585	0.000043	0.28161501	0.000043	-0.75	1.52	2.45
ZR26	1821	0.035400	0.0011464	0.28153179	0.000029	0.28149812	0.000029	-4.63	1.02	2.67
ZR11	1835	0.032055	0.0001575	0.28152136	0.000041	0.28149063	0.000041	-4.57	1.47	2.68
ZR25	1841	0.063268	0.0026504	0.28164692	0.000038	0.28158607	0.000038	-1.05	1.36	2.49
ZR33	1848	0.097346	0.0008713	0.28168660	0.000046	0.28159262	0.000046	-0.65	1.65	2.48
ZR4	1855	0.057658	0.0024021	0.28174016	0.000031	0.28168428	0.000031	2.76	1.09	2.29
ZR19	1868	0.049818	0.0001467	0.28164299	0.000041	0.28159436	0.000041	-0.13	1.46	2.46
ZR18	1873	0.079976	0.0008830	0.28168642	0.000039	0.28160814	0.000039	0.47	1.40	2.43
ZR5N	1873	0.061289	0.0004197	0.28160742	0.000032	0.28154743	0.000032	-1.68	1.12	2.55
ZR16	1877	0.055001	0.0012576	0.28161271	0.000036	0.28155876	0.000036	-1.19	1.27	2.53
ZR3N	1889	0.089693	0.0034353	0.28171999	0.000037	0.28163144	0.000037	1.67	1.33	2.38
ZR15	1891	0.088112	0.0034949	0.28171704	0.000036	0.28162996	0.000036	1.66	1.29	2.38
SAMPLE		**CLR-04 (Santana Gneiss)**								
ZR4	1722	0.066811	0.0010602	0.28175857	0.000058	0.28169854	0.000058	0.22	2.05	2.32
ZR3	1755	0.056875	0.0005658	0.28176627	0.000069	0.28171417	0.000069	1.53	2.45	2.28
ZR2	1766	0.028562	0.0001813	0.28161863	0.000047	0.28159230	0.000047	-2.55	1.69	2.51
ZR10	1768	0.065455	0.0015391	0.28166475	0.000041	0.28160434	0.000041	-2.07	1.44	2.49

4.4.4. Sm-Nd isotope data for whole-rock samples

Sm-Nd isotope data for samples ST-02 and ST-03 from the Santa Terezita Granite gave slightly positive $\varepsilon_{Nd(1.85\ Ga)}$ of +1.76 and +0.25 and Paleoproterozoic Nd T_{DM} ages of 1.96 and 2.08 Ga. Two samples from the Santo Corazón Granite gave negative $\varepsilon_{Nd\ (1.87\ Ga)}$ of -2.73 and -1.07 and Paleoproterozoic Nd T_{DM} ages of 2.27 and 2.14 Ga. For the Correreca Granite, three samples yielded negative $\varepsilon_{Nd\ (1.86\ Ga)}$ values between -1.18 and -0.45, and Paleoproterozoic Nd T_{DM} ages of 2.08 to 1.96 Ga. Samples RM-33 and CLR-04 from the Santana Gneiss provided slightly negative to positive $\varepsilon_{Nd\ (1.76\ Ga)}$ values of -0.21 and +0.62 and Nd T_{DM} ages of 2.04 and 2.00 Ga (Table 4.4; Fig. 4.15).

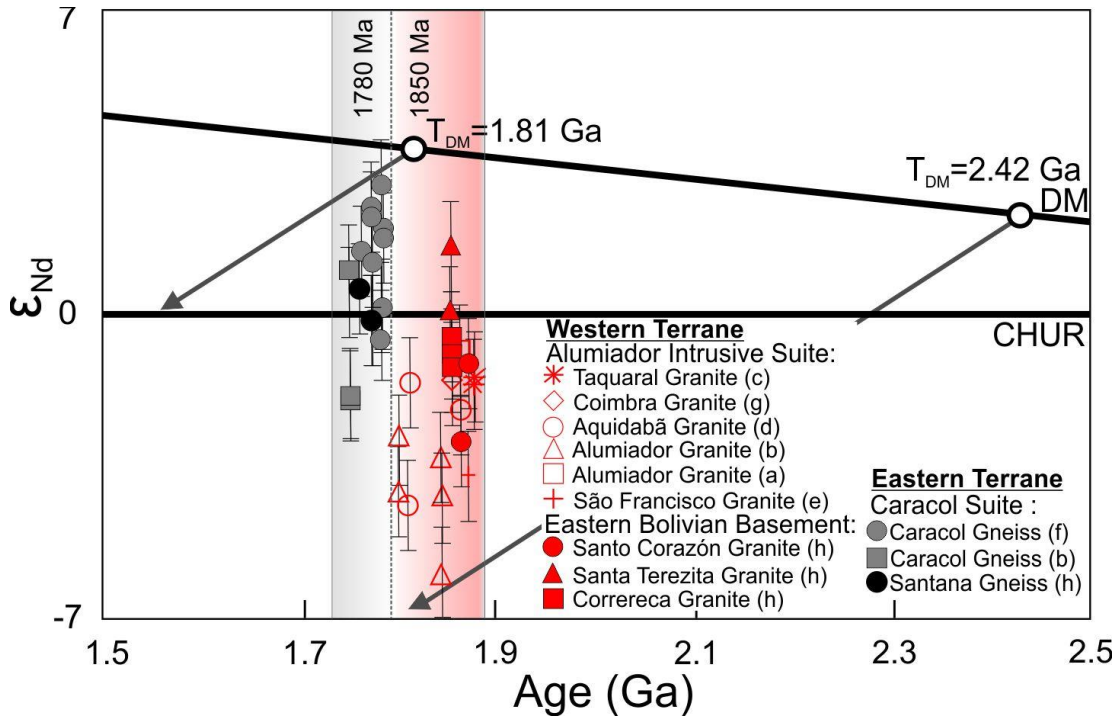

Figure 4.15. (A) Age (Ga) vs. ε_{Nd} diagram for Santo Corazón, Santa Terezita and Correreca granite samples, and the Santana Gneiss. For comparison, values from the Alumiador Intrusive Suite and from the Caracol Suite that represent the Western and Eastern terranes of the Rio Apa Block, respectively, are also plotted. Data from (a) Lacerda Filho *et al.* (2006); (b) Cordani *et al.* (2010); (c) Redes *et al.* (2015); (d) Nogueira (2015); (e) Souza *et al.* (2016); (f) Plens (2018); (g) Santos *et al.* (2019); and (h) the present study.

Table 4.4. Sm-Nd data for the Santo Corazón, Santa Terezita, and Correreca granites and the Santana Gneiss.

Sample	Lithology	Age (Ma)	Sm (ppm)	Nd (ppm)	$^{147}Sm/^{144}Nd$	$^{143}Nd/^{144}Nd_m$ (±2σ)	$\varepsilon_{Nd(0)}$	$\varepsilon_{Nd(t)}$	T_{DM} (Ga)
SC-824	Santo Corazón Granite	1874	5.637	32.011	0.1065	0.511388±15	-24.38	-2.73	2.27
SC-1328	Santo Corazón Granite	1874	5.371	32.031	0.1014	0.511410±13	-23.95	-1.07	2.14
CO-1329	Correreca Granite	1862	9.479	52.911	0.1083	0.511496±15	-22.28	-1.18	2.08
CO-822	Correreca Granite	1862	9.331	53.099	0.1062	0.511508±8	-22.04	-0.45	1.96
CO-820	Correreca Granite	1862	8.323	50.411	0.0998	0.511412±13	-23.92	-0.79	2.12
ST-03	Santa Terezita Granite	1853	8.771	45.528	0.1165	0.511669±6	-18.90	0.25	2.08
ST-02	Santa Terezita Granite	1849	7.602	42.821	0.1073	0.511634±10	-19.58	1.76	1.96
RM-33	Santana Gneiss	1764	5.4900	26.5600	0.1249	0.511839±7	-15.59	0.62	2.00
CLR-04	Santana Gneiss	1764	5.1500	26.2100	0.1188	0.511725±7	-17.81	-0.21	2.04

4.5. DISCUSSION

4.5.1. Tectonic environment of the Eastern Bolivian basement granites and Santana Gneiss (Brazil)

The Santo Corazón, Correreca, and Santa Terezita granites represent the oldest basement of Eastern Bolivia. Their U-Pb zircon crystallization ages vary from 1874 to 1849 Ma, and the Nd isotopic compositions suggest that the Epsilon Nd values changed from negative to positive with time. The Santo Corazón Granite with a crystallization age of ~1.87 Ga exhibits negative initial $\varepsilon_{Nd\ (1.87)}$ values of -2.73 and -1.07, the Correreca Granite with an age of 1.86 Ga shows similar but less negative initial ε_{Nd} values of -1.18 and -0.45, and the Santa Terezita Granite with an age of 1.85 Ga that represents the youngest granite of the basement of Eastern Bolivia displays a rather narrow, positive range of initial $\varepsilon_{Nd\ (1.85)}$ values of +0.25 and +1.76. All of these bodies have Paleoproterozoic Nd model ages between 2.27 and 1.96 Ga.

The geochemical data indicate that the granites from the Eastern Bolivian basement are magnesium-rich, peraluminous, and classified as S-type granites generated in a volcanic arc setting. The negative to positive range of initial $\varepsilon_{Nd(t)}$ values, that become more positive for the youngest granite, the Santa Terezita Granite, and the negative to positive $\varepsilon_{Hf(t)}$ values between -4.63 and +2.76 shown by the Correreca Granite, as well as the abundant xenocrysts allow to infer that these granites represent reworking of a Paleoproterozoic crust and that a mantellic input was important.

Possible decoupling between Nd (negative) and Hf (positive to negative) data can be observed for the Correreca Granite. This decoupling could be explained by the model of Zhang *et al*. (2019a), who discussed a case in which sediment recycled in a subduction zone lead to decoupling of the Nd and Hf isotope systems. Neodymium isotopes provide more accurate estimates of features of granitic magma sources. Thus, it is possible to interpret that the difference between negative $\varepsilon_{Nd(t)}$ and positive $\varepsilon_{Hf(t)}$ values recorded for the Correreca Granite may be based on the recycling of components that return towards the crust during subduction, a process that

may be related to granites generated in a magmatic arc environment. At this point, we have no other information that could be used to further analyse these ideas.

In the Corumbá region, iron-rich, peraluminous granitoids of granodioritic and quartz-monzonitic composition, and with–calc-alkaline to alkaline-calcic character, represent the protoliths for the Santana Gneiss. These protoliths have low to high potassium, and were seemingly generated in a magmatic arc environment later than the Eastern Bolivian basement granites, at 1764±23 Ma. In terms of Nd isotopic composition, the Santana Gneiss has slightly positive to negative ε_{Nd} values (+0.62 to -0.21) and T_{DM} between 2.00 and 2.04 Ga, which indicates derivation from Paleoproterozoic crust.

4.5.2. Spatial association of the Eastern Bolivian basement granites and Santana Gneiss (Brazil) with the Rio Apa Block

The Rio Apa Block (Cordani *et al*., 2010) is part of a cratonic domain in the Paraguay Belt, which is composed of medium-grade metamorphic rocks of Paleo- to Mesoproterozoic ages and extends further south into Paraguay territory and into the southwestern Mato Grosso do Sul State of Brazil (Figs. 4.1 and 4.2). The block is composed of a series of plutonic and supra-crustal units of Orosirian and Statherian age (ca. 2050 – 1600 Ma, Cordani *et al*., 2010; Teixeira *et al*., 2020). This crustal fragment was intruded by Orosirian and Statherian granites that, in turn, are covered by Neoproterozoic carbonates of the Corumbá and Itapocumi groups (Almeida, 1965, 1967; Alvarenga *et al*., 2000; Boggiani and Alvarenga, 2004).

Lacerda Filho *et al*. (2006) subdivided the Rio Apa Block into three different geotectonic parts: i) the Alto Tererê Metamorphic Complex, which was considered a remnant of oceanic crust of Riacian age; ii) the Rio Apa Magmatic Arc of Orosirian age, which is equivalent to gneiss from the Rio Apa Complex; and iii) the Amonguijá Magmatic Arc of Statherian age, which comprises the Serra da Bocaina Formation and granites of the Alumiador Intrusive Suite. Cordani *et al.* (2010) divided the Rio Apa Block in Western and Eastern terranes (Fig. 4.2). Supplementary Table 4.I.1 summarizes the published U-Pb, Rb-Sr, Ar-Ar, and Sm-Nd data for rocks of the Rio Apa Block.

The geochemical signature, the U-Pb ages, the ε_{Nd} values and model ages of the monzogranitic to syenogranitic rocks seem to indicate that the Eastern Bolivian granites are similar with the Alumiador Intrusive Suite related to the evolution of the Amonguijá Magmatic Arc (Lacerda Filho *et al*., 2006), which is located in the Western Terrane of the Rio Apa Block (Fig. 4.2). The geochemical data, U-Pb ages, and Nd-Hf isotopic composition of the Santana Gneiss indicate that it could be related with the Caracol Suite of the Eastern Terrane of the Rio Apa Block.

The Alumiador Intrusive Suite involves biotite granitoids of granodiorite to syenogranite compositions and~~,~~ of syn-collisional to post-collisional calc-alkaline character (Teixeira *et al*., 2020). This suite is exposed in the Alumiador, São Miguel, São Paulo and Paraguai mountains, and in some isolated locations along~~at~~ the western border of the Bodoquena Mountain (MS), and in the Corumbá region (Cordani *et al.*, 2010; Redes *et al.*, 2015; Santos *et al.*, 2019, Teixeira *et al*., 2020), where it is represented by the Taquaral and Coimbra granites of the Alumiador Intrusive Suite (Redes *et al*., 2015; Santos *et al*., 2019). Based on the data fromour current study, it is possible to propose that the Rio Apa Block extends towards Western Bolivia, into the Southern Tucavaca Aulacogen. This, then allows to delineate a new border between the Paraguá and Rio Apa blocks (Fig.4.1 and 4.17). With this assumption, the. Santa Terezita, Santo Corazón and Correreca granites could represent an extension of the Rio Apa Block into the eastern part of Bolivia.

Older concordant populations with ages older than 1900 Ma were also found, and those crystals are interpreted as xenocrysts. Such older ages were also found for the Piatã Granite of the Alumiador Intrusive Suite and the host rock to this suite, the Porto Murtinho Complex (1.9 Ga) (Cordani *et al*., 2010; Pavan *et al*., 2014). It can be interpreted that these zircon crystals and those that gave upper intercept ages of ~ 1900 to 2260 Ma were inherited from the Porto Murtinho Complex.

The older zircon population with ages of ~1800-1790 Ma from the Santana Gneiss may correspond to zircon xenocrysts that could have been inherited from the gneiss of the Paso Bravo

Complex or Morraria Gneiss that are intruded by the Caracol Suite (~1.8 to ~1.9 Ga; Cordani *et al*., 2010).

The Orosirian granites and the Santana Gneiss from Eastern Bolivia and the Corumbá (MS) region of Brazil analyzed in this study, thus, could have been part of the evolution of the Rio Apa Block. The Orosirian granites would belong to the Alumiador Intrusive Suite and correspond to the development of the Western Terrane of the Rio Apa Block. In contrast, the Santana Gneiss would be part of the Caracol Suite related to the evolution of the Eastern Terrane of the block. Thus, in the further discussion we will call the Eastern Bolivian basement granites and Santana Gneiss "EBB-SG".

This interpretation of the basement in Eastern Bolivia constitutes a new development, as in earlier literature the rocks of the study region were treated as part of the basement of the Paraguá Block, without any specific designation or interpretation of the occurrence of the gneissic rocks in the Corumbá region. Our work contributes something new, namely the possible extension of the Rio Apa Block (RAB) to the north of the state of Mato Grosso do Sul (Corumbá), and to the east into Bolivia.

4.5.3. Crustal growth of the EBB-SG+RAB

Using Nd model ages, Cordani *et al*. (2010) proposed that the Rio Apa Block is composed of two different tectonic terranes with different evolution, known as the Western and Eastern terranes. These terranes are delimited by a N-S suture zone (ibid) and have diferent Nd model ages. The first metamorphic event took place at approximately 1670 Ma and was marked by medium to high grade metamorphism and ductile tectonics, and regional homogenization of Sr isotope systematics (ibid). Metamorphic age data suggest that these terranes were attached to each other during a second, low grade metamorphic event. The age of this event was constrained by K-Ar and Ar-Ar ages to ~ 1300 Ma (ibid). This second metamorphic event was responsible for an increase of temperature to 350-400°C, as determined from the argon blocking temperature of mica).

The Western Terrane, composed the Orosirian granites of the eastern part of the Bolivian basement (EBB, this work) and the granites from the Alumiador Intrusive Suite (Fig. 4.3) older than the Eastern Terrane, having been built up between 1880 and 1811 Ma ago. The Eastern Terrane, represented by the Santana Gneiss (this work) and the Caracol Suite (Plens, 2018), is comparatively younger, with the main construction period constrained to about 1760 to 1720 Ma ago. Here, we suggest that two cycles (C1 and C2) can be identified - in terms of $^{207}Pb/^{206}Pb$ ages - during the construction of the Rio Apa Block (Fig.4.14). The term cycle designates intervals of maximum zircon generation, which would represent peaks of magmatic input, possibly related to flare-up phases (Ducea *et al*., 2015). In this way, Cycle 1 corresponds to the evolution of the Western Terrane and Cycle 2 corresponds to the evolution of the Eastern Terrane. The $^{207}Pb/^{206}Pb$ ages obtained during this study are plotted together with data from the literature in Fig. 4.14, where it is possible to see that the EBB and Alumiador Intrusive Suite were built up over a long period of ~170 Ma between 1890 and 1720 Ma.

Cycle C1 (1.8 Ga), represented by the EBB granites analyzed here, is characterized by ε_{Hf} values between +2.76 and -4.63 and Hf T_{DM} of 2.29 Ga to 2.68 Ga. **Cycle C2 (1.7 Ga**) is represented by the Santana Gneiss and shows positive to negative ε_{Hf} values between +1.53 and -2.07 and Hf T_{DM} of 2.28 Ga and 2.51 Ga. In contrast, the Caracol Suite granites falling into the same cycle (Plens, 2018) have mainly positive but also a few negative ε_{Hf} values between +5.32 and -4.64, and Hf T_{DM} of 1.92 to 2.30 Ga (also Plens, 2018). These data indicate that Cycle 2, which is younger than Cycle 1, has more juvenile characteristics compared to Cycle 1 (Fig. 4.14).

4.5.4. Spatial relationship between the EBB-SG+RAB and neighbouring terranes: Rio Negro Juruena Province (Amazonian Craton) and Paraguá Block

The Orosirian granites from the eastern basement of Bolivia (EBB), as well as the Rio Apa Block, are limited by the Paraguá Block to the west and the Rio Negro-Juruena Province to the northeast (Fig. 4.1). These terranes are, to a large extent, built up of granites (Tassinari and Macambira, 2004, Bettencourt *et al*., 2010; Cordani *et al*., 2010). When the Eastern Bolivian granites are compared with the granitic rocks of the Rio Negro-Juruena Province (Fig. 4.16), they

show similar characteristics in terms of petrology and age. Cordani *et al*. (2010), Lacerda Filho (2015), and Plens (2018) positioned the Rio Apa Block as a segment of the Amazonian Craton, into the general evolutionary scheme of the Rio Negro-Juruena Province (Tassinari and Macambira, 1999).

As discussed already, the Rio Apa Block is composed of two parts, the Eastern Terrane formed by granitic and gneissic rocks of ~1760 Ma age, and the Western Terrane composed of comparatively older rocks of ~1900-1800 Ma age. For the evolution of the Amazonian Craton, several authors (e.g., Tassinari and Macambira 1999; Santos *et al*., 2000) suggested crustal accretion episodes along a trend from the east to the west, with the youngest rocks ocurring in the western part of the craton. When this age zonation is compared with the age zonation of the Rio Apa Block, with oldest rocks to the west and youngest rocks to the east, it is possible to see that the geochronological disposition exhibited by the Amazonian Craton is the opposite of the geochronological disposition indicated by rocks from the Rio Apa Block. Consequently, it is difficult to imagine that the Rio Apa Block was part of the Amazonian craton around that time.
Most of the available U-Pb geochronological data indicate that the basement of the Paraguá Block is dominated by rocks younger than the EBB+RAB. The Nd isotopic data show that rocks from this block (T_{DM} of 1500-2050 Ma) are derived from different, mainly younger sources than the source(s) for the basement of the Rio Apa Block (T_{DM} of 2000-2600 Ma). Besides being younger, the rocks from the Paraguá Block were derived from isotopically different sources, and this is strong evidence against a common evolution for the Paraguá and Rio Apa blocks (Lacerda Filho *et al.*, 2006, Cordani *et al.*, 2010; Santos *et al.*, 2008; Matos *et al.*, 2009; this work).

The present study argues that the Rio Apa Block extends for approximately 300 km towards the western region of Bolivia. This means that a new delimitation between the Paraguá and Rio Apa blocks must be considered, based on the presence of Orosirian granitic rocks and Nd model age constraints that previously had not been registered, as well as analysis of satellite and relief images that allowed to estimate the suture zone between these blocks. Previous research considered the basement of Eastern Bolivia as part of the Paraguá Block that involved the rocks of the Lomas Maneches Complex, Chiquitania Complex, and San Ignácio Group with ages

between 1660 and 1700 Ma, and also of 1820 Ma (Litherland *et al*., 1986,1989; Boger *et al*., 2005; Santos *et al*., 2008).

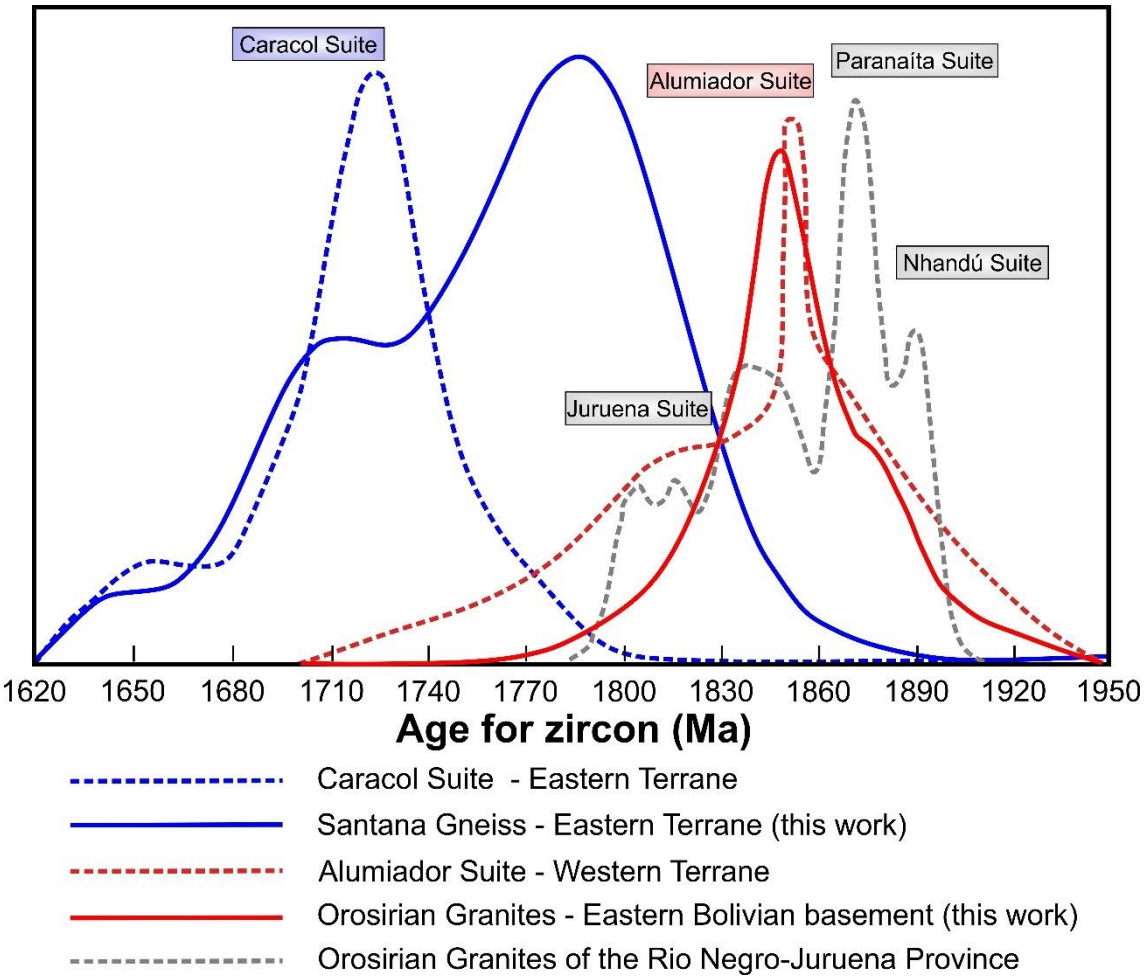

Figure 4.16. Histogram of U-Pb concordia ages for zircon crystals from the Orosirian granites from the Eastern Bolivian Basement (EBB) and Santana Gneiss (SG), and from the Alumiador and Caracol suites of the Rio Apa Block, as well as the Orosirian granites from the Rio Negro-Juruena Province of the Amazonian Craton (data from: Lacerda Filho *et al*., 2006; Cordani *et al*., 2010; Redes *et al*., 2015; Nogueira, 2015; Souza *et al*., 2016; Plens, 2018; Santos *et al.*, 2019; Pinho *et al*., 2003; Silva e Abram, 2008; Santos *et al*., 2000, JICA/MMAJ, 2000; Tassinari *et al*., 1996; Assis, 2011; Assis, 2015; Silva *et al*., 2014; Moura 1998; Lamarão, 2001; Vasquez *et al*., 2000; Vasquez *et al*., 2001).

4.5.5. Accretionary Events

The evolution of the Rio Apa Block has been discussed for a long time. Some authors (Ruiz *et al*., 2005; Lacerda Filho *et al*., 2006; Lacerda Filho, 2015) postulated that the Rio Apa Block was a segment of the Amazonian Craton and constituted basement of the Paraguá Belt and Tucavaca Aulacogen. These workers interpreted the Rio Apa Block as an extension of the Rio Negro-Juruena Province (Tassinari and Macambira, 1999; Cordani *et al*., 2010; Lacerda Filho, 2015; Plens, 2018). Others (eg., Tassinari and Macambira, 1999, 2004; Santos *et al*., 2000, 2008) considered the Rio Apa Block as an allochthonous crustal fragment that was separated from the Neoproterozoic Tucavaca Belt. According to these authors, the Rio Apa Block became attached to the Amazonian Craton during the amalgamation of Gondwana or, alternatively, during the Sunsas Orogeny (1.0 Ga). On the basis of our new data, we can interpret the following events:

Paleoproterozoic Accretionary Events: ~1700 and 1690 Ma

This event is indicated by the Santa Terezita Granite located at the border between the Rio Apa and Paraguá blocks. Three rims of zircon from this granite gave a concordia age of 1722±7 Ma (Fig. 4.10 B);-the Th/U ratios for these rims are 0.1, which is normal for metamorphic zircon, according to Rubatto (2017). Thus, the age of ca. 1.7 Ga found only at the western border of the EBB + Rio Apa Block, specifically in the Santa Terezita Granite, can be interpreted as related to the collision between the Rio Apa and Paraguá blocks. The ages of ~1.7 Ga found in zircon crystals from the Chiquitania Complex (Redes *et al*., in final preparation) reinforce this hypothesis.

We determined, for the Santana Gneiss, a U-Pb interval of ~1770-1755 Ma that likely represents a population of antecrysts/autocrysts, but a second range of ages of ~1730-1690 Ma was also observed. This interval could be related with the metamorphic event linked to the collision event between the Eastern and Western terranes of the Rio Apa Block, which according to Cordani *et al*. (2010) occurred at about 1690 Ma.

Mesoproterozoic Accretionary Events: 1.3 Ga

An age of 1.3 Ga, commonly related to the San Ignácio Orogeny (Bettencourt *et al*., 2010), was obtained from the rims of four zircon crystals from the Santa Terezita Granite and also for zircon from the Santana Gneiss (1475±45 Ma). These results may indicate a metamorphic stage related to the San Ignácio Orogeny. This might suggest that the Paraguá Block and the EBB+RAB collided with the Amazonian Craton in the course of the San Ignácio orogeny (Fig. 4.17). The Rondonian-San Ignácio Orogeny was a significant event between 1560 and 1300 Ma, which affected a large area along the Brazil-Bolivia border (Cordani *et al*., 2010; Bettencourt *et al*., 2010). The age of ~1.3 Ga for the rims of zircon crystals from the westernmost body investigated here, the Santa Terezita Granite, and from the Santana Gneiss, indicates that higher temperature affected these bodies during times of the San Ignácio Orogeny, when compared with other rocks of the Aluminador Intrusive Suite.

Until now, an indication of this collision was supported only by K-Ar and $^{40}Ar/^{39}Ar$ ages of 1300 Ma obtained on mica and amphibole from the Alumiador Intrusive Suite (Cordani *et al*., 2010). This orogeny is also registered in other units of the Paraguá Block, such as the Chiquitania Complex, which is characterized by deformation and metamorphism (Bettencourt *et al*., 2010). This demonstrates that the San Ignácio Orogeny generated metamorphism of regional extension. At approximately 1000-1100 Ma ago, the collision between the Amazonian and Laurentian blocks resulted in the Sunsas Orogeny (Brito Neves and Fuck, 2014) that resulted in the amalgamation of the Rodinia supercontinent. The Paraguá Block and EBB+RAB registered this orogeny but behaved as a stable cratonic terrane (Litherland *et al.*, 1989; Boger *et al.*, 2005; Teixeira *et al.*, 2010; Cordani *et al.*, 2010).

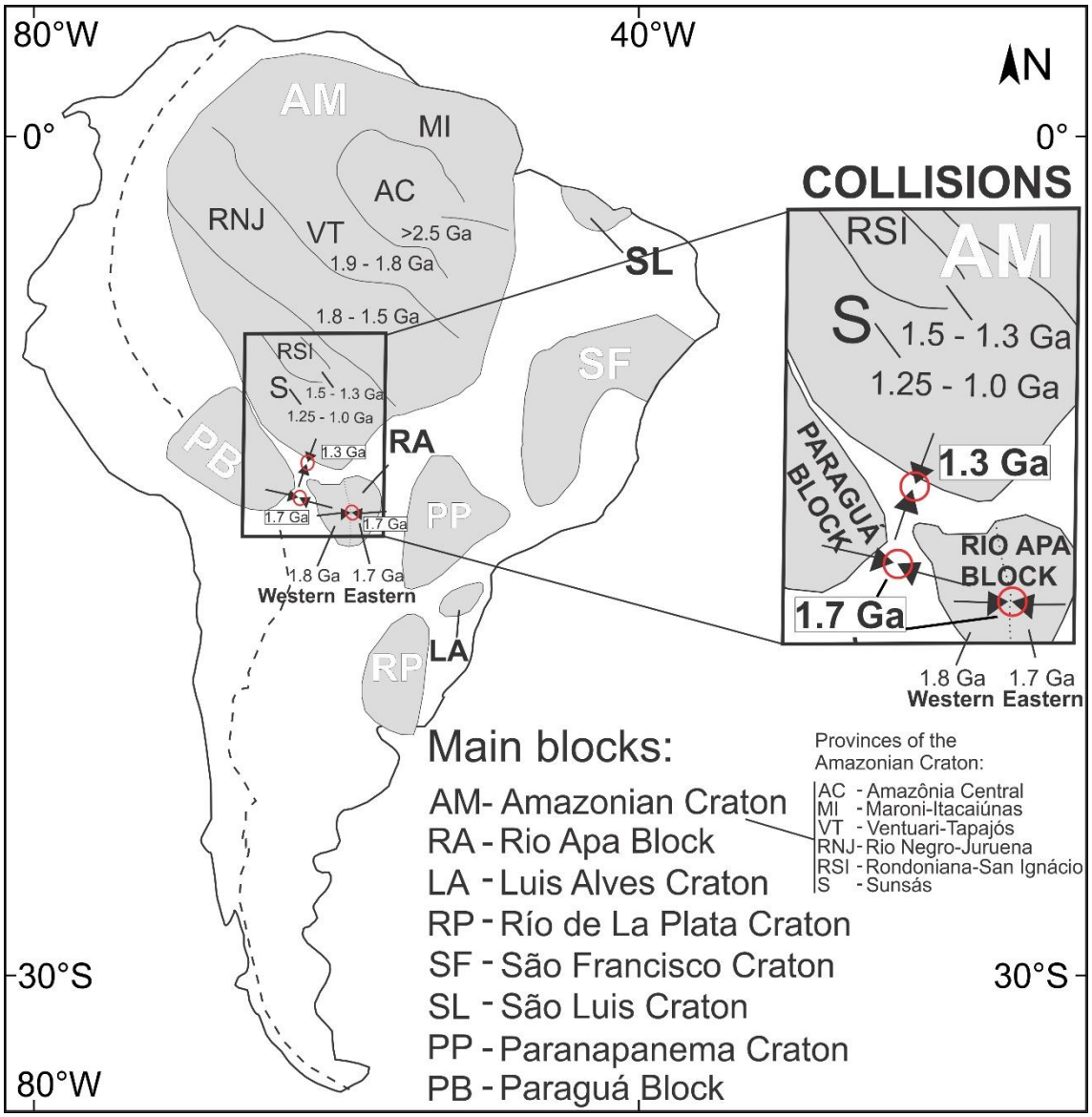

Figure 4.17. Schematic geotectonic map of South America, where the positions of the main cratons and blocks are indicated, with emphasis on suggested collisions between the EBB-SG+Rio Apa and Paraguá blocks, and the Amazonian Craton – as based on the results from this study (cf. Discussion of detail).

4.6. CONCLUSIONS

We are presenting new U-Pb, Sm-Nd, and Lu-Hf isotope data for zircon from three Orosirian granites and the Santana Gneiss body. Major results of this work and implications for tectonic processes along the western margin of Gondwana are:

1. The Santa Terezita Granite occurs at the southern margin of the Tucavaca Aulacogen, in the San José de Chiquitos region. A 1.85 Ga age obtained in cores of zircon from this granite is

considered the age of crystallization. In addition, Nd T_{DM} and slightly positive ε_{Nd} values allow to interpret that the Santa Terezita Granite has a crustal signature that includes a mantle-derived component.

- A ~1.3 Ga age determined in rims of zircon crystals from the Santa Terezita Granite shows that this granite was affected by the San Ignácio Orogeny.

- The Santa Terezita Granite is located in the far west of the study area at the border between the Rio Apa and Paraguá blocks. Given its location and assuming that the age of ~1.7 Ga obtained in rims of some zircon crysrals is associated with the deformation of this granite, this intrusion can be related to the collision between the EBB+RAB and Paraguá blocks. The age of 1.3 Ga related to the San Ignácio

Orogeny also suggests that these two blocks collided with the Amazonian Craton during this orogeny.

2. The Santo Corazón and Correreca granites are located in the southern San Diablo Shear Zone of the Santo Corazón region. A 1874 Ma age obtanied for the Santo Corazón Granite is interpreted as the age of crystallization. The negative ε_{Nd} and Paleoproterozoic T_{DM} indicate that this body has a Paleoproterozoic crustal origin. The Correreca Granite has a crystallization age of 1862 Ma, a Paleoproterozoic Nd T_{DM}, and a negative ε_{Nd} also suggestive of a Paleoproterozoic crustal signature. The Hf on zircon data for the Correreca Granite could indicate mantellic derivation with crustal contamination.

3. Granites from Western Bolivia typically have magmatic arc signature and have been associated with the Amonguijá Magmatic Arc. The protoliths for the Santana Gneiss, in contrast, were likely related to the Rio Apa Magmatic Arc.

4. The Santana Gneiss has a Statherian age of 1764 Ma that is considered as the crystallization age for the igneous protolith. The slightly positive to negative ε_{Nd} and the Nd T_{DM} ages indicate derivation from Paleoproterozoic protoliths. Hafnium isotopic results suggest assimilation of older crust by a mantellic parental magma. The ~1.7 Ga age for the protolith of the Santana Gneiss is related to collision between the Western and Eastern terranes, which were amalgamated into the Rio Apa Block between 1680 and 1700 Ma (Cordani *et al*., 2010).

5. The Correreca, Santa Terezita, and Santo Corazón granites can be correlated with the Alumiador Intrusive Suite of the Western Terrane of the Rio Apa Block. In contrast, the Santana Gneiss can be correlated with the Caracol Suite of the Eastern Terrane. The Rio Apa Block, thus, can be extended into Eastern Bolivia. The studied granites registered at least two collisions, one between the Rio Apa and Paraguá blocks at approximately 1.7 Ga, and the second one between the resulting fragment with the Amazonian craton at 1.3 Ga during the Rondonian-San Ignacio orogeny. Thus, the Rio Apa Block would be related to the end of the evolution of the southwestern Amazonian Craton, and it became agglutinated to the Amazonian Craton during the San Ignácio Orogeny.

6. Our results for the eastern region of Bolivia provide a new perspective on the geological evolution of this terrane and on the Rio Apa Block. However, our results are demonstrably highly complex, and more robust U-Pb dating would certainly be important to better delineate both magmatic and metamorphic events. For metamorphic events, it would be of great value to obtain U-Pb data from other minerals, such as monazite and titanite. Regarding the classification of autocrysts and antecrysts, it is necessary to apply a U-Pb method with great spatial in-situ resolution, i.e. ion-probe dating, to obtain smaller errors. This may perhaps show that the intervals between magmatic pulses were actually shorter than currently assumed, and as has been proposed in the literature (e.g., Matzel *et al*., 2006, Miller *et al*., 2007).

4.7. ACKNOWLEDGEMENTS

This work was possible thanks to financial support from the National Council for Scientific and Technological Development (CNPq) of Brazil under grant 141387/2015-7 to L.A.R., and an INCTET grant. The work by NH, E.L.D and WUR has been in part supported by Brazilian National Council for Scientific and Technological Development (CNPq) fellowships (grants 309878/2019-5, 465613/2014-4 and 305761/2019-6, respectively).

We would like to dedicate this manuscript to the memory of Márcio M. Pimentel, for his support and dedication.

4.8. REFERENCES

Albarède, F., Telouk, P., Blichert-Toft, J., Boyet, M., Agranier, A., Nelson, B., 2004. Precise and accurate isotopic measurements using Multiple-Collector ICPMS. Geochimica et Cosmochima Acta, 68, 2725–44.

Almeida, F.F.M., 1965. Geologia da Serra da Bodoquena (Mato Grosso). Boletim da Divisão de Geologia e Mineralogia, 219, 1-137.

Almeida, F.F.M., 1967. Origem e evolução da plataforma brasileira. Rio de Janeiro. Boletim da Divisão de Geologia e Mineralogia, 241, 29- 36.

Alvarenga, C. J. S., Moura, C. A. V., Gorayeb, P. S. S., Abreu, F. A. M. 2000. Paraguay and Araguaia belts. In: Cordani, U. G., Milani, E. J., Thomaz Filho, A., Campos, D. A. (Eds.). Tectonic Evolution of South America. Rio de Janeiro, 31st. IGC, 183-193.

Assis, R.R., 2011. Depósitos Auríferos Associados ao Magmatismo Granítico do Setor Leste da Província Aurífera Alta Floresta (MT), Cratón Amazônico: Tipologia dasMineralizações, Modelos Genéticos e Implicações Prospectivas. Dissertação de Mestrado, Instituto de Geociências, Universidade de Campinas.

Assis, R.R., 2015. Depósitos Auríferos Associados ao Magmatismo Félsico da Província de alta Floresta (MT), Cratón Amazonico: Litogeoquímica, Idade das mineralizações e Fonte dos Fluidos. Tese de Doutorado, Universidade de Campinas.

Barker, F., 1979. Trondhjemites: definition, environment and hypotheses of origin. In: Barker F. (Ed.), Trondhjemites, Dacites and Related Rocks. Amsterdam, Elsevier, pp.1-12.

Berrangé, J. P., 1982. The Eastern Bolivia mineral exploration project "Proyecto Precámbrico". Episodes, 4, 3-8.

Bettencourt, J.S., Leite, Jr. W.B., Ruiz, A.S., Matos, R., Payolla, B.L., Tosdal, R.M., 2010. The Rondonian-San Ignácio Province in the SW Amazonian Craton: an overview. Journal of South American Earth Sciences, 29, 28-46.

Boger, S.D., Raetz M., Giles, D., Etchart, E., Fanning, C.M., 2005. U and Pb age data from the Sunsas region of eastern Bolivia, evidence for the allochtonous origin of the Paraguá Paragua Block. Precambrian Research, 139, 121-146.

Boggiani, P. C., Alvarenga, C.J.S., 2004. Faixa Paraguai. In: Mantesso-Neto, V., Bartorelli, A., Carneiro, C. D. R., Brito-Neves, B. (Eds.), Geologia do Continente Sul-Americano. São Paulo, Beca, 1, 113-118.

Bouvier, A., Vervoort, J. D., Patchett, J. P., 2008. The Lu–Hf and Sm–Nd isotopic composition of CHUR: Constraints from unequilibrated chondrites and implications for the bulk composition of terrestrial planets. Earth and Planetary Science Letters, 273, 48–57.

Brito Neves B.B., Fuck R.A. 2014. Basement of the South american platform: Half Laurentian (N-NW) + Half Gondwanan. Precambrian Research, 244, 75-86.

Chauvel, C., Blichert-Toft Je., 2001. A hafnium isotope and trace element perspective on melting of the depleted mantle. Earth and Planetary Science Letters, 190, 137–151.

Chu, N.C., Taylor, R.N., Chavagnac, V., Nesbitt, R.W., Boella, R.M., Milton, J. A., German, C.R., Bayon, G., Burton, K., 2002. Hf isotope ratio analysis using multi-collector inductively coupled plasma mass spectrometry: an evaluation of isobaric interference corrections. Journal of Analytical Atomic Spectrometry, 17, 1567-1574.

Cohen, K. M., Finney, S. C., Gibbard, P. L., and Fan, J.-X., 2013. The International Chronostratigraphic Chart. Episodes, 36, 199–204.

Cordani, U.G., Teixeira, W., 2007. Proterozoic Accretionary Belts in the Amazonian Craton. In: Hatcher Jr., R.D., Carlson, M.P., McBride, J.H. (Eds.), 4-D Framework of Continental Crust. Memoir 220, Geological Society of America, 297-320.

Cordani, U.G., Teixeira, W., D'Agrella-Filho, M.S., Trindade, R.I., 2009. The position of the Amazonian Craton in supercontinents. Gondwana Research, 15, 396–407.

Cordani, U.G., Teixeira, W., Tassinari, C.C.G., Coutinho, J.M.V., Ruiz A.S., 2010. The Rio Apa Craton in Mato Grosso do Sul (Brazil) and Northern Paraguay: Geochronological evolution, correlations and tectonic implications for Rodinia and Gondwana. American Journal of Science, 310, 981–1023.

Darbyshire, F. A., White, R. S., Priestley, K. F., 2000. Structure of the crust and uppermost mantle of Iceland from a combined seismic and gravity study. Earth and Planetary Science Letters, 181, 409-428.

DePaolo, D. J., 1981. Trace elemento and isptopic effects of combined wallrock assimilation and fractional crystallization. Earth and Planetary Science Letters, 53, 189-202.

Ducea, M.N., Saleeby, J.B., Bergantz, G., 2015. The Architecture, Chemistry, and Evolution of Continental Magmatic Arcs. Annual Review of Earth and Planetary Sciences, 3, 10.1–10.33.

Faleiros, F.M., Pavan M., Remédio, M.J., Rodrigues, J.B., Almeida, V.V., Caltabeloti, F.P., Pinto, L.G.R., Oliveira, A.A., Pinto de Azevedo, E.J., Costa, V.S., 2016. Zircon U-Pb ages of rocks from the Rio Apa Cratonic Terrane (Mato Grosso do Sul, Brazil): New insights for its connection with the Amazonian Craton in pre-Gondwana times. Gondwana Research, 34, 187-204.

Frost, B.R., Barnes, C.G., Collins, W.J., Arculus, R.J., Elis, D.J., Frost, C.D., 2001. A Geochemical Classification for Granitic Rocks. Journal of Petrology, 42, 2033–2048.

Gerdes, A., Zeh, A., 2009. Zircon formation versus zircon alteration – New insights from combined U-Pb and Lu-Hf in-situ LA-ICP-MS analyses, and consequences for the interpretation of Archean zircon from the Central Zone of the Limpopo Belt. Chemical Geology, 261, 230–243.

Gioia, S. M. C. L., Pimentel, M. M., 2000. The Sm-Nd isotopic method in the geochronology laboratory of the University of Brasilia. Brazilian Academy of Sciences, 72, 219-245.

Hoffman, P.F., 1988. United plates of America, the birth of a craton. Earth and Planetary Science Letters, 16, 543–603.

Jackson, S.E., Pearson, N.J., Griffin, W.L., Belousova, E.A., 2004. The application of laser ablation inductively coupled plasma mass spectrometry to in situ U-Pb zircon geochronology. Chemical Geology 211, 47-69.

JICA/MMAJ. 2000. Japan International Cooperation Agency – JICA/Metal Mining Agency of Japan - MMAJ. Report on the Mineral Exploration in the Alta Floresta Area, Brazil, Final Report, Projeto Alta Floresta - MT, Japan, March, 137p.

Kelemen, P.B., N.Shimizu, T. Dunn, 1993. Relative depletetion of niobium in some arc magmas and the continental crust: partitioning of K, Nb, La, and Ce during melt/rock reaction in the upper mantle, Earth and Planetary Science Letters, 120, 111-134.

Lacerda Filho, J. V., 2015. Bloco Rio Apa: Origem e Evolução Tectônica. Universidade Federal de Brasília, Brasilia, DF, Tese de Doutorado, 181 pp.

Lacerda Filho, J. V., Brito R.S.C., Silva M.G., Oliveira C.C., Moreton L.C., Martins E.G., Lopes R.C., Lima T.M., Larizatti J.H., Valente C.R., 2006. Geologia e Recursos Minerais do Estado de Mato Grosso do Sul, Programa Integração, Atualização e Difusão de Dados da Geologia do Brasil, 10-128.

Litherland, M., Annells, R.N., Appleton, J.D., Berrangé, J.P., Bloomfield, K., Burton, C.C.J., Darbyshire, D.P.F.M., Fletcher C.J.N., Hawkins M.P., Klinck B.A., Lanos A., Mithcell W.I., O Connor E.A., Pitfield P.E.J., Power G. E Webb B.C., 1986. The Geology and Mineral Resources of the Bolivian Precambrian Shield. British Geological Survey Overseas Memoir, 9, 153 pp.

Litherland, M., Annels, R.N., Appleton, J.D., Berrange, J.P., Bloomfield, K., Burton, C.C.J., Darbyshire, D.P.F.M Fletcher C.J.N., Hawkins, M.P., Klink, B.A., Llanos, A., Mitchell, W.I., O Connor, E. A., Pitfield, P.E.J., Power, G. e Werb B.C., 1989. The Proterozoic of eastern Bolivia and its relationship to the Andean Mobile Belt. Precambrian Research, 43, 157-174.

Litherland, M., Bloomfield, K., 1981. The Proterozoic history of eastern Bolivia. Precambrian Research, 15, 157–179.

Klinck, B.A., Litherland, M., 1982. A model for the Proterozoic structural history of eastern Bolivia. Report on Eastern Bolivia Mineral Exploration Project, Santa Cruz, number BAK/15 (unpublished).

Lamarão, C.N. 2001. Geologia, Geoquímica e Geocronologia do Magmatismo Paleoproterozoico da Região de Vila Riozinho, Província Aurífera do Tapajós, Cráton Amazônico. Tese de doutorado, Universidade Federal do Pará.

Ludwig, K.R., 2012. Isoplot 3.75. A Geochronological Toolkit for Microsoft Excel. Special Publication, Berkeley Geochronology Center, 4, 75 pp.

Lugmair, G.W., Marti, K., 1978. Lunar initial $^{143}Nd/^{144}Nd$: differential evolution of the lunar crust and mantle. Earth and Planetary Science Letters, 39, 349-357.

Maniar, P. D. e Piccoli, P.M., 1989. Tectonic discrimination of granitoids. Geological Society of America Bulletin 101, 635-643.

Matos, R., 2010. Geocronologia e Evolução Tectônica Paleo-Mesoproterozoica do Oriente Boliviano – Região Sudoeste do Cráton Amazônico. Universidade de São Paulo, Tese de Doutorado, 240 pp.

Matos, R., Teixeira W., Geraldes, M.C., Bettencourt, J.S., 2009. Geochemistry and Nd–Sr isotopic signatures of the Pensamiento Granitoid Complex, Rondonian- San Ignacio Province. Eastern Precambrian shield of Bolivia: petrogenetic constraints for a Mesoproterozoic magmatic arc setting. Revista Geologia USP - Série Científica, 9, 89–117.

Matteini, M., Dantas, E. L., Pimentel, M. M., Bühn, B., 2010. Combined U-Pb and Lu-Hf isotope analyses by laser ablation MC-ICP-MS: methodology and applications. Academia Brasileira de Ciências, 82, 479-491.

Matzel, J.E.P., Miller, J.S., Mundil, R., Paterson, S.R., 2006. Zircon saturation and the growth of the Cathedral Peak Pluton, CA. 16th Annual V.M. Goldschmidt Conference abstract.

Middlemost, E.A.K., 1985. Magmas and magmatic rocks. An Introduction to Igneous Petrology. London: Longman, 206 pp.

Miller, J.S., Matzel, J.E.P., Miller, C.F., Burgess, S.D., Miller, R.B., 2007. Zircon growth and recycling during the assembly of large, composite arc plutons. Journal of Volcanology and Geothermal Research, 167, 282–299.

Mitchell, W.I., 1979. La geología y potencial de minerales del área de Santo Corazón – Rincón del Tigre (Folha SE 21-5, parte da Folha SE 21-9, parte da Folha SE 21-6 e parte da Folha SE 21-10). Santa Cruz de la Sierra, Serviço Geológico da Bolívia. British Geological Survey, 131pp.

Morel, M.L.A., Nebel O., Nebel-Jacobsen, Y.L., Miller, J.S., Vroon, P.Z., 2008. Hafnium isotope characterization of the GJ-1 zircon reference material by solution and laser ablation MC–ICPMS. Chemical Geology, 255, 231 –235.

Moura, M.A., 1998. O Maciço Granítico Matupá no Deposito Serrinha (Mt): Petrologia, Alteração Hidrotermal e Metalogenia. Tese de Doutorado, Instituto de Geociências, Universidade de Brasília.

Nebel, O., Nebel-Jacobsen, Y., Mezger, K. e Berndt, J., 2007. Initial Hf isotope compositions in magmatic zircon from early Proterozoic rocks from the Gawler Craton, Australia: A test for zircon model ages. Chemical Geology, 241, 23-37.

Nogueira, S. F., 2015. Petrologia, Geocronologia (U-Pb SHRIMP) e Geologia Isotópica (Sm-Nd) do Granito Aquidabã, Arco Magmático Amonguijá-Terreno Rio Apa-Sul do Cráton Amazônico. Dissertação de Mestrado, Universidade Federal de Mato Grosso.

O'Connor, J.T., 1965. A classification for quartz-rich igneous rocks based on feldspar ratios. US Geological Survey, 525B, 79-84.

Oliveira, E.C., Lafon J.M., Gioia S.M.C.L., Pimentel M.M., 2008. Datação Sm-Nd em rocha total e granada do metamorfismo granulítico da região de Tartarugal Grande, Amapá Central. Revista Brasileira de Geociências 38, 114-127.

Oliveira, F. V., 2015. Chronus: Um novo suplemento para a redução de dados U-Pb obtidos por LAMC-ICPMS. Universidade Federal de Brasília, Brasilia, DF, Dissertação de Mestrado, 91 pp.

Patchett, P.J., 1983. Importance of the Lu–Hf isotopic system in studies of planetary chronology and chemical evolution. Geochimica et Cosmochima Acta, 47-81.

Pavan, M., Caltabeloti, F.P., Pinto, L.G.R.., 2014. Programa Geologia do Brasil. Folha SF.21-V-D-III - Fazenda Santa Otília, Estado de Mato Grosso do Sul. Companhia de Pesquisa de Recursos Minerais - CPRM, Carta Geológica, Escala 1:100.000.

Pearce, J.A., Harris N.B.W., Tindle, A.G., 1984. Trace element discrimination diagrams for the tectonic interpretation of granitic rocks. Journal of Petrology, 25, 956-983.

Pinho, M. A., Chemale Jr, F., Van Schmus, W. R., and Pinho, F. E. 2003. U–Pb and Sm–Nd evidence for 1.76– 1.77 Ga magmatism in the Moriru region, Mato Grosso, Brazil: implications for province boundaries in the SW Amazon Craton. Precambrian Research, 126, 1-25.

Plens, D. P., 2018. Petrogênese e Análise Estrutural e a Suíte Caracol: Implicações para a Evolução Geodinâmica do Bloco Rio Apa - Sul do Cráton Amazônico. Tese de Doutorado, Universidade Federal de Brasília.

Redes, L. A, Sousa, M. Z. A., Ruiz, A. S., Lafon, J. M., 2015. Petrogenesis and U-Pb and Sm-Nd geochronology of the Taquaral granite: record of an orosirian continental magmatic arc in the region of Corumba – MS. Brazilian Journal of Geology, 45, 431-451.

Rollinson, H., 1993. Using geochemical data: evaluation, presentation, interpretation. Longman, London, 351pp.

Rubatto, D., 2017. Zircon: the metamorphic mineral. Revista Mineral Geochemical 83, 261–265.

Ruiz, A. S., 2005. Evolução geológica do sudoeste do Cráton Amazônico região limítrofe Brasil-Bolívia-Mato Grosso. Tese de Doutorado, Universidade Estadual Paulista.

Ruiz, A.S., Simões, L.S.A., Brito-Neves, B.B., 2005. Maciço Rio Apa: Extremo Meridional do Cráton Amazônico. In: 10º Simpósio de Estudos Tectônicos. Curitiba-PA, Brasil. Sociedade Brasileira de Geologia, 301-304.

Ruiz, A.S., D'Agrella-Filho, M.S., Sousa, M.Z.A., Lima, G.A., 2010. Tonian sills and mafic dike swarms of the S-SW Amazonian craton, records of Rodinia Supercontinent break-up? In: Meeting of the Americas 91. EOS Transactions American Geophysical Union, 3, p. 26.

Ruiz, A. S., 2009. Compartimentação Tectônica (Pré-Sunsas) do Sudoeste do Cráton Amazônico: Ênfase em Mato Grosso – Brasil. *In*: XVIII Congresso Geológico Boliviano. Potosí, Bolívia, 159-163.

Saes, G.S., Leite, J.A.D., Alvarenga, C.J.S., 1992. Evolução tectono-sedimentar do Grupo Aguapeí, Proterozoico Médio na porção meridional do Cráton Amazônico: Mato Grosso e Oriente Boliviano. Revista Brasileira de Geociências 23, 31–37.

Santos, G., Ruiz A. S., Sousa, M. Z. A., Batata, M. E. F., Cabrera, R. F., Lafon, J. M., 2019. Petrology, deformation and geochronology U-Pb (SHRIMP) of Coimbra Granite – Rio Apa Block in the region of Corumbá, Brazil. Geologia USP-Série Científica, 9, 17-192.

Santos, J. O. S., Hartmann, L. A., Gaudette, H. E., Groves, D. I., Mcnaughton, N. J., Fletcher, I. R., 2000. A new understanding of the Amazon Craton Provinces based on integration of field mapping and U-Pb and Sm-Nd Geochronology. Gondwana Research, 3, 453-488.

Santos, J.O.S., Rizzotto, G.J., McNaughton, N.J., Matos, R., Hartmann, L.A., Chemale Junior, F., Potter, P.E., Quadros, M.L.E.S., 2008. The age and autochthonous evolution of Sunsas Orogen in West Amazon Craton. Precambrian Research, 165, 120–152.

Santos, J.O.S., Rizzotto, G., Easton, M.R., Potter, P.E., Hartmann, L.A., McNaughton, N.J., 2002. The Sunsas Orogen in Western Amazon Craton, South America and Correlation with the Grenville Orogen of Laurentia, based on U-Pb Isotopic Study of Detrital and Igneous Zircons. In: Geological Society of America, Denver Annual Meeting, Precambrian Geology, 27-30.

Sato K., Basei M. A. S., Siga Junior O., Sprosser W. M., Passarelli C. R., 2008. Novas técnicas aplicadas ao método U-Pb no CPGeo – Igc/USP: avanços na digestão química, espectrometria de massa (TIMS) e exemplos de aplicação integrada com SHRIMP. Geologia USP-Série Científica, 8, 76-99.

Shand, S.J., 1943. The Eruptive Rocks. John Wiley, New York, Second Edition, 444 pp.

Scherer, E., Münker, C., Mezger, K., 2006. Calibration of the lutetium–hafnium clock. Science, 293, 683–687.

Schmitt, R.S., Trouw, R.A.J., Van Schmus, W.R., Pimentel, M.M., 2004. Late amalgamation in the central part of Western Gondwana: new geochronological data and the characterization of a Cambrian collisional orogeny in the Ribeira belt (SE Brazil). Precambrian Research, 133, 29- 61.

Siivola, J., Schmid, R., 2007. List of Mineral Abbreviation. In: Fettes, D., Desmonds, J. (Eds.). Metamorphic Rocks. A Classification and Glossary of Terms. Cambridge University Press, Cambridge, pp. 93-110.

Silva, M. G., Abram, M. B. 2008. Projeto Metalogenia da Província Aurífera Juruena-Teles Pires, Mato Grosso. Informe de Recursos Minerais, Série Ouro, 16. Companhia de Pesquisa de Recursos Minerais - CPRM. Goiânia. 212p.

Silva, M. G; Rocha Neto, M.B.; Jost, H.; Kuyumjian, R.M., 2014. Metalogênese das Províncias Tectônicas Brasileiras. Belo Horizonte: Companhia de Pesquisa e Recursos Minerais - CPRM. 589 p. : il.

Souza, C. D., Sousa, M. Z. A., Ruiz, A. S., Batata, M. E. F., Brittes, A. F. N., Lafon, J. M., 2016. Formação Serra da Bocaina: Contribuição do Vulcanismo Paleoproterozoico do Arco Magmático Amonguijá no Bloco Rio Apa, Sul do Cráton Amazônico. Geochimica Brasiliensis, 30, 136 – 157.

Sun, S.S., McDonough, W.S., 1989. Chemical and isotopic systematics of oceanic basalts: implications for mantle composition and processes. Geological Society London, Special Publications, 42, 313-345.

Tassinari, C. C. G., Cordani, U. G., Nutman, A. P, Van Schmus, W. R., Bettencourt, J. S., Taylor, P. N., 1996. Geochronological systematics on basement rocks from the Rio Negro-Juruena Province (Amazonian Craton) and tectonic implications. International Geology Review 38 (2), 161–175.

Tassinari, C.C.G., Macambira, M.J.B., 1999. Geochronological provinces of the Amazonian Craton. Episodes, 38,174-182.

Tassinari, C.G.C., Macambira, M.J.B., 2004. A Evolução Tectônica do Cráton Amazônico. In: Neto-Mantesso V., Bartorelli A, Carneiro C. D. R., Brito-Neves B.B. (Eds.), Geologia do

Continente Sul-Americano: Evolução da Obra de Fernando Flávio Marques de Almeida, Editora Beca, 471-486.

Taylor, S.R., McLennan, S.M., 1985. The Continental Crust: its Composition and Evolution. Blackwell, Oxford, 312 pp.

Teixeira, W., Cordani, U.G., Faleiros, F.M., Sato, K., Maurer, V.C., Ruiz, A.S., Azevedo, E.J.P., 2020. The Rio Apa Terrane reviewed: UePb zircon geochronology and provenance studies provide paleotectonic links with a growing Proterozoic Amazonia. Earth-Science Reviews, 202, 1-35.

Teixeira, W., Geraldes, M. C., Matos, R., Ruiz, A. S., Saes, G., Vargas-Mattos, G., 2010. A review of the tectonic evolution of the Sunsas belt, SW Amazonian Craton. Journal of South American Earth Sciences, 29, 47–60.

Thiéblemont, D., Tégyey, M., 1994. Une discrimination géochimique des roches différenciés témoin de la diversité d'órigine et de situation tectonique des magmas calco-alcalins. C. R. Paris Academy of Science, 319, 87–94.

Vargas-Mattos, G.L., 2006. Caracterização geocronológica e geoquímica dos granitos proterozoicos: implicação para a evolução crustal da borda SW do Cráton Amazônico na Bolívia. Universidade do Estado do Rio de Janeiro, Dissertação de Mestrado, 110 pp.

Vargas-Mattos, G.L., Geraldes, M.C., Teixeira, W., Salinas, R.M., 2010. Paleoproterozoic granites in Bolivian Precambrian shield: the 1.92–1.89 Ga Correreca magmatic rocks and tectonic implications. In: VI Simpósio de Geologia Isotópica da América do Sul. Brasília, Brasil. Sociedade Brasileira de Geologia, 65.

Vasquez M.L. e Klein E.L. 2000. Geologia e recursos minerais da Folha Rio Novo - SB.21 - Z-C, Estado do Pará. Nota explicativa. Projeto Especial Província Mineral do Tapajós. Brasília, CPRM, PROMIM Tapajós, escala 1:250.000. 1 CD-Rom.

Vasquez M.L., Klein E.L., Ricci P.S.F. 2001. Granitoides pós-colisionais da porção leste da Provincia Tapajós. In: SBG, Simpósio de Geologia da Amazônia. 1 CD-Rom.

Wedepohl, K.H., 1995. The compositions of the continental crust. Geochimica et Cosmochima Acta, 59, 1217–1232.

White, A.J.R., Chappell, B.W., 1977. Ultrametamorphism and granitoid genesis. Tectonophysics 43, 7–22.

Wiedenbeck, M., Hanchar, J.M., Peck, W.H., Sylvester, P., Valley, J.W., Whitehouse, M.J., Kronz, A., Morishita, Y., Nasdala, L., Fiebig, J., Franchi, I., Girard, J.P., Greenwood, R.C., Hinton, R., Kita, N., Mason, P.R.D., Norman, M., Ogasawara, M., Piccoli, R., Rhede, D., Satoh, H., Schulz-Dobrick, B., Skar, O., Spicuzza, M.J., Terada, K., Tindle, A., Togashi, S., Vennemann, T., Xie, Q., Zheng, Y.F., 2004. Further characterisation of the 91500 zircon crystal. Geostandards and Geoanalytical Research, 28, 9-39.

Wiedenbeck, M., Allé, P., Corfu, F., Griffin, W.L., Meier, M., Oberli, F., von Quadt, A., Roddick, J.C., Spiegel, W., 1995. Three natural zircon standards for U-Th-Pb, Lu-Hf, trace element and REE analyses. Geostandards Newsletter, 19, 1-23.

Zhao, G., Sun, M., Wilde, S.A., Li, S., 2004. A Paleo-Mesoproterozoic supercontinent: assembly, growth and breakup. Earth-Science Reviews, 67, 91–123.

Zhang, C., Liua, D., Zeng, J., Jiang S., Luo, Q., Kong, X., Yang, W, Liu, L., 2019a. Nd-O-Hf isotopic decoupling in S-type granites: Implications for ridge subduction. Lithos, 332, 261–273.

Zhang, C., Santosh, M., Luo, Q., Jiang S., Liu, L, Liu, D., 2019b. Impact of residual zircon on Nd-Hf isotope decoupling during sediment recycling in subduction zone. Geoscience Frontiers, 10, 241-251.

Supplementary Table 4.I.1. Summary of geochronological data of Rio Apa Block. (a) Araújo *et al*. (1982); (b) Brittes *et al*. (2013); (c) Cordani *et al*. (2010); (d) Faleiros *et al*. (2016); (e) Lacerda Filho *et al*. (2006); (f) Lacerda Filho (2015); (g) Nogueira (2015); (h) Pavan *et al*. (2014); (i) Plens *et al*. (2013); (j) Redes *et al*. (2015); (k) Remédio *et al*. (2013); (l) Santos *et al*. (2019); (m) Souza (2016); (n) Souza *et al*. (2016); (o) Plens (2018).

UNITY			Lithology	Author	U-Pb (Ma)	Rb-Sr (Ma)	Ar-Ar (Ma)	T_{DM} (Ga)	$\varepsilon_{Nd(t)}$
Rio Perdido Suite			Microgabronorite (d)	Faleiros *et al*. (2016) (d)	1589±44 (d)			2.35 to 2.09 (f)	-4.44 to -0.86 (f)
Amolar Group			Metaquartzite (f) Metasiltite (f) Metaquartzite (f) Quartzite (f)	Lacerda Filho (2015) (f) Lacerda Filho (2015) (f) Lacerda Filho (2015) (f) Lacerda Filho (2015) (f)	2034 to 1764 (f) 2489 to 1752 (f) 2572 to 1831 (f) 2738 to 1709 (f)			2.00 to 2.34 (f)	-19.4 to -20.4 (f)
Caracol Suite	Caracol Gneiss (d) Caracol Gneiss (f) Caracol Gneiss (c) Caracol Gneiss (d) Caracol Gneiss (o) Caracol Gneiss (o) Caracol Gneiss (o) Caracol Gneiss (o) Caracol Gneiss (o) Caracol Gneiss (o)		Muscovite Biotite Gneiss Syenogranite (d) Pink Syenogranite (f) Leucogneiss (c) Biotite Granodiorite (d) Biotite Gneiss Granite (o) Gneiss Granitic Syenogranite (o) Gneiss Granitic Syenogranite (o) Gneiss Granitic Syenogranite (o) Gneiss Granitic (o) Amphibole Gneiss Granitic (o)	Faleiros *et al*. (2016) (d) Lacerda Filho (2015) (f) Cordani *et al*. (2010) (c) Faleiros *et al*. (2016) (d) Plens (2018) (o) Plens (2018) (o) Plens (2018) (o) Plens (2018) (o) Plens (2018) (o) Plens (2018) (o)	1753±13 (d) 1768±27 (f) 1774±26 (c) 1781±7 (d) 1773±11 (o) 1748±19 (o) 1776±13 (o) 1760±15 (o) 1776±13 (o) 1761±6 (o)	Caracol Gneiss 1680 to1710 (d)		Caracol Gneiss 1.82 to 2.25 (o) 1.97 to 2.23 (c)	Caracol Gneiss -1.75 to +3.25 (o) -1.94 to +0.97 (c)
Rio Apa Complex	Espinilho Orthogneiss (k) Espinilho Orthogneiss (d) Sanga Bonita Granite (c) Baía das Garças Granite (c) Santa Clarinha Granite (k) Tamanduá Granite (f) Cerro Porã Granite (i) Santa Clarinha Orthogneiss (d) Baía das Garças Granite (c) Santo Antônio Granite (f)		Monzogranite Biotite Gneiss (k) Porphyritic Monzogranite (d) Porphyritic Biotite monzogranite (c) Pink Isotropic granite (c) Hornblenda biotite mylonitic granite (k) Monzogranite mylonitic pink (f) Gray Monzogranite (i) Hornblenda Biotita Gneiss Syenogranite (d) Pink Biotita Granite (c) Pink Granite (f)	Remédio *et al*. (2013) (k) Faleiros *et al*. (2016) (d) Cordani *et al*. (2010) (c) Cordani *et al*. (2010) (c) Remédio *et al*. (2013) (k) Lacerda Filho (2015) (f) Plens *et al*. (2013) (i) Faleiros *et al*. (2016) (d) Cordani *et al*. (2010) (c) Lacerda Filho (2015) (f)	1716±11 (k) 1719±11 (d) 1721±25 (c) 1727±29 (c) 1735 ±12 (k) 1736±19 (f) 1749 ±45 (i) 1750±9 (d) 1754±42 (c) 1794±14 (f)	Baía das Garças Granite 1570 to1700 (c)	1302±4 (f) ~ 1300 (c)	Baía das Garças Granite 1.96 to 2.81 (c) ~2.09 (f)	Baía das Garças Granite -4.95 to +0.87 (c) -4.75 to +3.87 (f)
Alto Tererê Group			Garnet-muscovite Schist (f) Amphibolite (f) Garnet-muscovite Schist (f) Amphibolite (f)	Lacerda Filho (2015) (f) Lacerda Filho (2015) (f) Lacerda Filho (2015) (f) Lacerda Filho (2015) (f)	1773 to 2120 (f) 1727 to 1962 (f) 1769±9 (f) 1793±36 (f)			2.20 to 2.28 (c) Mafic rocks 2.75 to 1.67 (f)	-1.09 to -0.09 (c) Mafic rocks -4.97 to +3.74 (f)
Serra da Alegria Anorthosite			Anorthosite Gabbro (f)	Lacerda Filho *et al*. (2006) (f)	1791 (f)			2.50 to 2.64 (c) 2.51 (f)	-4.31 to -2.31 (c) -4.32 to -2.89 (f)
Paso Bravo Province			Biotite hornblende Gneiss (c) Biotite hornblende Gneiss (c)	Cordani *et al*. (2010) (c) Cordani *et al*. (2010) (c)	1559±55 (c) 1839±33 (c)	1730 to1835 (c)		2.20 to 2.37 (c)	-0.50 to -1.13 (c)
Amoguijá Supersuite	Intrusive Alumiador Suite	Aquidabã Granite (g) Corrégo do Cervo Granite (d) Alumiador Granite (c) Santa Otília Granite (d) Coimbra Granite (l) Taquaral Granite (j) Alumiador Granite (e) São Francisco Granite (m) Piatã Granite (f)	Granodiorite (g) Syenogranite (d) Syenogranite to monzogranite (c) Syenogranite (d) PorphyroclasticMonzogranite (l) Granodiorite (j) Biotite Granite to monzogranite (e) Porphyritic Monzogranite (m) Muscovite biotite garnet Monzogranite (f)	Nogueira (2015) (g) Faleiros *et al*. (2016) (d) Cordani *et al*. (2010) (c) Faleiros *et al*. (2016) (d) Santos *et al*. (2019) (n) Redes *et al*. (2015) (j) Lacerda Filho *et al*. (2006) (e) Souza (2016) (m) Lacerda Filho (2015) (f)	1811±7 (g) 1830±12 (d) 1839±33 (c) 1841±15 (d) 1859±4 (n) 1861±5 (j) 1867 (e) 1878±7 (m) 1892±31 (f)	1600±40 (a) 1440 to 1740 (c)		2.38 to 2.58 (c) 2.36 to 2.60 (m) 2.35 to 2.57 (g) 2.32 (j) 2.27 (n)	-5.90 to -2.86 (c) -3.65 to -2.53 (m) -4.37 to -1.50 (g) -1.48 to -1.28 (j) -1.35 (l)
	Rio Naitaca Formation		Andesite Lapilli Tuff (d)	Faleiros *et al*. (2016) (d)	1813±18 (d)				

	Serra da Bocaina Formation	Rhyolite (e) Ignimbrite (b) Riolite (f) Lava (n)	Lacerda Filho *et al*. (2006) (e) Brittes *et al*. (2013) (b) Lacerda Filho (2015) (f) Souza *et al*. (2016) (n)	1794 (e) 1877±4 (b) 1877±9 (f) 1897±5 (n)	1650±63 (a) 1440 to1740 (c)		2.26 (c)	-2.4 (c)
Paraíso Complex	Scardine Granite (k) Rio da Areia Granite (k)	Biotite hornblende Monzogranite (k) Porphyroclastic Monzogranite (k)	Remédio *et al*. (2013) (k) Remédio *et al*. (2013) (k)	1791±19 (k) 1820±18 (k)			1.99 (f)	-0.2 (f)
Porto Murtinho Complex	Microgabbro (f) Córrego Cabrito Dyke (f) Chatelodo Granite (d) Morro da Lenha Granite (d) Morraria Gneiss (e) Porto Murtinho Gneiss (d) Córrego Jiboia Gneiss Granitic (d) Morraria Gneiss (c) Fazenda Matão Gabbro (f) Gneiss tonalite (f) Córrego Jiboia Gneiss Granitic (d) Biotite hornblende Gneiss (f) Gneiss (h)	Microgabbro (f) Dark grey Microgabbro (f) Retrometrophoric Gneiss (d) Syenogranite (d) Biotite Gneiss migmatitic (e) Biotite porphyritic Monzogranite (d) Mylonitic Gneiss Granitic (d) Biotite Gneiss migmatitic (c) Isotropic dark gray Metagabbro (f) Tonalitic migmatitic Gneiss (f) Mylonitic Gneiss Granitic (d) Biotite hornblende tonalitic Gneiss (f) Paragneiss (h)	Lacerda Filho (2015) (f) Lacerda Filho (2015) (f) Faleiros *et al*. (2016) (d) Faleiros *et al*. (2016) (d) Lacerda Filho *et al*. (2006) (e) Faleiros *et al*. (2016) (d) Faleiros *et al*. (2016) (d) Cordani *et al*. (2010) (c) Lacerda Filho (2015) (f) Lacerda Filho (2015) (f) Faleiros *et al*. (2016) (d) Lacerda Filho (2015) (f) Pavan *et al*. (2014) (h)	1778±5 (f) 1819±13 (f) 1902±6 (d) 1910 to 1950 (d) 1941 (e) 1941±13 (d) 1947±9 (d) 1950±23 (c) 1969± 5 (f) 1985±19 (f) 1989±11 (d) 2074±7 (f) 3200 to 1900 (h)	1650 (c)		Gneiss 2.17 to 2.53 (c) 2.14 to 2.60 (f) Gabbro 2.60 (f)	Gneiss -5.97 to +0.08 (c) -5.70 to +2.92 (f) Gabbro -2.74 (f)

Supplementary Table 4.II.1. Results of U-Pb isotope analysis by LA-ICP-MS on zircon from sample ST-02 (Santa Terezita Granite). Data in black were used for Concordia diagrams. Data in red, were excluded. (*) Data are grouped according to $^{207}Pb/^{206}Pb$ apparent ages. See text for discussion.

SAMPLE	ST-02																	
	Ratios											Apparent ages						
GRAIN	*f* 206 (%)	Th/U	$^{206}Pb/^{204}Pb$	$^{207}Pb/^{206}Pb$	err (%) 1 б	$^{207}Pb/^{235}U$	err (%) 1 б	$^{206}Pb/^{238}U$	err (%) 1 б	Rho	$^{207}Pb/^{206}Pb$	2 б (abs)	$^{207}Pb/^{235}U$	2 б (abs)	$^{206}Pb/^{238}U$	2 б (abs)	conc. (%)
ZR11	0.02	0.23	73992	0.10726	0.9	4.14337	1.8	0.28015	1.4	0.82	1753	34	1663	28	1592	40	91
ZR24	0.20	0.24	7864	0.10819	1.2	4.34394	1.5	0.29118	0.9	0.57	1769	43	1702	25	1647	25	93
ZR15	0.01	0.51	206275	0.11419	0.4	4.68073	1.2	0.29727	1.1	0.90	1867	13	1764	20	1678	32	90
(*) Group 1849±11 Ma																		
ZR7N	0.01	0.47	202226	0.11063	1.3	4.72598	1.8	0.30980	1.2	0.65	1810	47	1772	30	1740	35	96
ZR35	0.00	0.56	639161	0.11141	0.6	4.99975	1.1	0.32544	0.8	0.76	1823	21	1819	18	1816	25	100
ZR12N	0.00	0.29	470877	0.11203	0.6	4.92968	1.2	0.31913	0.9	0.77	1833	23	1807	20	1785	28	97
ZR10	0.01	0.56	258839	0.11238	0.4	4.78681	1.0	0.30890	0.8	0.81	1838	16	1783	16	1735	24	94
ZR23N	0.01	0.71	270101	0.11266	0.7	5.39262	1.2	0.34713	0.9	0.74	1843	27	1884	21	1921	31	104
ZR23B	0.01	0.63	226797	0.11278	0.6	5.21357	1.2	0.33527	1.0	0.81	1845	22	1855	20	1864	31	101
ZR17N	0.01	0.58	289407	0.11278	0.6	5.05673	1.4	0.32516	1.2	0.84	1845	23	1829	23	1815	37	98
ZR39	0.00	0.57	332645	0.11354	0.6	4.94475	0.9	0.31584	0.6	0.68	1857	20	1810	15	1769	19	95
ZR32	0.01	0.58	252694	0.11361	0.5	5.03926	0.8	0.32166	0.6	0.70	1858	17	1826	14	1798	18	97
ZR29	0.65	0.77	2349	0.11383	1.1	4.90914	1.7	0.31277	1.2	0.73	1861	39	1804	28	1754	38	94
ZR7B	0.66	0.06	2301	0.11453	0.7	5.42504	1.8	0.34351	1.6	0.90	1873	24	1889	31	1904	53	102
Group 2104±220 Ma																		
ZR38	0.07	0.61	22233	0.11718	0.6	4.14147	1.5	0.25632	1.3	0.88	1914	22	1663	24	1471	34	77
ZR19	1.13	0.18	1362	0.12179	1.8	4.82856	2.3	0.28751	1.4	0.62	1983	62	1790	38	1629	41	82
ZR3	0.54	0.56	2848	0.12208	0.4	4.57252	3.2	0.27164	3.1	0.98	1987	15	1744	53	1549	86	78
ZR34	0.21	0.72	7458	0.12336	0.7	4.90814	1.5	0.28853	1.2	0.84	2005	25	1804	24	1634	35	81
ZR16	0.28	0.04	5452	0.12494	0.8	5.28851	1.3	0.30697	1.0	0.75	2028	28	1867	22	1726	30	85
ZR20	0.65	0.42	2347	0.12584	2.5	6.20824	3.9	0.35778	3.0	0.77	2041	87	2006	67	1972	102	97
ZR8	1.38	0.36	1106	0.12833	1.8	5.44286	2.0	0.30759	0.9	0.45	2075	62	1892	35	1729	28	83
ZR14	0.01	0.50	120088	0.12840	0.7	4.45790	2.0	0.25178	1.8	0.91	2076	25	1723	32	1448	46	70
Group 2212±77 Ma																		
ZR6	2.13	0.66	722	0.13571	3.7	5.37261	3.9	0.28711	1.4	0.36	2173	125	1880	66	1627	41	75
ZR22	2.24	0.51	666	0.13615	4.3	8.42105	5.1	0.44856	2.7	0.53	2179	145	2277	90	2389	106	110

ZR5	1.16	0.31	1331	0.13732	2.2	3.27032	5.8	0.17271	5.3	0.92	2194	75	1474	88	1027	101	47
ZR33	1.68	0.09	919	0.13782	2.6	4.65925	3.4	0.24517	2.2	0.65	2200	88	1760	56	1414	56	64
ZR27N	3.48	0.84	437	0.14244	3.2	6.89776	3.5	0.35118	1.3	0.38	2257	108	2098	61	1940	44	86
Excluded Data																	
ZR2	*0.01*	*0.71*	*177581*	*0.10449*	*4.1*	*4.64585*	*4.3*	*0.32245*	*1.2*	*0.28*	*1705*	*148*	*1758*	*71*	*1802*	*37*	*106*
ZR18	*4.35*	*0.48*	*354*	*0.10514*	*10.3*	*3.65718*	*10.4*	*0.25225*	*1.6*	*0.15*	*1717*	*356*	*1562*	*159*	*1450*	*41*	*84*
ZR21	*0.03*	*0.43*	*52383*	*0.10677*	*5.8*	*4.47932*	*5.9*	*0.30425*	*1.3*	*0.23*	*1745*	*204*	*1727*	*96*	*1712*	*40*	*98*
ZR30	*2.69*	*0.33*	*565*	*0.11026*	*5.6*	*5.43899*	*5.8*	*0.35774*	*1.5*	*0.25*	*1804*	*198*	*1891*	*98*	*1971*	*49*	*109*
ZR31	*3.42*	*0.33*	*395*	*0.11903*	*7.8*	*11.77312*	*8.5*	*0.71732*	*3.6*	*0.42*	*1942*	*265*	*2587*	*154*	*3486*	*191*	*180*
ZR37	*0.08*	*0.48*	*19972*	*0.11956*	*2.8*	*4.95861*	*3.1*	*0.30078*	*1.2*	*0.38*	*1950*	*99*	*1812*	*51*	*1695*	*34*	*87*
ZR1	*2.11*	*0.30*	*728*	*0.11997*	*4.5*	*4.64042*	*4.6*	*0.28051*	*0.8*	*0.18*	*1956*	*155*	*1757*	*75*	*1594*	*23*	*81*
ZR36	*3.23*	*0.45*	*471*	*0.12578*	*4.2*	*6.14421*	*4.4*	*0.35426*	*1.1*	*0.25*	*2040*	*145*	*1997*	*75*	*1955*	*37*	*96*
ZR26	*1.22*	*0.86*	*1256*	*0.13057*	*4.8*	*5.90623*	*5.3*	*0.32806*	*2.3*	*0.43*	*2106*	*162*	*1962*	*90*	*1829*	*73*	*87*
ZR9	*7.75*	*0.54*	*200*	*0.14453*	*8.4*	*3.98144*	*8.5*	*0.19977*	*1.8*	*0.21*	*2282*	*274*	*1630*	*134*	*1174*	*38*	*51*
ZR13	*2.39*	*0.46*	*643*	*0.14852*	*3.2*	*5.78135*	*3.3*	*0.28230*	*0.8*	*0.25*	*2329*	*108*	*1944*	*57*	*1603*	*24*	*69*
ZR17B	*2.85*	*0.13*	*514*	*0.14986*	*3.1*	*10.94661*	*4.2*	*0.52973*	*2.8*	*0.66*	*2344*	*105*	*2519*	*77*	*2740*	*124*	*117*
ZR4	*8.02*	*0.59*	*186*	*0.18863*	*9.1*	*12.04663*	*11.0*	*0.46315*	*6.1*	*0.56*	*2730*	*285*	*2608*	*196*	*2453*	*247*	*90*
ZR27B	*3.54*	*0.33*	*435*	*0.19304*	*4.3*	*7.01058*	*4.4*	*0.26338*	*1.1*	*0.24*	*2768*	*137*	*2113*	*77*	*1507*	*29*	*54*
ZR28	*0.92*	*0.41*	*1667*	*0.30153*	*3.1*	*11.18609*	*3.2*	*0.26904*	*0.9*	*0.29*	*3478*	*93*	*2539*	*59*	*1536*	*26*	*44*
ZR25	*3.06*	*0.52*	*503*	*0.16691*	*3.0*	*6.09325*	*3.4*	*0.26475*	*1.6*	*0.47*	*2527*	*98*	*1989*	*58*	*1514*	*43*	*60*
ZR12B	*2.39*	*0.34*	*647*	*0.16728*	*1.2*	*4.78649*	*2.8*	*0.20751*	*2.5*	*0.89*	*2531*	*41*	*1783*	*46*	*1216*	*55*	*48*

Supplementary Table 4.II.2. Results of U-Pb isotope analysis by LA-ICP-MS on zircon from sample ST-03 (Santa Terezita Granite). Data in black were used for Concordia diagrams. Data in red, were excluded. (*) Data are grouped according to $^{207}Pb/^{206}Pb$ apparent ages. See text for discussion.

SAMPLE	ST-03																
	Ratios										Apparent ages						
GRAIN	*f* 206 (%)	Th/U	$^{206}Pb/^{204}Pb$	$^{207}Pb/^{206}Pb$	err (%) 1 б	$^{207}Pb/^{235}U$	err (%) 1 б	$^{206}Pb/^{238}U$	err (%) 1 б	Rho	$^{207}Pb/^{206}Pb$	2 б (abs)	$^{207}Pb/^{235}U$	2 б (abs)	$^{206}Pb/^{238}U$	2 б (abs)	conc. (%)
ZR33	0.02	10.01	94247	0.08323	0.5	2.51247	0.9	0.21891	0.6	0.68	1275	21	1276	13	1276	14	95
ZR42B	0.01	0.41	215279	0.08637	0.7	2.78624	1.7	0.23395	1.5	0.88	1346	27	1352	25	1355	36	101
ZR35B	0.04	0.07	41412	0.10637	0.3	4.44070	1.2	0.30277	1.1	0.92	1738	11	1720	20	1705	33	97
ZR22	0.01	0.08	210919	0.10720	0.9	5.10713	1.7	0.34549	1.4	0.84	1752	31	1837	29	1913	48	94
ZR44	0.74	0.27	2075	0.10908	0.8	4.02123	1.3	0.26734	1.0	0.76	1784	28	1638	21	1527	27	86
ZR23	0.65	0.07	2350	0.10963	1.6	5.04703	2.8	0.33388	2.3	0.82	1793	57	1827	47	1857	75	104
ZR58	0.50	0.23	3061	0.11009	0.6	4.96577	1.2	0.32711	1.0	0.80	1801	23	1814	21	1824	31	101
ZR24	0.01	0.39	139677	0.11026	2.7	5.53427	3.5	0.36401	2.2	0.63	1804	98	1906	60	2001	76	111
ZR28	0.08	0.17	18571	0.11075	1.9	5.21870	2.5	0.34172	1.6	0.63	1812	69	1856	42	1895	52	105
ZR26	0.30	0.21	5191	0.11135	0.5	4.68751	0.9	0.30529	0.6	0.72	1822	17	1765	15	1718	19	94
ZR42N	0.02	0.57	100457	0.11145	0.5	5.49525	1.1	0.35759	0.9	0.83	1823	17	1900	18	1971	31	108
ZR4	0.02	0.35	65232	0.11152	1.5	5.36962	1.8	0.34918	0.9	0.50	1824	53	1880	30	1931	29	106
ZR49	1.15	0.22	1332	0.11464	1.5	4.82419	2.0	0.30517	1.2	0.61	1874	54	1789	33	1717	36	92
ZR21	0.00	0.24	386048	0.11467	0.5	5.24665	1.4	0.33182	1.3	0.90	1875	19	1860	24	1847	41	99
ZR9	0.01	0.72	127364	0.11499	0.4	5.10875	0.7	0.32221	0.5	0.67	1880	15	1838	13	1801	16	96
ZR6	0.01	0.53	212267	0.11563	0.5	5.39915	1.2	0.33862	1.1	0.87	1890	17	1885	21	1880	35	99
ZR7	0.50	0.45	3038	0.11571	1.9	5.56321	2.8	0.34868	2.0	0.73	1891	66	1910	48	1928	68	102
ZR50	0.20	0.12	7534	0.11572	0.6	4.95063	1.5	0.31026	1.3	0.86	1891	23	1811	25	1742	39	92
ZR10	0.00	0.39	640712	0.11578	0.6	5.38122	1.3	0.33708	1.1	0.84	1892	21	1882	22	1873	35	99
ZR8B	0.04	0.64	38194	0.11652	0.3	5.40829	0.8	0.33662	0.6	0.76	1903	11	1886	13	1870	19	98
ZR20	0.57	0.37	2670	0.11735	0.4	5.49107	1.1	0.33936	0.9	0.85	1916	15	1899	18	1884	30	98
ZR12	0.55	0.74	2766	0.11787	0.4	5.14610	1.2	0.31661	1.0	0.87	1924	16	1844	20	1773	31	92
ZR13B	1.56	0.01	984	0.11966	0.9	4.31485	1.2	0.26150	0.8	0.63	1951	30	1696	20	1498	20	77
ZR37	1.12	0.13	1367	0.12059	0.9	4.57817	1.5	0.27532	1.1	0.74	1965	33	1745	24	1568	30	80
Group 1722±7 Ma																	
ZR31	0.05	0.02	30620	0.10076	3.3	4.21598	3.5	0.30345	1.3	0.38	1638	118	1677	57	1708	40	59
ZR54B	1.12	0.10	1367	0.09931	0.8	3.84878	1.3	0.28105	1.0	0.73	1611	30	1603	21	1597	27	84

ZR51	0.11	0.07	13664	0.10510	1.0	4.36808	1.8	0.30142	1.4	0.78	1716	38	1706	29	1698	41	164
Group 1853±5 Ma																	
ZR27	0.00	0.49	423686	0.11276	0.5	5.24150	1.0	0.33709	0.8	0.78	1844	19	1859	17	1873	26	102
ZR17	0.01	0.54	205727	0.11292	0.4	5.27713	0.8	0.33892	0.6	0.77	1847	13	1865	14	1881	20	102
ZR55N	0.01	0.43	298262	0.11295	0.4	5.40032	0.8	0.34674	0.6	0.73	1847	15	1885	14	1919	20	104
ZR52	0.01	0.59	164741	0.11299	0.5	5.30236	0.9	0.34033	0.7	0.78	1848	17	1869	16	1888	24	102
ZR1N	0.00	0.79	571548	0.11310	0.3	5.22026	0.7	0.33472	0.5	0.73	1850	10	1856	12	1861	16	101
ZR1B	0.00	0.73	535628	0.11312	0.3	5.18943	0.7	0.33268	0.5	0.75	1850	11	1851	12	1851	18	100
ZR25	0.00	0.46	369732	0.11313	0.6	5.16303	1.0	0.33098	0.7	0.73	1850	20	1847	16	1843	22	100
ZR54N	0.01	0.41	264885	0.11315	0.5	5.13687	0.9	0.32924	0.6	0.68	1851	19	1842	15	1835	20	99
ZR2	0.11	0.21	14453	0.11341	0.2	5.26408	1.5	0.33662	1.4	0.95	1855	9	1863	25	1870	46	100
ZR14	0.01	0.80	253583	0.11344	0.4	5.05450	0.9	0.32312	0.7	0.78	1855	16	1829	15	1805	22	97
ZR46	0.00	0.41	429750	0.11347	0.3	5.35715	0.8	0.34240	0.6	0.78	1856	13	1878	14	1898	21	102
ZR8N	0.01	0.56	167415	0.11396	0.4	5.17248	0.7	0.32916	0.5	0.70	1864	13	1848	12	1834	16	98
Excluded Data																	
ZR47	*0.01*	*0.78*	*172308*	*0.09310*	*4.6*	*4.54462*	*4.7*	*0.35399*	*0.9*	*0.18*	*1490*	*168*	*1739*	*76*	*1954*	*29*	*131*
ZR53	*0.10*	*0.29*	*14547*	*0.09632*	*3.4*	*6.45053*	*3.6*	*0.48566*	*1.2*	*0.34*	*1554*	*126*	*2039*	*63*	*2552*	*52*	*99*
ZR5	*0.04*	*0.47*	*36422*	*0.09871*	*3.9*	*4.24444*	*4.4*	*0.31184*	*2.0*	*0.45*	*1600*	*142*	*1683*	*71*	*1750*	*60*	*109*
ZR34	*1.87*	*0.11*	*819*	*0.11227*	*0.9*	*4.82515*	*3.0*	*0.31168*	*2.8*	*0.95*	*1836*	*32*	*1789*	*50*	*1749*	*86*	*98*
ZR30	*0.37*	*0.05*	*4142*	*0.11246*	*2.0*	*4.77771*	*2.2*	*0.30811*	*0.8*	*0.35*	*1839*	*71*	*1781*	*36*	*1731*	*23*	*104*
ZR35N	*0.54*	*0.77*	*2839*	*0.11434*	*1.8*	*5.11206*	*1.9*	*0.32424*	*0.7*	*0.34*	*1870*	*63*	*1838*	*32*	*1810*	*21*	*76*
ZR45	*3.89*	*0.28*	*396*	*0.11731*	*1.8*	*3.85008*	*2.0*	*0.23802*	*0.6*	*0.32*	*1916*	*65*	*1603*	*31*	*1376*	*15*	*72*
ZR36N	*0.50*	*1.24*	*3055*	*0.11887*	*3.2*	*4.93980*	*3.4*	*0.30136*	*1.1*	*0.33*	*1939*	*112*	*1809*	*56*	*1698*	*33*	*69*
ZR48	*0.07*	*0.45*	*21190*	*0.12835*	*5.9*	*6.53845*	*6.1*	*0.36944*	*1.1*	*0.19*	*2076*	*202*	*2051*	*104*	*2027*	*39*	*98*
ZR36B	*2.67*	*0.45*	*574*	*0.13504*	*7.8*	*5.42947*	*7.9*	*0.29158*	*1.3*	*0.17*	*2165*	*260*	*1890*	*131*	*1649*	*39*	*88*
ZR38	*5.76*	*0.31*	*266*	*0.16460*	*6.0*	*6.95001*	*6.1*	*0.30620*	*1.1*	*0.19*	*2504*	*194*	*2105*	*105*	*1722*	*34*	*78*
ZR16	*6.28*	*0.26*	*244*	*0.16756*	*6.7*	*6.54289*	*7.5*	*0.28317*	*3.5*	*0.46*	*2533*	*216*	*2052*	*129*	*1607*	*98*	*70*
ZR32	*5.49*	*0.11*	*279*	*0.21614*	*3.3*	*9.28201*	*3.7*	*0.31144*	*1.6*	*0.43*	*2952*	*104*	*2366*	*66*	*1748*	*49*	*100*
ZR43	*2.14*	*0.11*	*700*	*0.21709*	*2.2*	*13.54150*	*2.4*	*0.45237*	*0.9*	*0.38*	*2959*	*71*	*2718*	*46*	*2406*	*38*	*81*
ZR39	*2.37*	*0.06*	*646*	*0.12494*	*1.0*	*5.37326*	*1.4*	*0.31190*	*0.8*	*0.61*	*2028*	*36*	*1881*	*23*	*1750*	*25*	*86*
ZR15	*1.39*	*0.18*	*1107*	*0.12500*	*1.1*	*5.06744*	*1.4*	*0.29400*	*0.8*	*0.57*	*2029*	*37*	*1831*	*23*	*1661*	*23*	*82*
ZR55B	*2.91*	*0.14*	*525*	*0.12716*	*1.5*	*5.36895*	*1.9*	*0.30619*	*1.1*	*0.58*	*2059*	*53*	*1880*	*33*	*1722*	*34*	*63*
ZR18	*0.47*	*0.57*	*3319*	*0.12816*	*0.9*	*3.29058*	*3.1*	*0.18620*	*2.9*	*0.95*	*2073*	*32*	*1479*	*47*	*1101*	*58*	*53*
ZR40	*0.84*	*0.22*	*1825*	*0.13055*	*0.7*	*5.24562*	*1.2*	*0.29139*	*0.9*	*0.75*	*2105*	*25*	*1860*	*21*	*1648*	*27*	*99*
ZR3	*1.03*	*0.57*	*1500*	*0.13096*	*1.8*	*3.63905*	*2.4*	*0.20152*	*1.6*	*0.66*	*2111*	*61*	*1558*	*38*	*1183*	*35*	*56*

ZR56	*1.95*	*0.32*	*791*	*0.13265*	*0.5*	*4.25529*	*1.0*	*0.23265*	*0.8*	*0.76*	*2133*	*18*	*1685*	*16*	*1348*	*19*	*73*
ZR29	*1.44*	*0.33*	*1067*	*0.13563*	*2.4*	*5.09331*	*2.9*	*0.27234*	*1.6*	*0.56*	*2172*	*81*	*1835*	*49*	*1553*	*45*	*71*
ZR41	*2.04*	*0.04*	*751*	*0.14191*	*1.2*	*6.11340*	*1.4*	*0.31242*	*0.7*	*0.47*	*2251*	*42*	*1992*	*25*	*1753*	*21*	*78*
ZR57	*1.88*	*0.22*	*815*	*0.14577*	*1.1*	*5.97037*	*1.7*	*0.29702*	*1.2*	*0.72*	*2297*	*38*	*1972*	*29*	*1677*	*36*	*61*
ZR13N	*5.07*	*0.04*	*299*	*0.14627*	*1.3*	*7.54778*	*3.6*	*0.37422*	*3.3*	*0.92*	*2303*	*46*	*2179*	*63*	*2049*	*114*	*63*
ZR11	*3.67*	*0.04*	*420*	*0.14686*	*3.6*	*4.97948*	*3.8*	*0.24590*	*1.3*	*0.33*	*2310*	*121*	*1816*	*64*	*1417*	*33*	*89*
ZR19	*1.42*	*0.15*	*1082*	*0.14704*	*3.4*	*5.74462*	*3.7*	*0.28332*	*1.4*	*0.39*	*2312*	*114*	*1938*	*63*	*1608*	*41*	*109*

Supplementary Table 4.II.3. Results of U-Pb isotope analysis by LA-ICP-MS on zircon from sample SC-824(Santo Corazón Granite). Data in black were used for Concordia diagrams. Data in red, were excluded. (*) Data are grouped according to $^{207}Pb/^{206}Pb$ apparent ages. See text for discussion.

SAMPLE	SC-824																	
	Ratios										Apparent ages							
GRAIN	*f* 206 (%)	Th/U	$^{206}Pb/^{204}Pb$	$^{207}Pb/^{206}Pb$	err %) 1 б	$^{207}Pb/^{235}U$	err (%) 1 б	$^{206}Pb/^{238}U$	err (%) 1 б	Rho	$^{207}Pb/^{206}Pb$	2 б (abs)	$^{207}Pb/^{235}U$	2 б (abs)	$^{206}Pb/^{238}U$	2 б (abs)	conc. (%)
ZR23	0.01	0.88	59727	0.11037	1.3	5.63094	4.5	0.37001	4.3	0.96	1805	47	1921	77	2029	150	112
ZR26	0.00	0.73	2496	0.11053	1.4	4.44564	2.2	0.29168	1.6	0.75	1808	50	1721	36	1650	48	91
ZR14	0.01	0.61	4665	0.11413	0.8	5.87107	2.0	0.37305	1.8	0.89	1866	30	1957	35	2044	63	110
ZR13	0.01	0.65	2621	0.11428	1.9	6.00359	3.9	0.38100	3.4	0.87	1868	68	1976	67	2081	121	111
ZR4	0.01	0.66	3547	0.11717	0.6	7.15195	4.0	0.44265	3.9	0.98	1914	22	2131	70	2362	154	123
ZR19	0.01	0.46	4954	0.11806	1.2	5.85744	2.3	0.35980	2.0	0.85	1927	41	1955	40	1981	68	103
ZR7	0.01	0.83	1481	0.12470	3.1	6.54004	4.4	0.38033	3.1	0.69	2025	109	2051	76	2078	108	103
(*) Group 1874±15 Ma																		
ZR16B	0.01	0.78	129598	0.11285	0.8	5.03465	1.9	0.32355	1.7	0.88	1846	30	1825	32	1807	54	98
ZR29N	0.01	0.88	14759	0.11318	0.5	4.69428	1.6	0.30079	1.4	0.91	1851	19	1766	26	1695	42	92
ZR3	0.01	0.66	443174	0.11342	0.4	4.86254	1.6	0.31090	1.5	0.93	1855	15	1796	26	1745	45	94
ZR2	0.02	0.74	9777	0.11358	0.7	5.32963	3.6	0.34030	3.5	0.98	1857	24	1874	60	1888	114	102
ZR20N	0.01	1.09	11667	0.11446	0.6	4.98766	2.3	0.31603	2.2	0.95	1871	23	1817	39	1770	68	95
ZR9B	0.01	0.66	53103	0.11508	0.4	5.52451	2.1	0.34814	2.0	0.96	1881	16	1904	36	1926	67	102
ZR27	0.01	0.64	9840	0.11557	0.7	5.12243	2.4	0.32143	2.3	0.95	1889	24	1840	41	1797	72	95
Excluded Data																		
ZR8B	*0.01*	*0.76*	*40096*	*0.06819*	*16.9*	*3.90911*	*17.6*	*0.41577*	*4.7*	*0.27*	*874*	*632*	*1616*	*266*	*2241*	*175*	*256*
ZR34N	*0.01*	*0.66*	*794*	*0.07792*	*15.5*	*4.43437*	*15.9*	*0.41273*	*3.4*	*0.21*	*1145*	*563*	*1719*	*248*	*2227*	*126*	*195*
ZR11	*0.01*	*0.75*	*10282*	*0.10627*	*17.9*	*5.17673*	*18.1*	*0.35328*	*2.6*	*0.14*	*1736*	*593*	*1849*	*286*	*1950*	*86*	*112*
ZR18	*0.02*	*0.48*	*4883*	*0.10956*	*4.3*	*4.53686*	*4.6*	*0.30032*	*1.5*	*0.33*	*1792*	*153*	*1738*	*75*	*1693*	*46*	*94*
ZR30	*0.01*	*0.69*	*3343*	*0.11210*	*4.1*	*5.07170*	*5.1*	*0.32809*	*3.0*	*0.59*	*1834*	*145*	*1831*	*84*	*1829*	*94*	*100*
ZR34B	*0.01*	*0.59*	*1846*	*0.12001*	*8.4*	*5.87335*	*9.4*	*0.35493*	*4.1*	*0.44*	*1956*	*287*	*1957*	*157*	*1958*	*138*	*100*
ZR6N	*0.01*	*0.73*	*9770*	*0.12016*	*1.4*	*5.10697*	*3.7*	*0.30823*	*3.4*	*0.92*	*1959*	*50*	*1837*	*63*	*1732*	*104*	*88*
ZR28	*0.01*	*0.79*	*1123*	*0.12046*	*8.4*	*5.36854*	*8.9*	*0.32319*	*2.8*	*0.32*	*1963*	*286*	*1880*	*146*	*1805*	*88*	*92*
ZR6B	*0.00*	*0.90*	*1995*	*0.12234*	*2.1*	*5.62275*	*3.1*	*0.33331*	*2.2*	*0.71*	*1991*	*74*	*1920*	*52*	*1854*	*70*	*93*
ZR24N	*0.00*	*0.50*	*1318*	*0.13276*	*11.3*	*5.56457*	*11.7*	*0.30396*	*3.2*	*0.27*	*2135*	*370*	*1911*	*193*	*1711*	*95*	*80*
ZR15	*0.01*	*0.71*	*571*	*0.14436*	*3.1*	*7.15204*	*4.7*	*0.35930*	*3.6*	*0.75*	*2280*	*105*	*2131*	*83*	*1979*	*122*	*87*
ZR5	*0.01*	*0.32*	*142*	*0.28963*	*2.6*	*6.35758*	*4.8*	*0.15919*	*4.0*	*0.84*	*3416*	*80*	*2026*	*83*	*952*	*71*	*28*

ZR21	*0.01*	*0.47*	*115*	*0.29270*	*7.3*	*11.19867*	*9.0*	*0.27747*	*5.2*	*0.58*	*3432*	*219*	*2540*	*161*	*1579*	*144*	*46*
ZR24B	*0.01*	*0.31*	*114*	*0.30091*	*2.7*	*7.33245*	*5.6*	*0.17672*	*4.8*	*0.87*	*3475*	*83*	*2153*	*97*	*1049*	*93*	*30*
ZR29B	*0.01*	*0.63*	*2319*	*0.12665*	*0.9*	*4.66737*	*2.3*	*0.26726*	*2.1*	*0.91*	*2052*	*32*	*1761*	*39*	*1527*	*58*	*74*
ZR25	*0.01*	*0.76*	*2979*	*0.12823*	*1.8*	*5.36787*	*2.3*	*0.30357*	*1.5*	*0.63*	*2074*	*63*	*1880*	*40*	*1709*	*44*	*82*
ZR20B	*0.00*	*0.75*	*1046*	*0.12910*	*0.9*	*5.27539*	*3.2*	*0.29635*	*3.0*	*0.95*	*2086*	*31*	*1865*	*53*	*1673*	*89*	*80*
ZR17	*0.01*	*0.71*	*869*	*0.13204*	*3.3*	*6.34655*	*4.4*	*0.34858*	*2.9*	*0.66*	*2125*	*114*	*2025*	*76*	*1928*	*97*	*91*
ZR33	*0.01*	*0.52*	*576*	*0.13630*	*3.3*	*4.13873*	*9.7*	*0.22020*	*9.1*	*0.94*	*2181*	*114*	*1662*	*153*	*1283*	*210*	*59*
ZR12	*0.01*	*0.57*	*1314*	*0.15280*	*6.0*	*5.00795*	*11.5*	*0.23768*	*9.8*	*0.85*	*2378*	*198*	*1821*	*185*	*1375*	*239*	*58*
ZR31B	*0.01*	*0.25*	*406*	*0.15655*	*3.4*	*1.52605*	*16.2*	*0.07069*	*15.9*	*0.98*	*2419*	*112*	*941*	*190*	*440*	*134*	*18*
ZR11B	*0.01*	*0.61*	*3358*	*0.16413*	*1.4*	*6.12853*	*1.8*	*0.27080*	*1.0*	*0.58*	*2499*	*46*	*1994*	*30*	*1545*	*28*	*62*
ZR16N	*0.00*	*1.02*	*1430*	*0.16604*	*4.4*	*7.87354*	*10.8*	*0.34390*	*9.8*	*0.91*	*2518*	*145*	*2217*	*186*	*1905*	*321*	*76*
ZR1	*0.02*	*0.91*	*2085*	*0.17421*	*1.8*	*7.91324*	*3.5*	*0.32942*	*2.9*	*0.84*	*2599*	*61*	*2221*	*61*	*1836*	*92*	*71*
ZR32	*0.01*	*0.69*	*293*	*0.18542*	*4.6*	*7.50485*	*6.0*	*0.29353*	*3.8*	*0.64*	*2702*	*147*	*2174*	*104*	*1659*	*111*	*61*
ZR9N	*0.01*	*0.93*	*361*	*0.19015*	*3.2*	*12.30237*	*4.9*	*0.46921*	*3.7*	*0.75*	*2743*	*104*	*2628*	*90*	*2480*	*150*	*90*
ZR31N	*0.01*	*0.45*	*280*	*0.20326*	*1.6*	*4.26276*	*6.0*	*0.15209*	*5.7*	*0.96*	*2853*	*53*	*1686*	*96*	*913*	*97*	*32*
ZR8N	*0.01*	*0.90*	*185*	*0.20796*	*4.3*	*6.20352*	*6.9*	*0.21633*	*5.3*	*0.78*	*2890*	*137*	*2005*	*117*	*1262*	*122*	*44*
ZR10	*0.01*	*0.52*	*199*	*0.23097*	*4.1*	*12.06415*	*5.1*	*0.37881*	*3.1*	*0.60*	*3059*	*129*	*2609*	*94*	*2071*	*108*	*68*
ZR22	*0.00*	*0.56*	*304*	*0.24250*	*7.9*	*9.35133*	*9.7*	*0.27966*	*5.6*	*0.58*	*3136*	*240*	*2373*	*170*	*1590*	*157*	*51*

Supplementary Table 4.II.4. Results of U-Pb isotope analysis by LA-ICP-MS on zircon from sample CO-820 (Correreca Granite). Data in black were used for Concordia diagrams. Data in red, were excluded. (*) Data are grouped according to $^{207}Pb/^{206}Pb$ apparent ages. See text for discussion.

SAMPLE	CO-820																
	Ratios										Apparent ages						
GRAIN	*f* 206 (%)	Th/U	$^{206}Pb/^{204}Pb$	$^{207}Pb/^{206}Pb$	err (%) 1 б	$^{207}Pb/^{235}U$	err (%) 1 б	$^{206}Pb/^{238}U$	err (%) 1 б	Rho	$^{207}Pb/^{206}Pb$	2 б (abs)	$^{207}Pb/^{235}U$	2 б (abs)	$^{206}Pb/^{238}U$	2 б (abs)	conc. (%)
(*) Group 1861±7 Ma																	
ZR34B	0.01	0.66	62815	0.10964	1.8	5.58317	3.0	0.36931	2.3	0.78	1793	66	1914	50	2026	80	113
ZR24	0.00	1.32	46281	0.10726	1.8	5.03633	1.8	0.33031	1.3	0.74	1809	41	1825	30	1840	42	102
ZR29	0.00	0.59	96622	0.11119	1.6	5.28099	1.2	0.34418	1.0	0.80	1820	23	1866	21	1907	32	105
ZR26	0.00	0.80	59732	0.08629	9.9	5.02761	2.2	0.32748	1.6	0.72	1821	53	1824	37	1826	50	100
ZR11	0.00	0.42	39596	0.10882	1.5	5.12766	1.2	0.33158	0.9	0.76	1835	26	1841	21	1846	30	101
ZR16B	0.00	0.87	30614	0.11256	1.2	5.04246	1.7	0.32525	1.3	0.77	1839	37	1826	29	1815	41	99
ZR28	0.00	0.97	138288	0.11253	0.6	5.16866	1.2	0.33326	1.0	0.80	1840	22	1847	21	1854	31	101
ZR25	0.00	0.90	80056	0.11365	0.9	4.71799	2.4	0.30401	1.9	0.77	1841	53	1770	40	1711	56	93
ZR3B	0.00	0.70	181943	0.11285	0.6	5.76729	1.4	0.37161	1.0	0.72	1841	34	1942	25	2037	36	111
ZR5B	0.00	0.57	201614	0.11213	0.8	5.28773	1.2	0.34067	0.8	0.69	1841	28	1867	20	1890	26	103
ZR31	0.00	0.57	63772	0.11147	1.9	5.33305	2.2	0.34335	1.7	0.76	1842	50	1874	38	1903	56	103
ZR32	0.00	0.94	402944	0.11353	0.9	5.48440	1.5	0.35278	1.1	0.71	1844	36	1898	26	1948	35	106
ZR33	0.00	0.63	77464	0.11242	0.8	5.32574	1.2	0.34179	0.8	0.65	1848	29	1873	20	1895	25	103
ZR23	0.00	0.80	69814	0.11333	1.2	5.04577	1.9	0.32362	1.5	0.81	1849	37	1827	31	1807	48	98
ZR8	0.00	0.98	40221	0.11244	0.7	5.44601	1.8	0.34916	1.6	0.88	1850	26	1892	30	1931	52	104
ZR2	0.01	1.56	70759	0.11384	0.4	5.39014	1.0	0.34534	0.7	0.78	1851	17	1883	16	1912	25	103
ZR22	0.00	0.81	30522	0.11466	0.6	6.21193	2.2	0.39790	2.0	0.93	1852	24	2006	38	2159	74	117
ZR21	0.00	0.82	38226	0.11342	1.7	5.24121	2.0	0.33552	1.4	0.71	1853	48	1859	33	1865	45	101
ZR9	0.00	0.50	77342	0.11343	1.1	6.30487	4.6	0.40352	4.5	0.98	1853	26	2019	79	2185	166	118
ZR4	0.00	1.40	45276	0.11485	2.0	5.83748	3.0	0.37319	2.3	0.78	1855	65	1952	51	2044	82	110
ZR12	0.00	1.30	50014	0.11359	2.6	5.70445	1.5	0.36428	1.3	0.87	1857	24	1932	26	2002	46	108
ZR13B	0.01	0.66	219303	0.11379	0.4	5.25136	1.0	0.33524	0.8	0.82	1858	16	1861	17	1864	27	100
ZR30	0.00	0.83	55707	0.11297	1.3	5.43701	1.9	0.34683	1.4	0.76	1859	42	1891	32	1919	47	103
ZR14	0.00	0.70	98173	0.11958	1.2	6.66442	2.2	0.42458	1.9	0.87	1861	37	2068	39	2281	75	123
ZR6	0.00	0.89	20989	0.11516	2.1	5.78788	2.0	0.36782	1.4	0.73	1866	46	1945	34	2019	50	108
ZR17B	0.00	0.54	70762	0.11425	0.5	5.10983	1.0	0.32434	0.8	0.76	1868	19	1838	17	1811	24	97

ZR19	0.00	0.68	38868	0.11496	0.8	5.25805	1.2	0.33373	0.9	0.77	1868	23	1862	20	1856	29	99
ZR18	0.00	0.89	51379	0.11519	1.0	5.27008	1.2	0.33369	0.7	0.60	1873	32	1864	21	1856	23	99
ZR5N	0.00	0.90	83013	0.11468	1.0	5.47415	1.5	0.34659	1.1	0.76	1873	32	1897	25	1918	37	102
ZR23B	0.01	0.65	89149	0.11460	1.4	5.28139	1.7	0.33421	0.9	0.55	1874	49	1866	28	1859	29	99
ZR7	0.00	1.08	84440	0.11511	0.9	4.91857	2.3	0.31115	2.1	0.92	1874	31	1805	39	1746	66	93
ZR16N	0.00	1.10	39987	0.11497	0.9	5.12211	1.3	0.32351	1.0	0.77	1877	27	1840	22	1807	32	96
ZR4B	0.01	0.87	10680	0.11509	0.8	4.89572	1.2	0.30848	0.8	0.64	1881	30	1802	20	1733	23	92
ZR7B	0.00	1.04	38567	0.11538	1.4	4.94757	1.9	0.31097	1.2	0.65	1886	49	1810	31	1745	37	93
ZR13N	0.00	0.81	50353	0.11432	1.3	5.62092	2.2	0.35277	1.8	0.82	1889	42	1919	37	1948	59	103
ZR3N	0.00	0.95	118441	0.11391	0.5	4.57172	2.3	0.28692	1.9	0.81	1889	47	1744	38	1626	53	86
ZR17	0.00	1.05	69032	0.12513	3.7	5.21038	2.3	0.32675	1.8	0.78	1890	49	1854	38	1823	56	96
ZR15	0.00	1.02	40676	0.11525	0.8	5.00245	1.4	0.31360	1.2	0.84	1891	23	1820	23	1758	35	93
ZR10	0.00	1.26	6432	0.11543	1.1	5.00499	1.4	0.31095	1.0	0.70	1907	34	1820	24	1745	30	92
ZR2B	0.01	0.87	2817	0.11882	0.6	5.45399	1.1	0.33287	0.9	0.76	1939	23	1893	19	1852	27	96
Excluded Data																	
ZR24B	*0.00*	*1.41*	*3304*	*0.12271*	*3.6*	*5.76862*	*4.1*	*0.34092*	*1.9*	*0.45*	*1996*	*127*	*1942*	*70*	*1891*	*61*	*95*
ZR1	*0.00*	*1.10*	*2180*	*0.15381*	*2.5*	*4.06566*	*5.2*	*0.18732*	*4.3*	*0.82*	*2428*	*99*	*1647*	*84*	*1107*	*87*	*46*
ZR20	*0.00*	*0.63*	*1438*	*0.12337*	*1.2*	*5.75597*	*1.7*	*0.33735*	*1.3*	*0.77*	*2011*	*35*	*1940*	*29*	*1874*	*42*	*93*
ZR27	*0.00*	*0.51*	*731*	*0.12373*	*1.5*	*3.64432*	*3.1*	*0.21187*	*2.8*	*0.89*	*2025*	*47*	*1559*	*49*	*1239*	*62*	*61*

Supplementary Table 4.II.5. Results of U-Pb isotope analysis by LA-ICP-MS on zircon from sample CLR-04 (Santana Gneiss). Data in black were used for Concordia diagrams. Data in red, were excluded. (*) Data are grouped according to $^{207}Pb/^{206}Pb$ apparent ages. See text for discussion.

SAMPLE	CLR-04																
	Ratios										Apparent ages						
GRAIN	*f* 206 (%)	Th/U	$^{206}Pb/^{204}Pb$	$^{207}Pb/^{206}Pb$	err (%) 1 б	$^{207}Pb/^{235}U$	err (%) 1 б	$^{206}Pb/^{238}U$	err (%) 1 б	Rho	$^{207}Pb/^{206}Pb$	2 б (abs)	$^{207}Pb/^{235}U$	2 б (abs)	$^{206}Pb/^{238}U$	2 б (abs)	conc. (%)
ZR19	0.01	1.660	6577	0.101665	1.2	2.295	3.4	0.164	3.16	0.93	1655	43	1211	47	977	57	59
ZR7	0.02	1.13	5848	0.104498	1.8	3.623	1.3	0.252	1.13	0.87	1701	19	1555	21	1449	29	85
ZR4	0.00	0.55	48204	0.119053	2.0	5.199	2.3	0.358	1.45	0.49	1722	65	1852	39	1971	49	114
ZR6	0.01	0.70	119963	0.107785	1.9	5.340	2.3	0.361	2.06	0.76	1752	35	1875	39	1988	70	113
ZR16	0.01	0.81	4341	0.107468	1.1	3.519	5.9	0.237	5.84	0.98	1757	38	1532	92	1374	144	78
ZR12	0.01	0.86	232997	0.105212	0.6	7.935	2.8	0.531	2.68	0.99	1773	28	2224	50	2745	119	155
ZR14	0.02	0.95	251752	0.106914	0.9	5.510	1.4	0.363	1.22	0.91	1798	20	1902	24	1999	42	111
ZR11	0.02	0.81	200685	0.110142	0.4	4.905	1.2	0.321	1.02	0.96	1811	17	1803	20	1796	32	99
ZR18	0.00	0.59	227707	0.111829	0.9	4.847	1.6	0.315	1.25	0.79	1826	32	1793	26	1764	39	97
Group 1475±46 Ma																	
ZR20	0.00	0.35	203807	0.091440	0.7	2.938	1.1	0.233	0.85	0.81	1458	23	1392	17	1349	21	93
ZR17	0.00	0.54	107991	0.109784	4.3	4.678	4.1	0.358	2.20	0.56	1521	127	1763	67	1975	75	130
(*) Group 1764±23 Ma																	
ZR1	0.01	0.49	133816	0.103815	0.0	4.476	1.0	0.313	0.77	0.743	1693	21	1727	17	1754	24	104
ZR9	0.00	0.76	37520	0.110288	2.7	4.670	2.6	0.321	1.71	0.73	1726	70	1762	43	1792	53	104
ZR8	0.00	0.43	120859	0.104902	3.9	4.468	4.2	0.306	3.04	0.68	1728	102	1725	68	1722	92	100
ZR3	0.00	0.43	97752	0.107475	1.1	4.705	1.6	0.318	1.22	0.77	1755	35	1768	27	1779	38	101
ZR2	0.00	0.51	42945	0.108434	1.0	4.661	1.5	0.313	1.02	0.77	1766	39	1760	25	1756	31	99
ZR10	0.00	0.59	130064	0.108416	0.8	4.525	1.3	0.304	1.01	0.92	1768	28	1736	22	1709	30	97
ZR5	0.00	0.35	57436	0.091669	7.1	4.835	1.4	0.320	1.02	0.38	1790	31	1791	23	1791	32	100
ZR15	0.00	0.43	32457	0.110595	1.4	5.147	1.7	0.339	1.32	0.72	1803	35	1844	28	1881	43	104
Excluded Data																	
ZR13	*0.00*	*0.68*	*56196*	*0.062766*	*3.2*	*0.996*	*2.9*	*0.113*	*1.93*	*0.64*	*741*	*87*	*702*	*29*	*690*	*25*	*93*
ZR21	*0.00*	*0.47*	*14344*	*0.166911*	*7.9*	*7.764*	*8.4*	*0.340*	*3.00*	*0.37*	*2513*	*251*	*2204*	*145*	*1887*	*98*	*75*

CAPÍTULO 5 - ARTIGO 2

"THE POLYCYCLIC EVOLUTION OF THE PARAGUÁ BLOCK, BOLIVIA-SW BRAZIL: A Sm-Nd AND U-Pb/Hf ISOTOPE STUDY OF THE PALEO- TO MESOPROTEROZOIC CHIQUITANIA COMPLEX"

Letícia A. Redes[1], Natalia Hauser[1], Amarildo S. Ruiz[2], Ramiro S. Matos[3], Wolf Uwe Reimold[1], Elton L. Dantas[1], Ralf-Thomas Schmitt[4], Márcio Martins Pimentel[1] (*in memoriam*)

[1] Laboratory of Geochronology and Isotope Geochemistry, University of Brasília, Brazil., Geosciences Institute, Asa Norte, Brasília, DF, Brazil, 70910-900. E-mail: leticiaredes@hotmail.com

[2]Geology Faculty, Geosciences School, University of Mato Grosso, Fernando Corrêa da Costa Avenue, 2367, Boa Esperança, Cuiabá, MT, Brazil, 78060-900.

[3]Instituto de Investigaciones Geológicas y del Medio Ambiente, University Mayor of San Andrés, Street 27, Geology Pavilion, La Paz, Bolivia.

[4]Museum für Naturkunde, Leibniz-Institute for Evolution and Biodiversity Science, Invalidenstrasse 43, 10115 Berlin, Germany.

ABSTRACT

Geochemical analysis, as well as Sm-Nd and U-Pb/Hf on zircon isotope analysis was conducted on gneisses from the Chiquitania Complex, Paraguá Block, Eastern Bolivia, to improve the understanding of the evolution of this terrane and its relationship with the neighboring Amazonian Craton and Rio Apa Block. The protoliths of these gneisses are related with magmatic arc settings. We distinguish the older Miraflores Gneiss with an upper intercept age of 1747±11 Ma, and the younger Rio Fortuna, San Miguel and Rosário gneisses with upper intercept ages of 1699±9 Ma, 1681±13 Ma, and 1678±21 Ma. Based on available U-Pb age data, the Eastern Bolivia basement including the Paraguá Block had a polycyclic evolution. Three major events are recognized: Event 1 related with emplacement of Orosirian granites of the Rio Apa Block at ca.

1.84 Ga; Event 2 related with magmatic arc development on the Paraguá Block at 1.75-1.65 Ga, and Event 3 related with the San Ignácio Orogeny at ca. 1.3 Ga. Event 2 comprises three cycles: Cycle 1 related with the Miraflores Arc at ca. 1.75 Ga, Cycle 2 with the surrounding more juvenile Rio Fortuna tonalite and Rosário/San Miguel monzogranites of ca. 1.69 Ga age, and Cycle 3 with the Triunfo/Matão/Turvo Granitoid Arc and the more juvenile, ca. 1.65 Ga Refugio Granite Arc. Negative ε_{Nd} values for the Miraflores Gneiss indicate mainly reworked crust, whereas the other arcs yielded positive values of $\varepsilon_{Nd(t)}$ and $\varepsilon_{Hf(t)}$ indicating that parental magmas represent mixing between mantle-derived material and reworked crust. Paleoproterozoic Nd and Hf T_{DM} indicate older, 2.64 to 1.82 Ga, crust was reworked in a volcanic arc setting at ca. 1.75 and 1.69 Ga. We interpret the Paraguá Block as a constituted block formed by accretionary belts, with an older central part (Miraflores Granodiorite Arc), akin to the Lomas Maneches terrane, surrounded by progressively younger magmatic arcs. Collision between the Paraguá Block and Amazonian Craton occurred at ca. 1.5 Ga; these continental blocks were later detached at ca. 1.4 Ga. Final amalgamation of the Paraguá and Rio Apa blocks with the Amazonian Craton occurred at ca. 1.3 Ga (San Ignácio Orogeny).

Keywords: Chiquitania Complex; Paraguá Block; Bolivian basement; Paleoproterozoic gneisses; Sm-Nd isotopes; U-Pb/Lu-Hf on zircon.

5.1. INTRODUCTION

The Paraguá Block was introduced as a "Paraguá Craton" by Litherland *et al*. (1986) as a region that was tectonically stable during the Meso- to Neoproterozoic Sunsas Orogeny (1.25-1.00 Ga, Teixeira *et al*., 2010) (Fig. 5.1 and 5.2). The Paraguá Block was an important addition during crustal growth along the western margin of South America during Paleo-/Mesoproterozoic times, and its relationship with the SW Amazonian craton and the Rio Apa Block has been a matter of intense debate over some 30 years (e.g., Litherland *et al*., 1986; Condie, 2002; Boger *et al*., 2005; Cordani and Teixeira *et al*., 2007; Santos *et al*., 2008; Bettencourt *et al*., 2010; Brito Neves and Fuck 2014; Teixeira *et al*., 2020, and others).

The relevant stratigraphic sequence comprises the Lomas Maneches Complex of ca. 1.96 Ga age (Litherland *et al*., 1986; Boger *et al*., 2005; Santos *et al*., 2008; Matos *et al*., 2013), followed by a suite of orthogneisses and paragneisses of the Chiquitania Gneiss Complex dated to ca. 1.75-1.69 Ga (Litherland *et al*., 1986; Boger *et al*., 2005; Santos *et al*., 2008; Faria *et al*., 2014; Figueiredo *et al*., 2013; Nedel *et al*., 2017), and an even younger unit comprising ca. 1.58 Ga old schist of the San Ignácio Group (Litherland *et al*., 1986; Boger *et al*., 2005).

There are two main controversies about the Paraguá Block. One is related to the stratigraphic relation between the Lomas Maneches and Chiquitania complexes (Litherland *et al*., 1986), and the other to the nature - allochthonous or par-/autochthonous of the Paraguá Block (Litherland *et al*., 1986; Boger *et al*., 2005; Santos *et al*., 2008; Bettencourt *et al*., 2010). Some authors (Litherland *et al*., 1986; Boger *et al*., 2005; Cordani and Tassinari, 2007; Ruiz, 2009; Bettencourt *et al*., 2010) postulated that the Paraguá Block represents an allochthonous crustal fragment that was added to the southern margin of the Amazonian proto-Craton between the Mesoproterozoic and Neoproterozoic. Other authors (Santos *et al*., 2008) discussed that there is no evidence for the existence of a microcraton (the supposed Paraguá Block) between the Sunsas Orogen and the Amazon Craton. These authors claimed that the Paraguá Block is almost totally composed of arc-related granitoids formed during the Candeias Orogeny (ca. 1.37–1.32 Ga).

As there are scarce isotopic data for the basement of the Paraguá Block, especially for the gneisses of the Lomas Maneches and Chiquitania complexes, more extensive, combined geochemical and isotopic, data for this basement are required. This would help to elucidate the role that the Paraguá Block could have had in the context of craton construction, magmatic and metamorphic events, namely crustal evolution, in this part of South America. To this effect, new geochemical and isotopic data (Sm-Nd and U-Pb/Hf on zircon) were obtained from the Miraflores Gneiss in the central part, and from the Rosário, San Miguel, and Rio Fortuna gneisses along the borders of the Paraguá Block (Fig. 5.3). These data will improve the knowledge about the position and crustal evolution of the Paraguá Block, as well as the sources and the tectonic environment of the protoliths and can contribute to the discussion about the controversy about the relationship between the Chiquitania and the Lomas Maneches complexes.

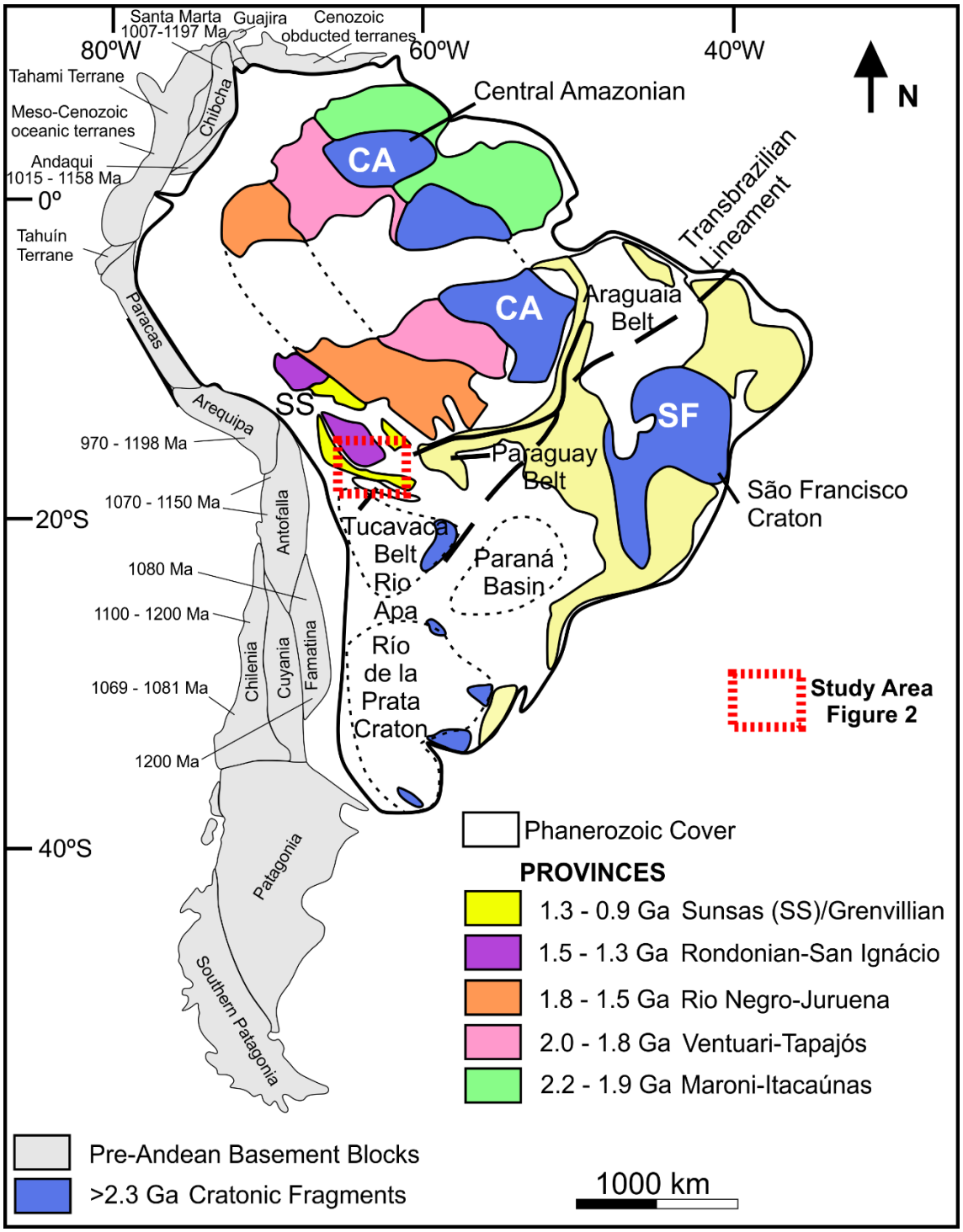

Figure 5.1. Geological provinces of the South American continent. Adapted from Cordani *et al*. (2000), Tassinari *et al*. (2000), Loewy *et al*. (2004), and Ramos (2010).

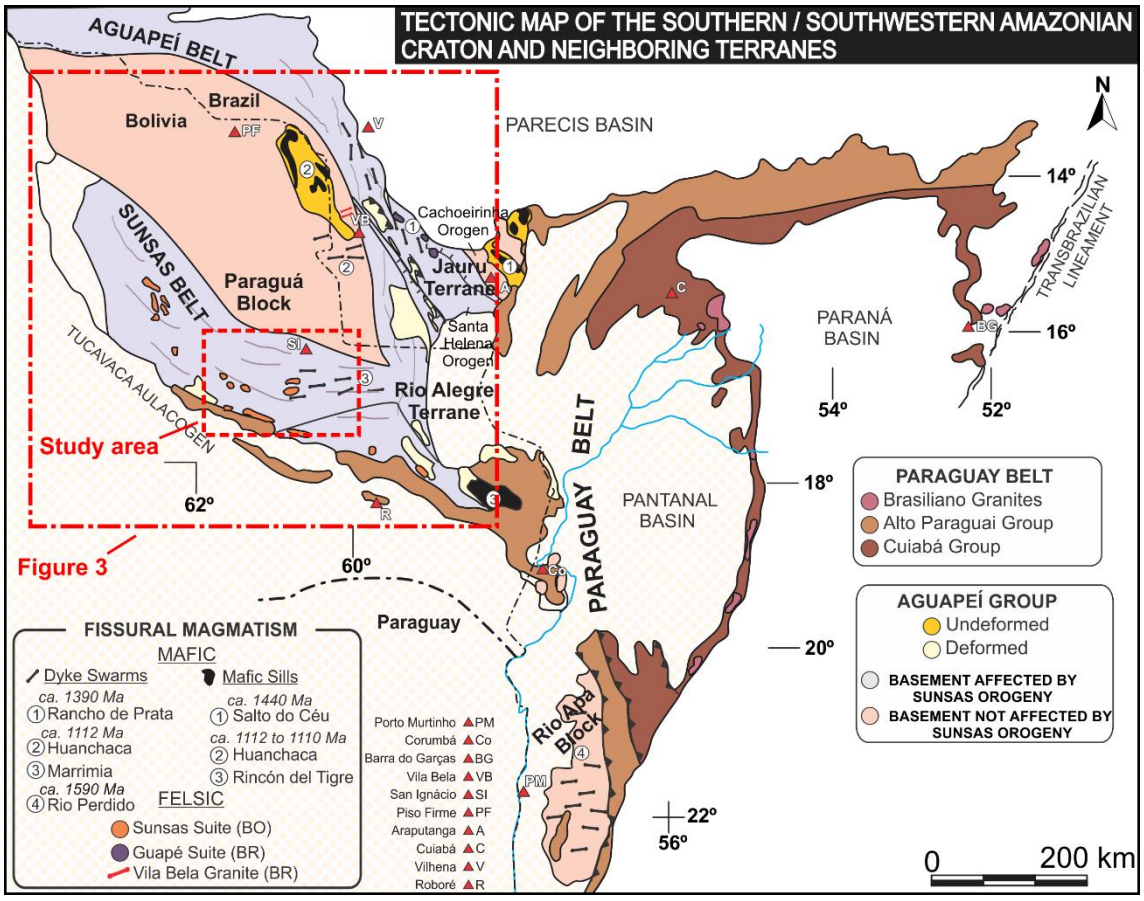

Figure 5.2. Tectonic map of the southern and southwestern parts of the Amazonian Craton (modified after Ruiz *et al*., 2010).

5.2. GEOLOGICAL SETTING AND GEOTECTONIC CONTEXT OF THE PARAGUÁ BLOCK

The vast Paraguá Block (Fig. 5.1 and 5.2) extends from the eastern part of Bolivia to the western part of Mato Grosso State in Brazil. The study area (Fig. 5.1 and 5.2) for the present work involves the Rondonian-San Ignácio and Sunsas-Aguapeí provinces (Cordani and Teixeira, 2007). The study area is bordered to the east by a remnant of oceanic crust, the Rio Alegre Terrane (Geraldes, 2000; Ruiz, 2005, 2009; Bettencourt *et al*., 2010). To the west, it is covered by the Phanerozoic sedimentary rocks of the Parecis Basin and volcano-sedimentary sequences from the Andes. To the north, the block is covered by the sedimentary strata of the Alto Paraguai and Pantanal do Orinoco basins, and to the south by the wetlands of the Beni-Mamoré (Chaco) basin. Tohver *et al*. (2004) increased the limits of the Paraguá Block to comprise an expansive area of Mato Grosso state and suggested that the east-west trending Nova Brasilândia belt of about 2000

km length represented the boundary between the Amazonian Craton and the Paraguá Block at the end of the Mesoproterozoic (Fig. 5.2).

Litherland *et al*. (1986) were the first to publish about a possible Precambrian block to the north of Bolivia, which they named the Paraguá Craton. They defined it as a tectonically stable region during the Meso- to Neoproterozoic deformation associated with the Sunsas and Aguapeí belts. The Paraguá Block has an extent of some 124,000 km^2 and hosts the units collectively called the pre-San Ignácio assemblage (Bettencourt *et al*., 2010). This terrane includes the Lomas Maneches Complex (ca. 1.82-1.69 Ga), Chiquitania Complex (ca. 1.80-1.66 Ga), and the San Ignácio Group (> 1.69 Ga), as well as the Pensamiento Granitoid Complex with ages between ca. 1.37 and 1.34 Ga that has been associated to the San Ignácio Orogeny (Bettencourt *et al*., 2010).

According to Matos (2012), the Serie Yarituses represents a magmatic event during the ca. 1.67-1.62 Ga period, with T_{DM} from 1.7 to 1.8 Ga and ε_{Nd} from +4.1 to + 0.2. Matos (2012) included in this series the La Cruz (ca. 1.67 Ga), Refúgio (ca. 1.67 Ga) and San Pablo (ca. 1.62 Ga) granites, which intrude the Lomas Maneches Complex.

The San Diablo Shear Zone (ZCSD) was proposed by Litherland *et al*. (1986) as the San Diablo Front (Fig. 5.3). The ZCSD is more than 5 km wide and characterized by intense deformation in a curvilinear zone, where the west and east portions of the shear zone have ENE and WNW orientation, with a sinistral kinematic direction. Originally the region to the south of the San Diablo Shear Zone, called the Cristal Block by Klinck and Litherland (1982), and the San Pablo Terrane by Saes *et al*. (1993), was described as an allochthonous block. Saes and Fragoso César (1996) pointed out that the ZCSD represents a tectonic discontinuity of the San Pablo Terrane and interpreted the zone as a suture zone between the Paraguá Block and the San Pablo Terrane. However, recent studies such as those by Nedel *et al*. (2017) have suggested that the ZCSD does not represent a suture zone between the Paraguá Block and the San Pablo Terrane, and that the Paraguá Block extends to the south of this shear zone. The Sunsas Orogeny (1.0 to 0.9 Ga) would have reworked the Paraguá Block in the areas affected by the Sunsas-Aguapeí belts, causing low-grade metamorphism and involving the emplacement of granites of dominantly acidic nature (Bettencourt *et al*., 2010).

Table 5.1. Geochronological review for the basement of the Paraguá Block, with information from (a) Litherland *et al*. (1986); (b) Boger *et al*. (2005); (c) Santos *et al*. (2008); (d) Figueiredo *et al*. (2013); (e) Matos *et al*., (2013); (f) Faria *et al*. (2014); (g) Nedel *et al*. (2017); and (h) this study

Unit	Lithology	Rb/Sr (Ma)		K/Ar (Ma)	Ages U/Pb (Ma)		$\varepsilon_{Nd(t)}$	T_{DM} (Ga)
		metamorphic	magmatic		metamorphic	magmatic		
San Ignácio Group	Micaschist (a), Metarkose (a), Gabbro (a), Amphibolite (a), Pelitic schists (b)			868±24 (a) 926±20 (a) 947±27 (a) 1032±22 (a) 1090±29 (a) 1198±31 (a)		1690 (b) 1764±6 (b)		
Chiquitania Complex	Refúgio Orthogneiss (c)					1641± 4 (c)	+4.06 (c)	1.66 (c)
	Turvo Gneiss (d)					1651±4 (d)		
	Rosário Gneiss (g)				1111±10 (g)	1685±5 (g)		
	San Miguel Gneiss (h)					1681±13 (h)	+1.93 (h)	1.81 (h)
	Las Madres Paragneiss (c)				1118±15 (c)	1690-1630 (c)	-4.88 (c)	1.86 (c)
	Rio Fortuna Gneiss (h)					1699±9 (h)	+0.75 (h)	1.95 (h)
	Rosário Gneiss (h)					1678±21 (h)	+0.92 (h)	1.89 (h)
	Rio Fortuna Gneiss (f)					1711±13 (f)		
	Rio Triunfo Gneiss (f)					1722±68 (f)		
	Rio Fortuna Orthogneiss (c)				1336±3 (c)	1734-1722 (c)	-3.83 (c)	2.06 (c)
	Miraflores Gneiss (h)					1747±11 (h)	-2.42 (h)	2.15 (h)
	Gneiss Biotite (b)				1333± 6 (a)	1764±6 (b)		
Lomas Maneches Complex	Orthogneiss (a)	1344±18 (a)	1970 (a)	1991 (a)				
	Orthogneiss (a)		1961 (a)					
	Charnockite (b)				1320±10 (b)	1663±13 (b)		
	Granodioritic gneiss (c)				1334±2 (c)		-3.97 (c)	2.06 (c)
	Orthoderived granulite (e)				1190±250 (e)	1640±12 (e)		
	Orthoderived granulite (e)					1658±15 (e)		
	Charnockite (b)					1755±70-1714±18 (b)		
	Orthoderived granulite (e)					1759±5 (e)		
	Orthogneiss (b)					1773±50-1689±5 (b)		
	Granulitic gneiss (c)				1339±4 (c)	1818±13 (c)	+0.57 (c)	2.07 (c)

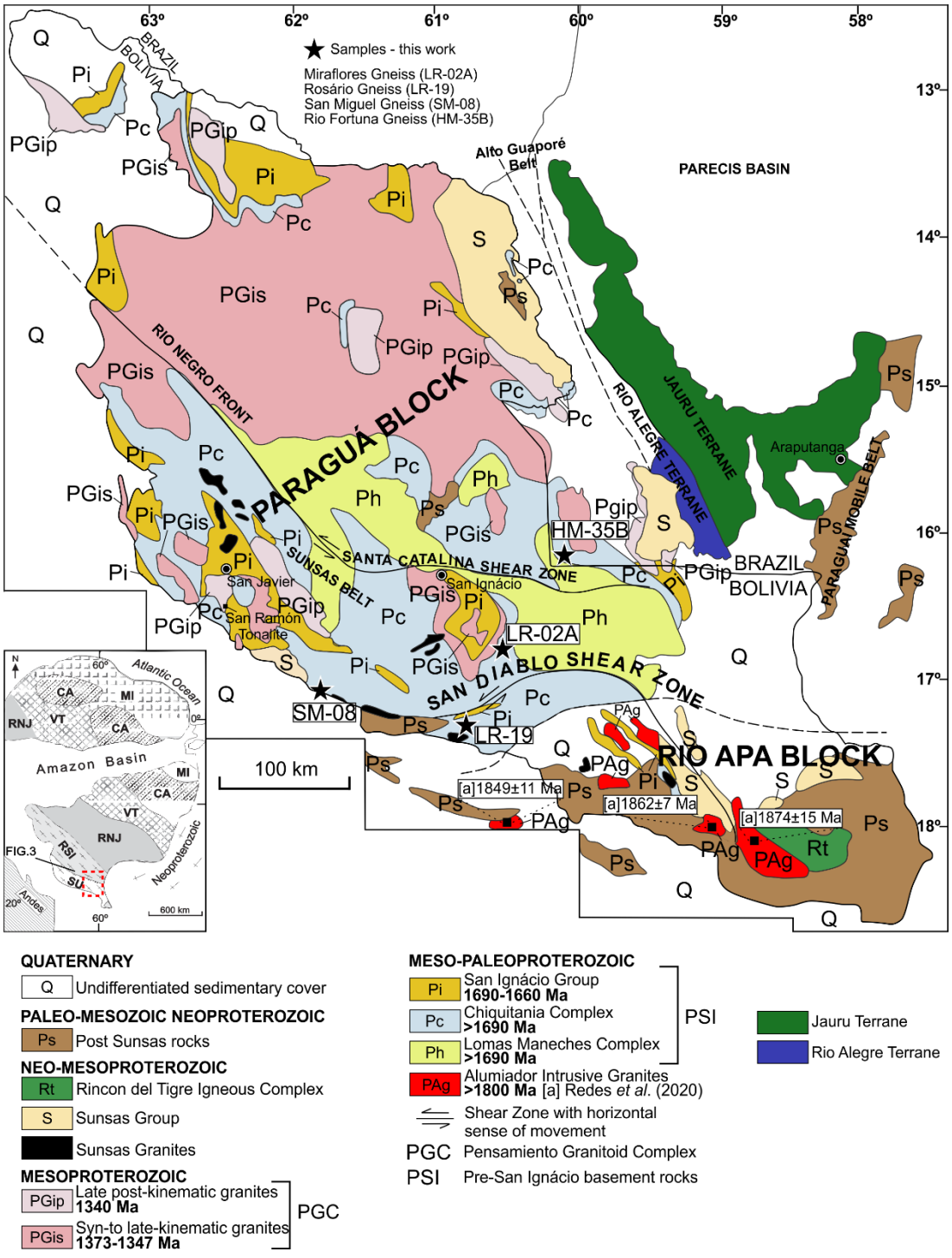

Figure 5.3. Major geological units and tectonic elements of the Paraguá Block and the northwestern Rio Apa Block in eastern Bolivia (modified after Litherland *et al.*, 1986; Ruiz, 2005; Matos *et. al*, 2009). Inset: The Amazonian craton with inferred limits between the Proterozoic provinces after Cordani and Teixeira (2007). Acronyms: Central Amazon - CA (> 2.6 Ga); Maroni-Itacaiúnas - MI (2.25 - 2.05 Ga); Ventuari-Tapajós - VT (1.98 - 1.81 Ga); Rio Negro-Juruena - RNJ (1.78 - 1.55 Ga); Rondonian-San Ignácio - RSI (1.55 - 1.30 Ga) and Sunsas - SU (1.25 - 0.97 Ga).

The Rondonian-San Ignácio and Sunsas-Aguapeí provinces

The term Rondonia-San Ignácio Province was proposed by Tassinari *et al*. (1996). This province comprises igneous and metamorphic rocks with ages between 1.56 and 1.3 Ga (Bettencourt *et al*., 2010), which are preserved in the regions around Rondônia (Brazil) and San Ignácio (eastern Bolivia, Fig. 5.1). The evolution of the Rondonian-San Ignácio Province was related with the formation of oceanic volcanic arcs and the development of continental arcs and accretionary prisms related to the closing of oceans and microcontinent-continent collisions, including late- to post-collision stages of collapse on a tectonically active Mesoproterozoic margin (Cordani *et al*., 1979, 2009; Teixeira *et al*., 1989, 2010; Tassinari and Macambira, 1999; Geraldes *et al*., 2001; Ruiz, 2005; Bettencourt *et al*., 2010). Continental collision occurred along the SW boundary of the Rio Negro-Juruena Province (Cordani and Teixeira, 2007). Evidence for this collision is well preserved in the Paraguá Block, in the form of the Pensamiento Granitoid Complex (Matos *et al*., 2009).

On the basis of geological mapping, petrographic and geochemical studies, and U-Pb (by ID-TIMS and SHRIMP) and ^{40}Ar-^{39}Ar data, the Rondonian-San Ignácio Province was divided by Bettencourt *et al*. (2010) into two evolutionary periods at about1.56–1.37 and 1.37–1.3 Ga. The older period is marked by diachronous events that formed the Cachoeirinha, Santa Helena and Rio Alegre (Bolivia-Mato Grosso border) accretional orogens and caused oceanic expansion (Bolivia-Rondônia border). The second period is synchronous along the continental margin and comprises subduction of the lithosphere and collision of an oceanic microcontinent (Paraguá Block) with the Amazonian proto-Craton (containing the Jauru and Rio Alegre terranes, see Figure 5.2 and Table 5.2). This latter period has been characterized as a collisional stage (ca. 1.34-1.32 Ga, Bettencourt *et al*., 2010). The Chiquitania and Lomas Maneches complexes in the Paraguá Block and the Alto Guaporé Belt in the Rio Negro-Juruena Province were mostly affected by deformation, high-grade metamorphism, and partial melting during the metamorphic peak of the Rondônia Region (Bettencourt *et al*., 2010). Subsequently, the Rondonian-San Ignácio Province was reached by deformation related to the collisions and metamorphism along the

Sunsas Orogeny (ca. 1.25-1.0 Ga, Teixeira *et al*., 2010). The Sunsas Orogeny has been identified in the Amazonian Craton and in the rocks of eastern Bolivia (Bettencourt *et al*., 2010).

The Sunsas-Aguapeí Province was formed at the end of the amalgamation of the Amazonian Craton during the construction of Rodinia and has been related to the Grenvillian Orogen of Laurentia (Tohver *et al*., 2004 2005; Cordani *et al*., 2009; Chew *et al*., 2008). Some models considered that the Sunsas Belt evolved over an extended time between ca. 1.45 and 1.10 Ga (Santos *et al*., 2000, 2008). However, this idea contrasts with the allochthonous characteristics observed in the Sunsas Orogen (Litherland *et al*., 1986, 1989), such as the folded layers of the Aguapeí Belt in relation to the less deformed Paraguá Block (Litherland and Bloomfield, 1981). The Sunsas Province includes the Sunsas and Vibosi groups (alluvial to deltaic lithologies) that were deposited in a passive margin environment and subsequently affected by the late Mesoproterozoic Sunsas Orogeny (Litherland and Bloomfield, 1981).

Table 5.2. Accretionary orogens of the Rondonian-San Ignácio Orogeny after (a) Geraldes (2000); (b) Geraldes *et al*. (2001); (c) Geraldes *et al*. (2004); (d) Matos *et al*. (2004); (e) Teixeira *et al*. (2010); (-- information not available).

TIMING OF ACCRETIONARY ORGENS	**1.37 Ga**	**1.48 - 1.42 Ga**	**1.56 - 1.52 Ga**
TERRANE	RIO ALEGRE TERRANE	JAURU TERRANE	JAURU TERRANE
ACCRETIONARY OROGENS	Rio Alegre Orogen	Santa Helena Orogen	Cachoeirinha Orogen
UNITS	Santa Rita Intrusive Suite (a) Mafic to Ultramafic Suites (d) Rio Alegre Volcanosedimentary Unit (a)	Rio Branco Intrusive Suite (c) Pindaituba Intrusive Suite (b) Santa Helena Intrusive Suite (b) Água Clara Intrusive Suite (a)	Alvorada Intrusive Suite (a) Santa Cruz Intrusive Suite (a) Figueira Branca Intrusive Suite (e)
U-Pb (Ma)	1379 to 1412 (a) 1494 to 1509 (d) 1509 to 1503 (a)	1471 to 1427 (c) 1465 to 1425 (b) 1455 to 1420 (b) 1485±4 (a)	1440±6 (a) 1549±10 (a) 1425±4 (e)
T_{DM} (Ga)	1.50 (a) 1.67 (d) 1.54 to 1.48 (a)	--- 1.50 to 1.60 (b) 1.50 to 1.60 (b) 1.80 (a)	1.70 - 1.80 (a) 1.80 (a) ---
$\varepsilon_{Nd(t)}$	+3.60 (a) +4.25 to +2.25 (d) -2.70 to -2.40 (a)	-15.20 to -8.30 (c) +2.06 to +2.04 (b) +3.10 to +3.90 (b) +1.70 (a)	-0.30 (a) +0.90 (a) ---

The Lomas Maneches and Chiquitania complexes: the stratigraphic controversy

There is some controversy concerning the regional stratigraphic relationship between the Lomas Maneches and Chiquitania complexes. Klinck and Litherland (1982), on the basis of regional unconformity, interpreted that the Lomas Maneches granulites represented oldest Paleoproterozoic basement. Litherland *et al*. (1986) proposed two models to explain the stratigraphy of the basement of eastern Bolivia. In the first, they suggested that the Lomas Maneches and Chiquitania complexes and the San Ignácio schists formed during the same Paleoproterozoic Orogeny, and that these units would represent a single stratigraphic sequence that transgresses the metamorphic sequence from schist, to gneisses, and granulites. In the second model, they considered a "cold basement" of Paleoproterozoic age and a younger supracrustal sequence, namely the sedimentary stage related to the San Ignácio Orogeny. Thus, the granulites of the Lomas Maneches Complex were considered the basement for the supracrustal shales of the San Ignácio Group, and the discontinuity was suggested to occur somewhere within the Chiquitania Complex (Litherland and Bloomfield, 1981). Litherland *et al*. (1986) considered that the pre-San Ignácio crust was older than ca. 1.96 Ga.

Boger *et al*. (2005) interpreted that the Lomas Maneches and Chiquitania complexes contained metasedimentary rocks derived from a ca. 1.76 Ga source and deposited after ca. 1.69 Ga. Santos *et al*. (2008) obtained an age of ca. 1.81 Ga for magmatic zircons from the Lomas Maneches Complex, and ages of ca. 1.77 and- 1.72 Ga for the Rio Fortuna and Santa Rita orthogneisses of the Chiquitania Complex. These relatively old zircon crystals were interpreted to be inherited from the Lomas Maneches Complex. Hence, Santos *et al*. (2008) interpreted the Lomas Maneches Complex as older than the Chiquitania Complex, and the San Ignácio Group as the youngest unit of the basement to the Paraguá Block.

Nedel *et al*. (2017) characterized the Miraflores and Rosário orthogneisses of the Chiquitania Complex in eastern Bolivia and obtained a crystallization age of ca. 1.68 Ga (Table 5.1). One zircon gave a possible age of metamorphism of ca. 1.11 Ga (Table 5.1) for this gneiss. The predominantly orthoderived Rio Fortuna, Matão, Triunfo and Retiro gneisses (Faria, 2015; Nascimento, 2015) form the Serra do Baú Complex (Ruiz, 2005; Faria, 2015). They occur in Mato

Grosso state at the Brazil-Bolivia border near Serra de Santa Bárbara and correspond to the orthogneisses of the Chiquitania Complex. Table 5.1 provides a summary of petrography, U-Pb, Sm-Nd and K-Ar data for the rocks comprising the basement of the Paraguá Block.

5.3. MATERIALS AND ANALYTICAL METHODS

The studied gneisses of the Chiquitania Complex occur in the eastern part of Santa Cruz department in eastern Bolivia. The Miraflores, Rio Fortuna and San Miguel gneisses occur north of the San Diablo Shear Zone (ZCSD), and the Rosário gneiss occurs in the southwestern part of the Paraguá Block (Fig. 5.2 and 5.3). Samples were collected for petrographic analysis, geochemistry, and Sm-Nd isotope analysis on whole rock samples, as well as for U-Pb/Lu-Hf isotope analysis on zircon (Laboratory of Geochronology and Isotope Geochemistry of Brasilia, see Supplementary Table 5.I.2). Thirty thin sections were prepared in the Lamination Laboratory at the Institute of Geosciences of the University of Brasilia (IG-UnB) for determination of the main mineral compositions, textural features, metamorphic grade, and deformation features (Supplementary Table 5.I.1). Details about the samples and the geochemical and isotope geochemical methods of this study are provided in the Supplementary Material 5.I.1 and Tables 5.I.2 to 5.I.9.

5.4. RESULTS

5.4.1. Geochemistry

The gneisses have a wide range of intermediate to acidic compositions, with silica contents between 65.4 and 73.7 wt% (Table 5.3; Fig. 5.4). The cationic classification diagram of Debon and Le Fort (1983; Fig. 5.4 A) indicates that the protolith of the Miraflores Gneiss would correspond to monzogranite and granodiorite, of the Rio Fortuna Gneiss to tonalite, of the San Miguel Gneiss to monzogranite, and of the Rosário Gneiss to granite. These protoliths plot into the I-type field and are related with calcium-alkaline to alkali-calcium magmatism (Fig. 5.4 B and C). They also have a magnesian to ferrous signature but are more affiliated to the magnesian domain (Fig. 5.4 D). The protoliths for the Miraflores and Rio Fortuna granodiorite and tonalite,

respectively, are classified as peraluminous, and the samples from the San Miguel and Rosário gneisses as metaluminous (Fig. 5.4 E).

All four gneisses are enriched in the LILE (Large-Ion Lithophile Elements) compared to HFSE (High Field Strength Elements) and have positive anomalies of K, Rb and Th that indicate crustal contributions (Rollinson, 1993) or the activity of fluids rich in these elements (Wilson, 1989). The HFSE show positive anomalies for Ce and Sm in comparison to Ta, Nb, Hf, Zr, Y and Yb. In Figure 5.5 A, the typical negative anomaly for Ta and Nb, which is normally referred to as an "arc-like signature" (Niu *et al*., 2013), was observed for all gneisses.

The gneisses have Rare Earth Element patterns (Fig. 5.5 B) compatible with calc-alkaline series magmatism (Rollinson, 1993), with La/Yb ratios between 5.04 and 34.30, and Eu/Eu* ratios around 0.058 (Table 5.3). The positive Eu anomaly observed for the samples from the Miraflores Gneiss is thought to be related to a higher abundance of plagioclase.

According to tectonic setting diagrams (Fig. 5.5 C and D), the protoliths would belong to the Volcanic Arc Granites (VAG), except for the Rio Fortuna Gneiss protolith that is positioned on the boundary between the Collision and Subduction fields.

Table 5.3. Geochemical data for the Rio Fortuna Gneiss (open square), Miraflores Gneiss (filled square), Rosário Gneiss (open triangle), and the San Miguel Gneiss (open circle). Major element data in wt% and trace element data in ppm.

Samples	**HM-35B** ☐	**LR-02D** ■	**LR-02B** ■	**LR-02C** ■	**LR-02A** ■	**LR-19** △	**SM-08** ○
Major elements (wt %)							
SiO_2	65.4	71.8	71.4	71.1	70.8	71.6	73.0
TiO_2	0.56	0.30	0.33	0.33	0.24	0.40	0.46
Al_2O_3	16.5	14.0	14.3	14.3	15.2	13.0	12.0
Fe_2O_3	5.00	2.23	2.29	2.31	2.31	2.87	3.48
MnO	0.12	0.06	0.07	0.07	0.04	0.02	0.05
MgO	1.30	0.48	0.52	0.63	0.40	0.83	0.86
CaO	4.31	2.93	2.28	2.19	1.92	1.59	1.74
Na_2O	4.46	3.67	3.85	4.61	4.22	3.57	3.11
K_2O	1.30	3.82	4.40	3.16	3.75	5.96	3.71
P_2O_5	0.12	0.06	0.06	0.06	0.04	0.07	0.07
LOI	0.30	0.40	0.40	0.80	0.70	0.40	1.20
Total	99.37	99.75	99.90	99.56	99.62	99.31	99.68
Trace elements (ppm)							
Sc	28	5	5	5	5	5	5
Ni	11	6	6	6	7	11	7
Cu	15	15	15	16	15	16	15
Zn	67	40	39	41	29	29	54
Ga	21	16	16	16	17	14	16
Rb	55	86	87	74	82	177	134
Sr	290	303	292	315	408	132	265
Y	46	21	17	7	5	14	18
Zr	264	279	291	301	205	406	368
Nb	13	8	11	6	5	8	10
Cs	0.8	0.5	0.6	0.9	0.6	2.3	0.7
Ba	287	1725	1360	1230	1820	893	903
Hf	6	7	7	7	5	11	9
Ta	1	1	1	1	0.3	0.8	2
Pb	15	15	15	55	15	15	15

Th	4	4	5	8	2	15	14
U	1	1	1	1	0	2	1
La	34	52	36	46	16	37	45
Ce	66	84	76	83	24	73	86
Pr	8	10	7	9	3	9	10
Nd	34	35	25	29	10	34	32
Sm	8	6	4	4	2	6	6
Eu	2	1	1	1	1	1	1
Gd	8	5	4	3	1	6	4
Tb	1	0.7	0.6	0.3	0.2	0.8	0.6
Dy	8	4	3	2	0.9	4	4
Ho	2	0.7	0.7	0.3	0.1	0.5	0.7
Er	5	2	2	0.9	0.4	1	2
Tm	0.8	0.3	0.3	0.1	1	0.2	0.3
Yb	5	2	2	1	0.6	0.8	2
Lu	0.7	0.3	0.3	0.2	0.1	0.1	0.2
$(La/Yb)_N$	5	19	14	34	21	34	19
$(La/Sm)_N$	3	6	6	7	7	4	5
$(Gd/Yb)_N$	1	2	2	2	2	6	2
Ba/La	9	33	38	27	112	24	20
Sr/Y	6	15	17	43	91	10	15
Eu/Eu*	0.06	0.06	0.06	0.06	0.06	0.06	0.06

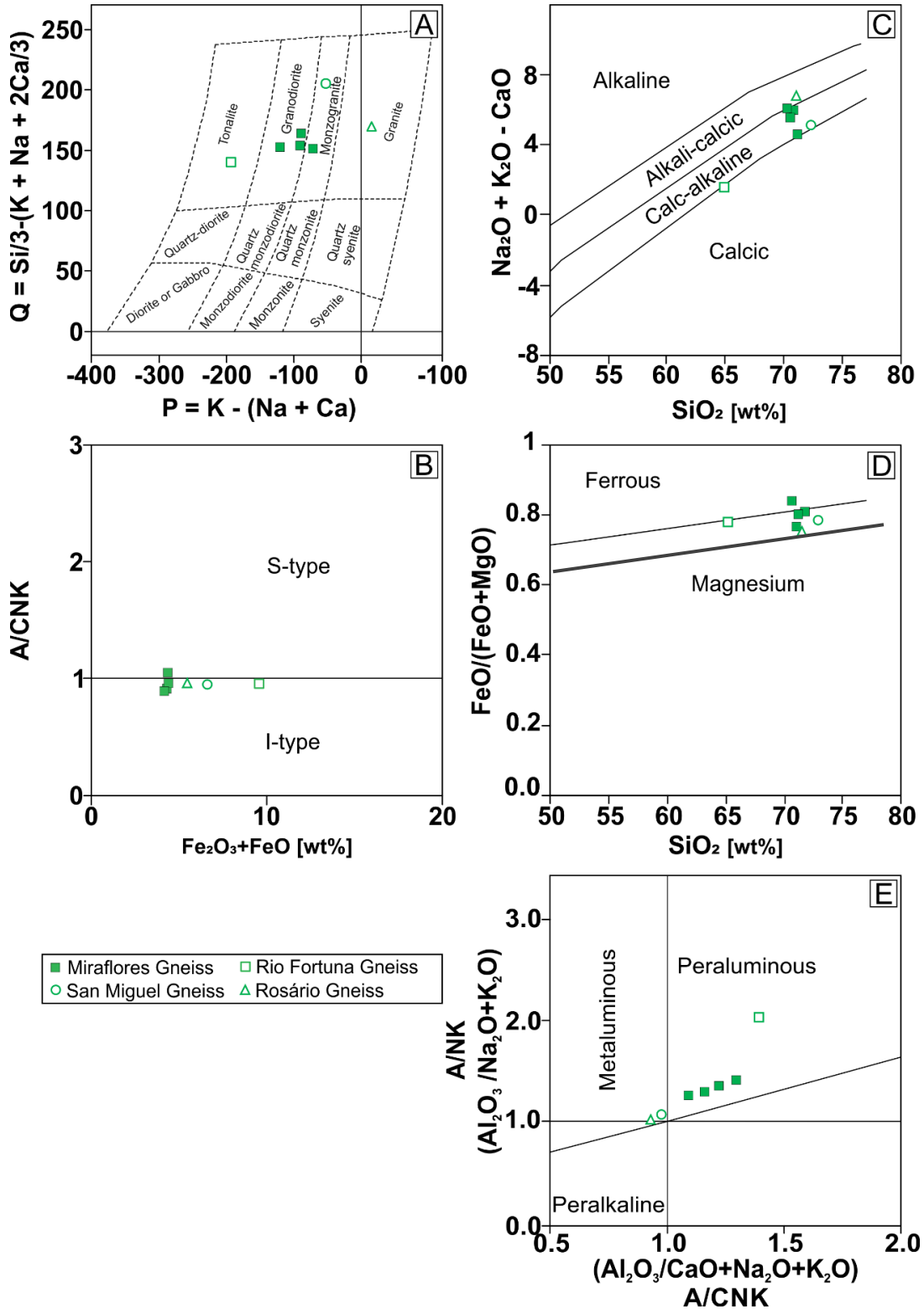

Figure 5.4. Geochemical characteristics of the Chiquitania Complex. (A) Q/P (Si/3 – (K+Na+2Ca/3)) data plot (Debon e Le Fort, 1983). (B) A/CNK (Al_2O_3/CaO+Na_2O+K_2O) *versus* Fe_2O_3+FeO data plot (Pearce *et al.*, 1984). (C) Na_2O+K_2O-CaO *versus* SiO_2 (Frost *et al.*, 2001). (D) FeO_t/(FeO_t+MgO) *versus* SiO_2 (Frost *et al.*, 2001). (E) A/NK (Al_2O_3 /Na_2O+K_2O) *versus* A/CNK (Al_2O_3/CaO+Na_2O+K_2O) after Maniar and Piccoli (1989).

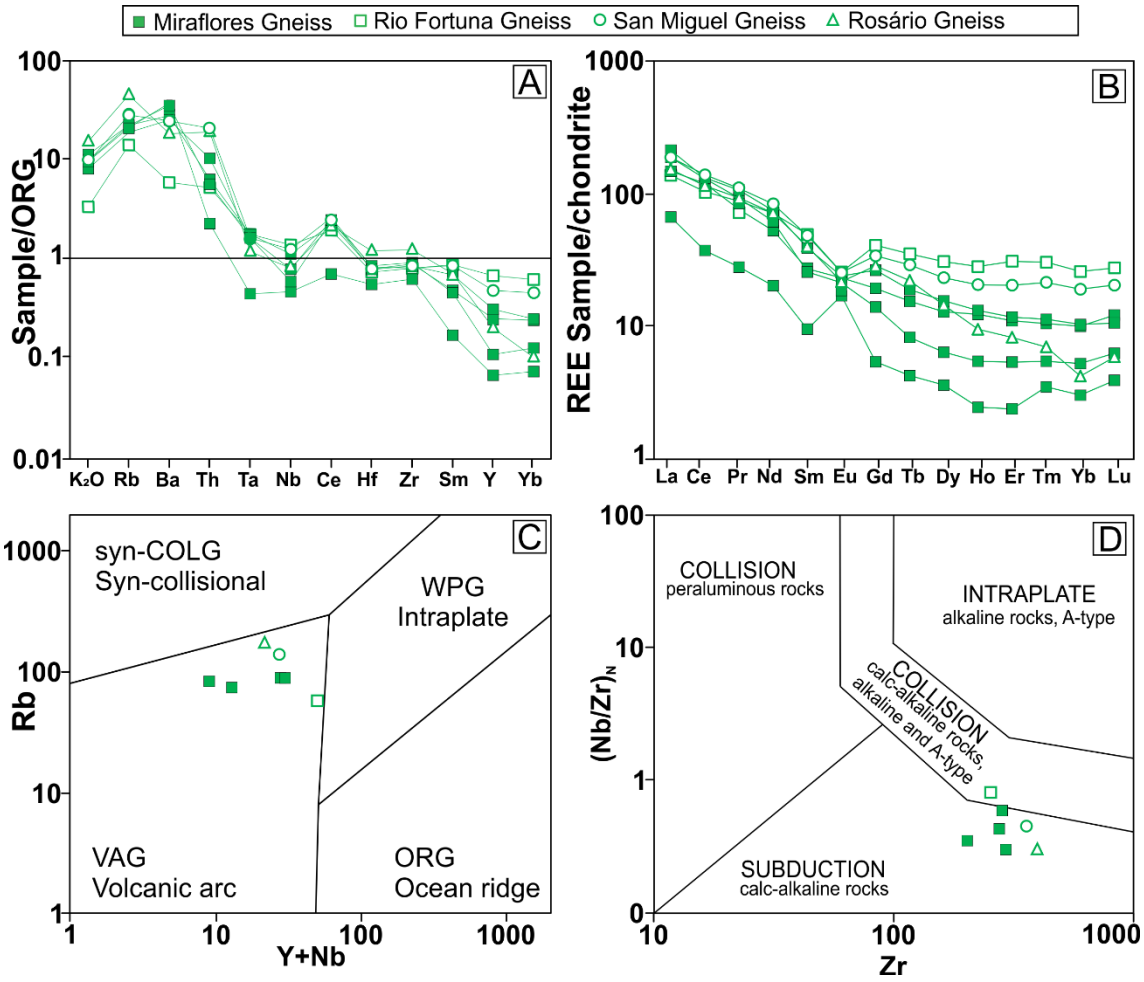

Figure 5.5. Element distribution patterns for the Miraflores, Rio Fortuna, San Miguel and Rosário gneisses. (A) Trace elements and K_2O normalised to granites from Mid-Ocean Ridges (ORG – Ocean Ridge Granites (Pearce *et al.*, 1984). (B) REE diagram normalised to C1 chondrite (normalization factors from Evensen *et al*., 1978). Tectonic setting diagrams for the Miraflores, Rio Fortuna, San Miguel, and Rosário gneisses: (C) Rb *versus* Y+Nb (Pearce *et al.*, 1984). (D) $(Nb/Zr)_N$ *versus* Zr (Thiéblemont and Tegyey, 1994). The Nb and Zr values were normalised to Zr = 9.714 and Nb = 0.617), as suggested by Hoffman (1988).

5.4.2. U-Pb and Lu-Hf isotope analysis on zircon

Miraflores Gneiss (sample LR-02A)

For this sample, 33 U-Pb isotope analyses were performed (Supplementary Table 5.I.5). Lu-Hf isotopic data were not obtained for this sample. Taking into account the apparent $^{207}Pb/^{206}Pb$ ages, four populations (I, II, III and IV) of concordant and discordant data were identified (Fig.

5.6 A), each anchored in the Concordia diagram by concordant data.

(I) Zircon crystals with darker cores and without zonation (Supplementary Table 5.I.4) define an upper intercept age of 1847±37 Ma (MSWD = 0.2) and have Th/U ratios of 0.07 to 0.93. (II) Concordant ages between ca. 1780 and 1732 Ma were obtained for the largest zircon population with Th/U ratios of 0.10-1.05. From this group, an upper intercept age of 1747±11 Ma (MSWD = 1.1; Fig. 5.6 A) was obtained for prismatic zircon crystals with irregular zonation, sometimes with cores that display magmatic zonation (Supplementary Table 5.I.4). We interpret this age as the crystallization age for the granodioritic protolith. (III) A population with an upper intercept age of 1425±32 Ma (MSWD = 0.3; Fig. 5.6 A) was obtained on zircon rims and cores with chaotic zonation (Supplementary Table 5.I.4). The Th/U ratios for this group of crystals are low, between 0.03 and 0.07. (IV) The youngest population of data that gave an upper intercept age of 1291±26 Ma (MSWD = 0.8) was obtained exclusively from rims of 5 zircon crystals with metamorphic characteristics (BSE images in Fig. 5.6 A). The Th/U ratios for these analyses are between 0.08 and 0.15. One zircon crystal (ZR8) has a core with a U-Pb age of ca. 1813 Ma and a rim of 1291±26 Ma. It is a typical example of an inherited crystal reworked during a metamorphic event.

Rio Fortuna Gneiss (sample HM-35B)

Thirty analyses were performed on zircon from this sample (Supplementary Table 5.I.6). Two main populations (I and II) were identified (Fig. 5.6 B). (I) A main group of data representing 86 % of the analyzed crystals with $^{207}Pb/^{206}Pb$ ages between ca. 1716 and 1670 Ma and with Th/U ratios of 0.28 to 0.60. They give an upper intercept age of 1699±9 Ma (MSWD = 0.3; Fig. 5.6 B) that is interpreted as the crystallization age of the tonalitic protolith of the Rio Fortuna Gneiss. (II) The analyzed rims (Supplementary Table 5.I.4), with $^{207}Pb/^{206}Pb$ ages between ca. 1625 and 1579 Ma and Th/U ratios of 0.20 and 0.36, give an upper intercept age of 1578±81 Ma. Only one concordant data point of 1415±14 Ma was obtained (Fig. 5.6 B) for ZR12 zircon crystal with a low Th/U ratio of 0.06.

Eleven zircon crystals with $^{207}Pb/^{206}Pb$ ages between ca. 1716 and 1670 Ma (Supplementary Table 5.I.9; Fig. 5.10 B) gave positive $\varepsilon_{Hf(t)}$ values between +1.70 and +7.40, and Paleoproterozoic Hf model ages between 2.23 and 1.87 Ga.

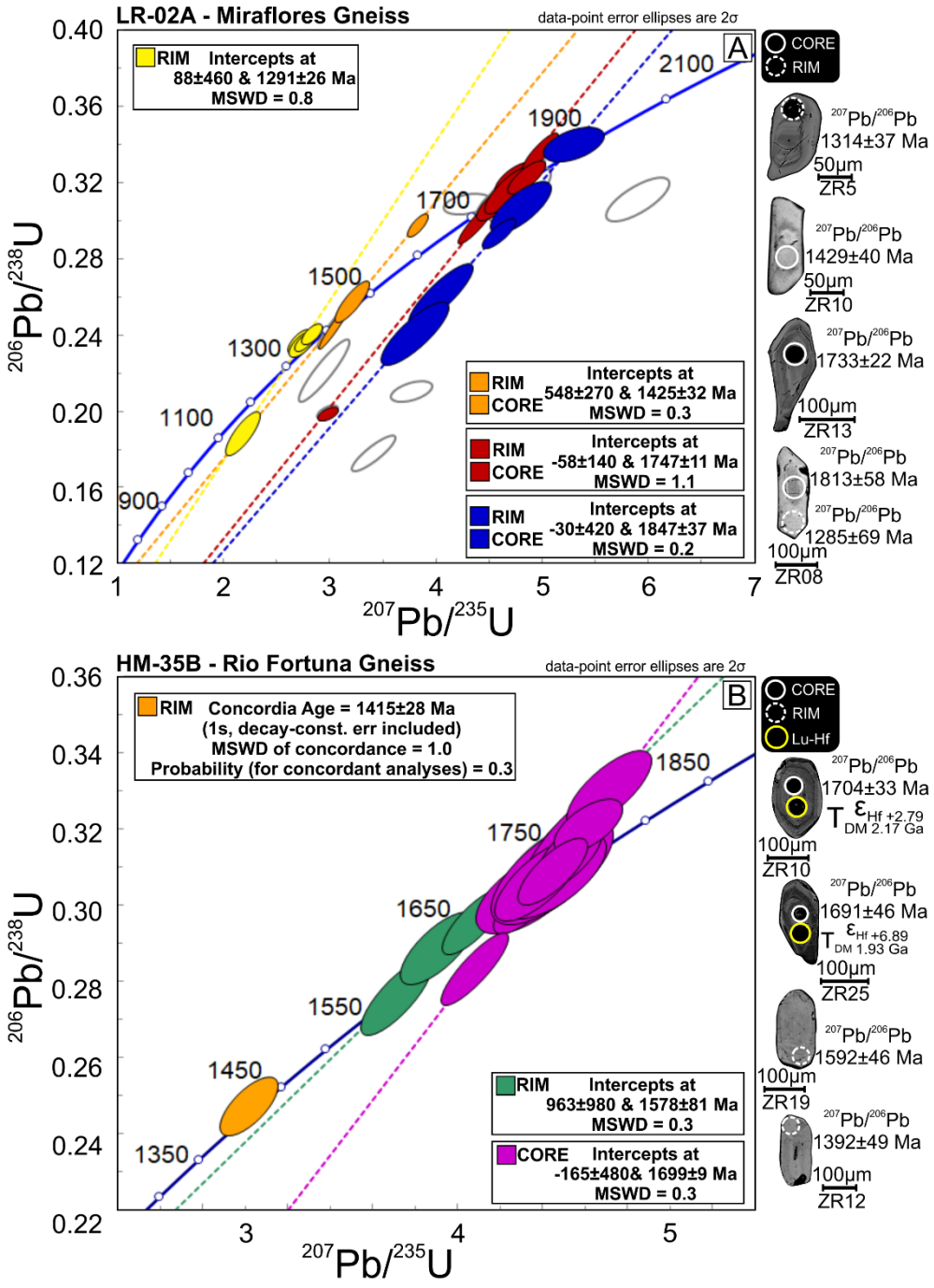

Figure 5.6. U-Pb Concordia diagram showing the LA-ICP-MS zircon spot data for (A) LR-02A (Miraflores Gneiss) and (B) HM-35B (Rio Fortuna Gneiss) samples. For the Miraflores Gneiss, the Discordia lines and error ellipses are red for the protolith age, blue for inherited crystals, green for data related with reworking, and yellow to metamorphic overprint. For the Rio Fortuna Gneiss, the Discordia lines and error ellipses are pink for the age of the tonalitic protolith, and green for

reworked grains. Concordant data are shown in yellow. Backscattered electron (BSE) images of some of the analyzed zircon crystals are shown on the right side. The 30 µm spots, related to U-Pb isotope analyses, are shown by white circles, and the 40 µm spots, related to the Lu-Hf isotope analyses, are shown as yellow circles.

San Miguel Gneiss (sample SM-08)

The 42 U-Pb isotope analyses carried out on zircon crystals from this sample (Supplementary Table 5.I.7) allow to define four populations (I, II, III and IV) with different apparent $^{207}Pb/^{206}Pb$ ages (Fig. 5.7 A). (I) The population of $^{207}Pb/^{206}Pb$ ages between ca. 1730 and 1599 Ma and Th/U ratios of 0.20 to 0.47 was obtained in cores and rims of crystals. An upper intercept age of 1681±13 Ma (MSWD = 1.1; Fig. 5.7 A) was calculated. It is interpreted as the crystallization age of the San Miguel monzogranitic protolith gneiss. (II) A population with $^{207}Pb/^{206}Pb$ apparent ages between ca. 1570 and 1527 Ma and Th/U ratios between 0.05 and 0.27 gave an upper intercept age of 1546±19 Ma (MSWD = 1.3; Fig. 5.7 A). These ages were obtained in zircon cores and rims with chaotic zonation, gulfs, and apparent flow structures (Supplementary Table 5.I.4). (III) The population with apparent $^{207}Pb/^{206}Pb$ ages between ca. 1364 and 1305 Ma and Th/U ratios between 0.03 and 0.11 was obtained solely on rims of crystals. These data enable the definition of an upper intercept age of 1320±19 Ma (MSWD = 0.8, Fig. 5.7 A) that is related to a metamorphic event. (IV) The youngest group of upper intercept ages of ca. 1271 and 1230 Ma was also obtained on rims. This population defines a Concordia age of 1256±26 Ma (MSWD = 0.5; Fig. 5.7 A), and the corresponding crystals have Th/U ratios of 0.10-0.14.

Lu-Hf isotope analysis (Supplementary Table 5.I.9; Fig. 5.10 B) was done on seven zircon crystals with U-Pb ages between ca. 1708 and 1599 Ma. Positive $\varepsilon_{Hf(t)}$ values between +0.30 and +6.90 and Paleoproterozoic Hf model ages between 2.32 and 1.88 Ga were obtained. One zircon with an age of ca. 1439 Ma gave a positive $\varepsilon_{Hf(t)}$ of +2.8 and a Paleoproterozoic Hf model age of 1.96 Ga.

Rosário Gneiss (sample LR-19)

Of 37 U-Pb isotope analyses on zircon crystals (Supplementary Table 5.I.8), 35 are represented on the Concordia diagram (Fig. 5.7 B). Three populations (I, II and III) with different $^{207}Pb/^{206}Pb$ apparent ages were identified. (I) A $^{207}Pb/^{206}Pb$ age set between ca. 1738 and 1627 Ma was obtained from analyses made on cores and rims of prismatic zircon crystals. These grains show irregular zoning, irregular core design, and sometimes magmatic zoning (Supplementary Table 5.I.4) and have Th/U ratios of 0.29 to 0.62. These data define an upper intercept age of 1678±21 Ma (MSWD = 3.0; Fig. 5.7 B). This age is interpreted as the crystallization age for the monzogranitic protolith of the Rosário Gneiss. (II) The second age population was obtained in zircon cores with convoluted zoning and flow structure. Apparent $^{207}Pb/^{206}Pb$ ages between ca. 1542 and 1531 Ma define an upper intercept age of 1538±24 Ma (Fig. 5.7 B). The Th/U ratios for this group are between 0.10 and 0.26. (III) Apparent $^{207}Pb/^{206}Pb$ ages of ca. 1390 to 1300 Ma were obtained on clear, typically metamorphic rims. The cores of this grain population gave ages between ca. 1649 and 1600 Ma.

Lu-Hf analyses were performed on six zircon crystals from the oldest group (I) with ages between ca. 1738 and 1632 Ma (Supplementary Table 5.I.9; Fig. 5.7 B). They yielded negative to positive $\varepsilon_{Hf(t)}$ values between -0.90 and +8.90 and Paleoproterozoic Hf model ages between 2.34 and 1.82 Ga.

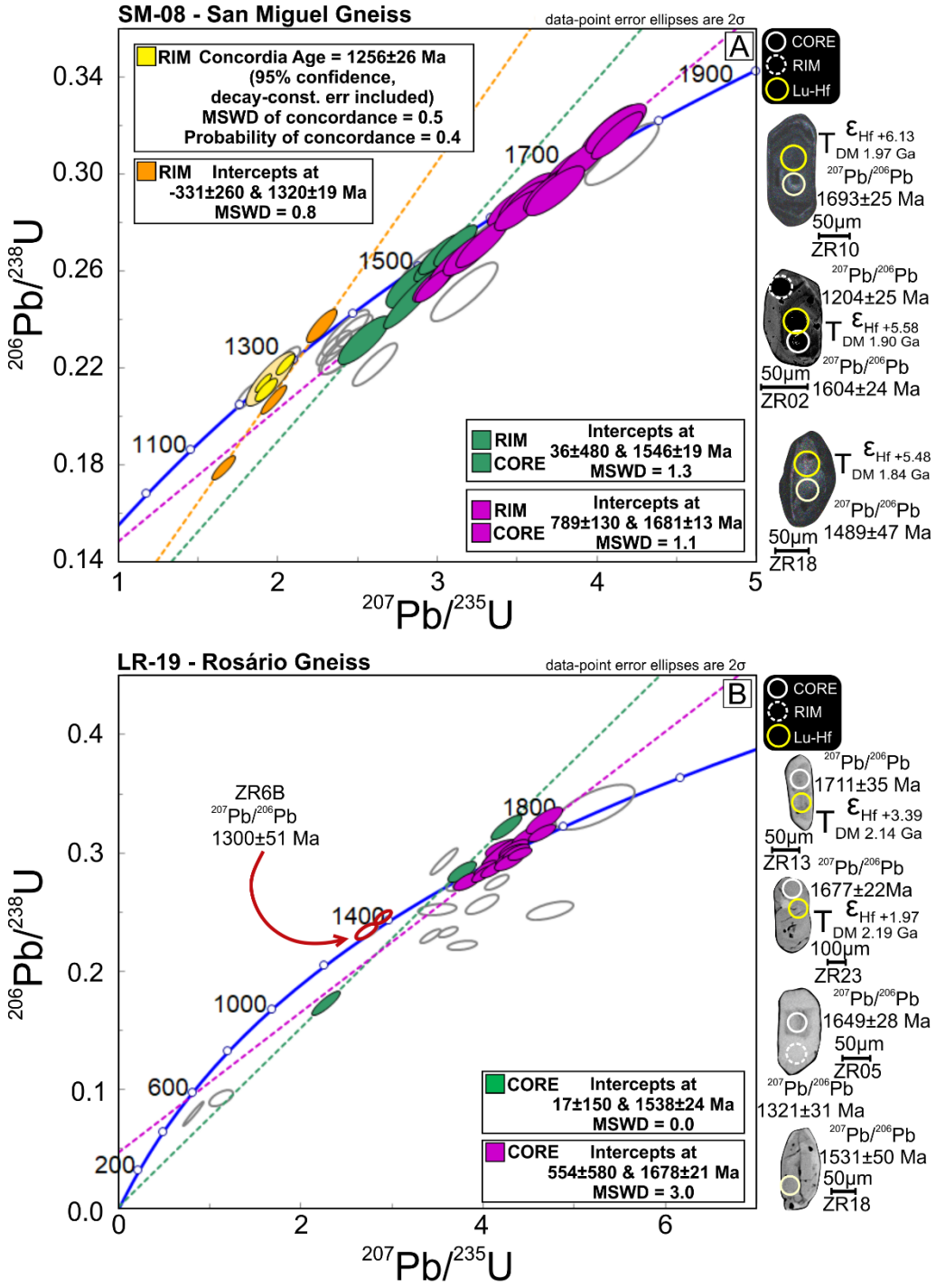

Figure 5.7. U-Pb Concordia diagram showing the LA-ICP-MS zircon spot data for samples: (A) SM-08 (San Miguel Gneiss) and (B) LR-19 (Rosário Gneiss). For the San Miguel Gneiss, the Discordia lines and error ellipses are blue for the age of monzogranitic protolith, pink for inherited grains, green for zircon related to reworking, and yellow for metamorphic overprint. The Concordia age of 1256±26 Ma reveals the youngest metamorphic event found for the San Miguel Gneiss. For the Rosário Gneiss, the Discordia lines and error ellipses are orange for the monzogranitic protolith age, pink for inherited zircon population and green for reworking. Scarce concordant and discordant data in grey that do not define a Discordia line are also shown. The 30

μm spots, related to the U-Pb analyses, are shown by white circles, and the 40 μm spots, related to the Lu-Hf analyses, as yellow circles.

5.4.3. Sm-Nd Isotope Data

The Sm-Nd isotope results for the four studied gneisses are shown in Table 5.4 and Figure 5.8. The Miraflores Gneiss (sample LR-02A) has a negative $\varepsilon_{Nd(1747)}$ of -2.42 and a model age of 2.15 Ga. The Rio Fortuna Gneiss (sample HM-35B) has a slightly positive $\varepsilon_{Nd(1699)}$ of +0.75 and a model age of 1.95 Ga. The San Miguel Gneiss (sample SM-08) has a positive $\varepsilon_{Nd(1681)}$ of +1.93 and a model age of 1.81 Ga, and the Rosário Gneiss (sample LR-19) a positive $\varepsilon_{Nd(1678)}$ of +0.92 and a model age of 1.89 Ga.

Table 5.4. Sm-Nd isotopic data for the gneisses from the Chiquitania Complex, Bolivia-Brazil border, of this study

Sample	Rock Type	Protolith	Unit	Age (Ma)	Sm (ppm)	Nd (ppm)	$^{147}Sm/^{144}Nd$	$^{143}Nd/^{144}Nd_m$ (±2σ)	$^{143}Nd/^{144}Nd_t$	$\varepsilon_{Nd(0)}$	$\varepsilon_{Nd(t)}$	T_{DM} (Ga)
LR-02A	Orthogneiss	monzogranite	Miraflores	1747	1.92	11.03	0.1050	0.511459 ± 26	0.510250	-22.99	-2.42	2.15
HM-35B	Orthogneiss	tonalite	Rio Fortuna	1699	8.65	41.13	0.1271	0.511898 ± 6	0.510477	-14.43	+0.75	1.95
SM-08	Orthogneiss	monzogranite	San Miguel	1681	4.71	27.48	0.1036	0.511708 ± 11	0.510591	-18.14	+1.93	1.81
LR-19	Orthogneiss	monzogranite	Rosário	1678	6.05	31.37	0.1165	0.511804 ± 8	0.510540	-16.26	+0.92	1.89

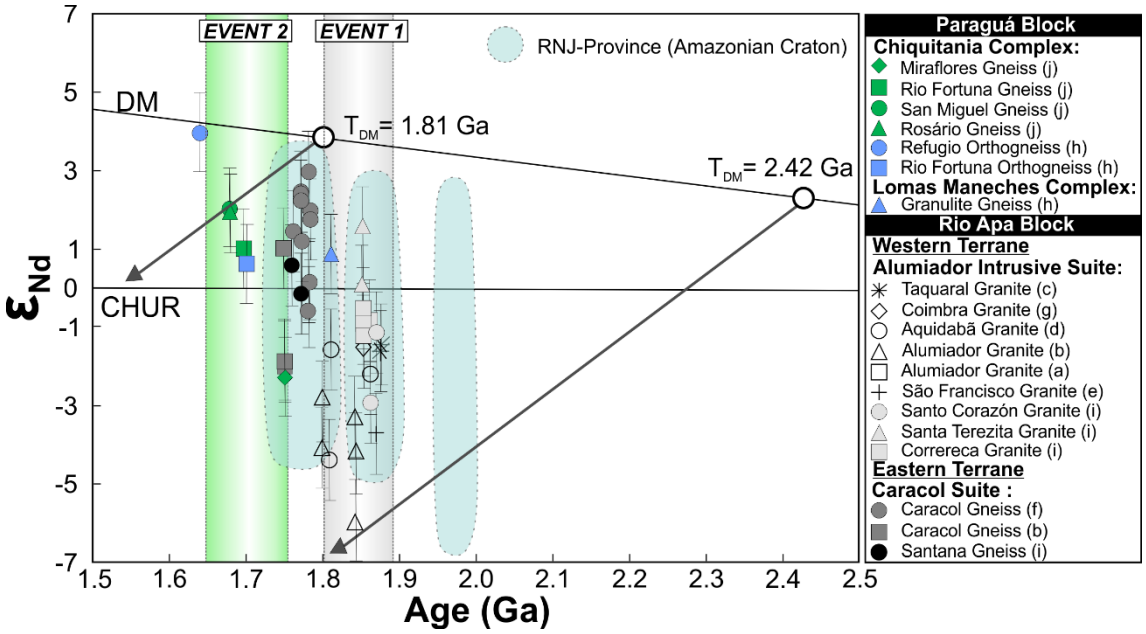

Figure 5.8. Age (Ga) versus ε_{Nd} diagram for the Miraflores, Rosário, San Miguel and Rio Fortuna gneisses from the Chiquitania Complex. The values for the Rio-Negro Juruena Province (RJN; Amazonian Craton), Eastern Bolivian basement (EBB) granites, Alumiador Suite (Western Terrane), the Santana Gneiss, and for the Caracol Gneiss Suite (Eastern Terrane) from the Rio Apa Block were also plotted for comparison. Data sources: (a) Lacerda Filho *et al*. (2006); (b) Cordani *et al*. (2010); (c) Redes *et al*. (2015); (d) Nogueira (2015); (e) Souza *et al*. (2016); (f) Plens (2018); (g) Santos *et al*. (2019); (h) Santos *et al*. (2008); (i) Redes *et al*., 2020; (j) This study.

5.5. DISCUSSION

5.5.1. Subdivision, age, and tectonic setting of the Chiquitania Complex gneiss terrane

Based on the U-Pb ages, the Chiquitania Complex can be divided into an older and a younger unit (Fig. 5.9 A).

The older unit of the Chiquitania Complex: Miraflores Gneiss

The Miraflores Gneiss represents the older unit of the Chiquitania Complex. This gneiss gave a zircon U-Pb age of 1747±11 Ma that is interpreted as the crystallization age of the protolith, a peraluminous granodiorite, with slightly negative $\varepsilon_{Nd(t)}$ of -2.42 and a Paleoproterozoic model age of 2.15 Ga. The geochemical data indicate that the Miraflores protolith had affinity with a magmatic arc setting. For that reason, we call this terrane the "*Miraflores Granodioritic Arc*".

Boger *et al*. (2005) described a felsic biotite-bearing gneiss from the Chiquitania Complex that was obtained close to the Miraflores Gneiss outcrop. These authors interpreted this gneiss as derived from a sedimentary or volcanic protolith that was unrelated to the Lomas Maneches or San Ignácio complexes. The U-Pb ages on zircon obtained for this paragneiss (their sample 235A) and its leucosome (235A-1) allowed Boger *et al*. (2005) to interpret that the protolith of the 235A paragneiss was derived from a source with ages around 1.76 Ga, but that it had been emplaced after ca. 1.69 Ga. (Fig. 5.9 A). This paragneiss yielded the same two ages of ca. 1.7-1.8 Ga and 1.35 Ga that we obtained for our sample from the Miraflores Gneiss. The oldest ages of ca. 1.84 Ga identified in zircon crystals from our sample, however, were not found by Boger *et al*. (2005).

Given the resemblance of the Miraflores Gneiss to the gneiss phases studied by Boger *et al*. (2005) with similar emplacement ages, there is a possibility that the Miraflores Gneiss and the paragneiss (+ leucosome) of Boger *et al*. (2005) are parts of the same body that would represent the oldest part of the Chiquitania Complex in the central region of the Paraguá Block (Fig. 9 A). The geochemical characteristics of these rocks allow to relate the respective protoliths to an arc of approximately 1.75 Ga (Fig. 5.9 B). We interpret that the Miraflores Gneiss protolith was

plutonic in origin, but in the view of Boger *et al*. (2005), this protolith could also have had a volcanic origin.

The intrusive, tectonic or transitional relationship between the Lomas Maneches and the Chiquitania complexes has been debated for a long time (e.g., Litherland *et al*., 1986, 1989; Boger *et al*., 2005; Santos *et al*., 2008). Both the Miraflores Gneiss and the Lomas Maneches granulites (Matos *et al*., 2013) have similar geochemical signatures, e.g., they are calc-alkaline, metaluminous to peraluminous, and have slightly negative to slightly positive $\varepsilon_{Nd(t)}$ (Santos *et al*., 2008). However, the proposed crystallization age for the Miraflores Gneiss of 1747±11 Ma makes this body slightly younger than the Lomas Maneches Complex. Some inherited zircon crystals with ages around 1.84 Ga indicate that a basement with nearly juvenile characteristics was reworked by the Miraflores granodiorite. This basement was either an unknown phase or belonged to the Lomas Maneches Complex (ca. 1.97 – 1.63 Ga, Litherland *et al*., 1986; Boger *et al*., 2005; Santos *et al*., 2008).

The younger unit of the Chiquitania Complex: Rio Fortuna, San Miguel and Rosário gneisses

The Rio Fortuna, San Miguel and Rosário gneisses of the exterior of the Paraguá Block represent the younger unit of the Chiquitania Complex. They were classified as orthogneisses, have crystallization ages around 1.69 Ga, and all of them were metamorphosed to amphibolite facies – now retrogressed to greenschist facies.

The Rio Fortuna Gneiss occurs in the NE border region of the Paraguá Block (Fig. 5.9 A). The gneiss is in contact to the east with the Aguapeí Belt and to the southwest with the granulites of the Lomas Maneches Complex (Santos *et al*., 2008; Faria *et al*., 2014). As the protolith to the Rio Fortuna Gneiss was a peraluminous I-type tonalite with a crystallization age of 1699±9 Ma, with a slightly positive $\varepsilon_{Nd(t)}$ of +0.75 and a Paleoproterozoic model age of 1.95 Ga, this arc is called the "*Rio Fortuna Tonalitic Arc*". Major and trace element systematics indicate that the tonalite was also associated with a magmatic arc environment. Peraluminous tonalites in the magmatic arc context could be interpreted as representing an assimilation of sedimentary rocks by a basaltic magma (e.g., Patiño-Douce 1995; Cuadros *et al*., 2017). The Hf

isotopic ratios obtained on zircon crystals from this gneiss would, thus, indicate such an assimilation, as they show positive $\varepsilon_{Hf(t)}$ values between +1.7 and +7.4 and gave Paleoproterozoic model ages between 2.23 and 1.87 Ga.

Santos *et al*. (2008) described two main U-Pb zircon populations for the Rio Fortuna Gneiss: 1) zoned magmatic zircon formed at ca. 1.33 Ga, and 2) inherited crystals and cores of ca. 1.77–1.73 Ga ages, besides one age for a core of ca. 1.67 Ga. Faria *et al*. (2014) interpreted the U-Pb zircon age of ca. 1.71 Ga (Fig. 5.10) as the crystallization age of the protolith of the Rio Fortuna Gneiss. Faria *et al*. (2014) also obtained an age of ca. 1761 Ma. The oldest ages between ca. 1.77 and 1.76 Ga for the Rio Fortuna Gneiss obtained by Santos *et al*. (2008) and Faria *et al*. (2014) are interpreted here as ages of zircon inherited from the Miraflores Gneiss. It is interesting to observe that zircon crystals of this age range were not identified in our sample of the Rio Fortuna Gneiss.

The San Miguel Gneiss crops out at the southwestern border of the Paraguá Block (Fig. 5.9 A), possibly bordering against the Arequipa Terrane (Ramos, 2008) - but this alleged contact zone is covered by Phanerozoic sediments. The Rosário Gneiss is located at the southern edge of the Paraguá Block and borders against the Rio Apa Block (Fig. 5.9 A). The protoliths of both gneisses are metaluminous, calc-alkaline, I-type monzogranite. The protolith of the San Miguel Gneiss is characterized by a positive $\varepsilon_{Nd(t)}$ value of +1.93 and a Paleoproterozoic model age of 1.81 Ga, and the Rosário protolith gave a positive $\varepsilon_{Nd(t)}$ value of +0.92 and also a Paleoproterozoic model age of 1.89 Ga. The Hf data for these protoliths indicate parental magmas with essentially positive $\varepsilon_{Hf(t)}$ values between +0.3 and +8.9 and Paleoproterozoic model ages between 2.32 and 1.82 Ga. Only one zircon (ZR26, 1632 Ma) from the Rosário Gneiss gave a negative $\varepsilon_{Hf(t)}$ value of -0.9 and model age of 2.34 Ga.

As the crystallization ages of the San Miguel Gneiss and Rosário protoliths are 1681±13 Ma and 1678±21 Ma, it is here considered that they have – within error limits - the same age. The age and the same geochemical affinity allow us to consider that these two gneisses could be part of the same body. As the chemical compositions indicate that they also developed in an arc environment, we refer to a "*Rosário/San Miguel Monzogranitic Arc*". These bodies are also

similar in age to the Rio Fortuna Gneiss, but this body occurs on the other side of the Paraguá Block (Fig. 5.9 A).

Matos (2012) interpreted that the granites of the Serie Yarituses, the La Cruz (1673 Ma), Refúgio (1673 Ma), San Pablo (1621 Ma), and the Turvo (1651 Ma; Figueiredo *et al*., 2009) intruded the Lomas Maneches Complex. However, here we propose that they are gneissic bodies that represent younger arcs that contributed to the Chiquitania Complex.

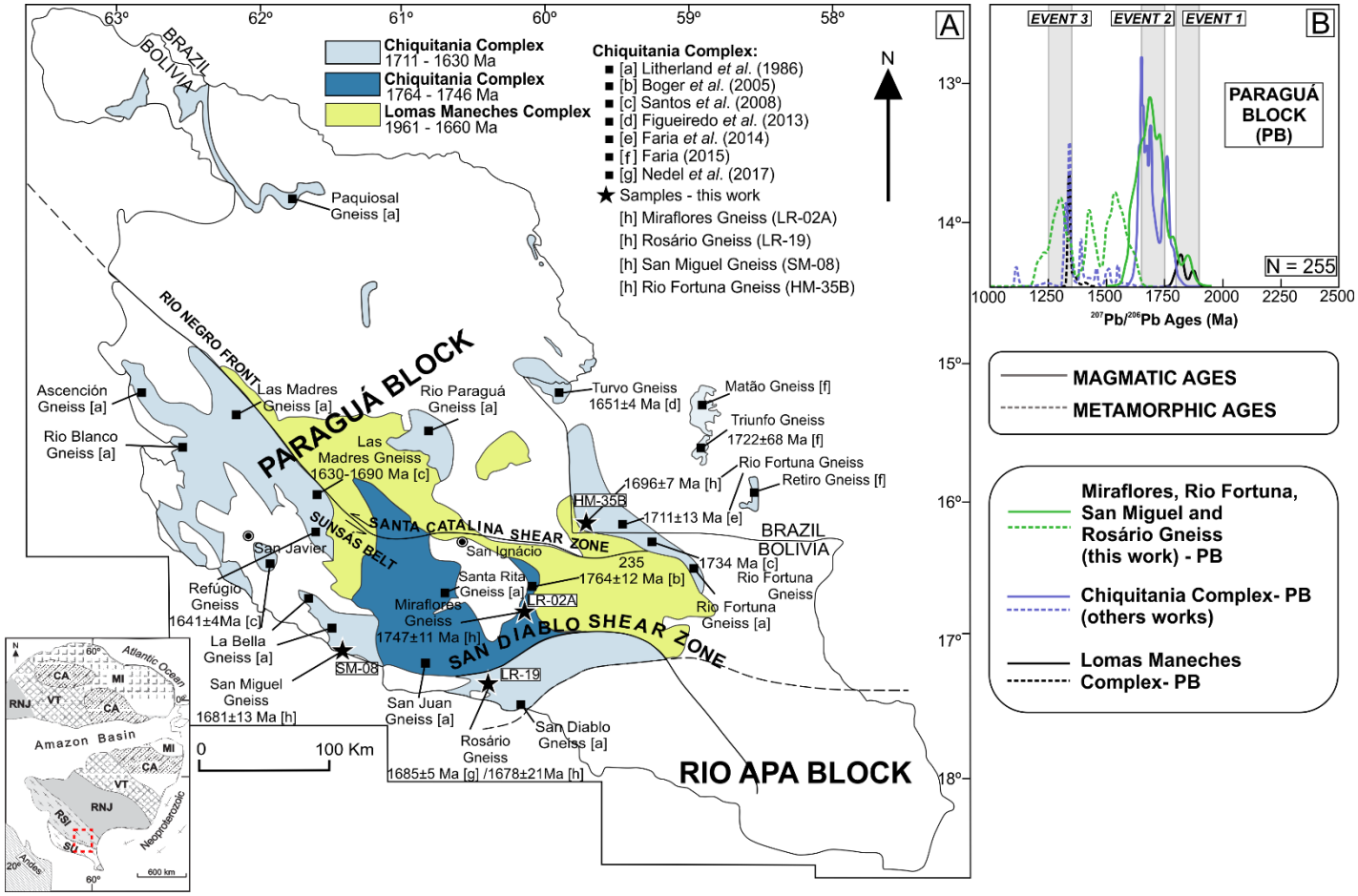

Figure 5.9. (A) Principal divisions and names of the gneisses of the Chiquitania Complex (Paraguá Block). Modified after Litherland *et al*. (1986). (B) Histogram of $^{207}Pb/^{206}Pb$ ages from Boger *et al*. (2005); Lacerda Filho *et al*. (2006); Santos *et al*. (2008); Cordani *et al*. (2010); Figueiredo *et al*. (2013); Faria *et al*. (2014); Faria (2015); Nogueira (2015); Redes *et al*. (2015); Souza *et al*. (2016); Nedel *et al*. (2017); Plens (2018); Santos *et al*. (2019); Redes *et al*. (2020); and from the present study.

5.5.2. Polycyclic evolution of the basement of Eastern Bolivia

The basement of Eastern Bolivia (Fig. 5.10 C) is composed of the Paraguá Block and granitoids of Orosirian ages (Redes *et al*., 2020) that represent the northwest extension of the Rio Apa Block into Bolivia. The Santa Terezita, Correreca and Santo Corazón granites were grouped by Redes *et al*. (2020) into the EBB (Eastern Bolivian Basement).

The oldest and youngest units of the Chiquitania Complex represent a polycyclic evolution. As discussed above, these units were generated in magmatic arc environments at ca. 1.75 and 1.70-1.65 Ga (Fig. 5.9). They then underwent periods of reworking (partial melting/migmatization?) and were finally metamorphosed at approximately 1.3 Ga (Litherland *et al*., 1986).

The Nd and Hf isotope data for these two units of the complex (Figs. 5.8 and 5.10 B) show similar model ages between 2.34 and 1.82 Ga (Rosário Gneiss) that indicate that the rocks of the Chiquitania Complex were the result of reworking of Riacian to Orosirian crust between 1.75 and 1.65 Ga, in a magmatic arc environment.

A compilation of 608 U-Pb age data from the EBB and the Lomas Maneches and Chiquitania complexes is shown in Figure 5.10 A. For comparison, 741 U-Pb data from the Rio Negro-Juruena Province of the Amazonian Craton and from the Rio Apa Block are shown. Based on this compilation, we suggest at least 3 events (E1, E2 and E3) related with the evolution of the Eastern Bolivian basement. We use the term "event" to indicate times of maximum zircon production, which would represent magmatic pulses, possibly related with flare-up phases (Ducea *et al*., 2015) or metamorphic events.

Event 1: ca. 1.84 Ga

This event (Fig. 5.10) is related with the evolution of the Orosirian granites in the basement of Eastern Bolivia that were correlated with the Alumiador Intrusive Suite of the Western Terrane of the Rio Apa Block (EBB + RAB, Redes *et al*., 2020; Ribeiro *et al*., 2020).

On the Paraguá Block, Santos *et al*. (2008) identified magmatic zircons with ages of ca. 1.81 Ga in the Lomas Maneches Complex and ages of ca. 1.77 and 1.72 Ga for the Rio Fortuna

and Santa Rita orthogneisses of the Chiquitania Complex. Inherited magmatic zircons of ca. 1.84 Ga with prismatic, euhedral and bipyramidal habits identified in the oldest unit of the Chiquitania Complex, the Miraflores Gneiss (Fig. 5.7 A), allow us to consider that they could be derived from the Lomas Maneches Complex. In agreement with Santos *et al*. (2008), we consider the Lomas Maneches Complex as the host terrane for the "*Miraflores Granodioritic Arc*" of ca.1.74 Ga age.

The Nd isotope data indicate that these granitoids represent reworking in Orosirian times of 2.23 to 1.96 Ga crust created in a magmatic arc setting (Redes *et al.*, 2020). As we do not have any Hf data for zircons from the Lomas Maneches or Miraflores gneisses, this event is only characterized by the Correreca Granite that gave negative to positive $\varepsilon_{Hf(t)}$ values and Hf model ages between 2.68 and 2.29 Ga (Redes *et al*., 2020). If we considered the Equation proposed by Vervoort *et al*. (2011) to transform $\varepsilon_{Nd(t)}$ into $\varepsilon_{Hf(t)}$ ($\varepsilon_{Hf(t)} = (1.55* \varepsilon_{Nd(t)}) +1.21$), the $\varepsilon_{Hf(t)}$ value for the Miraflores Gneiss would be -2.54.

Event 2: ca.1.75-1.65 Ga

This event is related to the generation of tonalitic to granitic protoliths of the Chiquitania Complex (Fig. 5.9) in arc environments between ca. 1.75 and 1.65 Ga. This event could be divided into three cycles - Cycle 1 (ca.1.75 Ga), Cycle 2 (ca.1.70 Ga), and Cycle 3 (ca.1.65 Ga), as distinguished in the Nd and Hf isotope diagrams (Figs. 5.8 and 5.10 B, respectively). We define a "cycle" as a main zircon peak inside an event record. Cycle 1 occurred in the center part and cycles 2 and 3 occurred at the borders of the Paraguá Block.

Cycle 1 corresponds to the mature "*Miraflores Granodioritic Arc*" that today is located in the interior of the Paraguá Block. This arc involved the reworking of an old basement (ca. 1.92 Ga) that could have represented the Lomas Maneches Complex (Fig. 5.10 A).

Cycle 2 corresponds to nearly juvenile arcs, one at the eastern border of the Paraguá Block, which is represented by the "*Rio Fortuna Tonalite Arc*", and the other at the southwestern border represented by the "*Rosário/San Miguel Monzogranite Arc*" (Fig. 5.9 A).

Cycle 3 must correspond with arcs of ca.1.65 Ga age, at both sides of the Paraguá Block. On the eastern side of the Paraguá Block occur the Triunfo (ca. 1.72 Ga, Faria, 2015), Matão

(Faria, 2015) and Turvo (ca. 1.65 Ga; Figueiredo *et al*., 2013) gneisses (Fig. 5.9) that could be part of a younger volcanic arc called here the "*Triunfo/Matão/Turvo Granitoid Arc*". The Triunfo and Turvo gneisses have protoliths that vary from metaluminous to peraluminous tonalites to syenogranites and have slightly positive $\varepsilon_{Nd(t)}$ and $\varepsilon_{Hf(t)}$ values (Faria, 2015; Figueiredo *et al*., 2013). The Matão Gneiss is an orthogneiss of tonalitic to syenogranitic composition with retrograde metamorphism to greenschist facies. The presence of granulitic and amphibolitic xenoliths in this gneiss establishes a clear stratigraphic relationship with the Luchese Granulite of the Lomas Maneches Complex (Nascimento, 2015).

Towards the northwestern part of the Paraguá Block, about 12 km east of San Javier in Bolivia (Fig. 5.9 A) and to the north of the "*Rosário/San Miguel Monzogranitic Arc"* occurs a leucocratic orthogneiss of syenogranitic to monzogranitic composition, the Refúgio Gneiss (Santos *et al*., 2008) with a crystallization age of ca. 1.64 Ga (Figueiredo *et al*., 2013; Faria, 2015). The protolith was formed in a nearly juvenile magmatic arc named here the "*Refúgio Granitic Arc*". It is younger and more juvenile than the Rosário and San Miguel gneisses, showing the possibility of a juvenile crust at 1641 Ma. A garnet-rich, migmatitic, leucocratic paragneiss with an amphibolitic paleosome, known as the Las Madres Gneiss (Litherland *et al*., 1986; Santos *et al*. 2008), gave ages between ca.1.69 and 1.63 Ga (Santos *et al*., 2008). It could be related with the evolution of the "*Refúgio Granitic Arc".*

Event 3: ca.1.35 and 1.25 Ga

This age interval (Fig. 5.9 B) was found only on rims of zircon crystals from the Miraflores, San Miguel and Rosário gneisses. These comparatively younger rims, interpreted to be of metamorphic origin, surround darker and older cores (Fig. 5.7 and 5.8), either with regular magmatic zonation (ages between ca.1.74-1.65 Ga) or with chaotic internal structure (ages of ca. 1.57-1.53 Ga or 1.42-1.41 Ga). For the Miraflores Gneiss an upper intercept age of 1291±26 Ma was obtained, whereas towards the southwest, the San Miguel Gneiss registered a youngest Concordia age of 1256±26 Ma and an upper intercept age of 1320±19 Ma. These rims enclose cores with $^{207}Pb/^{206}Pb$ ages of ca.1599 and 1535 Ma. Two metamorphic rims with $^{207}Pb/^{206}Pb$ ages

of ca.1300 and 1321 Ma were obtained on rounded zircon crystals from the Rosário Gneiss. These rims enclose cores that gave $^{207}Pb/^{206}Pb$ ages of ca.1600 and 1649 Ma.

We did not find any age from this interval for the Rio Fortuna Gneiss, but Santos *et al*. (2008) registered an upper intercept age of ca.1.33 Ga (rims of zircon crystals); the authors interpreted this to represent a metamorphic event. Boger *et al*. (2005) found the same ages on the rims of crystals from his paragneiss that could be related with the Miraflores Gneiss.

The combination of these results allows to relate the metamorphism of the studied gneisses to the second phase of the San Ignácio Orogeny (ca. 1.34-1.29 Ga), which Bettencourt *et al*. (2010) had linked to the collision of the Paraguá Block with the Amazonian Craton. Thus, this event marks the end of the San Ignácio orogeny. Boger *et al*. (2005) interpreted that the metamorphic age of the Chiquitania Complex was around 1.33 Ga. This age is also similar to the age of emplacement of syn- to post-kinematic granitoids and late- to post-kinematic granitoids that make up the Pensamiento Granitoid Complex in the northern Paraguá Block (Matos *et al*., 2009). The emplacement of these granites would have affected the pre-existing units, such as the Lomas Maneches Complex and the Chiquitania Complex.

Periods of Reworking: ca. 1.58 to 1.54 Ga and ca. 1.42 to 1.42 Ga

Upper intercept ages between ca.1.58 and 1.54 Ga were obtained for the Rio Fortuna, Rosário and San Miguel gneisses in the marginal zones of the Paraguá Block. These ages represent the second most important group of ages registered in the Paraguá Block. Zircon crystals with ages in this interval were not found in the Miraflores Gneiss (Fig. 5.10 A), probably because it acted as a stable block. U-Pb ages in this age interval were obtained both in cores and rims of zircon crystals with complex and chaotic areas that combine gradual growth patterns with flow structures. Corfu *et al*. (2003) described this type of internal structure as related to migmatization. According to observations by Litherland *et al*. (1986), the Chiquitania Complex gneisses show characteristics of migmatization, both macroscopic (typical banding) and microscopic. Further field work is, however, required, and we prefer to simply say that these ages are related with reworking of continental crust.

This reworking event was also identified in the Las Madres Paragneiss ($^{207}Pb/^{206}Pb$ age of 1550±8 Ma, Santos *et al*., 2008) and in the paragneiss analyzed by Boger *et al*. (2005). They did, however, not find any geological meaning for this age and interpreted only that it could represent partial mixing between core (ca. 1.76 Ga) and rim (ca. 1.33 Ga) portions of the analyzed zircon grains.

The existence of these ages in zircon from the margins of the Paraguá Block could, however, indicate that the evolution of these terranes was similar to that of the Amazonian Craton. According to Bettencourt *et al*. (2010) the period of generation of accretionary orogens in the Amazonian Craton occurred between ca.1.56 and 1.37 Ga. There, the Cachoeirinha (ca.1.56-1.52 Ga) and Santa Helena (ca.1.48-1.42 Ga) orogenies recognized in the Jauru Terrane and the Rio Alegre orogen (ca.1.51 - 1.38 Ga) in the Rio Alegre Terrane in Brazil would have been part of this event (Fig. 5.2 and 5.3). These findings would indicate that this reworking event could have been widespread in the Paraguá Block as well and could also relate to the beginning of the San Ignácio Orogeny.

A second group of upper intercept ages of ca.1.42 and 1.42 Ga was registered for both rims and cores of zircon crystals of the Miraflores, San Miguel and Rio Fortuna gneisses. The areas of zircon crystals from where these ages were obtained have chaotic appearance (Corfu *et al*., 2003). Ages around 1.40 Ga (Fig. 5.3) could be related to the period of arc generation, as evidenced by the San Ramón tonalite (ca.1.42 Ga, Nd T_{DM} of 1.6 Ga, and $\varepsilon_{Nd(t)}$ of +2.3; Santos *et al*., 2008), which is located about 80 km northwest of the San Miguel Gneiss.

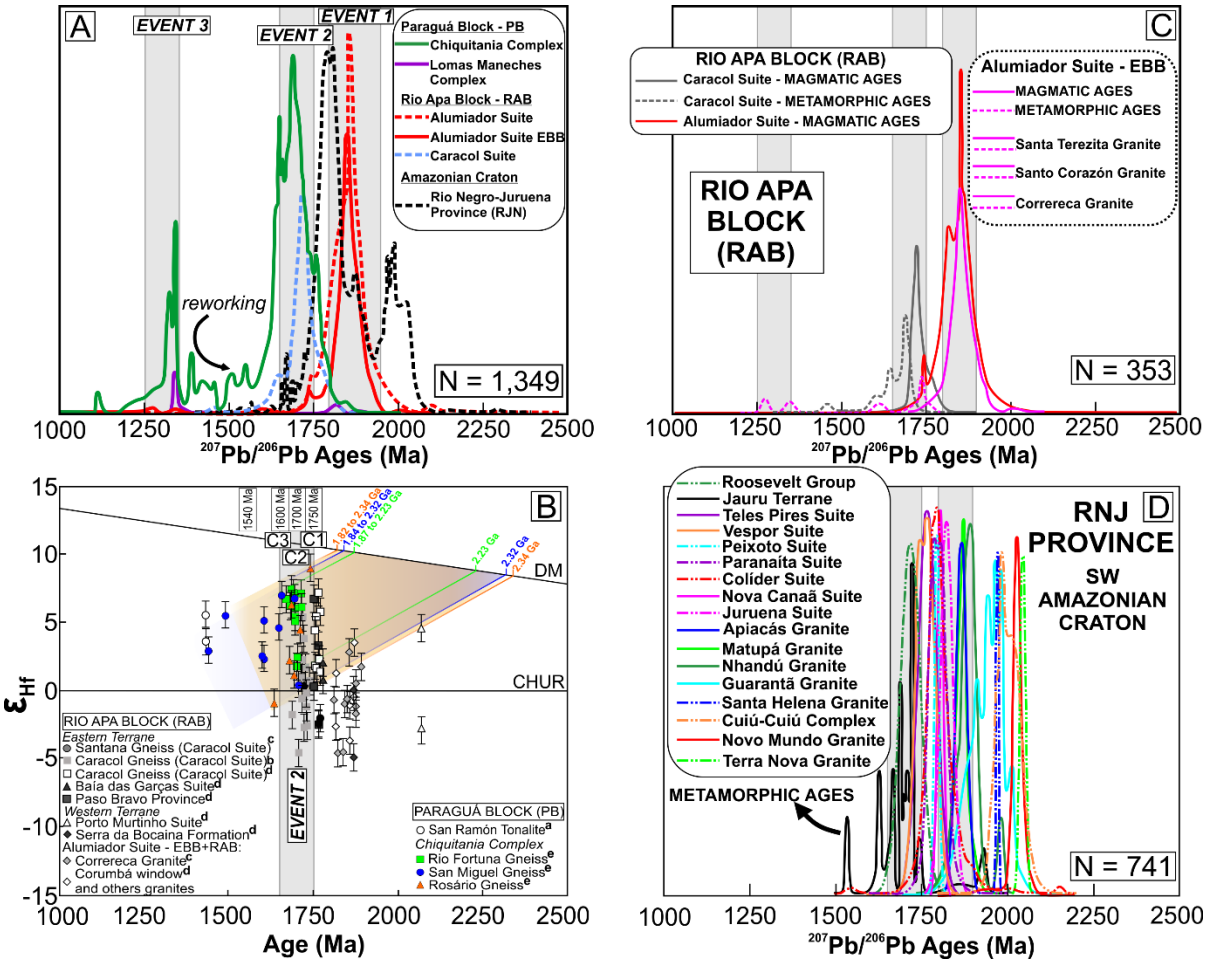

Figure 5.10. (A) Histogram of $^{207}Pb/^{206}Pb$ ages showing the main magmatic/metamorphic events that affected the Paraguá Block and Rio Apa Block (Alumiador and Caracol suites). Three events (E1, E2 and E3) were identified in the basement of Eastern Bolivia. Ages for the Paraguá Block are from: Boger *et al*. (2005); Santos *et al*. (2008); Figueiredo *et al*. (2013); Faria *et al*. (2014); Faria (2015); Nedel *et al*. (2017). Ages for the Rio Apa Block are from: Lacerda Filho *et al*. (2006); Cordani *et al*. (2010); Nogueira (2015); Redes *et al*. (2015, 2020); Souza *et al*. (2016); Plens (2018); Santos *et al*. (2019); Teixeira *et al*. (2020). (B) Age (Ga) *versus* ε_{Hf} diagram for (a) San Ramón Tonalite (Matos, 2010), (b) Caracol Gneiss (Plens, 2018), (c) Santana Gneiss and Correreca Granite (Redes *et al*., 2020), (d) Caracol Suite, Paso Bravo Suite, Baía das Garças Suite, Porto Murtinho Complex, Serra da Bocaina Formation, Corumbá Window, granites of the Alumiador Suite (Ribeiro *et al*., 2020), (e) Rosário (SR), San Miguel (SM) and Rio Fortuna (RF) Gneiss (present study); Protolith types for these gneisses: SR - monzogranite; SM - monzogranite; RF – tonalite. Three cycles (C1-C3) were identified for Event 2 - see text for discussion. (C) Histogram of $^{207}Pb/^{206}Pb$ ages for the Rio Apa Block. Ages are from: Lacerda Filho *et al*. (2006); Cordani *et al*. (2010); Nogueira (2015); Redes *et al*. (2015); Souza *et al*. (2016); Plens (2018); Santos *et al*. (2019); Redes *et al*. (2020); Teixeira *et al*. (2020). See text for discussion. (D) Histogram of $^{207}Pb/^{206}Pb$ ages for the Rio Negro-Juruena Province of the SW Amazonian Craton. Ages are from: Tassinari *et al*. (1996); Moura (1998); Santos *et al*. (2000); Geraldes *et al*. (2001); Payolla *et al*. (2002); Paes e Barros (2007); Silva and Abram (2008); Duarte *et al*. (2012), Prado *et al*. (2013); Scandolara *et al*. (2014); Silva *et al*. (2014); Assis (2015); Duarte (2015); Quispe (2016); Santos *et al*. (2016); Costa Testa (2018); Galé (2018); Santos *et al*. (2019).

5.5.3. Regional correlation

Correlation of the Paraguá Block with the Rio Apa Block

Various suggestions have been made regarding the tectonic positioning of the Paraguá Block with respect to the Rio Apa Block. It was suggested that the Rio Apa Block must be an extension of the Paraguá Block based on the continuity of the Grenvillian Belt (Nova Brasilândia, Aguapeí and Sunsas, Santos *et al*., 2000, 2008).

The most common ages for zircon crystallization found in rocks from the western terrane of the Rio Apa Block are around 1.85 Ga (Santa Terezita Granite of Alumiador Intrusive Suite; Redes *et al*., 2020). They correspond with Event 1 defined above. Ages around 1.85 Ga were only recorded in inherited zircon crystals from the oldest part of the Paraguá Block, the Miraflores Gneiss, and the Lomas Maneches Complex (Santos *et al*., 2008). In addition, a sample from the Lomas Maneches Complex also gave the two oldest inherited zircon grains with ages of ca. 1.87 Ga (Santos *et al*., 2008) that correspond to the crystallization age of the Santo Corazón Granite (Alumiador Intrusive Suite; Redes *et al*., 2020).

However, the U-Pb geochronological data, including our new results, and the Nd and Hf model ages indicate that the basement of the Paraguá Block is dominated by rocks younger than the basement of the Rio Apa Block, and the $\varepsilon_{Nd(t)}$ and $\varepsilon_{Hf(t)}$ values indicate a more juvenile signature for the sources of the Paraguá Block (Fig. 5.10 B). The Paraguá Block gave initial $\varepsilon_{Nd(t)}$ values of -3.97 to +4.06 and Nd model ages of 2.15 to 1.50 Ga (Matos *et al*., 2009; Santos *et al*., 2008; Bettencourt *et al*., 2010). In contrast, the Rio Apa Block gave positive to negative values of $\varepsilon_{Nd(t)}$ of -5.97 to +3.25 and Nd model ages between 2.60 and 1.82 Ga (Teixeira *et al*., 2020). Furthermore, the predominance of positive $\varepsilon_{Nd(t)}$ values for rocks from the Paraguá Block points to a more juvenile signature (Rio Fortuna and San Miguel/Rosário arcs) than obtained for the basement rocks of the Rio Apa Block (Fig. 5.8). The Paraguá Block gave positive values of $\varepsilon_{Hf(t)}$ between +0.3 and +8.9 and Hf model ages of 2.32 to 1.82 Ga. In contrast, the Rio Apa Block gave negative to positive values of $\varepsilon_{Hf(t)}$ of -5.97 to +7.06, with a predominance of negative values, and Hf model ages between 2.56 to 2.03 Ga, according to data from Plens (2018), Ribeiro *et al*. (2020) and Redes *et al.* (2020).

This indicates that the rocks of the Paraguá Block, in addition to being younger than the rocks from the Rio Apa Block, were derived from more juvenile sources (Fig. 5.10 C). This is strong evidence against correlation of the Paraguá Block with the Rio Apa Block, as also observed by Ribeiro *et al.* (2020). The attempt by Plens (2018) to correlate the gneissic rocks of the Chiquitania Complex with the gneissic rocks of the Caracol Suite of the Rio Apa Block, based on geochronological and isotopic results, should therefore be considered with caution. Plens (2018) also suggested that the San Ignácio Orogeny that affected the southwestern portion of the Amazonian Craton and the Paraguá Block at ca.1.3 Ga was responsible for the juxtaposition of the Eastern and Western Bolivian basement. In contrast, Cordani *et al*. (2010) argued that the juxtaposition between the Eastern and Western terranes of the Rio Apa Block occurred at ca. 1.69 Ga.

The Caracol Gneiss (Plens, 2018) and the Santana Gneiss (Redes *et al*., 2020), grouped together as the Caracol Suite of the Eastern Terrane of the Rio Apa Block, have similar ages (ca.1.76 and 1.72 Ga, respectively) to that of the Miraflores Gneiss that represents Cycle-1 of Event 2. The Caracol Suite yielded negative to positive $\varepsilon_{Hf(t)}$ values and Hf model ages between 2.68 and 1.92 Ga (Plens, 2018; Redes *et al*., 2020; Ribeiro *et al*., 2020). Comparison of U-Pb ages, $\varepsilon_{Hf(t)}$ values, and Hf model ages for the Caracol Suite and the Chiquitania Complex (Fig. 5.10) shows that the Chiquitania Complex was derived either from younger, more juvenile sources, or from a mixture between younger and older sources than those for the gneisses of the Rio Apa Block.

The Eastern Terrane of the Rio Apa Block contains rocks that could be correlated with Cycle 2 of Event 2. The Santa Terezita Granite is located in the eastern part of Bolivia and is part of the Eastern Bolivian Basement granites (EBB, Redes *et al*., 2020). It represents the westernmost portion of the Rio Apa Block. Metamorphic rims of ca. 1.70 Ga found on zircon crystals from Santa Terezita Granite were used to propose that the collision between EBB + Rio Apa Block and the Paraguá Block occurred around that time (Redes *et al*., 2020).

Correlation of the Paraguá Block with the Amazonian Craton

The growth of the Amazonian Craton began with an Archean nucleus (> 2.6 Ga in age; Central Amazonian Province; Cordani and Teixeira, 2007) and during the Proterozoic involved accretion/collision between ca. 2.2 and 1.0 Ga. Lithostratigraphic units and metamorphic episodes are progressively younger towards the SW of the Amazonian Craton (Fig. 5.10 D). The SW portion of this craton comprises, from east to west, the Rio Negro-Juruena (ca.1.84-1.54 Ga; Fig. 5.11 A and B), Rondoniana-San Ignácio (ca.1.56-1.30 Ga), and Sunsas (ca.1.25-1.00 Ga) provinces (Sadowski and Bettencourt, 1996; Geraldes *et al*., 2001; Ruiz, 2005; Teixeira *et al*., 2010; Bettencourt *et al*., 2010; Rizzotto and Hartmann, 2012).

The events and cycles recognized in the Paraguá Block allow us to compare with those recognized for the Amazonian Craton. For example, the ca. 1.75-1.60 Ga, 1.58-1.53 Ga, 1.40 Ga, and 1.35 - 1.25 Ga periods (Bettencourt *et al*., 2010; Scandolara *et al*., 2017) of the Rio Negro-Juruena Province are synchronous with those of the Paraguá Block. It means that the Rio Negro-Juruena Province and the Paraguá Block (Fig. 5.10 and 5.11) were affected by the same orogenies (San Ignácio and Sunsas).

The Juruena (ca.1.81-1.51 Ga), Jamari (ca.1.79-1.51 Ga) and Jauru terranes (ca.1.78-1.42 Ga) indicate the existence of pre-Rondonian-San Ignácio crust in SW Rondônia and Mato Grosso (SW of the Amazonian Craton). The Juruena Terrane is located in the northern part of Mato Grosso, the Jamari Terrane in the central-northern parts of Rondônia, and the Jauru Terrane in the southwestern part of Mato Grosso (Fig. 5.2 and 5.3). The Juruena granodiorite represents the first magmatic arc active at ca. 1.85-1.82 Ga (Santos *et al*., 2008). Magmatic zircon crystals from the Lomas Maneches Complex with an age of ca. 1.81 Ga (Santos *et al*., 2008) suggest even older crust in Eastern Bolivia, with ages comparable to the basement ages of the Juruena region in northern Mato Grosso (Fig. 5.2, 5.3 and 5.11; Bettencourt *et al*., 2010). Bettencourt *et al*. (2010) pointed out that the Paraguá Block could be a segment of the Rio Negro-Juruena Province, in agreement with a proposal by Sadowski and Bettencourt (1996), which then would discard the existence of a Paraguá Block.

The ca. 1.75 and 1.65 Ga crystallization ages obtained for the Chiquitania Complex gneiss (Event 2) are similar to those found in the Rio Negro-Juruena Province (Juruena Terrane, Jamari Terrane and Jauru Terrane; Fig. 5.11) in the SW Amazonian Craton.

Furthermore, the ca.1.65-1.67 Ga magmatic and metamorphic events in Rondônia are related to rocks from the Lomas Maneches Complex (Santos *et al*. 2000, 2008; Silva *et al*., 2002). However, Boger *et al*. (2005) maintained that the San Ignácio Group, Chiquitania Complex, and Lomas Maneches Complex had no equivalent in SW Mato Grosso or Rondônia states.

Granitic basement with ca.1.79-1.74 Ga ages was recognized in the Jauru Terrane (Geraldes *et al*., 2001). Similar to the Paraguá Block, the Jauru Terrane in the SW Amazonian Craton is dominated by granitic suites (e.g., the Santa Helena and Rio Branco batholiths) that were mainly emplaced during the ca. 1.56-1.33 Ga interval (Geraldes *et al*., 2001; Santos *et al*., 2008). In addition, the rocks of the Jauru Terrane have Nd model ages between 1.95 and 1.35 Ga (Fig. 5.8), indicating that they were not derived from a single source, and that the Paraguá Block and Jauru Terrane, thus, should not be correlated.

In the Jamari Terrane (SW Amazonian Craton), a collisional phase is characterized by high-grade metamorphism between ca. 1.69-1.63 Ga, and a post-collisional period that took place between ca. 1.6 and 1.51 Ga is evidenced by two A-type granitoids from the Serra da Providência and Rio Crespo areas (Scandolara *et al*., 2017). This indicates that these orogenic periods of the Amazonian Craton were not synchronous with the evolution of the Paraguá Block (Fig. 5.11).

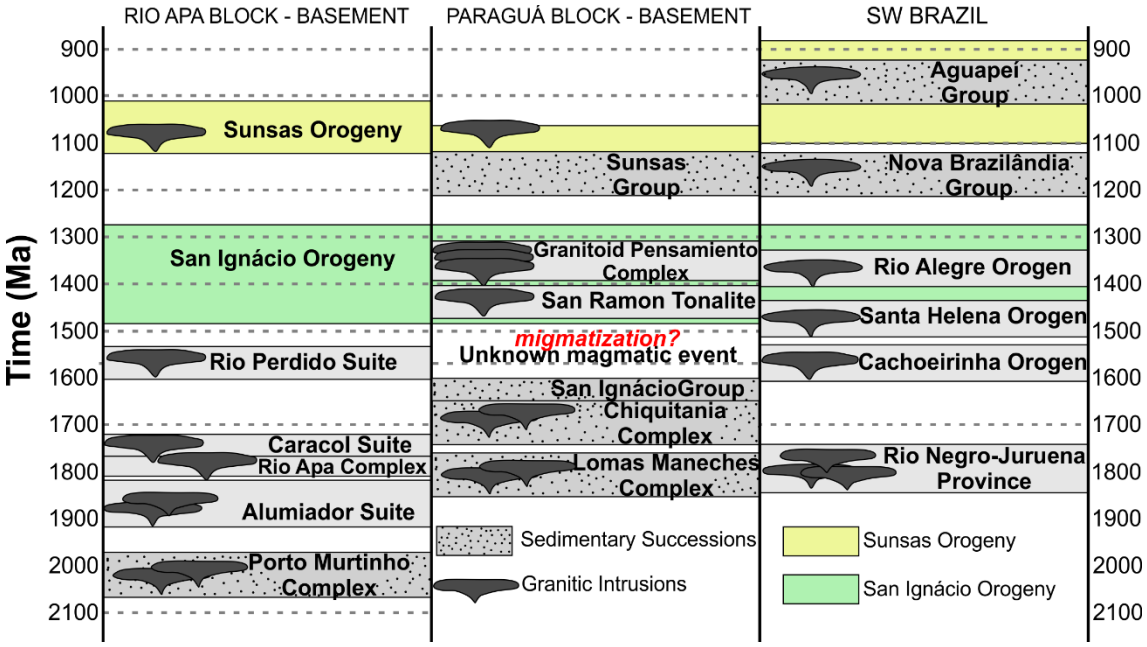

Figure 5.11. Space-time diagram for the Proterozoic magmatic/metamorphic events on the southwestern margin of South America. The data are from this study and the references mentioned in the text.

5.5.4. Tectonic evolution of the Paraguá Block: proposed scenarios

In view of the new data obtained from the Chiquitania Complex, and in the light of existing models (for example: Litherland *et al*., 1986; Boger *et al*., 2005; Bettencourt *et al*., 2010), some possible scenarios can be discussed for the evolution of the Paraguá Block (PB), the EBB + RAB (Redes *et al*., 2020), and the Amazonian Craton.

Scenario 1: Collision between the Paraguá Block (PB) and Rio Apa Block (EBB + RAB) at ca. 1.7 Ga and with the Amazonian Craton at ca. 1.30 Ga

This model suggests that the collision between the Eastern Bolivian basement and the Rio Apa Block (EBB + RAB) and the Paraguá Block (PB) took place at ca. 1.7 Ga. This involved EBB + RAB and the central and oldest part of the PB, the Lomas Maneches and Chiquitania complexes.

The few ages of ca.1.72 Ga found for rims on zircon from the Santa Terezita Granite of the Rio Apa Block in Bolivia are similar to the ages found for the Miraflores Gneiss protolith.

This evidence was used to indicate the collision between the Paraguá Block and EBB + RAB at this time (Redes *et al*., 2020).

In this context, the youngest units of the Chiquitania Complex that are around 50 to 125 Ma younger than the postulated collision age of ca. 1.7 Ga may have had granitic protoliths generated in transitional to post-collisional environments. The transition environment is more consistent with the geotectonic context and the geochemical characteristics of these gneisses, because transitional granitoids might have an origin in orogenic belts of 10 to 100 Ma formation periods, after collision and compression ended. Consequently, fusion conditions are then achieved by the collapse of the orogen, with decompression, relaxation and thinning of the crust (e.g., Winter, 2001) and bimodal magmatism. Post-collisional granitoids are more characterized by calc-alkaline, metaluminous to peraluminous compositions than transitional granitoids.

Still in this scenario, Event 3 would mark the second collision at ca. 1.3 Ga between the PB + EBB + RAB continent and the Amazonian Craton, which can be related to the ca. 1.35 to 1.25 Ga ages obtained on rims of zircon crystals of our gneisses. The ca.1.3 Ga age is also recorded by the metamorphic zircon rims of the Santa Terezita Granite (EBB + RAB) (Redes *et al*., 2020).

Scenario 2: Collision of the Paraguá Block (PB) with the Amazonian Craton occurred at ca. 1.5 Ga and with the EBB + RAB at ca. 1.3 Ga

This second scenario considers the possibility that the Paraguá Block could have been amalgamated with the SW Amazonian Craton between ca. 1.58 and 1.53 Ga (Fig. 5.12).

A) Before this collision, and during Event 2, the Paraguá Block was structured by the accretion of several orogens. The Miraflores Granodiorite Arc represents the oldest part (core) around which the other arcs were attached. Thus, several collisions, responsible for the framework of the Paraguá microcontinent, probably happened in a relatively short period of time, between ca.1.75-1.64 Ga (Fig. 5.12 A).

B) The age range between ca.1.58 and 1.53 Ga is the second most important one found in the gneisses from the Chiquitania Complex, except for the Miraflores Gneiss that occurs in the central

part of the Paraguá Block. This age interval is coincident with the first stage of the San Ignácio orogeny (Bettencourt *et al*., 2010). This period is also coeval with the generation of accretional orogens in the SW Amazon Craton between ca.1.56 and 1.37 Ga (Bettencourt *et al*., 2010), such as the Cachoeirinha (ca.1.56-1.52 Ga) and Santa Helena orogens (ca.1.48-1.42 Ga) of the Jauru Terrane and the Rio Alegre Orogen (ca.1.51 - 1.38 Ga) of the Rio Alegre Terrane. The ages registered in the Chiquitania gneisses are more similar to those found for the Cachoerinha orogen. Probably this time interval indicates the first collision between the amalgamated microcontinent of Paraguá and the proto-Amazonian Craton. The San Ramón Tonalite (ca. 1.43 Ga; Santos *et al*., 2008) is similar in age to the Santa Helena Tonalite in western Mato Grosso (Geraldes *et al*., 2001), also with juvenile characteristics. Intrusions such as that of San Ramón Tonalite around 1.43 Ga could be related with an arc setting. The reworking observed in the Miraflores and Rio Fortuna gneisses could be related with this event.

As records of magmatism or deformation at ca. 1.5 Ga have not been found so far in EBB + RAB rocks, the Rio Apa and Paraguá blocks may not have been amalgamated prior to ca. 1.3 Ga. Thus, if the collision between PB and EBB + RAB only happened at ca.1.3 Ga, the main evidence to justify the collision between PB and EBB + RAB - the ca. 1.7 Ga metamorphic rims on zircon crystals from the Santa Terezita Granite (EBB + RAB; Redes *et al*., 2020) - must be revisited (Fig. 5.12 B).

C) There is evidence for taphrogenesis at ca. 1.4 Ga marked by the occurrence of sills and swarms of mafic dykes in the S-SW portion of the Amazonian Craton in Mato Grosso state. This is represented by the Huanchaca Intrusive Suite, the Rancho de Prata dykes, and the Salto do Céu mafic sills (Lima, 2016; see Figure 5.2). In the SW Amazonian Craton, the Rancho de Prata dyke swarm and Salto do Céu sills (ca.1.44 Ga – Lima, 2016) intrude the Jauru Terrane. These dykes and sills have been related to the post-orogenic stages of the Santa Helena Magmatic Arc (Lima, 2016). The Rio Alegre Orogen in the SW Amazonian Craton indicates the occurrence of an extensional event at ca. 1.4 Ga (Bettencourt *et al*., 2010; Table 5.2).

Sills and mafic dykes of the Huanchaca Intrusive Suite intrude the Turvo orthogneiss at the border of the Paraguá Block (Lima, 2016). This indicates that the Paraguá Block could have become detached from the SW Amazonian Craton at this time (Fig. 5.12 C).

D) The Paraguá Block may have joined the SW Amazonian Craton at ca. 1.3 Ga (Fig. 5.12 D), during Event 3, synchronous with the collision with the EBB + RAB to the south of the Amazonian Craton (Redes *et al*., 2020). This is supported by the occurrence of granitoids from Pensamiento Intrusive Suite, such as the Colmena Granite of ca.1.3 Ga age exposed in the major San Diablo Shear Zone (Litherland *et al*., 1986; Nedel *et al*., 2017), and by ca. 1.34-1.29 Ga ages for metamorphic rims of zircon crystals from the Chiquitania Complex gneisses (Event 3) and the Santa Terezita Granite (EBB + RAB).

In view of the various existing proposals for the tectonic evolution that involves the Paraguá Block, even though several of them are plausible (e.g., Litherland *et al*., 1986; Bettencourt *et al*., 2010), we still believe that scenario 2 is the more likely and cohesive, mainly because it corroborates the available geochronological and isotopic data.

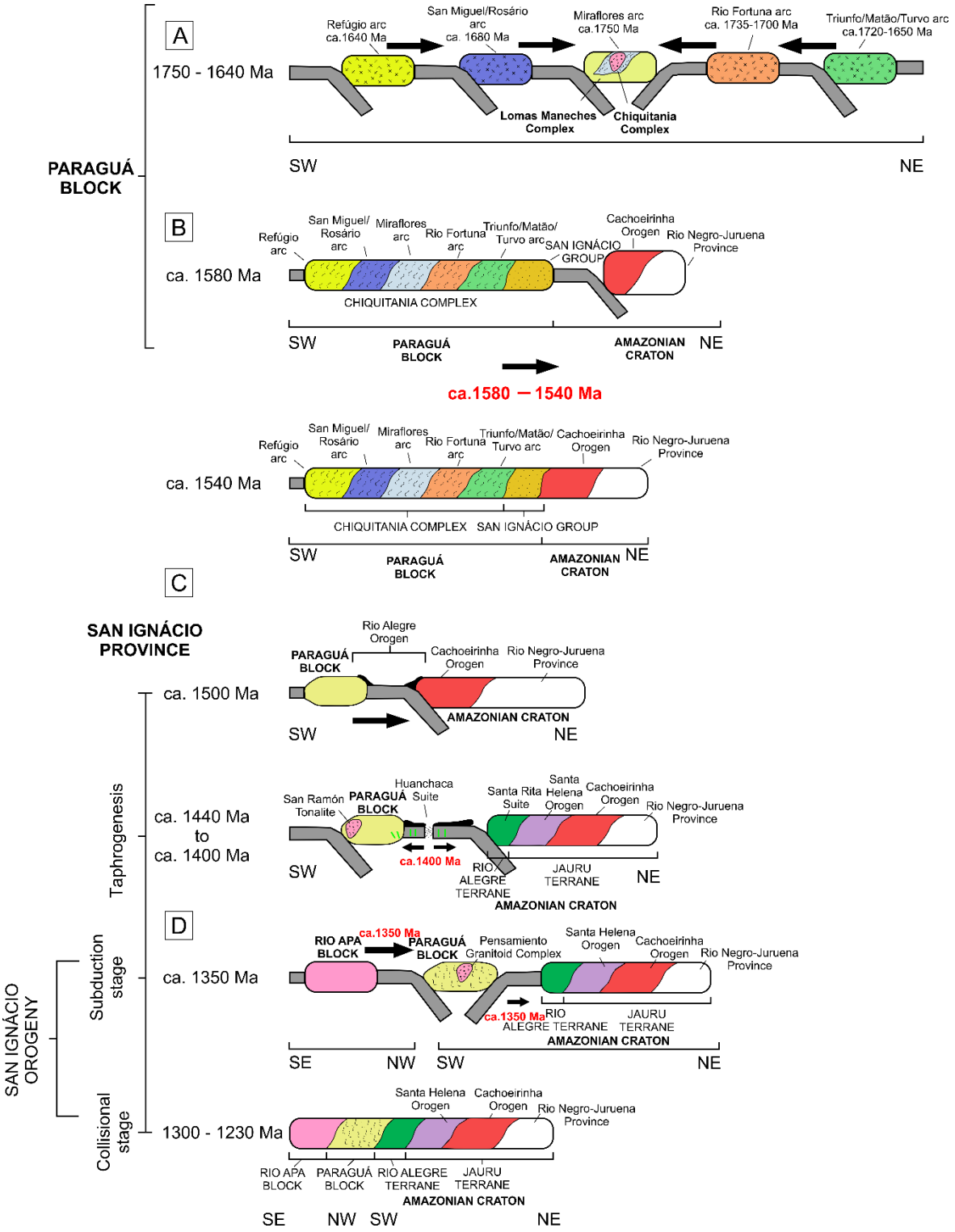

Figure 5.12. Proposed tectonic evolution of the Paraguá Block (see text for explanation). (A) During the ca. 1750–1640 Ma time interval. (B) During the approximate time interval between ca. 1580 and 1540 Ma. (C) During the ca. 1500–1400 Ma time interval. (D) During the ca. 1350–1230 Ma time interval.

5.6. CONCLUSIONS

1 - The Chiquitania Complex gneisses have magmatic arc affinity. They are here divided into an older unit, the Miraflores Gneiss (ca. 1.75 Ga) in the interior of the Paraguá Block, an intermediate unit (ca. 1.69 – 1.64 Ga) represented by the Rio Fortuna, San Miguel and Rosário gneisses at the borders of the Paraguá Block, and the youngest units (ca. 1.64 Ga), the Triunfo, Matão, Turvo and Refúgio gneisses.

2 - For the evolution of the Eastern Bolivian basement (Paraguá Block + Eastern Bolivia Basement), three events are proposed: Event 1 related to the Orosirian granites of the Eastern Bolivian basement, the Alumiador Intrusive Suite of the Western Terrane of the Rio Apa Block (EBB + RAB; Redes *et al*., 2020), and the inherited zircon of the Lomas Maneches Gneiss. Event 2 is related to the construction of at least two arcs: the Miraflores Arc at ca. 1.75 Ga and the Rio Fortuna and Rosário/San Miguel arcs at ca. 1.69 Ga. We have presented evidence for Event 3 (ca. 1.35-1.25 Ga ages) that it can be related with the metamorphism associated with the San Ignácio Orogeny.

3 - Event 2 is characterized by three magmatic cycles represented by the formation of different magmatic arcs, namely the *Miraflores Granodioritic Arc* at ca. 1.75 Ga (Cycle 1), the *Rio Fortuna Tonalite Arc*, and the *Rosário/San Miguel Monzogranitic Arc* at ca. 1.69 Ga (Cycle 2). This was followed by the emplacement of the *Triunfo/Matão/Turvo* and *Refúgio arcs* at ca. 1.64 Ga (Cycle 3). The *Miraflores Granodioritic Arc* is located in the central part of the Paraguá Block. The negative $\varepsilon_{Nd(t)}$ and the Nd T_{DM} ages indicate that it was a mature arc and that a Paleoproterozoic source was involved. The *Rio Fortuna Tonalitic Arc*, with an age of ca.1.70 Ga, is located to the east of the Paraguá Block on the Brazil-Bolivia border. The slightly positive $\varepsilon_{Nd(t)}$ and the Nd T_{DM} ages indicate derivation from Paleoproterozoic protoliths. The Hf isotopic results may indicate that the protolith formed from a mixture of basaltic magma with sedimentary rocks in an arc environment. The *Rosário/San Miguel Monzogranitic Arc* with an age ca. 1.68 Ga is located in the southwestern part of the Paraguá Block. The positive $\varepsilon_{Nd(t)}$ and the Paleoproterozoic Nd T_{DM} indicate a nearly juvenile source for this arc, which is further supported by Hf isotope data on zircon.

4 - Our data support that the Paraguá Block was an allochthonous continent. We consider that the Paraguá Block could have been amalgamated with the SW Amazonian Craton between ca. 1.58 and 1.53 Ga, could have become detached at ca. 1.4 Ga based on evidence for taphrogenesis, and later during Event 3 (ca. 1.3 Ga) collided again with the Amazonian Craton and with the EBB + RAB.

5 – We analyzed four samples from the Chiquitania Complex. Our results, together with those by others for the Chiquitania and Lomas Maneches complexes, reveal a variety of ages related to different processes (metamorphic, magmatic, and inherited zircons). These processes, here identified from the U-Pb point of view and related to Hf data, indicate that there is need for further study to better understand the stratigraphic relationships and evolution of this area. Because the study area is huge, it is also important to map it in more detail on a smaller scale than effected to date.

5.7. ACKNOWLEDGEMENTS

Financial support was provided by the National Council for Scientific and Technological Development (CNPq) of Brazil under grant number 141387/2015-7 to L.A.R., N.H, A.S.R, E.L.D, and W.U.R. We thank (CNPq – Brazil) for the research productivity scholarship of the first author. The research of NH and WUR is supported in part by CNPq fellowships (grants 309878/2019-5 and 305761/2019-6, respectively). We are also grateful for partial support of this study from the *Coordenação de Aperfeiçoamento de Pessoal de Nível Superior* – Brazil (CAPES) – under Finance Code 001. Special thanks are extended to Márcio M. Pimentel (*in memoriam*), who was an inspiration for us. We are dedicating this contribution to his memory and in his honor.

5.8. REFERENCES

Albarède, F., Telouk, P., Blichert-Toft, J., Boyet, M., Agranier, A., Nelson, B., 2004. Precise and accurate isotopic measurements using Multiple-Collector ICPMS. Geochimica et Cosmochimica Acta 68, 12, 2725–2744.

Andersen, T., Andersson, U.B., Graham, S., Åberg, G., Simonsen, S.L., 2009. Granitic magmatism by melting of juvenile continental crust: new constraints on the source of Palaeoproterozoic granitoids in Fennoscandia from Hf isotopes in zircon. Journal of the Geological Society of London 166, 233–247.

Assis, R.R., 2015. Depósitos auríferos associados ao magmatismo félsico da Província de Alta Floresta (MT), Cráton Amazônico: litogeoquímica, idade das mineralizações e fonte dos fluidos. Tese de Doutorado. Universidade de Campinas, Campinas, 326 pp. (in Portuguese with abstract in English).

Berrangé, J.P., 1982. The eastern Bolivia Mineral Exploration Project (Proyecto Precámbrico). Episodes 4, 3-8.

Bertotti, A.L., 2012. Lu-Hf em zircão por LA-MC-ICP-MS. Tese de Doutorado. Universidade Federal do Rio Grande do Sul, Porto Alegre, 162 pp. (in Portuguese with abstract in English).

Bertotti, A.L., Chemale Junior., F., Kawashita, K., 2013. Lu-Hf em zircão por LA-MC-ICP-MS: aplicação em gabro do Ofiolito Aburrá, Colômbia. Pesquisas em Geociências 40, 2, 117–127 (in Portuguese with abstract in English).

Bettencourt, J.S., Leite, Jr. W.B., Ruiz, A.S., Matos, R., Payolla, B.L., Tosdal, R.M., 2010. The Rondonian-San Ignacio Province in the SW Amazonian Craton: An overview. Journal of South American Earth Sciences 29, 28-46.

Blichert-Toft, J., Albarède, F., 1999. Hf isotopic compositions of the Hawaii Scientific Drilling Project Core and the source mineralogy of Hawaiian basalts. Geophysical Research Letters 26, 7, 935–938.

Blichert-Toft, J., Chauvel, C., Albarède, F., 1997. Separation of Hf and Lu for high-precision isotope analysis of rock samples by magnetic sector-multiple collector ICP-MS. Contributions to Mineralogy and Petrology 127, 248-260.

Boger, S.D., Raetz M., Giles, D., Etchart, E., Fanning, C.M., 2005. U–Pb age data from the Sunsas region of Eastern Bolivia, evidence for the allochthonous origin of the Paragua Block. Precambrian Research 139, 121-146.

Bouvier, A., Vervoort, J.D., Patchett, P.J., 2008. The Lu-Hf and Sm-Nd isotopic composition of CHUR: constraints from unequilibrated chondrites and implications for the bulk composition of the terrestrial planets. Earth and Planetary Science Letters 273, 48–57.

Brito Neves, B.B., Fuck, R.A., 2014. The basement of the South American platform: Half Laurentian (N-NW) + half Gondwanan (E-SE) domains. Precambrian Research 244, 75-86.

Buhn B., Pimentel, M.M., Matteini, M., Dantas, E.L., 2009. High spatial resolution analysis of Pb and U isotopes for geochronology by laser ablation multi-collector inductively coupled plasma spectrometry (LA-MC-ICPMS). Anais da Academia Brasileira de Ciências 81, 1, 99-114.

Chew, D.M., Magna, T., Kirkland, C.L., Miškovic, A., Cardona, A., Spikings, R., Schaltegger, U., 2008. Detrital zircon fingerprint of the Proto-Andes: evidence for a Neoproterozoic active margin? Precambrian Research 167, 186–200.

Chu, N.C., Taylor, R.N., Chavagnac, V., Nesbitt, R.W., Boella, R.M., Milton, J. A., German, C.R., Bayon, G., Burton, K., 2002. Hf isotope ratio analysis using multi-collector inductively coupled plasma mass spectrometry: an evaluation of isobaric interference corrections. Journal of Analytical Atomic Spectrometry 17, 1567-1574.

Cohen, K.M., Finney, S.C., Gibbard, P.L., Fan, J.-X., 2013. The International Chronostratigraphic Chart. Episodes 36, 199–204.

Condie, K.C., 2002. Breakup of a Paleoproterozoic Supercontinent. Gondwana Research 5, 41-43.

Cordani, U.G., Sato, K., Teixeira, W., Tassinari, C.C.G., Basei, M.A.S., 2000. Crustal evolution of the South American platform. In: Cordani, U. G., Milani, E. J., Thomaz Filho, A., Campos, D. A. (Eds.), Tectonic evolution of South America. Rio de Janeiro, pp. 19-40.

Cordani, U.G., Tassinari, C.C.G., Teixeira, W., Basei, M.A.S., Kawashita, K., 1979. Evolução Tectônica da Amazônia com base nos dados geocronológicos. In: II Congresso Geológico Chileno. Arica, Chile, Anais, 137-148.

Cordani, U.G., Teixeira, W., 2007. Proterozoic Accretionary Belts in the Amazonian Craton. In: Hatcher, Jr., R.D., Carlson, M.P., McBride, J.H. (Eds.), 4-D Framework of Continental Crust. Memoir, Geological Society of America, Boulder, Colorado, 200, pp. 297-320.

Cordani, U.G., Teixeira, W., D'Agrella-Filho, M.S., Trindade, R.I., 2009. The position of the Amazonian Craton in supercontinents. Gondwana Research 15, 396–407.

Cordani, U.G., Teixeira, W., Tassinari, C.C.G., Coutinho, J.M.V., Ruiz A.S., 2010. The Rio Apa Craton in Mato Grosso do Sul (Brazil) and Northern Paraguay: Geochronological evolution, correlations and tectonic implications for Rodinia and Gondwana. American Journal of Science 310, 981–1023.

Corfu, F, Hanchar, J.M., Hoskin, P..WO., Kinny, P., 2003. Atlas of zircon textures. In: Hanchar J.M., Hoskin, P.W.O. (Eds.), Reviews in Mineralogy and Geochemistry 53, pp. 469–500.

Cuadros, F.A., Botelho, N.F., Fuck, R.A., Dantas, E.L., 2017. The peraluminous Aurumina Granite Suite in central Brazil: An example of mantle-continental crust interaction in a Paleoproterozoic cordilleran hinterland setting? Precambrian Research 299, 75–100.

Debon, F., Le Fort, P.A., 1983. Chemical-mineralogical classification of common plutonic rocks and associations. Transactions of the Royal Society of Edinburgh Earth Sciences 73, 135-149.

DePaolo, D.J., 1981. Trace elemento and isptopic effects of combined wall rock assimilation and fractional crystallization. Earth and Planetary Science Letters 53, 189-202.

Duarte, T.B., 2015. Geologia, geoquímica e geocronologia do domínio vulcânico do Arco magmático Juruena, SW do Cráton Amazônico: implicações geotectônicas. Dissertação de Mestrado. Universidade Estadual de Campinas, Campinas, 124 pp. (in Portuguese with abstract in English).

Duarte, T.B., Rodrigues, J.B., Ribeiro, P.S.E., Scandolara, J.E., 2012. Tectonic evolution of the Juruena magmatic arc between the Aripuanã and Juruena rivers: northwest Mato Grosso state. Brazil. Revista Brasileira de Geociências 42, 824-840.

Ducea, M.N., Paterson, S.R., DeCelles, P.G., 2015. High-volume Magmatic Events in Subduction Systems. Elements 11, 2, 99-104.

Evensen, N.M., Hamilton, P.J., O'Nions, R.K., 1978. Rare-earth abundances in chondritic meteorites. Geochimica et Cosmochimica Acta 42, 1199–1212.

Faria, A.D., 2015. Petrografia, Análise deformacional e geocronologia (U-Pb) dos gnaisses do Terreno Paraguá: Provável Arco Vulcânico Orosiriano - SW do Cráton Amazônico. Tese de Doutorado. Universidade Federal do Pará, Belém, 135 pp. (in Portuguese with abstract in English).

Faria, A.D., Ruiz, A.S., Matos, J.B., Sousa, M.Z.A., Lima, G.A., Macambira, M.J.B., 2014. Geology, Geochemistry, and Geochronology (U-Pb) of the Rio Fortuna Gneiss – Serra do Baú Intrusive Suite – Paraguá Terrane – SW Amazonian Craton. Brazilian Journal of Geology 44, 139-154 (in Portuguese with abstract in English).

Figueiredo, F.L.P., Ruiz A.S., Sousa, M.Z.A., Macambira, M.J.B., 2009. Dados isotópicos Pb-Pb em zircão no Ortognaisse Turvo (Terreno Paraguá - SW do Cráton Amazônico). In: Simpósio de 45 anos de Geocronologia no Brasil, São Paulo-SP, Boletim de Resumos Expandidos, 177-179 (in Portuguese).

Figueiredo, F.L.P., Ruiz A.S., Sousa, M.Z.A., Macambira, M.J.B., 2013. Gnaisse Turvo: registro de magmatismo paleoproterozoico no Terreno Paraguá – Sudoeste do Cráton Amazônico, Vila Bela da Santíssima Trindade, Mato Grosso. Brazilian Journal of Geology 43, 401-422 (in Portuguese with abstract in English).

França, O. Ruiz, A.S., Sousa, MZ.A., Batata, M.E.F., Lafon, J.M., 2014. Geology, petrology, U-Pb (SHRIMP) geochronology of the Morrinhos granite – Paraguá Terrane, SW Amazonian craton: implications for the magmatic evolution of the San Ignácio orogeny. Brazilian Journal of Geology 44, 415-432.

Frost, B.R., Barnes, C.G., Collins, W.J., Arculus, R.J., Elis, D.J., Frost, C.D., 2001. A Geochemical Classification for Granitic Rocks. Journal of Petrology 42, 2033–2048.

Galé, M. G., 2018. Gênese das mineralizações associadas ao magmatismo ácido na região do Garimpo do Papagaio, Noroeste da Província Aurífera de Alta Floresta (MT). Tese de Doutorado. Universidade de São Paulo, São Paulo, 189 pp. (in Portuguese with abstract in English).

Geraldes, M.C., Bettencourt, J.S., Teixeira, W, Matos, J.M., 2004. Geochemistry and isotopic constraints on the origin of the mesoproterozoic Rio Branco 'anorogenic' plutonic suite, SW of Amazonian craton, Brazil: high heat flow and crustal extension behind the Santa Helena arc? Journal of South American Earth Sciences 17, 195-208.

Geraldes, M.C., Teixeira, W., Van Schmus, W.R., 2000. Isotopic and chemical evidence for three accretionary magmatic arcs (1.79–1.42 Ga) in the SW Amazon Craton, state of Mato Grosso, Brazil. Revista Brasileira de Geociências 30, 99–101.

Geraldes, M.C., Van Schmus, W.R., Condie, K.C., Bell, S., Teixeira, W., Babinski, M., 2001. Proterozoic geologic evolution of the SW part of the Amazonian Craton in Mato Grosso state, Brazil. Precambrian Research 111, 91–128.

Gerdes, A., Zeh, A., 2009. Zircon formation versus zircon alteration – New insights from combined U-Pb and Lu-Hf in-situ LA-ICP-MS analyses, and consequences for the interpretation of Archean zircon from the Central Zone of the Limpopo Belt. Chemical Geology 261, 230–243.

Gioia, S.M.C.L., Pimentel, M.M., 2000. The Sm-Nd isotopic method in the geochronology laboratory of the University of Brasilia. Anais da Academia Brasileira de Ciências 72, 2, 219-245.

Goodge, J.W., Vervoort, J.D., 2006. Origin of Mesoproterozoic A-type granites in Laurentia: Hf isotope evidence. Earth and Planetary Science Letters 243, 711-731.

Hoffman, P.F., 1988. United plates of America, the birth of a craton. Earth and Planetary Science Letters 16, 543–603.

Horstwood, M.S.A., Košler, J., Gehrels, G., Jackson, S.E., McLean, N.M., Paton, C., Pearson, N.J., Sircombe, K., Sylvester, P.S., Vermeesch, P., Bowring, J.F., Condon, D.J., Schoene, B., 2016. Community-Derived Standards for LA-ICP-MS U-(Th-)Pb Geochronology – Uncertainty Propagation, Age Interpretation and Data Reporting. Geostandards and Geoanalytical Research 40, 3, 311-332.

Jackson, S.E., Pearson, N.J., Griffin, W.L., Belousova, E.A., 2004. The application of laser ablation inductively coupled plasma mass spectrometry to in situ U-Pb zircon geochronology. Chemical Geology 211, 47-69.

Jesus, G.C., Sousa, M.Z.A., Ruiz, A.S., Matos, J.B., 2010. Petrologia e geocronologia (U/Pb–Sm/Nd) do Granito Passagem, Complexo Granitoide Pensamiento, SW do Cráton Amazônico (MT). Revista Brasileira de Geociências 40, 392-408 (in Portuguese).

Klinck, B.A., Litherland, M., 1982. A model for the Proterozoic structural history of eastern Bolivia. Report on Eastern Bolivia Mineral Exploration Project, Santa Cruz, number BAK/15 (unpublished).

Lacerda Filho, J.V., Brito R.S.C., Silva M.G., Oliveira C.C., Moreton L.C., Martins E.G., Lopes R.C., Lima T.M., Larizatti J.H., Valente C.R., 2006. Geologia e Recursos Minerais do Estado de Mato Grosso do Sul, Programa Integração, Atualização e Difusão de Dados da Geologia do Brasil. CPRM, Campo Grande, 1, 10-128.

Lima, G.A., 2016. Soleiras e Enxames de Diques Máficos do sul-sudoeste do Cráton Amazônico. Tese de Doutorado. Universidade Federal do Pará, Belém, 182 pp. (in Portuguese with abstract in English).

Litherland, M., Annells, R.N., Appleton, J.D., Berrangé, J.P., Bloomfield, K., Burton, C.C.J., Darbyshire, D.P.F.M., Fletcher, C.J.N., Hawkins, M.P., Klinck, B.A., Lanos, A., Mithcell, W.I., O Connor, E.A., Pitfield, P.E.J., Power, G. E Webb B.C., 1986. The Geology and Mineral Resources of the Bolivian Precambrian Shield. British Geological Survey Overseas Memoir 9, 153 pp.

Litherland, M., Annels, R.N., Appleton, J.D., Berrange, J.P., Bloomfield, K., Burton, C.C.J., Darbyshire, D.P.F.M, Fletcher, C.J.N., Hawkins, M.P., Klink, B.A., Llanos, A., Mitchell, W.I., O Connor, E.A., Pitfield, P.E.J., Power, G., Webb, B.C., 1989. The Proterozoic of eastern Bolivia and its relationship to the Andean Mobile Belt. Precambrian Research 43, 157-174

Litherland, M., Bloomfield, K., 1981. The Proterozoic history of eastern Bolivia. Precambrian Research 15, 157–179.

Loewy, S.L., Connelly, J.N., Dalziel, I.W.D., 2004. An orphaned block: the Arequipa–Antofalla basement of central Andean margin of South America. Geological Society of America Bulletin 116, 171-187

Ludwig, K.R., 2012. Isoplot 3.75. A Geochronological Toolkit for Microsoft Excel. Special Publication. Berkeley Geochronology Center 4, 75 pp..

Maniar, P.D., Piccoli, P.M., 1989. Tectonic discrimination of granitoids. Geological Society of America Bulletin 101, 635-643.

Matos, J.B., Juliani, C., Tokashik, C.C., Oliveira, R.F., Ruiz, A.S., 2013. Granulitos Ortoderivados da Suite Lomas Maneches, Fronteira Brasil-Bolívia: Geoquímica e Geocronologia. In: XIII Simpósio de Geologia da Amazônia, Belém-PA, Anais Sociedade Brasileira de Geologia 1, 305-308.

Matos, J.B., Schorscher, J.H.D., Geraldes, M.C., Souza, M.Z.A., Ruiz., A.S., 2004. Petrografia, geoquímica e Geocronologia das rochas do Orógeno Rio Alegre, Mato Grosso: um registro de crosta oceânica Mesoproterozoica no SW do Cráton Amazônico. Geologia USP. Série Científica 4, 75- 90 (in Portuguese).

Matos, R., 2012. Geocronología U-Pb y Sm-Nd de la Serie Yarituses y de la Granodiorita San Ramón, So del Craton Amazónico: implicaciones para la evolucíon cortical del escudo precámbrico de Bolivia. Revista Boliviana de Geociências 4, 33-44

Matos, R., Teixeira W., Geraldes, M.C., Bettencourt, J.S., 2009. Geochemistry and Nd–Sr isotopic signatures of the Pensamiento Granitoid Complex, Rondonian- San Ignácio Province. Eastern Precambrian shield of Bolivia: petrogenetic constraints for a Mesoproterozoic magmatic arc setting. Geologia USP, Série Científica 9, 89–117.

Matteini, M., Dantas, E.L., Pimentel, M.M., Bühn, B., 2010. Combined U-Pb and Lu-Hf isotope analyses by laser ablation MC-ICP-MS: methodology and applications. Anais da Academia Brasileira de Ciências 82, 2, 479-491.

Morel, M.L.A., Nebel O., Nebel-Jacobsen, Y.L., Miller, J.S., Vroon, P.Z., 2008. Hafnium isotope characterization of the GJ-1 zircon reference material by solution and laser ablation MC–ICPMS. Chemical Geology 255, 231 –235.

Moura, M.A., 1998. O Maciço Granítico Matupá e o Depósito de Ouro Serrinha (MT): Petrologia, Alteração Hidrotermal e Metalogenia. Tese de Doutorado. Universidade de Brasília, Brasília, 238 pp. (in Portuguese with abstract in English).

Nalon, P.A., Sousa M.Z.A., Ruiz, A.S., Macambira, M.B., 2013. Batólito Guaporeí uma extensão do Complexo Granitoide Pensamiento em Mato Grosso, SW do Cráton Amazônico. Revista Brasileira de Geociências 43, 85–100 (in Portuguese).

Nascimento, N.D.C., 2015. Geologia, Geocronologia U-Pb e Sm-Nd e Petrologia do migmatito Furna Azul: implicações sobre a evolução crustal mesoproterozoica da Orogenia San Ignácio? SW do Cráton Amazônico. Dissertação de Mestrado. Universidade Federal de Mato Grosso, Cuiabá, 104 pp. (in Portuguese with abstract in English).

Nebel, O., Nebel-Jacobsen, Y., Mezger, K., Berndt, J., 2007. Initial Hf isotope compositions in magmatic zircon from early Proterozoic rocks from the Gawler Craton, Australia: A test for zircon model ages. Chemical Geology 241, 23-37.

Nedel, I.M., Ruiz, A.S., Matos, G.R.S., Sousa, M.Z.A., Pimentel, M.M., Pavanetto, P., 2017. Front San Diablo na região de Miraflores, Faixa Sunsas, Bolívia: implicações tectônicas e estratigráficas San Diablo Front at Miraflores region, Sunsas Belt, Bolívia: tectonics and stratigraphics implications. Geologia USP, Série Científica 17, 125-147 (in Portuguese).

Niu, Y.L., Zhao, Z.D., Zhu, D.C., Mo, X.X., 2013. Continental collision zones are primary sites for net continental crust growth – A testable hypothesis. Earth-Science Reviews 127, 96–110.

Nogueira, S.F., 2015. Petrologia, Geocronologia (U-Pb SHRIMP) e Geologia Isotópica (Sm-Nd) do Granito Aquidabã, Arco Magmático Amonguijá-Terreno Rio Apa-Sul do Cráton Amazônico. Dissertação de Mestrado. Universidade Federal de Mato Grosso, Cuiabá, 80 pp. (in Portuguese with abstract in English).

Oliveira, F.V., 2015. Chronus: Um novo suplemento para a redução de dados U-Pb obtidos por LAMC-ICPMS. Dissertação de Mestrado. Universidade Federal de Brasília, Brasília, 107 pp. (in Portuguese with abstract in English).

Paes de Barros, A.J., 2007. Granitos da região de Peixoto de Azevedo – Novo Mundo e mineralizações auríferas relacionadas – Província Aurífera Alta Floresta (MT). Tese de Doutorado. Universidade Estadual de Campinas, Campinas, 171 pp. (in Portuguese with abstract in English).

Patchett, P.J., 1983. Importance of the Lu–Hf isotopic system in studies of planetary chronology and chemical evolution. Geochimica et Cosmochimica Acta 47, 81-97.

Patiño Douce, A.E., 1995. Experimental generation of hybrid silicic melts by reaction of high-Al basalt with metamorphic rocks. Journal of Geophysical Research 100, 15623–15639.

Payolla, B.L., Bettencourt, J.S., Kozuch, M., Leite Jr., W.B., Fetter, A.H., Van Schmus, W.R., 2002. Geological evolution of the basemente rocks in the east central part of the Rondonia Province, SW Amazonian Craton, Brazil: U e Pb and Sm-Nd isotopic constraints. Precambrian Research 119, 141-169.

Pearce, J.A., Harris N.B.W., Tindle, A.G., 1984. Trace element discrimination diagrams for the tectonic interpretation of granitic rocks. Journal of Petrology 25, 956-983.

Pietranik, A.B., Hawkesworth, C.J., Storey, C.D., Kemp, A.I.S., Sircombe, K.N., Whitehouse, M.J., Bleeker, W., 2008. Episodic, mafic crust formation from 4.5 to 2.8 Ga: New evidence from detrital zircons, Slave craton, Canada. Geology, 36, 11, 875–878. https://doi.org/10. 1130/ G248 61A.1

Plens, D.P., 2018. Petrogênese e Análise Estrutural e a Suíte Caracol: Implicações para a Evolução Geodinâmica do Bloco Rio Apa - Sul do Cráton Amazônico. Tese de Doutorado. Universidade Federal de Brasília, Brasília, 132 pp. (in Portuguese with abstract in English).

Prado, E.S., Barros M.A.S., Pinho F.E.C., Pierosan R., 2013. Granito Terra Nova - petrologia e geocronologia: um granito tipo-A da Província Aurífera Alta Floresta - Cráton Amazônico. Revista Brasileira de Geociências 43, 1, 101-116 (in Portuguese).

Quispe, P.E.C., 2016. Geologia, Geoquímica e Geocronologia dos Granitoides foliados e Rochas subvulcânicas da Região de Peixoto de Azevedo, Setor Leste da Província Aurífera de Alta Floresta, Mato Grosso. Dissertação de Mestrado. Universidade Estadual de Campinas, Campinas, 124 pp. (in Portuguese with abstract in English).

Ramos, V., 2008. The basement of the Central Andes: the Arequipa and related terranes. Annual Review of Earth and Planetary Sciences 36, 289-324.

Ramos, V., 2010. The Grenville-age basement of the Andes. Journal of South American Earth Sciences 29, 77-91.

Redes, L.A., Hauser, N., Ruiz, A.S., Ramiro, G.M., Reimold, U.W., Dantas, E.L., Schmitt R.T., Lima, B.A.F., Zacchi, E.N.P., Chaves, J.G.S., Osorio, L.F.B., Pimentel, M.M., 2020. U–Pb and Hf isotopes in granitoids from the Eastern Bolivian basement: Insights into the Paleoproterozoic evolution of the western part of South America. Journal of South American Earth Sciences 104, 102806. https://doi.org/10.1016/j.jsames.2020.102806

Redes, L. A, Sousa, M. Z. A., Ruiz, A. S., Lafon, J. M., 2015. Petrogenesis and U-Pb and Sm-Nd geochronology of the Taquaral granite: record of an orosirian continental magmatic arc in the region of Corumbá – MS. Brazilian Journal of Geology 45, 431-451.

Ribeiro, B.V., Cawood, P.A., Faleiros, F.M., Mulder, J.A., Martin, E., Finch, M.A., Raveggi, M., Teixeira, W., Cordani, U.G., Pavan, M., 2020. A long-lived active margin revealed by zircon U–Pb–Hf data from the Rio Apa Terrane (Brazil): New insights into the Paleoproterozoic evolution of the Amazonian Craton. Precambrian Research 350, 105919. https://doi.org/10.1016. /j.precamres.2020.105919

Rizzotto, G.J., Hartmann, L.A., 2012. Geological and geochemical evolution of the Trincheira Complex, a Mesoproterozoic ophiolite in the Southwestern Amazonian Craton, Brazil. Lithos 148, 277-295.

Rollinson, H., 1993. Using geochemical data: evaluation, presentation, interpretation. Longman, London, 386 pp.

Rubatto, D., 2017. Zircon: the metamorphic mineral. Reviews in Mineralogy and Geochemistry 83, 261–265.

Ruiz, A.S., 2005. Evolução geológica do sudoeste do Cráton Amazônico região limítrofe Brasil-Bolívia-Mato Grosso. Tese de Doutorado. Universidade Estadual Paulista, São Paulo, 299 pp. (in Portuguese).

Ruiz, A.S., 2009. Compartimentação Tectônica (Pré-Sunsas) do Sudoeste do Cráton Amazônico: Ênfase em Mato Grosso – Brasil. In: XVIII Congresso Geológico Boliviano. Potosí, Bolívia, 159-163.

Ruiz, A.S., D'Agrella-Filho, M.S., Sousa, M.Z.A., Lima, G.A., 2010. Tonian sills and mafic dike swarms of the S-SW Amazonian craton, records of Rodinia Supercontinent break-up? In: Meeting of the Americas. Foz do Iguaçu-PR. Abstracts, EOS Transactions American Geophysical Union 23, 3 pp.

Sadowski, G.R., Bettencourt, J.S., 1996. Mesoproterozoic tectonic correlations between eastern Laurentia and the western border of the Amazonian Craton. Precambrian Research 76, 213–227.

Saes, G.S., Fragoso Cesar, A.R.S., 1996. Acresção de terrenos mesoproterozoicos no SW da Amazônia. In: 39º Congresso Brasileiro de Geologia. Salvador-BA. Boletim de resumos expandidos, Sociedade Brasileira de Geologia 124–126.

Saes, G.S., Leite, J.A.D., 1993. Evolução tectono-sedimentar do Grupo Aguapeí, Proterozoico Médio na porção meridional do Cráton Amazônico: Mato Grosso e Oriente Boliviano. Revista Brasileira de Geociências 23, 31–37 (in Portuguese).

Santos, F.R.P., Silva, C.H., Costa, A.C.D., Siqueira, A.C.N., 2016. Geologia e petrografia do Grupo Alto Jauru na região da Fazenda Retiro Novo, SW do Cráton Amazônico: evidências de um prisma acrescionário estateriano. Brazilian Journal of Geology 46, 1, 129-146 (in Portuguese).

Santos, F.S., Pierosan, R., Barros, M.A.S., Geraldes, M.C., Lima, M.F., 2019. Petrology of the Colíder Group volcanic successions in the northernmost Mato Grosso, Brazil: A contribution to the knowledge of the felsic volcanism of the Alta Floresta Gold Province. Journal of South American Earth Sciences 89, 10–29.

Santos, G., Ruiz, A.S., Sousa, M.Z.A., Batata, M.E.F., Cabrera, R.F., Lafon, J.M., 2019. Petrology, deformation and geochronology U-Pb (SHRIMP) of Coimbra granite – Rio Apa block in the region of Corumbá, Brazil. Geologia USP. Série Científica 9, 17–192 (in Portuguese).

Santos, J.O.S., Hartmann, L.A., Gaudette, H.E., Groves, D.I., Mcnaughton, N.J., Fletcher, I.R., 2000. A new understanding of the Amazon Craton Provinces based on integration of field mapping and U-Pb and Sm-Nd Geochronology. Gondwana Research 3, 453-488.

Santos, J.O.S., Rizzotto, G.J., McNaughton, N.J., Matos, R., Hartmann, L.A., Chemale Junior, F., Potter, P.E., Quadros, M.L.E.S., 2008. The age and autochthonous evolution of Sunsas Orogen in West Amazon Craton. Precambrian Research 165, 120–152.

Sato, K., Basei, M.A.S., Siga, O.J., 2008. Novas técnicas aplicadas ao método U-Pb no CPGeo - IGc/USP: avanços na digestão química, espectrometria de massa (TIMS) e exemplos de aplicação integrada com SHRIMP. Geologia USP, Série Científica 8, 77-99 (in Portuguese).

Scandolara, J.E., Correa, R.T., Fuck, R.A., Souza, V.S., Rodrigues, J.B., Ribeiro, P.S.E., Frasca, A.A.S., Saboia, A.M., Lacerda Filho, J.V., 2017. Paleo-Mesoproterozoic arc-accretion along the southwestern margin of the Amazonian craton: The Juruena accretionary orogen and possible implications for Columbia supercontinent. Journal of South American Earth Sciences 73, 223-247.

Scandolara, J.E., Ribeiro, P.S.E., Frasca, A.A.S., Fuck, R.A., Rodrigues, J.B., 2014. Geochemistry and geochronology of mafic rocks from the Vespor suíte in the Juruena arc, Roosevelt-Juruena terrane, Brazil: implications for Proterozoic crustal growth and geodynamic setting of the SW Amazonian craton. Journal of South American Earth Sciences 53, 20-49.

Scherer, E., Münker, C., Mezger, K., 2006. Calibration of the lutetium–hafnium clock. Science. 293, 683–687.

Schmitt, R.S., Trouw, R.A.J., Van Schmus, W.R., Pimentel, M.M., 2004. Late amalgamation in the central part of Western Gondwana: new geochronological data and the characterization of a Cambrian collisional orogeny in the Ribeira belt (SE Brazil). Precambrian Research 133, 29- 61

Shand, S.J., 1943. Eruptive rocks: Their genesis, composition, classification, and their relation to ore-deposits, with a chapter on meteorites. Thomas Murby and Co., London, 444 pp.

Siivola, J., Schmid, R., 2007. List of Mineral Abbreviation. In: Fettes, D., Desmonds, J. (Eds.), Metamorphic Rocks. A Classification and Glossary of Terms. Cambridge University Press, Cambridge, United Kingdom, pp. 93-110.

Silva, F.R., Barros, M.A.S., Pierosan, R., Pinho, F.E.C., Rocha, M.L.B.P., Vasconcelos B.R., Dezula, S.E.M., Tavares, C., Rocha, J., 2014. Geoquímica e geocronologia U-Pb (SHRIMP) de granitos da região de Peixoto de Azevedo: Província Aurífera Alta Floresta, Mato Grosso. Brazilian Journal of Geology 44, 3, 433-455 (in Portuguese).

Silva, L.C., Armstrong, R., Pimentel, M.M., Scandolara, J.E., Ramgrab, G.E., Wildner, W., Angelim, L.A.A., Vasconcelos, A.M., Rizzoto, G.J., Quadros, M.L.E.S., Sander, A., Rosa, A.L.Z., 2002. Reavaliacão da evolução geológica em terrenos pré-cambrianos brasileiros com base em novos dados U-Pb SHRIMP, Parte III: Províncias Borborema, Mantiqueira Meridional e Rio Negro-Juruena. Revista Brasileira de Geociências 32, 529–544 (in Portuguese).

Silva, M.G., Abram, M.B., 2008. Projeto Metalogenia da Província Aurífera Juruena-Teles Pires, Mato Grosso. Informe de Recursos Minerais, Série Ouro, 16. Companhia de Pesquisa de Recursos Minerais - CPRM, Goiânia, 212 pp..

Souza, C.D., Sousa, M.Z.A., Ruiz, A.S., Batata, M.E.F., Brittes, A.F.N., Lafon, J.M., 2016. Formação Serra da Bocaina: Contribuição do Vulcanismo Paleoproterozoico do Arco Magmático Amonguijá no Bloco Rio Apa, Sul do Cráton Amazônico. Geochimica Brasiliensis 30, 136 – 157 (in Portuguese).

Stacey, J.S., Kramers, J.D., 1975. Approximation of terrestrial lead isotope evolution by a two-stage model. Earth and Planetary Science Letters 26, 207–221.

Tassinari, C.C.G., Bettencourt, J.S., Geraldes, M.C., Macambira, M.J.B.; Lafon, J.M., 2000. The Amazonian Craton, in: Cordani, U. G.; Milani, E. J.; Thomaz Filho, A.; Campos, D. A. (Eds.), Tectonic evolution of South America. 31º International Geological Congress, Rio de Janeiro, pp. 41-95.

Tassinari, C.C.G., Cordani, U.G., Nutman, A.P, Van Schmus, W.R., Bettencourt, J.S., Taylor, P.N., 1996. Geochronological systematics on basement rocks from the Rio Negro-Juruena Province (Amazonian Craton) and tectonic implications. International Geology Reviews 38, 2, 161–175.

Tassinari, C.C.G., Macambira, M.J.B., 1999. Geochronological provinces of the Amazonian Craton. Episodes 38, 174-182.

Teixeira, W., Cordani, U.G., Faleiros, F.M., Sato, K., Maurer, V.C., Ruiz, A.S., Azevedo, E.J.P., 2020. The Rio Apa Terrane reviewed: U-Pb zircon geochronology and provenance studies provide paleotectonic links with a growing Proterozoic Amazonia. Earth-Science Reviews 202, 1–35.

Teixeira, W., Geraldes, M.C., Matos, R., Ruiz, A.S., Saes, G., Vargas-Mattos, G., 2010. A review of the tectonic evolution of the Sunsas belt, SW Amazonian Craton. Journal of South American Earth Sciences 29, 47–60.

Teixeira, W., Tassinari, C.C.G., Cordani, U.G., Kawashita, K., 1989. A review of the geochronology of the Amazonian Craton: tectonic implications. Precambrian Research 42, 213–227.

Testa, A.L.G.C., 2018. Geologia, Petrologia e Geocronologia dos Granitos da Região de Novo Mundo (MT) e Implicações para a evolução magmática e regional. Dissertação de Mestrado. Universidade de Brasília, Brasília, 133 pp. (in Portuguese with abstract in English).

Thiéblemont, D., Tégyey, M., 1994. Une discrimination géochimique des roches différenciés témoin de la diversité d'órigine et de situation tectonique des magmas calco-alcalins. Comptes Rendus de l'Académie Des Sciences 319, 87-94.

Tohver, E., Bettencourt, J.S., Tosdal, R., Mezger, K., Leite, W.B., Payolla, B.L., 2004. Terrane transfer during Grenville orogeny: tracing the Amazonian ancestry of Southern Appalachian basement through Pb and Nd isotopes. Earth and Planetary Science Letters 228, 161-176.

Tohver, E., Pluijm, B.A.V.D., Scandolara, J.E., Essene, E., 2005. Late Mesoproterozoic deformation of SW Amazônia (Rondônia, Brazil): geochronological and structural evidence for collision with Southern Laurentia. Journal of Geology 113, 309–323.

Wiedenbeck, M., Allé, P., Corfu, F., Griffin, W.L., Meier, M., Oberli, F., von Quadt, A., Roddick, J.C., Spiegel, W., 1995. Three natural zircon standards for U-Th-Pb, Lu-Hf, trace element and REE analyses. Geostandards Newsletter 19, 1-23.

Wiedenbeck, M., Hanchar, J.M., Peck, W.H., Sylvester, P., Valley, J.W., Whitehouse, M.J., Kronz, A., Morishita, Y., Nasdala, L., Fiebig, J., Franchi, I., Girard, J.P., Greenwood, R.C., Hinton, R., Kita, N., Mason, P.R.D., Norman, M., Ogasawara, M., Piccoli, R., Rhede, D., Satoh, H., Schulz-Dobrick, B., Skar, O., Spicuzza, M.J., Terada, K., Tindle, A., Togashi, S., Vennemann, T., Xie, Q., Zheng, Y.F., 2004. Further characterization of the 91500 zircon crystal. Geostandards and Geoanalytical Research 28, 9-39.

Wilson, M., 1989. Igneous Petrogenesis – A Global Tectonic Approach. Harper Collins Academic Press, London, 466 pp.

Winter, J.D., 2001: An Introduction to Igneous and Metamorphic Petrology. Prentice-Hall Inc., New Jersey, 697 pp.

Zhao, G., Sun, M., Wilde, S.A., Li, S., 2004. A Paleo-Mesoproterozoic supercontinent: assembly, growth and breakup. Earth-Science Reviews. 67, 91–123.

Supplementary Table 5.I.1. Summary of petrographic information about the studied gneisses of the Chiquitania Complex of the Paraguá Block.

LITHOLOGY	PROTOLITH	MACROSCOPIC CHARACTERISTICS	MICROSCOPIC CHARACTERISTICS	ESSENTIAL MINERALOGY	ACCESSORY MINERALS	ALTERATION	METAMORPHIC
MIRAFLORES GNEISS (hornblende-biotite-gneiss)	monzogranite to granodiorite	light gray, medium-grained, leucocratic gneisses, with millimeter to centimeter wide compositional bands; banding is parallel and regular, continuous, or discontinuous; shows migmatitic structures (Fig. I.1)	inequigranular texture; porphyroblasts of microcline immersed in a fine-grained, quartz-feldspar dominated matrix with stretched biotite, muscovite and chlorite (Fig. I.3)	oligoclase and andesine (45-40 vol%), quartz (25-20 vol%), microcline (20-15 vol%), and biotite (15-10 vol%)	titanite, rutile, apatite, zircon and opaque minerals	sericitization, argillitization, saussuritization, and chloritization	retrograde greenschist facies after amphibolite grade
RIO FORTUNA GNEISS (hornblende-biotite-gneiss)	tonalite	light gray, medium-grained, leucocratic gneiss, with continuous and discontinuous, millimeter to centimeter wide banding (Fig. I.1)	inequigranular to equigranular texture of medium grain size, granoblastic; amphibole often exhibits sagenitic texture (Fig. I.3)	andesine (70-60 vol%), quartz (25-20 vol%), microcline (10-8 vol%), biotite (8-5 vol%), and hornblende (5-3 vol%)	garnet, titanite, zircon, apatite and opaque minerals	sericitization, argillitization, saussuritization, and chloritization	upper greenschist to lower amphibolite facies grade
SAN MIGUEL GNEISS (biotite gneiss)	monzogranite	light gray, medium-grained, leucocratic gneiss, with centimeter wide banding, sometimes irregular and folded on a meter scale (Fig. I.2)	medium grain size, with granoblastic to lepidoblastic, equigranular to inequigranular texture, myrmekitic texture involving intergrowth of quartz and plagioclase (Fig. I.4)	quartz (45-35 vol%), andesine (35-30 vol%), microcline (25-20 vol%) and biotite (10-8 vol%)	titanite, zircon, apatite, and opaque minerals	saussuritization and argillitization	greenschist facies grade

ROSÁRIO GNEISS **(biotite gneiss)**	monzogranite	medium gray, medium-grained, mesocratic gneiss, composed of alternating, millimeter to centimeter wide bands, with dark green bands and light bands. Banding is mostly continuous and regular, and sometimes also irregular and folded. Rounded xenoliths of amphibolite composition and quartz veins (Fig. I.2)	textures are granoblastic, the rock is medium-grained and inequigranular to equigranular, and sometimes it exhibits perthitic texture in K-feldspar (Fig. I.4)	microcline (35-30 vol%), quartz (30-25 vol%), andesine (30-25 vol%), and biotite (15 vol%)	apatite, zircon, and opaque minerals	chloritization, sericitization, and saussuritization	greenschist facies grade

Supplementary Table 5.I.2. Conditions and instrumentation for U-Pb and Lu-Hf analyses by LA-ICP-MS - Laboratory of Geochronology and Isotope Geochemistry, University of Brasília.

Laboratory and Sample Preparation	
Laboratory name	Laboratory of Geochronology and Isotope Geochemistry, University of Brasília - UnB
Sample type/mineral	Zircon
Sample preparation	Conventional mineral separation, 0.5 cm resin mount, 1 µm polish to finish
Imaging	BSE, FEI Quanta 450, 10 nA 20kV, 13.8 mm working distance
Laser ablation system	
Make, Model and type	ESI/New Wave Research, UP-213, Nd:YAG
Ablation cell and volume	Low volume cell, ca. 4 cm^3
Laser wavelength (nm)	213 nm
Pulse width (ns)	3 ns
Fluence (J cm^{-2})	3.0 - 3.5 J cm^{-2}
Repetition rate (Hz)	10 Hz (U-Pb) and 7 Hz (Lu-Hf)
Spot size	25 µm (U-Pb), 40 µm (Lu-Hf)
Sampling mode / pattern	single spot analyses
Carrier gas	100% He, Ar make-up gas combined using a Y-piece along the sample transport line close to the torch
Pre-ablation laser warm-up (background collection)	10 s
Ablation duration (s)	40 s
Wash-out delay	20 s
Ablation pit depth / ablation rate	~10 µm pit depth
Cell carrier gas flow (l min^{-1})	0.40 l min^{-1} He
ICP-MS Instrument	
Make, Model and type	Thermo-Fischer, Neptune, MC-ICP-MS
Sample introduction	Ablation aerosol
RF power (W)	1050 W
Make-up gas flow (l min^{-1})	0.7 l min^{-1}
Detection system	mixed Faraday cups and multiple ion counting (MIC) array
Masses measured for U-Pb	Faraday ^{232}Th, ^{238}U and ^{206}Pb; MIC ^{202}Hg, ^{204}Pb, ^{207}Pb and ^{208}Pb
Masses measured for Lu-Hf methodology	Faraday 171, 173, 175, 176, 177, 178, 179, 180
Integration time per peak/dwell times (ms); quadrupole settling time between mass jumps	#N.A.[1]

Total integration time per output data point (s)	1.049 s
Dead time (ns)	#N.A.[1]
Data Processing	
Gas blank	20 s
Calibration strategy	GJ-1 used as primary reference material, 91500 used as secondary reference material for validation
Reference Material	GJ-1 (Jackson *et al.* 2004, Horstwood *et al*. 2016)
	91500 (Wiedenbeck *et al*., 1995, 2004)
Data processing package used / Correction for LIEF	In-house U-Pb table (Buhn *et al*., 2009) and Lu-Hf table (Bertotti, 2012 – UFRGS[2])
Mass discrimination	Standard-sample bracketing with $^{207}Pb/^{206}Pb$ and $^{206}Pb/^{238}U$ ratios normalized to reference material GJ-1
Common-Pb correction, composition and uncertainty	none
Uncertainty level and propagation	Ages are quoted at 2σ absolute, propagation is by quadratic addition. Excess variance and age uncertainty of reference material are propagated where appropriate
Quality control / Validation	Systematic uncertainty for propagation is 1% (2s)

[1] #N.A. = not available
[2] UFRGS = Universidade Federal do Rio Grande do Sul

Supplementary Table 5.I.3. U-Pb isotope data by LA-ICP-MS on zircon from standard 91500.

STANDARD	91500											Apparent ages						
GRAIN	*f* 206 (%)	$\frac{Th}{U}$	$\frac{^{206}Pb}{^{204}Pb}$	$\frac{^{207}Pb}{^{206}Pb}$	err (%) 1 σ	$\frac{^{207}Pb}{^{235}U}$	err (%) 1 σ	$\frac{^{206}Pb}{^{238}U}$	err (%) 1 σ	Rho	$\frac{^{207}Pb}{^{206}Pb}$	2 σ (abs)	$\frac{^{207}Pb}{^{235}U}$	2 σ (abs)	$\frac{^{206}Pb}{^{238}U}$	2 σ (abs)	conc. (%)
Sample LR-02A - 91500																		
003-91500	0.15	0.26	69364	0.07456	1.0	1.81181	2.1	0.17562	1.8	0.87	1064	38	1050	27	1043	35	98
035-91500	0.11	0.26	41523	0.07482	0.7	1.84299	2.0	0.17925	1.5	0.71	1057	56	1061	27	1063	28	101
056-91500	0.11	0.27	36317	0.07647	0.9	1.92677	1.9	0.18272	1.4	0.73	1107	48	1090	25	1082	27	98
Sample HM-35B - 91500																		
003-91500	0.10	0.20	43652	0.07531	1.6	1.84405	2.3	0.17759	1.6	0.70	1077	65	1061	31	1054	32	98
023-91500	0.06	0.19	20891	0.07683	2.9	1.87662	4.2	0.17713	3.1	0.73	1117	112	1073	55	1051	59	94
Sample SM-08 - 91500																		
003-91500	0.12	0.21	40539	0.07555	1.3	1.79416	1.9	0.17222	1.4	0.71	1083	52	1043	25	1024	26	95
022-91500	0.09	0.22	42013	0.07392	1.7	1.82874	2.7	0.17942	2.1	0.76	1039	69	1056	35	1064	40	102
044-91500	0.08	0.21	25585	0.07466	2.0	1.80620	2.8	0.17545	2.0	0.70	1059	79	1048	37	1042	38	98
Sample LR-19 - 91500																		
003-91500	0.11	0.22	31972	0.07511	1.1	1.80424	2.3	0.17421	1.7	0.77	1071	56	1047	29	1035	33	97
023-91500	0.09	0.22	56501	0.07495	1.3	1.79187	2.4	0.17449	1.7	0.72	1054	64	1043	31	1037	33	98
050-91500	0.08	0.22	37499	0.07447	1.2	1.88839	2.5	0.18272	1.8	0.69	1067	71	1077	33	1082	35	101

Supplementary Table 5.I.4. Zircon characteristics for the studied gneisses of the Chiquitania Complex of the Paraguá Block.

SAMPLES	PROTOLITH	ZIRCON CHARACTERISTICS
MIRAFLORES GNEISS ***sample LR-02A***	monzogranite to granodiorite	The zircon crystals in sample LR-02A are colorless to pink, have mostly short, bipyramidal, prismatic habits (~70 %), and are less commonly elongated (~ 30 %). They are generally fractured with some inclusions and have sizes between 80 and 250 µm. In backscattered electron images (BSE), the zircon grains show variably regular to irregular zonation. Sometimes chaotic oscillatory zonation is also observed. Such textures are common in zircon crystals from magmatic sources (Sato *et al*., 2008). A clear rim was frequently observed and is interpreted as a metamorphic overgrowth (Fig. 6 A)
RIO FORTUNA GNEISS ***sample HM-35B***	tonalite	The zircon crystals from sample HM-35B are colorless to pinkish, and sometimes yellowish, and measure 150 to 400 µm in length. The larger crystals usually have a bipyramidal prismatic habit, and those between 150 and 200 µm length commonly show varied degrees of roundness. Inclusions and fractures are common. Back-scattered electron images reveal regular, and less common irregular zonation, whereby an external domain with chaotic zonation is noted, as well as embayments that may range from rims to cores and are considered typical for zircon affected by high-grade metamorphism (Fig. 6 B)
SAN MIGUEL GNEISS ***sample SM-08***	monzogranite	The zircon crystals of sample SM-08 are colorless to pink, and most of them exhibit a bipyramidal prismatic habit. They have lengths ranging from 50 to 250 µm. These crystals are characterized by regular zonation, with alternation of light and dark bands, with darker cores and light rims – considered typically as metamorphic texture (Rubatto, 2017). Less commonly, crystals exhibit complex growth zoning with intermediate local resorption features (Fig. 7 A)
ROSÁRIO GNEISS ***sample LR-19***	monzogranite	The zircon crystals of sample LR-19 are colorless to pink and have a bipyramidal prismatic habit, commonly with varying degrees of roundness. These grains usually have inclusions, are fractured, and have dimensions between 65 and 295 µm. Back-scattered electron images reveal an irregular, sometimes regular zonation banding with little homogeneous zoning. The zircon crystals in this sample have lighter rims around darker zircon cores, as well as chaotic zoning with some embayment (Fig. 7 B)

Supplementary Table 5.I.5. Results of U-Pb isotope analysis by LA-ICP-MS on zircon from sample LR-02A (Miraflores Gneiss). Data in black were used for Concordia diagrams. Data in red were excluded. (*) Data are grouped according to $^{207}Pb/^{206}Pb$ apparent ages. See text for discussion.

SAMPLE	LR-02A											Apparent ages						
GRAIN	*f* 206 (%)	Th/U	$^{206}Pb/^{204}Pb$	$^{207}Pb/^{206}Pb$	err (%) 1 σ	$^{207}Pb/^{235}U$	err (%) 1 σ	$^{206}Pb/^{238}U$	err (%) 1 σ	Rho	$^{207}Pb/^{206}Pb$	2 σ (abs)	$^{207}Pb/^{235}U$	2 σ (abs)	$^{206}Pb/^{238}U$	2 σ (abs)	conc. (%)
***Group 1291±26 Ma**																		
ZR15	0.01	0.08	157549	0.23690	0.0	2.70545	1.6	0.23690	1.1	0.689	1265	42	1371	27	1330	23	108
ZR8B	0.02	0.10	3972	0.18866	0.0	2.17674	3.1	0.18866	2.5	0.809	1285	69	1114	51	1174	43	87
ZR21	0.00	0.15	2083	0.23547	0.0	2.73211	1.8	0.23547	1.2	0.653	1296	50	1363	29	1337	26	105
ZR23	0.01	0.14	5170	0.23654	0.0	2.74503	1.2	0.23654	0.7	0.611	1296	34	1369	18	1341	18	106
ZR5	0.00	0.14	52806	0.24119	0.0	2.82522	1.4	0.24119	0.9	0.663	1314	37	1393	23	1362	21	106
***Group 1425±32 Ma**																		
ZR17	0.02	0.07	6811	0.24442	0.0	3.02909	1.9	0.24442	1.8	0.952	1423	17	1410	46	1415	29	99
ZR10	0.02	0.03	3454	0.25807	0.0	3.20782	2.1	0.25807	1.7	0.839	1429	40	1480	46	1459	32	104
ZR29	0.01	0.07	8105	0.29829	0.0	3.82562	1.1	0.29829	0.8	0.769	1488	21	1683	24	1598	17	113
***Group 1747±11 Ma**																		
ZR20	0.01	0.64	83299	0.30011	0.0	4.38616	1.7	0.30011	1.6	0.914	1732	22	1692	47	1710	28	98
ZR13	0.01	0.62	199283	0.31613	0.0	4.62454	1.1	0.31613	0.8	0.767	1733	22	1771	26	1754	18	102
ZR26	0.00	0.60	20212	0.30973	0.0	4.55724	1.6	0.30973	1.2	0.747	1744	37	1739	37	1741	27	100
ZR12	0.00	0.64	4707	0.32250	0.0	4.74940	1.7	0.32250	1.1	0.667	1746	43	1802	35	1776	28	103
ZR2	0.00	0.47	75655	0.31690	0.0	4.68121	2.0	0.31690	1.6	0.803	1751	41	1775	50	1764	33	101
ZR16	0.02	1.05	6443	0.33677	0.0	4.97934	1.4	0.33677	1.2	0.868	1753	22	1871	40	1816	24	107
ZR14B	0.02	0.10	2859	0.19942	0.0	2.97771	1.3	0.19942	0.7	0.560	1771	37	1172	16	1402	20	66
ZR11	0.00	0.70	28888	0.32334	0.0	4.85126	1.5	0.32334	1.1	0.767	1780	32	1806	36	1794	25	101
***Group 1847±37 Ma**																		
ZR18	0.01	0.15	4896	0.26147	0.0	4.03878	3.0	0.26147	2.6	0.856	1832	55	1497	69	1642	49	82
ZR7N	0.01	0.93	1942	0.34054	0.0	5.29419	2.2	0.34054	1.1	0.494	1844	68	1889	36	1868	38	102
ZR25	0.00	0.37	783	0.30737	0.0	4.78574	2.4	0.30737	1.8	0.740	1847	57	1728	54	1782	40	94
ZR19	0.01	0.48	39416	0.29397	0.0	4.59035	1.4	0.29397	1.1	0.792	1852	27	1661	32	1748	23	90
ZR28	0.01	0.07	1853	0.24132	0.0	3.80008	3.5	0.24132	2.8	0.823	1867	69	1394	71	1593	55	75
ZR27	*0.00*	*1.06*	*733*	*0.31117*	*0.0*	*5.90160*	*2.1*	*0.31117*	*1.5*	*0.736*	*2196*	*47*	*1746*	*47*	*1961*	*36*	*80*
ZR6B	*0.01*	*0.33*	*937*	*0.17766*	*0.0*	*3.40966*	*2.5*	*0.17766*	*2.2*	*0.869*	*2217*	*40*	*1054*	*42*	*1507*	*38*	*48*

ZR3	*0.01*	*0.19*	*5214*	*0.40165*	*0.0*	*5.30420*	*2.5*	*0.40165*	*2.3*	*0.896*	*1543*	*40*	*2177*	*83*	*1870*	*43*	*141*
ZR9	*0.00*	*0.47*	*22607*	*0.22144*	*0.0*	*2.94998*	*3.3*	*0.22144*	*3.0*	*0.914*	*1560*	*48*	*1289*	*71*	*1395*	*50*	*83*
ZR14N	*0.01*	*0.55*	*97434*	*0.30894*	*0.0*	*4.29433*	*2.1*	*0.30894*	*0.7*	*0.352*	*1639*	*71*	*1735*	*23*	*1692*	*34*	*106*
ZR24	*0.02*	*0.21*	*4248*	*0.36432*	*0.0*	*5.53029*	*1.7*	*0.36432*	*1.4*	*0.862*	*1801*	*27*	*2003*	*49*	*1905*	*28*	*111*
ZR1	*0.01*	*0.13*	*3511*	*0.25878*	*0.0*	*3.95009*	*2.0*	*0.25878*	*1.9*	*0.931*	*1811*	*23*	*1484*	*50*	*1624*	*33*	*82*
ZR8N	*0.00*	*0.73*	*4307*	*0.31347*	*0.0*	*4.79153*	*2.5*	*0.31347*	*1.9*	*0.750*	*1813*	*58*	*1758*	*58*	*1783*	*42*	*97*
ZR22	*0.01*	*0.14*	*720*	*0.21039*	*0.0*	*3.76868*	*2.1*	*0.21039*	*1.1*	*0.502*	*2097*	*63*	*1231*	*24*	*1586*	*34*	*59*
ZR4	*0.01*	*0.34*	*764*	*0.33791*	*0.0*	*6.21210*	*4.3*	*0.33791*	*1.4*	*0.322*	*2142*	*138*	*1877*	*45*	*2006*	*74*	*88*
ZR6N	*0.00*	*0.82*	*1423*	*0.30675*	*0.0*	*6.09377*	*4.7*	*0.30675*	*2.8*	*0.589*	*2277*	*128*	*1725*	*84*	*1989*	*81*	*76*
ZR7B	*0.00*	*0.13*	*871*	*0.09260*	*0.0*	*2.41826*	*7.1*	*0.09260*	*6.8*	*0.954*	*2737*	*68*	*571*	*74*	*1248*	*100*	*21*

Supplementary Table 5.I.6. Results of U-Pb isotope analysis by LA-ICP-MS on zircon from sample HM-35B (Rio Fortuna Gneiss). Data in black were used for Concordia diagrams. Data in red were excluded. (*) Data are grouped according to $^{207}Pb/^{206}Pb$ apparent ages. See text for discussion.

SAMPLE	HM-35B											Apparent ages						
GRAIN	*f* 206 (%)	Th/U	$^{206}Pb/^{204}Pb$	$^{207}Pb/^{206}Pb$	err (%) 1 σ	$^{207}Pb/^{235}U$	err (%) 1 σ	$^{206}Pb/^{238}U$	err (%) 1 σ	Rho	$^{207}Pb/^{206}Pb$	2 σ (abs)	$^{207}Pb/^{235}U$	2 σ (abs)	$^{206}Pb/^{238}U$	2 σ (abs)	conc. (%)
***Group 1415±14 Ma**																		
ZR12	0.41	0.06	107232	0.08845	1.3	3.01530	1.9	0.24724	1.3	0.69	1392	49	1411	28	1424	33	102
***Group 1578±81 Ma**																		
ZR09N	0.38	0.36	77201	0.09760	1.0	3.71381	1.8	0.27596	1.5	0.79	1579	39	1574	29	1571	41	100
ZR19	0.05	0.30	63217	0.09828	1.2	3.90777	1.9	0.28835	1.4	0.73	1592	46	1615	30	1633	39	103
ZR02	0.33	0.20	102363	0.10005	0.8	4.07992	1.5	0.29573	1.2	0.79	1625	31	1650	24	1670	35	103
***Group 1696±7 Ma**																		
ZR07	0.36	0.49	228653	0.10253	1.0	4.39617	1.6	0.31094	1.2	0.73	1670	38	1712	27	1745	36	104
ZR21	0.50	0.47	119114	0.10304	1.0	4.40234	1.7	0.30984	1.3	0.78	1680	36	1713	28	1740	41	104
ZR20	0.17	0.42	100998	0.10311	1.2	4.35322	1.8	0.30619	1.4	0.74	1681	43	1704	30	1722	42	102
ZR27	0.52	0.44	139673	0.10316	1.0	4.33517	2.3	0.30349	1.5	0.62	1689	65	1700	38	1709	44	101
ZR08	0.45	0.60	127378	0.10343	1.1	4.38179	1.8	0.30655	1.4	0.79	1691	39	1709	30	1724	44	102
ZR02B1	0.36	0.29	153283	0.10359	1.8	4.42191	1.2	0.30898	1.0	0.77	1693	25	1716	20	1736	29	103
ZR22	0.06	0.46	156471	0.10366	1.1	4.49966	1.4	0.31436	1.1	0.76	1693	31	1731	24	1762	34	104
ZR18	0.20	0.29	274447	0.10369	1.3	4.54833	1.4	0.31754	1.1	0.77	1694	31	1740	24	1778	35	105
ZR14	0.29	0.28	151312	0.10379	0.7	4.55926	1.6	0.31819	1.2	0.73	1695	33	1742	26	1781	37	105
ZR06	0.49	0.56	138261	0.10381	0.9	4.55545	1.7	0.31783	1.1	0.64	1696	45	1741	28	1779	34	105
ZR24	0.18	0.47	124186	0.10388	0.8	4.46653	1.9	0.31159	1.5	0.79	1696	39	1725	31	1749	45	103
ZR23	0.30	0.35	95210	0.10391	0.9	4.41892	1.8	0.30821	1.3	0.75	1696	40	1716	29	1732	41	102
ZR01	0.02	0.35	185161	0.10394	1.2	4.63158	1.3	0.32267	1.2	0.87	1698	19	1755	22	1803	36	106
ZR17	0.63	0.48	130574	0.10396	1.1	4.32893	1.5	0.30103	1.2	0.75	1702	34	1699	25	1696	34	100
ZR28	0.49	0.30	117543	0.10398	1.1	4.44631	2.7	0.30901	1.8	0.69	1703	69	1721	44	1736	56	102
ZR09	0.38	0.36	345725	0.10404	0.7	4.41261	1.5	0.30652	1.2	0.76	1704	33	1715	25	1724	35	101
ZR16	0.05	0.39	14747	0.10410	0.5	4.08411	1.6	0.28340	1.4	0.86	1706	26	1651	26	1608	39	94
ZR15	0.03	0.53	233886	0.10426	1.1	4.47596	1.2	0.30916	0.9	0.74	1714	28	1727	21	1737	28	101
ZR26	0.05	0.39	101486	0.10429	0.9	4.45699	2.2	0.30769	1.5	0.67	1715	59	1723	37	1729	45	101
ZR11	0.37	0.55	178250	0.10435	1.9	4.52196	1.4	0.31212	1.1	0.74	1716	33	1735	24	1751	33	102

ZR04	*0.37*	*0.498*	*170197*	*0.10440*	*0.9*	*4.522*	*2.0*	*0.3179*	*1.7*	*0.85*	*1682*	*35*	*1735*	*32*	*1780*	*52*	*106*
ZR05	*0.38*	*0.54*	*158399*	*0.10441*	*0.9*	*4.70674*	*1.7*	*0.33003*	*1.3*	*0.73*	*1686*	*41*	*1768*	*29*	*1839*	*41*	*109*
ZR25	*0.11*	*0.44*	*92623*	*0.10451*	*0.7*	*4.38114*	*1.9*	*0.30641*	*1.4*	*0.73*	*1691*	*46*	*1709*	*32*	*1723*	*43*	*102*
ZR03	*0.36*	*0.37*	*179029*	*0.10500*	*0.8*	*4.53065*	*1.4*	*0.31580*	*1.1*	*0.80*	*1697*	*27*	*1737*	*23*	*1769*	*35*	*104*
ZR13	*0.36*	*0.47*	*295041*	*0.10505*	*1.6*	*4.61222*	*1.5*	*0.32081*	*0.9*	*0.60*	*1701*	*39*	*1751*	*24*	*1794*	*28*	*105*
ZR10	*0.37*	*0.40*	*158486*	*0.10507*	*0.9*	*4.44774*	*1.5*	*0.30894*	*1.2*	*0.76*	*1704*	*33*	*1721*	*25*	*1735*	*35*	*102*
ZR10	*0.37*	*0.40*	*158486*	*0.10507*	*0.9*	*4.44774*	*1.5*	*0.30894*	*1.2*	*0.76*	*1704*	*33*	*1721*	*25*	*1735*	*35*	*102*

Supplementary Table 5.I.7. Results of U-Pb isotope analysis by LA-ICP-MS on zircon from sample SM-08 (San Miguel Gneiss). Data in black were used for Concordia diagrams. Data in red were excluded. (*) Data are grouped according to $^{207}Pb/^{206}Pb$ apparent ages. See text for discussion.

SAMPLE	SM-08											Apparent ages					
GRAIN	*f* 206 (%)	Th/U	$^{206}Pb/^{204}Pb$	$^{207}Pb/^{206}Pb$	err (%) 1 σ	$^{207}Pb/^{235}U$	err (%) 1 σ	$^{206}Pb/^{238}U$	err (%) 1 σ	Rho	$^{207}Pb/^{206}Pb$	2 σ (abs)	$^{207}Pb/^{235}U$	2 σ (abs)	$^{206}Pb/^{238}U$	2 σ (abs)	conc. (%)
***Group 1256±26 Ma**																	
ZR05B	0.81	0.10	235727	0.08136	0.6	2.40192	1.4	0.21409	1.2	0.862	1230	24	1243	20	1251	27	102
ZR016B	0.28	0.13	89064	0.08301	1.1	2.41970	1.8	0.21138	1.5	0.796	1270	41	1248	26	1236	33	97
ZR011B	0.81	0.14	208550	0.08307	0.8	2.54028	1.6	0.22178	1.3	0.818	1271	32	1284	23	1291	30	102
***Group 1320±19 Ma**																	
ZR09B	0.89	0.11	294126	0.08453	0.7	2.77189	1.4	0.23781	1.2	0.827	1305	27	1348	21	1375	29	105
ZR024B	1.06	0.03	9265	0.08637	0.5	2.46885	1.4	0.20729	1.2	0.891	1347	19	1263	20	1214	27	90
ZR06B	0.99	0.06	144663	0.08716	0.6	2.15151	1.4	0.17902	1.2	0.854	1364	23	1166	19	1062	23	78
***Group 1546±19 Ma**																	
ZR014N	0.30	0.24	77788	0.09493	1.2	3.03224	2.2	0.23165	1.8	0.818	1527	44	1416	33	1343	43	88
ZR010B	0.33	0.27	113202	0.09511	1.3	3.34985	2.1	0.25544	1.6	0.756	1530	50	1493	33	1466	42	96
ZR011N	1.15	0.05	134958	0.09533	0.7	3.47496	1.5	0.26436	1.3	0.857	1535	25	1522	23	1512	34	99
ZR04N	0.66	0.25	74211	0.09534	0.7	3.51426	1.5	0.26732	1.3	0.841	1535	28	1530	24	1527	35	100
ZR03B2	0.85	0.24	288366	0.09662	0.7	3.60921	1.5	0.27089	1.3	0.844	1560	28	1552	24	1545	36	99
ZR015N	0.92	0.23	10499	0.09717	0.8	3.33417	2.2	0.24885	2.0	0.913	1570	30	1489	33	1433	51	91
***Group 1681±13 Ma**																	
ZR05N	0.36	0.33	155026	0.09865	0.8	3.47451	1.6	0.25543	1.3	0.819	1599	30	1521	24	1466	33	92
ZR017	0.33	0.23	96015	0.09880	0.8	3.58593	1.7	0.26323	1.4	0.849	1602	30	1546	27	1506	39	94
ZR02N	0.41	0.24	146888	0.09892	0.7	3.47092	1.3	0.25446	1.1	0.830	1604	24	1521	21	1461	29	91
ZR27N	0.52	0.24	44062	0.09956	0.7	3.93273	1.3	0.28647	1.0	0.805	1616	25	1620	21	1624	30	100
ZR021B	0.20	0.29	56190	0.09992	1.0	3.68732	1.7	0.26763	1.4	0.788	1623	37	1569	27	1529	37	94
ZR024N	0.31	0.25	6580	0.10075	0.8	3.77871	1.8	0.27200	1.5	0.861	1638	30	1588	28	1551	42	95
ZR08	0.23	0.40	85244	0.10133	1.0	4.05660	1.8	0.29034	1.5	0.806	1649	38	1646	30	1643	43	100
ZR27B	0.39	0.20	50715	0.10143	0.8	4.05409	1.4	0.28985	1.1	0.781	1651	30	1645	23	1641	32	99
ZR09N	0.37	0.27	119437	0.10171	0.9	4.00437	1.5	0.28551	1.2	0.787	1656	32	1635	24	1619	34	98
ZR026	0.44	0.32	127500	0.10331	0.7	4.31838	1.3	0.30313	1.1	0.817	1684	24	1697	22	1707	32	101
ZR021B2	0.39	0.38	122053	0.10333	0.7	4.21603	1.3	0.29590	1.1	0.815	1685	24	1677	21	1671	31	99

ZR06N	0.39	0.43	147517	0.10380	0.7	4.34354	1.4	0.30346	1.2	0.829	1693	25	1702	23	1708	35	101
ZR023B	0.41	0.39	128343	0.10395	0.7	4.57077	1.6	0.31888	1.3	0.857	1696	26	1744	26	1784	42	105
ZR019	0.24	0.39	60812	0.10408	1.0	4.22081	1.7	0.29409	1.4	0.778	1698	38	1678	28	1662	40	98
ZR025B	0.25	0.37	101714	0.10433	0.8	4.40173	1.6	0.30596	1.3	0.833	1703	29	1713	26	1721	40	101
ZR012	0.41	0.40	84243	0.10465	1.0	4.23656	1.8	0.29358	1.4	0.802	1708	36	1681	29	1659	41	97
ZR013N	0.77	0.47	13678	0.10492	1.0	4.61799	1.7	0.31919	1.3	0.777	1713	36	1753	28	1786	41	104
ZR022	0.87	0.39	282016	0.10588	0.6	4.62252	1.4	0.31661	1.2	0.870	1730	22	1753	24	1773	38	103
ZR02B	*0.58*	*0.12*	*193980*	*0.08030*	*0.6*	*2.30696*	*1.3*	*0.20835*	*1.0*	*0.806*	*1204*	*25*	*1214*	*18*	*1220*	*23*	*101*
ZR05B	*0.81*	*0.10*	*235727*	*0.08136*	*0.6*	*2.40192*	*1.4*	*0.21409*	*1.2*	*0.862*	*1230*	*24*	*1243*	*20*	*1251*	*27*	*102*
ZR016B	*0.28*	*0.13*	*89064*	*0.08301*	*1.1*	*2.41970*	*1.8*	*0.21138*	*1.5*	*0.796*	*1270*	*41*	*1248*	*26*	*1236*	*33*	*97*
ZR011B	*0.81*	*0.14*	*208550*	*0.08307*	*0.8*	*2.54028*	*1.6*	*0.22178*	*1.3*	*0.818*	*1271*	*32*	*1284*	*23*	*1291*	*30*	*102*
ZR013B	*0.48*	*0.10*	*26861*	*0.09047*	*1.0*	*2.92504*	*2.0*	*0.23447*	*1.7*	*0.845*	*1435*	*38*	*1388*	*30*	*1358*	*41*	*95*
ZR01	*0.43*	*0.29*	*115390*	*0.09065*	*0.7*	*2.85124*	*1.5*	*0.22809*	*1.3*	*0.840*	*1439*	*28*	*1369*	*23*	*1325*	*31*	*92*
ZR020	*0.26*	*0.17*	*47445*	*0.09181*	*0.9*	*2.98221*	*1.5*	*0.23557*	*1.2*	*0.750*	*1463*	*36*	*1403*	*23*	*1364*	*28*	*93*
ZR018	*0.11*	*0.37*	*29162*	*0.09303*	*1.3*	*2.91060*	*2.2*	*0.22689*	*1.7*	*0.792*	*1489*	*47*	*1385*	*32*	*1318*	*41*	*89*
ZR014B	*0.44*	*0.16*	*116459*	*0.09320*	*1.0*	*2.92059*	*2.1*	*0.22726*	*1.8*	*0.855*	*1492*	*38*	*1387*	*31*	*1320*	*43*	*88*
ZR03B	*0.93*	*0.22*	*217490*	*0.09375*	*0.6*	*3.37449*	*1.5*	*0.26104*	*1.3*	*0.877*	*1503*	*22*	*1498*	*23*	*1495*	*34*	*99*
ZR04B	*0.79*	*0.28*	*13979*	*0.09391*	*0.7*	*3.28953*	*1.3*	*0.25403*	*1.0*	*0.802*	*1506*	*25*	*1479*	*20*	*1459*	*26*	*97*
ZR015B	*1.09*	*0.22*	*3202*	*0.10168*	*0.8*	*3.10624*	*1.8*	*0.22155*	*1.6*	*0.877*	*1655*	*30*	*1434*	*28*	*1290*	*38*	*78*
ZR010B2	*0.38*	*0.24*	*111737*	*0.10502*	*0.7*	*4.37716*	*1.6*	*0.30227*	*1.4*	*0.856*	*1715*	*27*	*1708*	*26*	*1703*	*41*	*99*
ZR07	*0.17*	*0.31*	*8939*	*0.10573*	*1.1*	*3.66552*	*2.3*	*0.25141*	*2.0*	*0.857*	*1727*	*42*	*1564*	*37*	*1446*	*52*	*84*
ZR023N	*0.20*	*0.27*	*65020*	*0.10951*	*1.0*	*4.65536*	*2.0*	*0.30830*	*1.7*	*0.851*	*1791*	*35*	*1759*	*33*	*1732*	*51*	*97*

Supplementary Table 5.I.8. Results of U-Pb isotope analysis by LA-ICP-MS on zircon from sample LR-19 (Rosário Gneiss). Data in black were used for Concordia diagrams. Data in red were excluded. (*) Data are grouped according to $^{207}Pb/^{206}Pb$ apparent ages. See text for discussion.

SAMPLE	LR-19											Apparent ages						
GRAIN	*f* 206 (%)	Th/U	$^{206}Pb/^{204}Pb$	$^{207}Pb/^{206}Pb$	err (%) 1 σ	$^{207}Pb/^{235}U$	err (%) 1 σ	$^{206}Pb/^{238}U$	err (%) 1 σ	Rho	$^{207}Pb/^{206}Pb$	2 σ (abs)	$^{207}Pb/^{235}U$	2 σ (abs)	$^{206}Pb/^{238}U$	2 σ (abs)	conc. (%)
***Group 1538±24 Ma**																		
ZR18	0.04	0.20	34539	0.09517	1.3	2.27594	2.8	0.17343	2.4	0.866	1531	50	1031	46	1205	39	79
ZR25	0.69	0.10	2220	0.09544	0.8	4.24828	1.6	0.32281	1.3	0.814	1537	33	1803	42	1683	27	110
ZR29	0.07	0.26	20973	0.09571	1.1	3.76748	1.7	0.28547	1.3	0.725	1542	42	1619	36	1586	28	103
***Group 1678±21 Ma**																		
ZR11	0.24	0.36	6447	0.10014	1.2	3.82623	1.7	0.27711	1.1	0.674	1627	44	1577	32	1598	27	98
ZR26	0.03	0.38	57922	0.10048	1.6	4.22015	1.9	0.30459	1.0	0.519	1633	60	1714	30	1678	32	103
ZR32	0.02	0.36	99001	0.10080	0.9	4.16990	1.4	0.30001	0.9	0.691	1639	33	1691	28	1668	22	102
ZR21	0.02	0.37	81287	0.10111	1.0	4.14020	1.5	0.29697	1.1	0.713	1645	37	1676	32	1662	25	101
ZR20	0.01	0.38	153692	0.10118	1.0	4.19000	2.1	0.30033	1.8	0.863	1646	36	1693	54	1672	34	102
ZR5N	0.01	0.49	147311	0.10137	0.8	4.02334	1.3	0.28784	0.9	0.744	1649	28	1631	27	1639	20	99
ZR27	0.01	0.36	125435	0.10219	0.8	3.98940	1.3	0.28312	0.9	0.736	1664	28	1607	26	1632	20	98
ZR1	0.02	0.49	62178	0.10267	0.8	4.46820	1.4	0.31563	1.1	0.785	1673	30	1768	35	1725	24	103
ZR23	0.01	0.45	132669	0.10288	0.6	4.30320	1.0	0.30334	0.7	0.711	1677	22	1708	21	1694	16	101
ZR8	0.03	0.62	49488	0.10298	1.1	4.66724	1.8	0.32868	1.4	0.771	1679	39	1832	43	1761	29	105
ZR9	0.05	0.38	33692	0.10329	1.0	4.33479	1.5	0.30436	1.1	0.710	1684	37	1713	32	1700	25	101
ZR19	0.01	0.38	140016	0.10342	0.9	4.10314	1.4	0.28771	1.0	0.741	1686	31	1630	29	1655	22	98
ZR22	0.03	0.37	43965	0.10369	1.0	4.31047	1.4	0.30148	0.9	0.688	1691	34	1699	28	1695	22	100
ZR17	0.01	0.37	104812	0.10441	0.9	4.26916	1.3	0.29652	1.0	0.730	1704	30	1674	28	1687	21	99
ZR13	0.68	0.41	2252	0.10484	1.0	4.35139	1.4	0.30101	1.0	0.683	1711	35	1696	29	1703	23	100
ZR10	0.02	0.49	101938	0.10600	0.9	4.64194	1.3	0.31757	0.9	0.729	1732	29	1778	29	1757	22	101
ZR15	0.30	0.29	5068	0.10637	0.9	4.39993	1.2	0.29997	0.7	0.603	1738	32	1691	21	1712	20	99
ZR16	*0.27*	*0.05*	*5853*	*0.07395*	*0.9*	*0.81412*	*5.5*	*0.07984*	*5.4*	*0.976*	*1040*	*46*	*495*	*51*	*605*	*50*	*58*
ZR6B	*0.02*	*0.02*	*93729*	*0.08430*	*1.1*	*2.72447*	*1.8*	*0.23437*	*1.1*	*0.639*	*1300*	*51*	*1357*	*28*	*1335*	*26*	*103*
ZR5B	*0.01*	*0.02*	*187666*	*0.08524*	*0.7*	*2.89151*	*1.3*	*0.24601*	*0.9*	*0.730*	*1321*	*31*	*1418*	*24*	*1380*	*19*	*104*
ZR4	*2.03*	*0.03*	*767*	*0.08722*	*3.4*	*1.11857*	*4.8*	*0.09300*	*2.9*	*0.593*	*1365*	*145*	*573*	*31*	*762*	*51*	*56*
ZR30	*0.00*	*0.06*	*373116*	*0.08835*	*0.4*	*3.56924*	*1.7*	*0.29299*	*1.6*	*0.932*	*1390*	*18*	*1656*	*45*	*1543*	*26*	*111*

ZR6N	*0.01*	*0.33*	*108090*	*0.09870*	*1.1*	*3.74152*	*1.6*	*0.27490*	*1.0*	*0.671*	*1600*	*40*	*1566*	*29*	*1580*	*25*	*99*
ZR14	*0.04*	*0.05*	*36002*	*0.10033*	*2.3*	*3.49058*	*2.5*	*0.25231*	*0.8*	*0.315*	*1630*	*84*	*1450*	*20*	*1525*	*38*	*94*
ZR28	*1.00*	*0.06*	*1550*	*0.10800*	*0.7*	*3.42208*	*1.4*	*0.22979*	*1.1*	*0.820*	*1766*	*25*	*1333*	*27*	*1509*	*21*	*85*
ZR31N	*1.09*	*0.11*	*1406*	*0.10931*	*0.8*	*4.14900*	*1.3*	*0.27526*	*0.9*	*0.752*	*1788*	*27*	*1567*	*26*	*1664*	*21*	*93*
ZR3	*0.99*	*0.52*	*1544*	*0.11195*	*2.8*	*5.22980*	*3.4*	*0.33878*	*2.3*	*0.674*	*1831*	*89*	*1881*	*75*	*1857*	*57*	*101*
ZR2	*1.60*	*0.50*	*962*	*0.11220*	*0.9*	*3.60927*	*1.2*	*0.23329*	*0.8*	*0.650*	*1835*	*30*	*1352*	*19*	*1552*	*19*	*85*
ZR33	*1.17*	*0.30*	*1321*	*0.11263*	*1.4*	*3.98311*	*1.9*	*0.25647*	*1.4*	*0.730*	*1842*	*44*	*1472*	*36*	*1631*	*30*	*89*
ZR31B	*1.99*	*0.18*	*770*	*0.11879*	*7.1*	*4.81046*	*6.0*	*0.29367*	*0.8*	*0.136*	*1938*	*205*	*1660*	*24*	*1787*	*99*	*92*
ZR34	*1.84*	*0.05*	*838*	*0.12326*	*2.0*	*3.76695*	*1.8*	*0.22164*	*0.7*	*0.404*	*2004*	*56*	*1291*	*17*	*1586*	*29*	*79*
ZR12	*2.30*	*0.17*	*671*	*0.13643*	*2.3*	*4.73232*	*2.2*	*0.25156*	*1.3*	*0.597*	*2182*	*59*	*1447*	*34*	*1773*	*36*	*81*
ZR24	*1.85*	*0.63*	*834*	*0.17835*	*50.2*	*6.16917*	*29.6*	*0.25086*	*9.0*	*0.304*	*2638*	*809*	*1443*	*230*	*2000*	*460*	*76*

Supplementary Table 5.I.9. Lu-Hf isotope data from the Chiquitania Complex.

HM-35B (Rio Fortuna Gneiss)																						
Crystal	AGE			$^{176}Hf/^{177}Hf$	± 2s	$^{176}Lu/^{177}Hf$	± 2s	$^{176}Hf/^{177}Hf$ (t)[1]	$\varepsilon_{Hf(t)}$[2]	± 2s	*Model age*				$^{176}Yb/^{177}Hf$	± 2s	Mean Ints ^{178}Hf (V)	$^{178}Hf/^{177}Hf$	± 2s	$^{179}Hf/^{177}Hf$	2SE	$^{173}Yb/^{171}Yb$	2SE
	$^{207}Pb/^{206}Pb$	2s (%)	Concordance								T_{DM}[3]	T_{DM} Crustal[3,4]	Mafic[5]	Felsic[5]									
ZR07	1670	2.28	104.48	0.281963	0.000119	0.002850	0.000210	0.281870	6.6	0.5	1.82	1.91	2.01	1.87	0.1396	0.011621	0.82629	1.467126	0.000103	0.745318	0.000081	1.150412	0.000341
ZR04	1682	2.10	105.82	0.281920	0.000146	0.002166	0.000021	0.281848	6.1	0.1	1.85	1.95	2.06	1.90	0.1055	0.001524	0.90810	1.467363	0.000282	0.745330	0.000105	1.150211	0.000572
ZR05	1686	2.43	109.02	0.281984	0.000212	0.003109	0.000123	0.281881	7.4	0.3	1.81	1.87	1.95	1.84	0.1547	0.006456	0.83282	1.467072	0.000171	0.745464	0.000128	1.151099	0.000714
ZR25	1691	2.71	101.88	0.281944	0.000175	0.002304	0.000101	0.281867	7.0	0.3	1.82	1.90	1.99	1.86	0.1266	0.005971	0.93388	1.467266	0.000197	0.745303	0.000138	1.150619	0.000695
ZR14	1695	1.97	105.06	0.281864	0.000116	0.001672	0.000176	0.281808	5.0	0.5	1.90	2.02	2.16	1.97	0.0849	0.009719	0.91147	1.467104	0.000126	0.745141	0.000138	1.150475	0.001000
ZR06	1696	2.68	104.92	0.281884	0.000212	0.001498	0.000012	0.281835	5.9	0.1	1.86	1.97	2.08	1.92	0.0603	0.004047	1.11922	1.467187	0.000335	0.745299	0.000174	1.150184	0.001164
ZR03	1697	1.61	104.23	0.281900	0.000147	0.002527	0.000084	0.281816	5.3	0.2	1.89	2.01	2.13	1.95	0.1242	0.004487	0.80189	1.467206	0.000128	0.745410	0.000108	1.150877	0.000543
ZR13	1701	2.31	105.43	0.281757	0.000065	0.001363	0.000021	0.281711	1.7	0.0	2.03	2.23	2.45	2.14	0.0656	0.001346	0.74769	1.467223	0.000087	0.745295	0.000058	1.150807	0.000623
ZR10	1704	1.94	101.85	0.281790	0.000083	0.001851	0.000044	0.281728	2.4	0.1	2.01	2.19	2.39	2.11	0.0979	0.001675	0.83763	1.467259	0.000129	0.745387	0.000103	1.150670	0.000469
ZR15	1714	1.61	101.30	0.281931	0.000086	0.002304	0.000084	0.281853	7.0	0.3	1.84	1.91	2.00	1.88	0.1179	0.005306	0.82366	1.467337	0.000121	0.745277	0.000095	1.150534	0.000493
ZR11	1716	1.91	102.08	0.281952	0.000174	0.003810	0.000179	0.281824	6.0	0.3	1.89	1.98	2.08	1.93	0.1837	0.008629	0.46873	1.467221	0.000203	0.745318	0.000133	1.150783	0.000669

SM-08 (San Miguel Gneiss)																						
Crystal	AGE			$^{176}Hf/^{177}Hf$	± 2s	$^{176}Lu/^{177}Hf$	± 2s	$^{176}Hf/^{177}Hf$ (t)[1]	$\varepsilon_{Hf(t)}$[2]	± 2s	*Model age*				$^{176}Yb/^{177}Hf$	± 2s	Mean Ints ^{178}Hf (V)	$^{178}Hf/^{177}Hf$	± 2s	$^{179}Hf/^{177}Hf$	2SE	$^{173}Yb/^{171}Yb$	2SE
	$^{207}Pb/^{206}Pb$	2s (%)	Concordance								T_{DM}[3]	T_{DM} Crustal[3,4]	Mafic[5]	Felsic[5]									
ZR01	1439	1.96	92.02	0.281999	0.000240	0.002883	0.000031	0.281918	2.8	0.0	1.77	1.96	2.17	1.87	0.0999	0.001525	0.51134	1.467199	0.000302	0.745500	0.000210	1.150267	0.001743
ZR018	1489	3.18	88.55	0.281993	0.000061	0.001228	0.000011	0.281957	5.4	0.1	1.71	1.84	1.99	1.78	0.0570	0.001135	0.90746	1.467300	0.000079	0.745332	0.000097	1.149489	0.000640
ZR05N	1599	1.89	91.72	0.281826	0.000079	0.000801	0.000058	0.281800	2.4	0.2	1.91	2.10	2.31	2.02	0.0363	0.002758	0.72431	1.467145	0.000110	0.745353	0.000065	1.150034	0.001531
ZR017	1602	1.89	94.06	0.281817	0.000102	0.000716	0.000011	0.281795	2.3	0.0	1.91	2.12	2.33	2.03	0.0315	0.000905	0.60839	1.467360	0.000239	0.745446	0.000173	1.148673	0.002510
ZR02N	1604	1.52	91.12	0.281917	0.000171	0.001495	0.000024	0.281870	5.0	0.1	1.82	1.95	2.10	1.89	0.0748	0.001443	0.89753	1.467244	0.000200	0.745259	0.000147	1.150114	0.001102
ZR08	1649	2.28	99.68	0.281875	0.000140	0.001542	0.000029	0.281825	4.5	0.1	1.88	2.02	2.17	1.95	0.0751	0.001721	0.62956	1.467207	0.000224	0.745316	0.000172	1.149750	0.000698
ZR09N	1656	1.91	97.79	0.281931	0.000109	0.001331	0.000017	0.281888	6.9	0.1	1.79	1.88	1.97	1.84	0.0678	0.000571	0.95875	1.467214	0.000112	0.745323	0.000095	1.150118	0.000771
ZR06N	1693	1.49	100.90	0.281933	0.000103	0.002319	0.000039	0.281856	6.6	0.1	1.84	1.92	2.02	1.88	0.1157	0.001587	0.77459	1.467318	0.000137	0.745322	0.000117	1.150576	0.000600
ZR012	1708	2.12	97.14	0.281723	0.000281	0.001671	0.000008	0.281667	0.3	0.0	2.09	2.32	2.57	2.21	0.0832	0.000349	0.80393	1.467261	0.000331	0.745362	0.000069	1.150974	0.001928

LR-19 (Rosário Gneiss)																						
Crystal	AGE			$^{176}Hf/^{177}Hf$	± 2s	$^{176}Lu/^{177}Hf$	± 2s	$^{176}Hf/^{177}Hf$ (t)[1]	$\varepsilon_{Hf(t)}$[2]	± 2s	*Model age*				$^{176}Yb/^{177}Hf$	± 2s	Mean Ints ^{178}Hf (V)	$^{178}Hf/^{177}Hf$	± 2s	$^{179}Hf/^{177}Hf$	2SE	$^{173}Yb/^{171}Yb$	2SE
	$^{207}Pb/^{206}Pb$	2s (%)	Concordance								T_{DM}[3]	T_{DM} Crustal[3,4]	Mafic[5]	Felsic[5]									
ZR26	1632	3.65	102.75	0.281725	0.000064	0.001336	0.000108	0.281682	-0.9	0.1	2.07	2.34	2.63	2.21	0.0572	0.000761	1.31770	1.467151	0.000088	0.744696	0.000153	1.150467	0.001007
ZR23	1677	1.31	101.03	0.281789	0.000103	0.001482	0.000162	0.281740	2.1	0.2	1.99	2.18	2.39	2.10	0.0626	0.007139	0.72787	1.467214	0.000157	0.745125	0.000105	1.149431	0.000898
ZR9	1684	2.17	100.95	0.281885	0.000096	0.001045	0.000019	0.281851	6.2	0.1	1.84	1.94	2.04	1.89	0.0416	0.000881	0.85928	1.467264	0.000130	0.745232	0.000123	1.148809	0.001159
ZR22	1691	2.00	100.25	0.281727	0.000112	0.000775	0.000020	0.281701	1.1	0.0	2.04	2.26	2.49	2.16	0.0320	0.000687	0.71809	1.467179	0.000125	0.745255	0.000090	1.150719	0.001815
ZR13	1711	2.05	99.52	0.281812	0.000131	0.000882	0.000030	0.281783	4.5	0.2	1.93	2.07	2.22	2.01	0.0388	0.001459	0.79331	1.467270	0.000132	0.745084	0.000089	1.149942	0.001260
ZR15	1738	1.84	98.51	0.281929	0.000081	0.001134	0.000013	0.281891	8.9	0.1	1.79	1.82	1.85	1.80	0.0469	0.000915	1.10461	1.467268	0.000121	0.745072	0.000078	1.150466	0.001069

[1] calculated using the ^{176}Lu decay constant of Blichert-Toft and Albarède (1999) at the assigned age, t
[2] calculated using the CHUR parameters of Bouvier *et al*. (2008)
[3] Present day Depleted Mantle (Andersen *et al*., 2009)
[4] Goodge and Vervoort (2006), EPSL 243, 711-731
[5] $^{176}Lu/^{177}Hf$ ratios of mafic and felsic crust from Pietranik *et al*. (2008)

Supplementary Figure I.1. (A) and (B) Macroscopic features of the Miraflores Gneiss. Typical slab outcrop of the fine- to medium-grained, leucocratic Miraflores Gneiss showing the folded gneissic banding. (C) Light grey, leucocratic, and medium grained aspect of the Rio Fortuna Gneiss with folded banding. (D) Hand specimen image of the Rio Fortuna gneiss, showing the proportion of different minerals. Notebook for scale 20 cm long; Pen for scale 14 cm long; Hammer for scale 40 cm long.

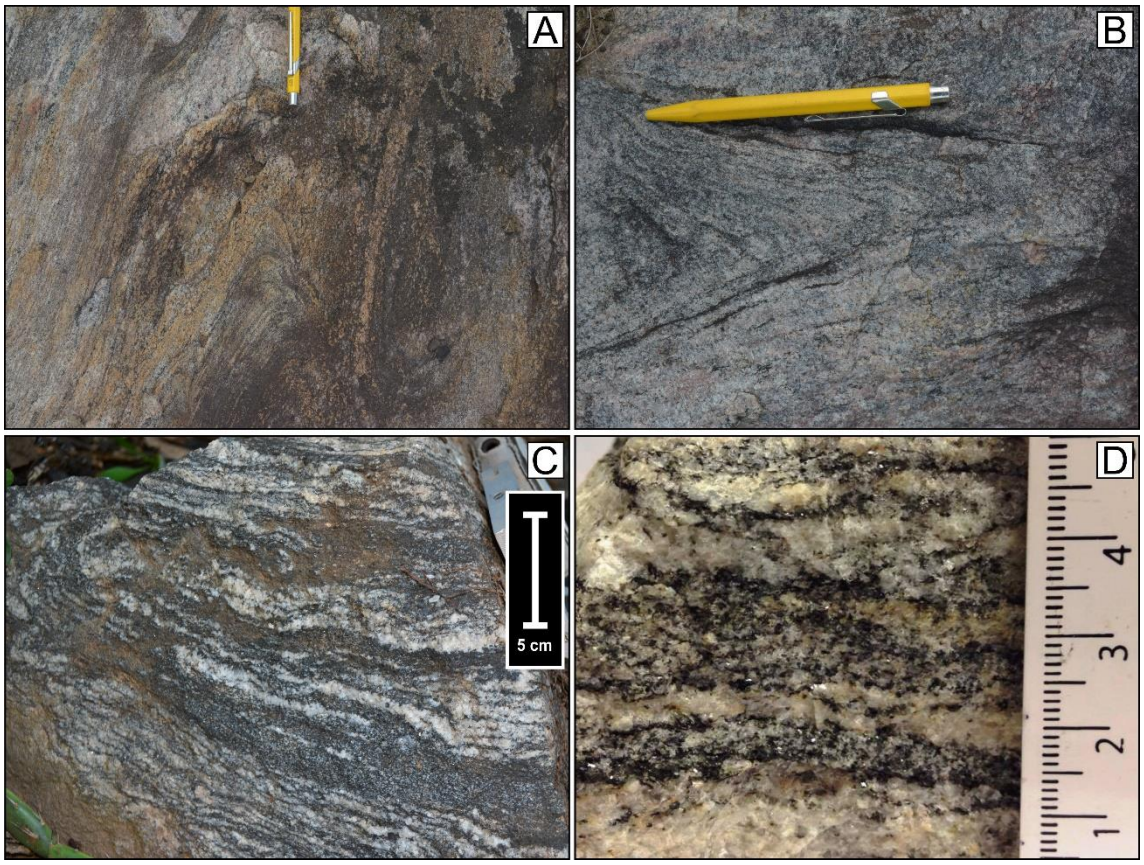

Supplementary Figure I.2. (A) and (B) Macroscopic features of the San Miguel Gneiss. Typical outcrop of a fine- to medium-grained slab with folded, leucocratic banding. (C) and (D) Rosário Gneiss: light grey, leucocratic, equigranular to inequigranular, medium grained rock, with alternating mafic and felsic bands. Pen for scale 14 cm long.

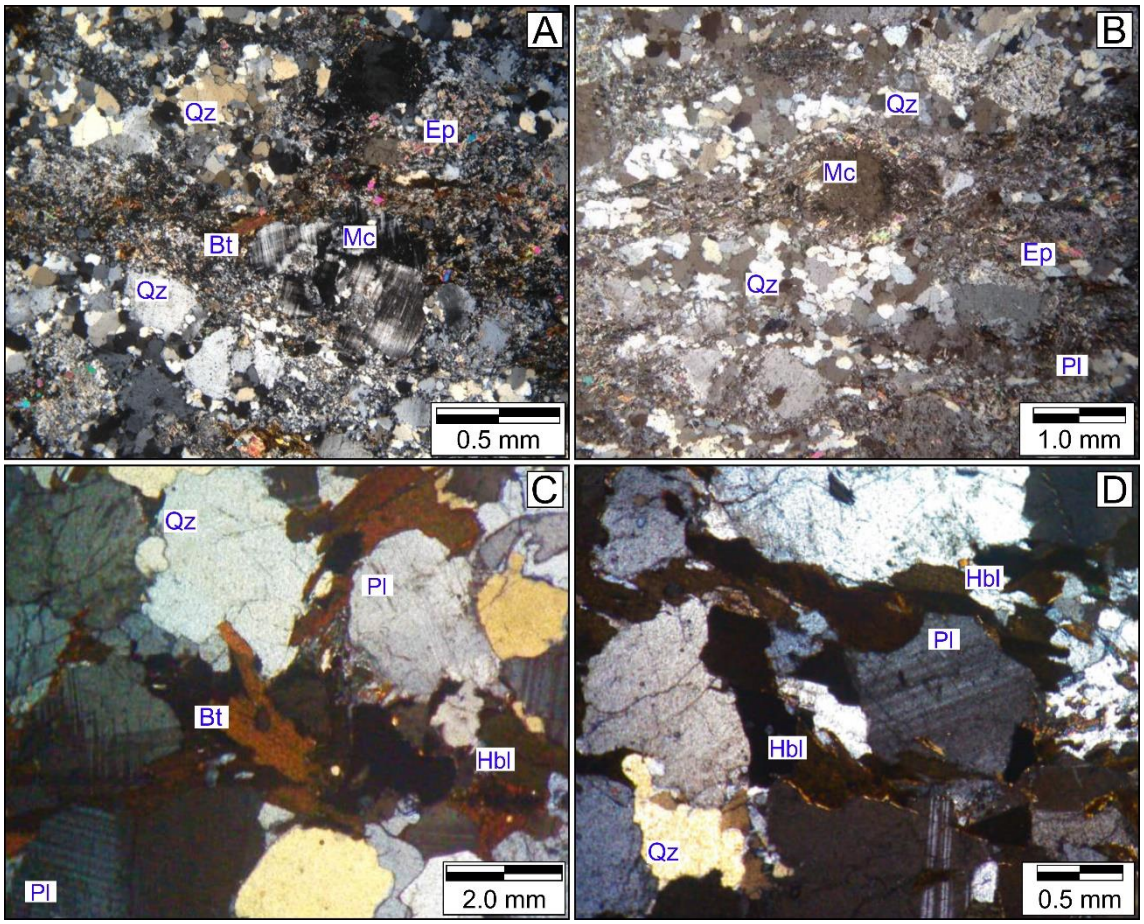

Supplementary Figure I.3. (A) Medium inequigranular granoblastic texture of the Miraflores Gneiss, with quartz, microcline, and intensely saussuritized plagioclase. (B) Porphyroblastic texture in the same gneiss, whereby the K-feldspar is immersed in a fine quartz-feldspar matrix. (C) and (D) Rio Fortuna Gneiss: Granoblastic, medium-grained, inequigranular to equigranular texture of quartz, plagioclase and K-feldspar in felsic bands, intercalated with biotite and hornblende rich bands, and plagioclase porphyroblasts. Pl = plagioclase; Qz = quartz; Kfs = K-feldspar; Mc = microcline, Bt = biotite; Hbl = hornblende; Ep = epidote. Abbreviations based on Siivola and Schmid (2007).

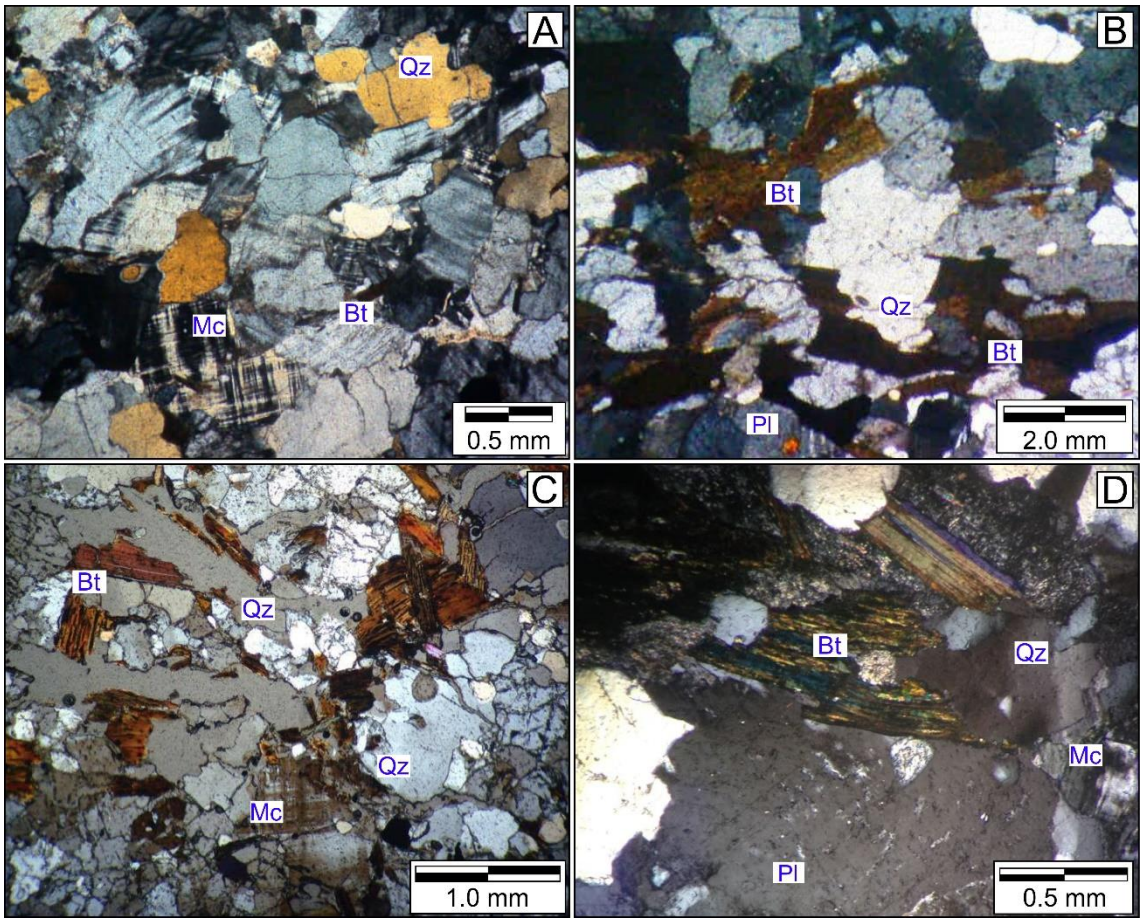

Supplementary Figure I.4. Photomicrographs (A) and (B) of the San Miguel Gneiss, and (C) and (D) of the Rosário Gneiss. (A) Granoblastic, inequigranular to equigranular, medium-grained texture of quartz, microcline and plagioclase. (B) Granoblastic and lepidoblastic texture of quartz, plagioclase and microcline, interspersed with biotite rich bands. (C) Granoblastic inequigranular to equigranular, medium-grained texture of quartz, plagioclase and microcline, intercalated with biotite rich bands. (D) Another feature of this gneiss: Perthitic microcline and biotite with kink bands and partial chloritization. Pl = plagioclase; Qz = quartz; Kfs = K-feldspar; Mc = microcline, Bt = biotite; Hbl = hornblende; Ep = epidote. Abbreviations based on Siivola and Schmid (2007).

CAPÍTULO 6 - DISCUSSÕES E CONCLUSÕES

6.1. Idade e ambiente tectônico dos granitos do embasamento oriental da Bolívia, Gnaisse Santana (Brasil) e dos gnaisses do Complexo Chiquitania

Os granitos orosirianos do leste da Bolívia foram agrupados neste trabalho como EBB (*Eastern Bolivian basement*). Eles correspondem a um magmatismo cálcio-alcalino, peraluminoso, gerado em ambiente de arco magmático. Os granitos Santo Corazón, Correreca e Santa Terezita representam o embasamento mais antigo do leste da Bolívia. Sua idade U–Pb em zircão indicam que eles teriam cristalizado entre 1874 a 1849 Ma, com valores $\varepsilon_{Nd(t)}$ que mudaram de negativo para positivo com o tempo. O Granito Santo Corazón com uma idade de cristalização de ~ 1,87 Ga exibe valores iniciais $\varepsilon_{Nd(t)}$ negativos de - 2,73 a - 1,07. O Granito Correreca tem uma idade de cristalização semelhante de 1,86 Ga, mas com valores iniciais $\varepsilon_{Nd(t)}$ menos negativos de entre - 1,18 e - 0,45.

O Granito Santa Terezita, que ocorre na margem sul do Aulacógeno Tucavaca, na região de San José de Chiquitos encontra-se no limite dos blocos Rio Apa e Paraguá. Com uma idade de cristalização de 1,85 Ga representa o granito mais jovem deste grupo de granitos estudados. Ele exibe uma faixa estreita e positiva de valores iniciais de $\varepsilon_{Nd(t)}$ de +0,25 a + 1,76. Todos esses corpos têm idades modelo paleoproterozoicas entre 2,27 e 1,96 Ga. Idades de 1,7 Ga e 1,3 Ga encontradas nas bordas, são possivelmente metamórficas e a idade de ~ 1,3 Ga também obtida nas bordas de cristais de zircão indicam que este granito foi afetado pela Orogenia San Ignácio.

Os dados geoquímicos indicam que estes granitos são ricos em magnésio, peraluminosos e classificados como granitos do tipo S gerados em um ambiente de arco vulcânico. O fato que os valores iniciais $\varepsilon_{Nd(t)}$, se tornam mais positivos com o tempo, o Granito Santa Terezita, e os valores negativos a positivos de $\varepsilon_{Hf(t)}$ de entre - 4,63 e + 2,76 mostrados pelo granito Correreca bem como os abundantes xenocristais permitem inferir que estes granitos representam o retrabalho de uma crosta paleoproterozoica e que um *input* mantélico também foi importante.

Um possível *decoupling* foi observado entre os sistemas Sm-Nd e Lu-Hf, nos dados do Granito Correreca. Esse *decoupling* pode ser explicado pelo modelo de Zhang *et al*. (2019), quem discutiu um caso em que os sedimentos reciclados em uma zona de subducção levam ao desacoplamento dos sistemas isotópicos, mostrando ε_{Nd} (negativo) em rocha total e ε_{Hf} (positivo) nos cristais de zircão. Assim, é possível interpretar que a diferença entre ε_{Nd} negativo e valores positivos de ε_{Hf} registrados para o Granito Correreca podem ser baseados na reciclagem de componentes que retornam para a crosta durante a subducção, processo que pode estar relacionado aos granitos gerados em um ambiente de arco magmático.

Na região de Corumbá, granitoides peraluminosos ricos em ferro de composição granodiorítica e quartzo-monzonítica, e com caráter calcioalcalino a alcalino-cálcico, representam os protólitos para o Gnaisse Santana. Esses protólitos têm potássio baixo a alto e foram aparentemente gerados em um ambiente de arco magmático a 1764±23 Ma. Os resultados indicam que esse arco ra posterior a aqueles dos granitos do embasamento oriental da Bolívia. Em termos composição isotópica de Nd, o Gnaisse Santana tem valores $\varepsilon_{Nd(t)}$ ligeiramente positivos e negativos (+0,62 a - 0,21) e idades modelo entre 2,00 e 2,04 Ga, o que indica derivação da crosta paleoproterozoica também.

Os granitos Correreca, Santa Terezita e Santo Corazón foram correlacionados com o a Suíte Intrusiva Alumiador do Terreno Ocidental do Bloco Rio Apa, especificamente associados ao Arco Magmático Amonguijá. Em contraste, o Gnaisse Santana foi correlacionado com a Suíte Caracol do Terreno Oriental e ao Arco Magmático Rio Apa. O Bloco Rio Apa, portanto, pode ser estendido para o leste da Bolívia cerca de 300 Km.

Ambos os arcos foram propostos por Lacerda Filho *et al*. (2006). No entanto, recentemente Teixeira *et al*. (2020) em seu trabalho de revisão sobre o Bloco Rio Apa, propôs os arcos Amonguijá (1,87–1,82 Ga) e Caracol (1,80-1,74 Ga).

Complexo Chiquitania

O Complexo Chiquitania representa uma das unidades mais antigas do embasamento do Bloco Paraguá. Esses gnaisses foram gerados em dois períodos distintos. A unidade mais antiga, o Gnaisse Miraflores (~ 1747 Ma), corresponderia com o interior do Bloco Paraguá. A segunda geração dos gnaisses do Complexo Chiquitania é composta por unidades mais jovem (~ 1690 - ~ 1640 Ma) representadas pelos gnaisses Rio Fortuna, San Miguel e Rosário que correspondem com as bordas do Bloco Paraguá. Os protólitos desses gnaisses possuem assinatura cálcio-alcalina e foram gerados em ambientes de arco magmático. Todos os protólitos são de composição granodiorítica a sienogranítica, com exceção do Gnaisse Rio Fortuna que possui protólito de composição tonalítica.

6.2. Evolução do embasamento do leste boliviano: três eventos

A história evolutiva do embasamento do leste boliviano está relacionada com o desenvolvimento e construção dos blocos Rio Apa e Paraguá. A parte do Bloco Rio Apa que aflora no extremo leste boliviano é representada pelos granitos Santa Terezita, Correreca e Santo Corazón (EBB).

Foram sugeridos três eventos para a evolução do embasamento no Leste da Bolívia, que engloba (Bloco Paraguá + EBB);

Evento 1 (~1.84 Ga): relacionado com os granitos do EBB da Suíte Intrusiva Alumiador do Terreno Ocidental do Bloco Rio Apa (EBB + RAB; Redes *et al*., 2020) e com os cristais de zircão herdados do Complexo Lomas Maneches.

Evento 2 (~1.75- ~1.64 Ga): foi associado com a construção de pelo menos dois arcos: o Arco granodiorítico Miraflores construído ao redor de 1747 Ma, e os arcos tonaliticos a graníticos de Rio Fortuna e San Miguel/Rosário construídos ao redor 1690 Ma (Fig. 6.1 A).

O evento 2 é caracterizado por três ciclos magmáticos representados por diferentes arcos magmáticos, nomeados de Arco granodiorítico Miraflores de ~ 1747 Ma (Ciclo 1), o Arco tonalitico Rio Fortuna e o Arco monzogranitico San Miguel / Santo Rosario ambos de ~ 1690 Ma

(Ciclo 2), e posteriormente a colocação dos granitoides Triunfo / Matão / Turvo e Arco Refúgio em ~ 1640 Ma também em ambiente de arco (Ciclo 3).

O Arco Miraflores está localizado na parte central do Bloco Paraguá. Os dados Sm-Nd indicam que se tratava de um arco maduro que teria retrabalhado uma fonte paleoproterozoica. O Arco de Rio Fortuna, com idade de 1699 Ma, está localizado a leste do Bloco Paraguá, na fronteira do Brasil com a Bolívia. O $\varepsilon_{Nd(t)}$ ligeiramente positivo e as T_{DM} indicam derivação de protólitos paleoproterozoicos. Os resultados isotópicos de Hf podem indicar que o protólito se formou a partir de uma mistura de magma basáltico com rochas sedimentares em um ambiente de arco. O Arco San Miguel/Santo Rosario, com idade de 1680 Ma, está localizado na parte sudoeste do Bloco Paraguá. O $\varepsilon_{Nd(t)}$ positivo e as T_{DM} paleoproterozoicas também indicam a participação de uma fonte quase juvenil para este arco, o que é posteriormente suportado por dados de isótopos Hf de zircão.

Os gnaisses do Complexo Chiquitania registraram também idade de ~1,5 Ga, ~1,4 Ga e ~1,3 Ga. As idades de ~1,5 Ga e 1,4 Ga estão associadas a eventos de retrabalhamento. (Fig. 6.1 B e C).

<u>Evento 3 (~1.35 - ~1.25 Ga)</u>: As idades de ~1,3 Ga foi encontrada somente nas bordas dos cristais de zircão dos gnaisses Miraflores, San Miguel e Rosário. Em geral, essas bordas comparativamente mais jovens, interpretadas como sendo de origem metamórfica, circundam núcleos mais escuros e mais antigos seja com zonação magmática regular (idades entre 1,74-1,65 Ga) ou com estrutura interna caótica (idades de 1,57 -1,53 Ga ou 1,42-1,41 Ga). Para o Gnaisse Miraflores foi obtida uma idade de intercepto superior de 1291 Ma, enquanto na região sudoeste da área de estudo, o Gnaisse de San Miguel registrou a idade Concórdia mais jovem de 1256±26 Ma e uma idade de intercepto superior de 1320 Ma, em tornos de núcleos ^{207}Pb / ^{206}Pb de 1599 e 1535 Ma. O Gnaisse Rosário apresentou em cristais de zircão bordas metamórficas ^{207}Pb / ^{206}Pb de 1300 e 1321 Ma, com núcleos de idades ^{207}Pb / ^{206}Pb de 1600 e 1649 Ma. Boger *et al*. (2005)

e Santos *et al*. (2008) também já haviam encontrado cristais de zircão com borda metamórfica de 1,3 Ga para os gnaisses do Complexo Chiquitania e nas rochas do Complexo Lomas Maneches. Nesse período, também ocorreu um intenso magmatismo que produziu os numerosos granitoides do Complexo Granitoide Pensamiento, principalmente na parte norte do Bloco Paraguá. Esses granitoides ocupam aproximadamente 70% do Bloco Paraguá (Matos *et al*., 2009).

A combinação desses resultados permite relacionar o metamorfismo dos gnaisses estudados à segunda fase da Orogenia de San Ignácio (1,34-1,29 Ga), que Bettencourt *et al*. (2010) associou à colisão do Bloco Paraguá com o Cráton Amazônico. Assim, este evento marca o fim da orogenia de San Ignácio (Fig. 6.1 D).

6.3. Evolução Tectônica

Tendo em vista, os novos dados geocronológicos obtidos no embasamento do leste boliviano foram levantados algumas hipóteses sobre a evolução tectônica esta área.

Desta forma, acreditamos que o Bloco Paraguá foi estruturado pelo acúmulo de orôgenos acrecionais. O Arco Miraflores representaria a parte mais antiga (núcleo) em torno da qual os outros arcos foram amalgamados mais tarde. Assim, várias colisões provavelmente ocorreram em um curto período de tempo, entre 1,75-1,64 Ga, e foram responsáveis pelo arcabouço do microcontinente Paraguá (Fig. 6.1)

Este microcontinente poderia ter sido amalgamado com o sudoeste do Cráton Amazônico entre 1,58 e 1,53 Ma. Essas idades são encontradas praticamente em todas as amostras analisadas do Complexo Chiquitania, exceto pelo Gnaisse Miraflores que ocorre na parte central do Bloco Paraguá. Este período é coevo com a geração de orógenos de acrecionais no sudoeste do Cráton Amazônico entre 1,56 e 1,37 Ga (Bettencourt *et al*., 2010). Durante esse período, desenvolveram-se os orógenos Cachoeirinha (1,56-1,52 Ga) e Santa Helena (1,48-1,42 Ga) do terreno Jauru e o orógeno Rio Alegre (1,51-1,52 Ga) do terreno Rio Alegre. As idades registradas nos gnaisses do Complexo Chiquitania são mais semelhantes às encontradas no orógeno Cachoerinha.

Provavelmente, esse intervalo de tempo indica a primeira colisão entre o microcontinente do Paraguá e o Cráton proto-Amazônico.

Como registros de magmatismo ou deformação em ~ 1,5 Ga não foram encontrados até agora em rochas EBB + RAB, isso pode indicar que os blocos do Rio Apa e Paraguá podem não ter sido amalgamados antes de ~ 1,3 Ga. Assim, se a colisão entre PB e EBB + RAB ocorreu apenas a 1,3 Ga, a principal evidência para justificar a colisão entre PB e EBB + RAB - os aros metamórficos de 1,7 Ga em cristais de zircão do Granito Santa Terezita (EBB + RAB; Redes *et al*., 2020).

As evidências de tarogênese em ~ 1,4 Ga são marcadas pela ocorrência de soleiras e enxames de diques máficos na porção S-SW do Cráton Amazônico no estado de Mato Grosso. Isto é representado pela Suite Intrusiva Huanchaca e pelas soleiras máficas Rancho de Prata e Salto do Céu (Lima, 2016; ver Figura 2). No sudoeste do Cráton Amazônico, o enxame de diques Rancho de Prata e as soleiras Salto do Céu (1,44 Ma - Lima, 2016) intrudem o Terrano Jauru. Esses diques e soleiras têm sido relacionados aos estágios pós-orogênicos do Arco Magmático de Santa Helena (Lima, 2016). O Orógeno Rio Alegre no sudoeste do Cráton Amazônico indica a ocorrência de um evento extensional em ~ 1,4 Ga (Bettencourt *et al*., 2010). Sills e diques máficos da Suíte Intrusiva Huanchaca intrudem os ortognaissesTurvo na divisa do Bloco Paraguá (Lima, 2016). Isso indica que o Bloco Paraguá pode ter se destacado do sudoeste do Cráton Amazônico neste período.

O Bloco Paraguá possivelmente colidiu com o sudoeste do Cráton Amazônico em ~ 1,3 Ga em sincronia com a colisão com o EBB + RAB ao sul do Cráton Amazônico (Redes *et al*., 2020). Isso é apoiado pela ocorrência de granitoides da Suíte Intrusiva Pensamiento, como o Granito Colmena de 1,3 Ga exposto na Zona de Cisalhamento de San Diablo (Litherland *et al*., 1986; Nedel *et al*., 2017), e por idades entre 1,34 e 1,29 Ga para bordas metamórficas de cristais de zircão dos gnaisses do Complexo Chiquitania (Evento 3) e do Granito Santa Terezita (EBB + RAB).

De maneira sintetizada concluímos que o Bloco Paraguá foi um continente alóctone, que consideramos a possibilidade de que o Bloco Paraguá pudesse ter sido amalgamado com o SW do Cráton Amazônico entre 1,58 e 1,53 Ma, posteriormente ter se destacado em ~ 1,4 Ga, com base em evidências de tatrogênese, e aproximadamente 100 milhões depois, em 1,3 Ga, possa ter ocorrido a colisão entre o Bloco Paraguá com EBB + RAB.

A região leste da Bolívia passou a fornecer uma nova perspectiva na evolução geológica dos blocos Rio Apa e Paraguá. Os dados desta pesquisa são baseados em análises U-Pb, Lu-Hf e geoquímica, que se somam aos dados pré-existentes. No entanto seria de grande valia, novas análises, principalmente U-Pb em zircão, mas como também em minerais, como monazita e titanita, a fim de identificar processos magmáticos, metamórficos e de herança, tanto nas rochas graníticas do EBB, quanto nas rochas que compõem o embasamento do Bloco Paraguá. Estudos com enfoque em outras unidades, como o Complexo Lomas Maneches e o Grupo San Ignácio, podem revelar uma variedade de idades relacionadas com diferentes processos e eventos, os estudos seriam úteis também, para ampliação do entendimento sobre as relações estratigráficas. Como essa área de estudo é de grande proporção, também é importante mapeá-la com mais detalhes em uma escala maior.

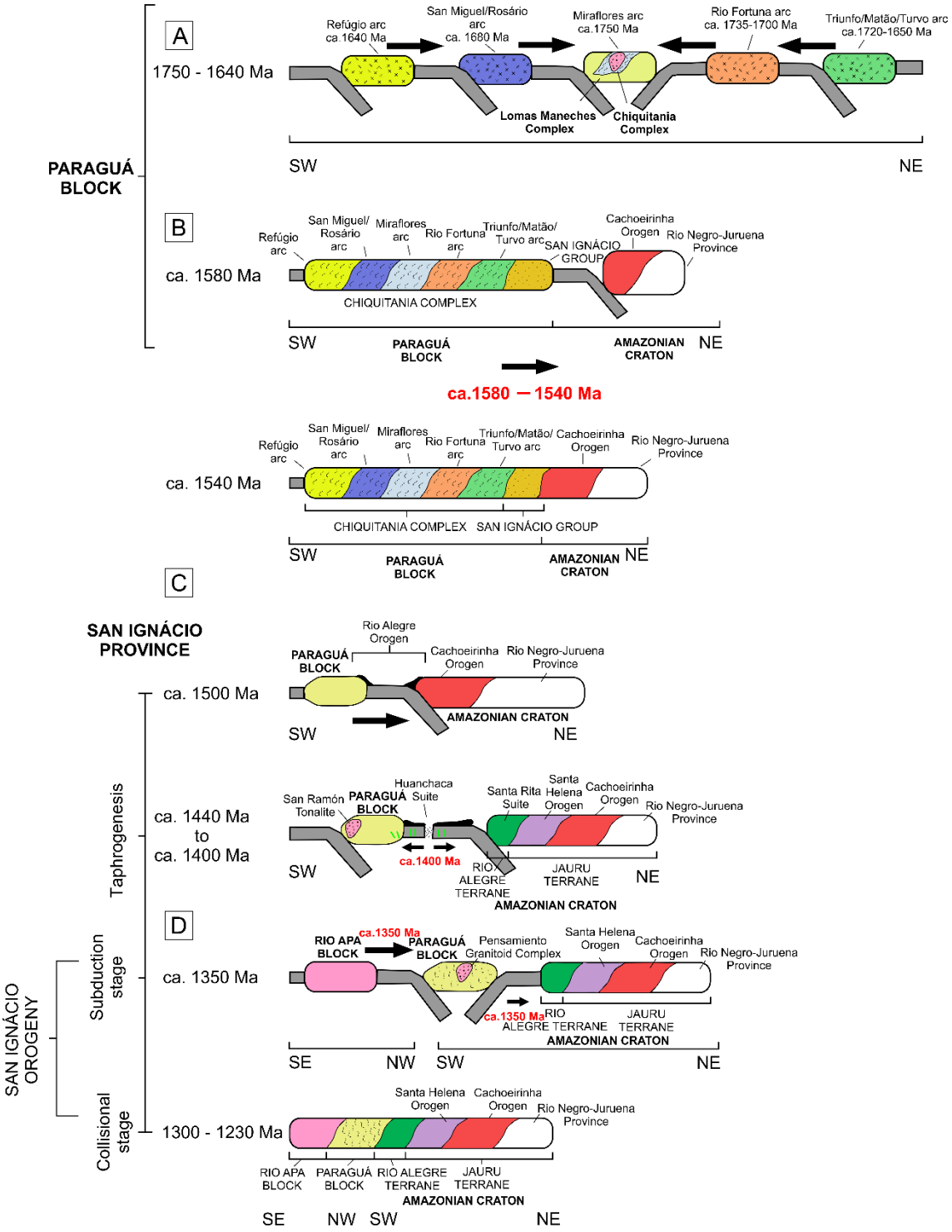

Figure 6.1. Proposta de evolução tectônica do Bloco Paraguá (ver texto para explicação). (A) Intervalo de tempo 1750–1640 Ma. (B) Intervalo de tempo aproximadamente entre 1580-1540 Ma. (C) Intervalo de tempo de 1500–1400 Ma. (D) Intervalo de tempo 1350–1230 Ma.

CAPÍTULO 7 - REFERÊNCIAS

Adamek, P.M., Troeng, B., Landivar, G., Llanos, A., Matos, R., 1996. Evaluación del los recursos minerales del Distrito San Ramón. Boletim do Serviço Geológico da Bolívia 10, 77

Albarède, F., Telouk, P., Blichert-Toft, J., Boyet, M., Agranier, A., Nelson, B., 2004. Precise and accurate isotopic measurements using Multiple-Collector ICPMS. Geochimica et Cosmochimica Acta 68, 12, 2725–2744.

Almeida F.F.M., 1965. Geologia da Serra da Bodoquena (Mato Grosso). Boletim DNPM, Divisão de Geologia e Mineralogia, 219, 1-137.

Almeida F.F.M., 1967. Origem e evolução da plataforma brasileira. Rio de Janeiro, Boletim da Divisão de Geologia e Mineralogia, 241, p. 36.

Alvarenga, C.J.S., Moura, C.A.V., Gorayeb, P.S., Abreu, F.A.M., 2000. Paraguai and Araguaia belts. In: Cordani U.G., Milani E.J., Thomaz Filho A., Campos D.A. (Eds.), Tectonic evolution of South America, 183-193.

Araújo, H.J.T., Santos, Neto, A., Trindade, C..H., Pinto, J.C.A., Montalvão, R.M.G., Dourado, T.D.C.; Palmeira, R.C.B., Tassinari, C.C.G., 1982. Geologia e Levantamento dos Recursos Naturais da Folha SF. 21 – Campo Grande. Projeto Radam Brasil, 28, 23-124.

Berrangé, J.P., 1982. The eastern Bolivia Mineral Exploration Project (Proyecto Precámbrico). Episodes 4, 3-8.

Berrangué J.P. & Litherland M., 1982. Sinopses da Geologia e potencial de mineral da área do Projeto Pré-câmbrico. Boletim do Serviço Geológico da Bolívia, informe 21, 120 pp.

Bettencourt, J.S., Leite, Jr. W.B., Ruiz, A.S., Matos, R., Payolla, B.L., Tosdal, R.M., 2010. The Rondonian-San Ignacio Province in the SW Amazonian Craton: An overview. Journal of South American Earth Sciences 29, 28-46.

Boger, S.D., Raetz M., Giles, D., Etchart, E., Fanning, C.M., 2005. U–Pb age data from the Sunsas region of Eastern Bolivia, evidence for the allochthonous origin of the Paragua Block. Precambrian Research 139, 121-146.

Boggiani, P. C., Alvarenga, C.J.S., 2004. Faixa Paraguai. In: Mantesso-Neto, V., Bartorelli, A., Carneiro, C. D. R., Brito-Neves, B. (Eds.), Geologia do Continente Sul-Americano. São Paulo, Beca, 1, 113-118.

Bouvier, A., Vervoort, J.D., Patchett, P.J., 2008. The Lu-Hf and Sm-Nd isotopic composition of CHUR: constraints from unequilibrated chondrites and implications for the bulk composition of the terrestrial planets. Earth and Planetary Science Letters 273, 48–57.

Brittes, A. F. N., Sousa, M. Z. A. M., Ruiz, A. S., Batata, E. F., Lafon, J.M., Plens, D. P., 2013. Geologia, petrologia e geocronologia (Pb-Pb) da Formação Serra da Bocaina: evidências de um Arco Magmático Orosiriano no Terreno Rio Apa, sul do Cráton Amazônico. Brazilian Journal of Geology, 43, 48-69.

Chauvel, C., Blichert-Toft Je., 2001. A hafnium isotope and trace element perspective on melting of the depleted mantle. Earth and Planetary Science Letters, 190, 137–151.

Chu, N.C., Taylor, R.N., Chavagnac, V., Nesbitt, R.W., Boella, R.M., Milton, J. A., German, C.R., Bayon, G., Burton, K., 2002. Hf isotope ratio analysis using multi-collector inductively coupled plasma mass spectrometry: an evaluation of isobaric interference corrections. Journal of Analytical Atomic Spectrometry, 17, 1567-1574.

Cordani, U.G., Sato, K., Teixeira, W., Tassinari, C.C.G., Basei, M.A.S., 2000. Crustal evolution of the South American platform. In: Cordani, U. G., Milani, E. J., Thomaz Filho, A., Campos, D. A. (Eds.), Tectonic evolution of South America. Rio de Janeiro, pp. 19-40

Cordani, U.G., Teixeira, W., 2007. Proterozoic Accretionary Belts in the Amazonian Craton. In: Hatcher, Jr., R.D., Carlson, M.P., McBride, J.H. (Eds.), 4-D Framework of Continental Crust. Memoir, Geological Society of America, Boulder, Colorado, 200, pp. 297-320.

Cordani, U.G., Teixeira, W., D'Agrella-Filho, M.S., Trindade, R.I., 2009. The position of the Amazonian Craton in supercontinents. Gondwana Research 15, 396–407.

Cordani, U.G., Teixeira, W., Tassinari, C.C.G., Coutinho, J.M.V., Ruiz A.S., 2010. The Rio Apa Craton in Mato Grosso do Sul (Brazil) and Northern Paraguay: Geochronological evolution, correlations and tectonic implications for Rodinia and Gondwana. American Journal of Science 310, 981–1023.

Correia Filho, F.C.L Martins, E.G. Araújo, E.S., 1981. Projeto Rio Apa: Relatório da área I. CPRM, Convênio CODESUL/CPRM,v. 2.

DePaolo, D.J., 1981. Trace elemento and isptopic effects of combined wall rock assimilation and fractional crystallization. Earth and Planetary Science Letters 53, 189-202.

Faleiros, F.M., Caltabeloti, F.P., Pinto, L.G.R., 2014. Programa Geologia do Brasil – PGB. Aldeia Tomázia. Folha SF.21-V-B-VI. Estado de Mato Grosso do Sul. Carta Geológica. São Paulo: CPRM, 2014, 1 mapa colorido, 95 x 70 cm. Escala 1:100.000.

Faleiros, F.M., Pavan M., Remédio, M.J., Rodrigues, J.B., Almeida, V.V., Caltabeloti, F.P., Pinto, L.G.R., Oliveira, A.A., Pinto de Azevedo, E.J., Costa, V.S., 2016. Zircon U-Pb ages of rocks from the Rio Apa Cratonic Terrane (Mato Grosso do Sul, Brazil): New insights for its connection with the Amazonian Craton in pre-Gondwana times. Gondwana Research, 34, 187-204.

Faria, A.D., 2015. Petrografia, Análise deformacional e geocronologia (U-Pb) dos gnaisses do Terreno Paraguá: Provável Arco Vulcânico Orosiriano - SW do Cráton Amazônico. Tese de Doutorado. Universidade Federal do Pará, Belém, 135 pp.

Faria, A.D., Ruiz, A.S., Matos, J.B., Sousa, M.Z.A., Lima, G.A., Macambira, M.J.B., 2014. Geology, Geochemistry, and Geochronology (U-Pb) of the Rio Fortuna Gneiss – Serra do Baú Intrusive Suite – Paraguá Terrane – SW Amazonian Craton. Brazilian Journal of Geology 44, 139-154.

Figueiredo, F.L.P., Ruiz A.S., Sousa, M.Z.A., Macambira, M.J.B., 2013. Gnaisse Turvo: registro de magmatismo paleoproterozoico no Terreno Paraguá – Sudoeste do Cráton Amazônico, Vila Bela da Santíssima Trindade, Mato Grosso. Brazilian Journal of Geology 43, 401-422.

França, O. Ruiz, A. S., Sousa, M. Z. A., Batata, M. E. F., Lafon, J.M., 2014. Geology, petrology, U-Pb (SHRIMP) geochronology of the Morrinhos granite – Paraguá Terrane, SW Amazonian craton: implications for the magmatic evolution of the San Ignácio orogeny. Brazilian Journal of Geology, 44, 415-432

Gerdes, A., Zeh, A., 2009. Zircon formation versus zircon alteration – New insights from combined U-Pb and Lu-Hf in-situ LA-ICP-MS analyses, and consequences for the interpretation of Archean zircon from the Central Zone of the Limpopo Belt. Chemical Geology, 261, 230–243.

Godoi H.O., Martins E.G., Mello C.R., Scislewski G., 1999. Geologia. MME/SG. Projeto Radam - Brasil. Programa Levantamentos Geológicos Básicos do Brasil. Folhas Corumbá (SE. 21-Y-D), Aldeia Tomázia, (SF. 21-V-B) e Porto Murtinho (SF. 21-V-D), Mato Grosso do Sul, escala 1: 250.000.

Godoi, H.O., Martins, E.G., Mello, J.C.R., 2001. Programa de Levantamentos Geológicos Básicos do Brasil: Folha SE.21-Y-D – Corumbá, Folha SF.21-V-B- Aldeia Tomázia, Folha SF.21-V-D - Porto Murtinho, Mato Grosso do Sul, escala 1:250 000. CPRM, 88pp.

Godoy, A.M., Ruiz, A.S., Manzano, J.C., Araújo, L.M.B., 2007. Contexto geológico do magmatismo do Grupo Amonguijá, Suíte Intrusiva Alumiador e Vulcânica Serra da Bocaina, Maciço Rio Apa, sul do Cráton Amazônico – MS. In: 11º Simpósio Nacional de Estudos Tectônicos, Natal-RN, Brasil. SBG, 277-279.

Godoy, A.M.; Pinho, F.E.C., Manzano, J.C., Araújo, L.M.B., Silva, J.A., Fig.ueiredo, M., 2010. Estudos Isotópicos das Rochas Granitoides Neoproterozoicas da Faixa de Dobramento Paraguai. Revista Brasileira Geociências, 40, 380–391.

Jackson, S.E., Pearson, N.J., Griffin, W.L., Belousova, E.A., 2004. The application of laser ablation inductively coupled plasma mass spectrometry to in situ U-Pb zircon geochronology. Chemical Geology 211, 47-69.

Jesus, G.C., Sousa, M.Z.A., Ruiz, A.S., Matos, J.B., 2010. Petrologia e geocronologia (U/Pb–Sm/Nd) do Granito Passagem, Complexo Granitoide Pensamiento, SW do Cráton Amazônico (MT). Revista Brasileira de Geociências 40, 392-408

Klinck, B.A., Litherland, M., 1982. A model for the Proterozoic structural history of eastern Bolivia. Report on Eastern Bolivia Mineral Exploration Project, Santa Cruz, number BAK/15 (unpublished).

Lacerda Filho, J. V., 2015. Bloco Rio Apa: Origem e Evolução Tectônica. Universidade Federal de Brasília, Tese de Doutorado, 181 pp.

Lacerda Filho, J.V., Brito R.S.C., Silva M.G., Oliveira C.C., Moreton L.C., Martins E.G., Lopes R.C., Lima T.M., Larizatti J.H., Valente C.R., 2006. Geologia e Recursos Minerais do Estado de Mato Grosso do Sul, Programa Integração, Atualização e Difusão de Dados da Geologia do Brasil. CPRM, Campo Grande, 1, 10-128.

Lima, G.A., 2016. Soleiras e Enxames de Diques Máficos do sul-sudoeste do Cráton Amazônico. Tese de Doutorado. Universidade Federal do Pará, Belém, 182 pp.

Litherland, M., Annells, R.N., Appleton, J.D., Berrangé, J.P., Bloomfield, K., Burton, C.C.J., Darbyshire, D.P.F.M., Fletcher, C.J.N., Hawkins, M.P., Klinck, B.A., Lanos, A., Mithcell, W.I., O Connor, E.A., Pitfield, P.E.J., Power, G. E Webb B.C., 1986. The Geology and Mineral Resources of the Bolivian Precambrian Shield. British Geological Survey Overseas Memoir 9, 153 pp.

Litherland, M., Annels, R.N., Appleton, J.D., Berrange, J.P., Bloomfield, K., Burton, C.C.J., Darbyshire, D.P.F.M, Fletcher, C.J.N., Hawkins, M.P., Klink, B.A., Llanos, A., Mitchell, W.I., O Connor, E.A., Pitfield, P.E.J., Power, G., Webb, B.C., 1989. The Proterozoic of eastern Bolivia and its relationship to the Andean Mobile Belt. Precambrian Research 43, 157-174

Litherland, M., Bloomfield, K., 1981. The Proterozoic history of eastern Bolivia. Precambrian Research 15, 157–179.

Loewy, S.L., Connelly, J.N., Dalziel, I.W.D., 2004. An orphaned block: the Arequipa–Antofalla basement of central Andean margin of South America. Geological Society of America Bulletin 116, 171-187

Ludwig, K.R., 2012. Isoplot 3.75. A Geochronological Toolkit for Microsoft Excel. Special Publication. Berkeley Geochronology Center 4, 75 pp.

Lugmair, G.W., Marti, K., 1978. Lunar initial $^{143}Nd/^{144}Nd$: differential evolution of the lunar crust and mantle. Earth and Planetary Science Letters, 39, 349-357.

Manzano J. C., Godoy A. M., Araújo L. M. B., Godoy L. P., 2012. Suíte Plutônica Alumiador, Grupo Amonguijá, Maciço Rio Apa – MS. São Paulo, UNESP, Geociências. 31, 3, 351-370.

Matos R., 2010. Geocronologia e Evolução Tectônica Paleo-Mesoproterozoica do Oriente Boliviano – Região Sudoeste do Cráton Amazônico. Instituto de Geociências, Universidade de São Paulo, Tese de Doutorado, 240pp.

Matos, J.B., Juliani, C., Tokashik, C.C., Oliveira, R.F., Ruiz, A.S., 2013. Granulitos Ortoderivados da Suite Lomas Maneches, Fronteira Brasil-Bolívia: Geoquímica e Geocronologia.

In: XIII Simpósio de Geologia da Amazônia, Belém-PA, Anais Sociedade Brasileira de Geologia 1, 305-308.

Matos, R., Teixeira W., Geraldes, M.C., Bettencourt, J.S., 2009. Geochemistry and Nd–Sr isotopic signatures of the Pensamiento Granitoid Complex, Rondonian- San Ignácio Province. Eastern Precambrian shield of Bolivia: petrogenetic constraints for a Mesoproterozoic magmatic arc setting. Geologia USP, Série Científica 9, 89–117.

Matteini, M., Dantas, E.L., Pimentel, M.M., Bühn, B., 2010. Combined U-Pb and Lu-Hf isotope analyses by laser ablation MC-ICP-MS: methodology and applications. Anais da Academia Brasileira de Ciências 82, 2, 479-491

Mitchell, W.I., 1979. La geología y potencial de minerales del área de Santo Corazón – Rincón del Tigre (Folha SE 21-5, parte da Folha SE 21-9, parte da Folha SE 21-6 e parte da Folha SE 21-10). Santa Cruz de la Sierra, Serviço Geológico da Bolívia. British Geological Survey, 131pp.

Morel, M.L.A., Nebel O., Nebel-Jacobsen, Y.L., Miller, J.S., Vroon, P.Z., 2008. Hafnium isotope characterization of the GJ-1 zircon reference material by solution and laser ablation MC–ICPMS. Chemical Geology 255, 231 –235.

Nalon, P.A., Sousa M.Z.A., Ruiz, A.S., Macambira, M.B., 2013. Batólito Guaporeí uma extensão do Complexo Granitoide Pensamiento em Mato Grosso, SW do Cráton Amazônico. Revista Brasileira de Geociências, 43, 85–100.

Nebel, O., Nebel-Jacobsen, Y., Mezger, K., Berndt, J., 2007. Initial Hf isotope compositions in magmatic zircon from early Proterozoic rocks from the Gawler Craton, Australia: A test for zircon model ages. Chemical Geology 241, 23-37.

Nedel, I.M., Ruiz, A.S., Matos, G.R.S., Sousa, M.Z.A., Pimentel, M.M., Pavanetto, P., 2017. Front San Diablo na região de Miraflores, Faixa Sunsas, Bolívia: implicações tectônicas e estratigráficas San Diablo Front at Miraflores region, Sunsas Belt, Bolívia: tectonics and stratigraphics implications. Geologia USP, Série Científica 17, 125-147.

Nogueira, S.F., 2015. Petrologia, Geocronologia (U-Pb SHRIMP) e Geologia Isotópica (Sm-Nd) do Granito Aquidabã, Arco Magmático Amonguijá-Terreno Rio Apa-Sul do Cráton Amazônico. Dissertação de Mestrado. Universidade Federal de Mato Grosso, Cuiabá, 80 pp.

Oliveira, E.C., Lafon J.M., Gioia S.M.C.L., Pimentel M.M., 2008. Datação Sm-Nd em rocha total e granada do metamorfismo granulítico da região de Tartarugal Grande, Amapá Central. Revista Brasileira de Geociências 38, 114-127.

Oliveira, F.V., 2015. Chronus: Um novo suplemento para a redução de dados U-Pb obtidos por LAMC-ICPMS. Dissertação de Mestrado. Universidade Federal de Brasília, Brasília, 107 pp.

Pavan, M., Caltabeloti, F.P., Pinto, L.G.R., 2014. Programa Geologia do Brasil – PGB. Folha SF.21-V-D-III - Fazenda Santa Otília, Estado de Mato Grosso do Sul. Carta Geológica, Escala 1:100.000.

Plens, D. P., 2018. Petrogênese e Análise Estrutural e a Suíte Caracol: Implicações para a Evolução Geodinâmica do Bloco Rio Apa - Sul do Cráton Amazônico. Tese de Doutorado, Universidade Federal de Brasília.

Plens, D.P., Ruiz, A.S., Sousa, M.Z.A., Batata, M.E.F., Lafon, J. M., Brittes, A.F.N., 2013. Cerro Porã Batholith: post-orogenic A-type granite from the Amonguijá Magmatic Arc – Rio Apa Terrane – South of the Amazonian Craton. Brazilian Journal of Geology, 43, 515-534.

Redes L. A., Sousa M.Z.A., Ruiz A. S., Lima G. A., Martins L. C.D., 2013. Geologia, Petrografia e Geoquímica do Granito Taquaral - Embasamento das Coberturas Neoproterozoicas do Aulacógeno Tucavaca na região de Corumbá-MS. *In:* 13º Simpósio de Geologia da Amazônia. Belém-PA. Anais: SBG, CD-ROM.

Redes, L. A, Sousa, M. Z. A., Ruiz, A. S., Lafon, J. M., 2015. Petrogenesis and U-Pb and Sm-Nd geochronology of the Taquaral granite: record of an orosirian continental magmatic arc in the region of Corumbá – MS. Brazilian Journal of Geology 45, 431-451.

Redes, L.A., Hauser, N., Ruiz, A.S., Ramiro, G.M., Reimold, U.W., Dantas, E.L., Schmitt R.T., Lima, B.A.F., Zacchi, E.N.P., Chaves, J.G.S., Osorio, L.F.B., Pimentel, M.M., 2020. U–Pb and Hf isotopes in granitoids from the Eastern Bolivian basement: Insights into the Paleoproterozoic evolution of the western part of South America. Journal of South American Earth Sciences 104, 102806. https://doi.org/10.1016/j.jsames.2020.102806

Remédio, M.J., Costa, V.S., Almeida, V.V., Pinto-Azevedo, E.J.H.C.B., Ferrari, V.C., Brumatti, M., Pinto, L.G.R., Caltabeloti, F.P., Faleiros, F.M., 2013. Programa Geologia do Brasil – PGB.

Folha SF.21-X-C-IV - Fazenda Margarida, Estado de Mato Grosso do Sul. Carta Geológica - Escala 1:100.000.

Ruiz, A.S., 2005. Evolução geológica do sudoeste do Cráton Amazônico região limítrofe Brasil-Bolívia-Mato Grosso. Tese de Doutorado. Universidade Estadual Paulista, São Paulo, 299 pp. (in Portuguese).

Ruiz, A.S., 2009. Compartimentação Tectônica (Pré-Sunsas) do Sudoeste do Cráton Amazônico: Ênfase em Mato Grosso – Brasil. In: XVIII Congresso Geológico Boliviano. Potosí, Bolívia, 159-163.

Saes, G.S., Leite, J.A.D., 1993. Evolução tectono-sedimentar do Grupo Aguapeí, Proterozoico Médio na porção meridional do Cráton Amazônico: Mato Grosso e Oriente Boliviano. Revista Brasileira de Geociências 23, 31–37.

Santos, F.S., Pierosan, R., Barros, M.A.S., Geraldes, M.C., Lima, M.F., 2019. Petrology of the Colíder Group volcanic successions in the northernmost Mato Grosso, Brazil: A contribution to the knowledge of the felsic volcanism of the Alta Floresta Gold Province. Journal of South American Earth Sciences 89, 10–29.

Santos, J.O.S., Rizzotto, G., Easton, M.R., Potter, P.E., Hartmann, L.A., McNaughton, N.J., 2002. The Sunsas Orogen in Western Amazon Craton, South America and Correlation with the Grenville Orogen of Laurentia, based on U-Pb Isotopic Study of Detrital and Igneous Zircons. In: Geological Society of America, Denver Annual Meeting, Precambrian Geology, 27-30.

Santos, J.O.S., Rizzotto, G.J., McNaughton, N.J., Matos, R., Hartmann, L.A., Chemale Junior, F., Potter, P.E., Quadros, M.L.E.S., 2008. The age and autochthonous evolution of Sunsas Orogen in West Amazon Craton. Precambrian Research, 165, 120–152.

Scherer, E., Münker, C., Mezger, K., 2006. Calibration of the lutetium–hafnium clock. Science. 293, 683–687.

Schmitt, R.S., Trouw, R.A.J., Van Schmus, W.R., Pimentel, M.M., 2004. Late amalgamation in the central part of Western Gondwana: new geochronological data and the characterization of a Cambrian collisional orogeny in the Ribeira belt (SE Brazil). Precambrian Research 133, 29- 61

Souza, C.D., Sousa, M.Z.A., Ruiz, A.S., Batata, M.E.F., Brittes, A.F.N., Lafon, J.M., 2016. Formação Serra da Bocaina: Contribuição do Vulcanismo Paleoproterozoico do Arco Magmático Amonguijá no Bloco Rio Apa, Sul do Cráton Amazônico. Geochimica Brasiliensis 30, 136 – 157

Tassinari, C.C.G., Bettencourt, J.S., Geraldes, M.C., Macambira, M.J.B.; Lafon, J.M., 2000. The Amazonian Craton, in: Cordani, U. G.; Milani, E. J.; Thomaz Filho, A.; Campos, D. A. (Eds.), Tectonic evolution of South America. 31º International Geological Congress, Rio de Janeiro, pp. 41-95.

Tassinari, C.C.G., Cordani, U.G., Nutman, A.P, Van Schmus, W.R., Bettencourt, J.S., Taylor, P.N., 1996. Geochronological systematics on basement rocks from the Rio Negro-Juruena Province (Amazonian Craton) and tectonic implications. International Geology Reviews 38, 2, 161–175.

Taylor, S.R., McLennan, S.M., 1985. The Continental Crust: its Composition and Evolution. Blackwell, Oxford, pp. 312.

Teixeira, W., Cordani, U.G., Faleiros, F.M., Sato, K., Maurer, V.C., Ruiz, A.S., Azevedo, E.J.P., 2020. The Rio Apa Terrane reviewed: U-Pb zircon geochronology and provenance studies provide paleotectonic links with a growing Proterozoic Amazonia. Earth-Science Reviews 202, 1–35.

Teixeira, W., Geraldes, M.C., Matos, R., Ruiz, A.S., Saes, G., Vargas-Mattos, G., 2010. A review of the tectonic evolution of the Sunsas belt, SW Amazonian Craton. Journal of South American Earth Sciences 29, 47–60.

Tohver E., Bettencourt J.S., Tosdal R., Mezger K., Leite W.B., Payolla B.L., 2004. Terrane transfer during Grenville orogeny: tracing the Amazonian ancestry of Southern Appalachian basement through Pb and Nd isotopes. Earth and Planetary Science Letters, 228, 161-176.

Vargas-Mattos, G.L., 2006. Caracterização geocronológica e geoquímica dos granitos proterozoicos: implicação para a evolução crustal da borda SW do Cráton Amazônico na Bolívia. Universidade do Estado do Rio de Janeiro, Dissertação de Mestrado, 110 pp.

Vargas-Mattos, G.L., Geraldes, M.C., Teixeira, W., Salinas, R.M., 2010. Paleoproterozoic granites in Bolivian Precambrian shield: the 1.92–1.89 Ga Correreca magmatic rocks and tectonic

implications. In: VI Simpósio de Geologia Isotópica da América do Sul. Brasília, Brasil. SBG, 65.

Wedepohl, K.H., 1995. The compositions of the continental crust. Geochimica et Cosmochima Acta, 59, 1217–1232.

Wiedenbeck, M., Allé, P., Corfu, F., Griffin, W.L., Meier, M., Oberli, F., von Quadt, A., Roddick, J.C., Spiegel, W., 1995. Three natural zircon standards for U-Th-Pb, Lu-Hf, trace element and REE analyses. Geostandards Newsletter, 19, 1-23.

Wiedenbeck, M., Hanchar, J.M., Peck, W.H., Sylvester, P., Valley, J.W., Whitehouse, M.J., Kronz, A., Morishita, Y., Nasdala, L., Fiebig, J., Franchi, I., Girard, J.P., Greenwood, R.C., Hinton, R., Kita, N., Mason, P.R.D., Norman, M., Ogasawara, M., Piccoli, R., Rhede, D., Satoh, H., Schulz-Dobrick, B., Skar, O., Spicuzza, M.J., Terada, K., Tindle, A., Togashi, S., Vennemann, T., Xie, Q., Zheng, Y.F., 2004. Further characterization of the 91500 zircon crystal. Geostandards and Geoanalytical Research, 28, 9-39.

Wiens, F., ms, 1986, Zur lithostratigraphischen, petrographischen und strukturellen Entwicklung des Rio-Apa Hochlandes, Nordost Paraguay: Clausthal, Geologisches Institut der Technischen Universita¨t Clausthal, Clausthaler Geowissenschaftliche, Ph. D. dissertation, 19, 280 p.

Zhang, C., Liua, D., Zeng, J., Jiang S., Luo, Q., Kong, X., Yang, W, Liu, L., 2019a. Nd-O-Hf isotopic decoupling in S-type granites: Implications for ridge subduction. Lithos, 332, 261–273.

Zhao, G., Sun, M., Wilde, S.A., Li, S., 2004. A Paleo-Mesoproterozoic supercontinent: assembly, growth and breakup. Earth Science Reviews, 67, 91–123.